THE UNIVERSITY *of* EDINBURGH

THE UNIVERSITY
of EDINBURGH

IMPACT OF NORMAL AGEING AND CEREBRAL HYPOPERFUSION ON MYELINATED AXONS AND ITS RELATION TO THE DEVELOPMENT OF ALZHEIMER'S DISEASE

Kanelina Karali BSc, MSc

Submitted for the Degree of Doctor of Philosophy
The University of Edinburgh
2013

The aim of science is not to open the door to everlasting wisdom, but to set a limit to everlasting error.

"The Life of Galileo" by Bertolt Brecht

To my parents Katerina and Panagioti

Στους γονείς μου Κατερίνα και Παναγιώτη

TABLE OF CONTENTS

I declare that this thesis has been composed by me, and that all of the work is my own unless otherwise stated. It has not been presented for any other degree or qualification.

Edinburgh, November 2013

Kanelina Karali

ACKNOWLEDGEMENTS

First of all, I would like to thank my supervisors Prof. Karen Horsburgh and Dr Jill Fowler for their constant guidance, advice and support during the course of my PhD. I would also like thank Dr David Lyons and Dr Emma Wood for their scientific advice and expertise. Moreover, I need to extent my thanks to the academic and technical staff at the Centres for Cognitive and Neural Systems and Neuroregeneration at the University of Edinburgh who helped in aspects of my PhD.

During my PhD in Edinburgh, I have been extremely lucky to have worked with some wonderful people within the Horsburgh lab, who were always willing to help, give advice or support through the ups and downs of my PhD. However, a few people need to be pointed out. Firstly, Dr Gillian Scullion whose help has been invaluable both scientifically and morally. Secondly, Mercede Panozzo and Jamie McQueen who have been my partners in PhD studentship. I thank them for being great colleagues and friends.

I am extremely grateful to my friends in Edinburgh and Athens for providing the necessary entertainment and support during my years as a student in Edinburgh. They made my life easier, happier and funnier, I am glad to have met them. In particular I want to thank my ex-flatmates Nefeli, Elisavet, Ioanna, Michalis and Konstantinos for making a flat feel like home. I also want to thank all the guys from the Real Democracy Now Edinburgh [GR] group for our long political and philosophical discussions and the camaraderie that inspired me. In addition, I want to thank Maro, Chara and Marianthi for being such good friends by always making me laugh, providing moral support and being my drinking buddies. Last, I want to thank

my close friend Amalia who has always been there to support me, no matter the distance between us.

Finally, I would like to thank my parents and my brother for their unconditional love and support. I owe them more than I can describe.

ABSTRACT

Cerebral hypoperfusion can occur in normal ageing and is proposed to underlie white matter disturbances observed in the ageing brain. Moreover, cerebral hypoperfusion and white matter attenuation are early events in the progression of Alzheimer's disease (AD). White matter mostly consists of myelinated axons which have distinct protein architecture, segregated into defined regions; the axon initial segment (AIS), the node of Ranvier, paranode, juxtaparanode, and internode. These sites are essential for action potential initiation and/or propagation and subsequently effective brain function. At the outset of the studies in the thesis there was evidence that the different regions within the myelinated axons are vulnerable to injury and disease. Thus it is hypothesised that in response to normal ageing and/or cerebral hypoperfusion these structures are altered and associated with cognitive impairment and that these effects are exacerbated in a transgenic mouse model (APPSw,Ind, J9 line) which develops age-dependent amyloid-β (Aβ) pathology.

The first study aims to investigate the effect of normal ageing and Aβ deposition on myelinated axons and on learning and memory. To address this, the effects of normal ageing on the integrity of the AIS, nodes of Ranvier, myelin, axons, synapses and spatial working memory are examined in young and aged wild-type and TgAPPSw,Ind mice. A significant reduction in the length of nodes of Ranvier is demonstrated in aged wild-type and TgAPPSw,Ind mice. In addition, the length of AIS, is significantly reduced in the aged wild-type animals while the young TgAPPSw,Ind have significantly shorter AIS than the young wild-type mice. These effects are not influenced by the presence of Aβ. Myelin integrity is affected by age but this is more prominent in the wild-type animals whilst axonal integrity is intact.

Moreover, there is an age-related decrease of presynaptic boutons only in the TgAPPSw,Ind mice. Contrary to the original hypothesis, working memory performance is not altered with age or influenced by increasing Aβ levels.

The second study aims to examine the effects of cerebral hypoperfusion in combination with Aβ pathology and/or ageing on cognitive performance and the structure of myelinated axons. To address this, the effects of surgically induced cerebral hypoperfusion on the integrity of the nodes of Ranvier, paranodes, myelin, axons and spatial working memory performance are investigated in young and aged wild-type and TgAPPSw,Ind mice. A decrease in nodal length is observed in response to hypoperfusion in young and aged animals. This effect is shown to be exacerbated in the young TgAPPSw,Ind animals. Moreover, the disruption of the nodal domain is shown to occur without any gross alterations in myelin and axonal integrity. It is also demonstrated that in response to hypoperfusion, spatial working memory performance is defected in young and aged animals of both genotypes. This deficit is exacerbated in the young TgAPPSw,Ind. The observed changes in the nodal structure are associated with poor working memory performance indicating functional implication for the nodal changes.

These data highlight that structures within myelinated axons are vulnerable to ageing and cerebral hypoperfusion. Therefore, the development of strategies that minimize injury or drive repair to these regions is necessary together with therapeutic approaches against the vascular insults that induce hypoperfusion and lead to white matter attenuation and cognitive decline. In the future, it would be interesting to investigate how alterations at the AIS/nodes of Ranvier affect neuronal excitability.

LIST OF FIGURES

LIST OF TABLES

LIST OF ABBREVIATIONS

2VO	2 vessel occlusion
AD	Alzheimer's disease
AIS	Axon initial segment
AnkG	Ankyrin G
AP	Action potential
APOE	Apolipoprotein E
APP	Amyloid precursor protein
ASL	Arterial spin labeling
ATP	Adenosine triphosphate
Aβ	Amyloid-beta
BACE	β-amyloid cleaving enzyme
BBB	Blood-brain barrier
BCCAO	Bilateral common carotid artery occlusion
BDNF	Brain-derived neurotrophic factor
CAA	Cerebral amyloid angiopathy
Caspr	Contactin associated protein
CBF	Cerebral blood flow
CNPase	2',3'- Cyclic Nucleotide 3'- Phosphodiesterase
CNS	Central nervous system
CT	Computed tomography
DAB	3, 3´-diaminobenzidine
DTI	Diffusion tensor imaging
FA	Fraction anisotropy

FDG-PET	2-deoxy-2-[F-18]fluoro-D-glucose
fMRI	Functional magnetic resonance imaging
GABA	γ-Aminobutyric acid
GDNF	Glial cell line-derived neurotrophic factor
IGF-1	Insulin-like growth factor-1
kDa	Kilo Dalton
K_v	Shaker-type potassium channels
LTP	Long-term potentiation
MAG	Myelin associated glycoprotein
MBP	Myelin basic
MCI	Mild cognitive impairment
MES-SDS	2-[N-morpholino]ethanesulfonic acid-sodiumdodecyl sulphate
MOG	Myelin oligodendrocyte glycoptotein
MRI	Magnetic resonance imaging
MRI	Magnetic resonance imaging
Na_v	Voltage-gated sodium channels
NF155	155 KDa neurofascin isoform
NF186	186 KDa neurofascin isoform
NF-H	Heavy neurofilament
NF-L	Light neurofilament
NF-M	Medium neurofilament
NFT	Neurofibrillary tangle
NrCAM	Neuronal cell adhesion molecule
OMgp	Oligodendrocyte-myelin glycoprotein

PB	Phosphate buffer (pH7.4)
PBS	Phosphate buffer saline (pH7.4)
PBSTx	Phosphate buffer saline (pH7.4) with 0.1% Triton-X100
PLP	Proteolipid protein
PNS	Peripheral nervous system
PS1	Presenilins
PS2	Presenilin 2
PW-MRI	Perfusion weighted magnetic resonance imaging
sAPP-α	Secreted amyloid precursor protein-α
sAPP-β	Secreted amyloid precursor protein-β
SPECT	sSingle photon emission computed tomography
TAG-1	Contactin-2

Chapter 1

Introduction

1.1 White matter

Early *post-mortem* observations of the central nervous system (CNS) introduced the concept of white matter and separated it from the grey matter (Meckel, 1817) on the basis of their colour difference upon examination with the naked eye (macroarchitecture). White matter is present throughout the CNS tissue of vertebrate animals. In humans, more than 50% of the total brain volume accounts for white matter (Figure 1.1A). This fraction of white matter abundance is by far the greatest seen in any species (Fields, 2008). In mice, for example, white matter is only 25% of the total brain volume.

The interest in white matter began in the 19th century. In 1858, Rudolf Virchow introduced the concept of neuroglia (Greek γλία,"glue, something sticky") for white matter. However, it was only considered to be a type of connective tissue without cellular components (Virchow, 1860). Later in the 19th century, Camillo Golgi was the first who showed that glia contains cellular components different from the nervous cells (Golgi, 1870). In the early 20th century, Santiago Ramon y Cajal and his pupil Pío del Río-Hortega described the three major cellular components: the astrocytes, the oligodendrocytes and the microglia. Hortega demonstrated the

myelinating properties of the oligodendrocytes rendering them the CNS equivalent of the Schawnn cell found in the peripheral nervous system (PNS).

It is now recognised that white matter integrity is essential for normal brain function. White matter maintains the communication between the different brain regions and disruption to its components could lead to breakdown of the communication between the neurons of different brain regions that may ultimately translate into cognitive impairment. Alterations to white matter have been implicated in ageing and neurodegenerative diseases and associated with cognitive dysfunction. Throughout the thesis the integrity of white matter components in response to normal ageing and challenges to the brain (low blood flow, amyloid-β) will be closely examined.

1.1.1 Components of white matter

White matter consists of glial cells, blood vessels and myelinated axons. Axons connect neurons residing in different grey matter areas of the CNS and facilitate their communication (Figure 1.1B). In the CNS, glial cells are approximately 10 times more abundant than the neurons (Coyle and Schwarcz, 2000). Glia include different cell types such as astrocytes, microglia and oligodendrocytes.

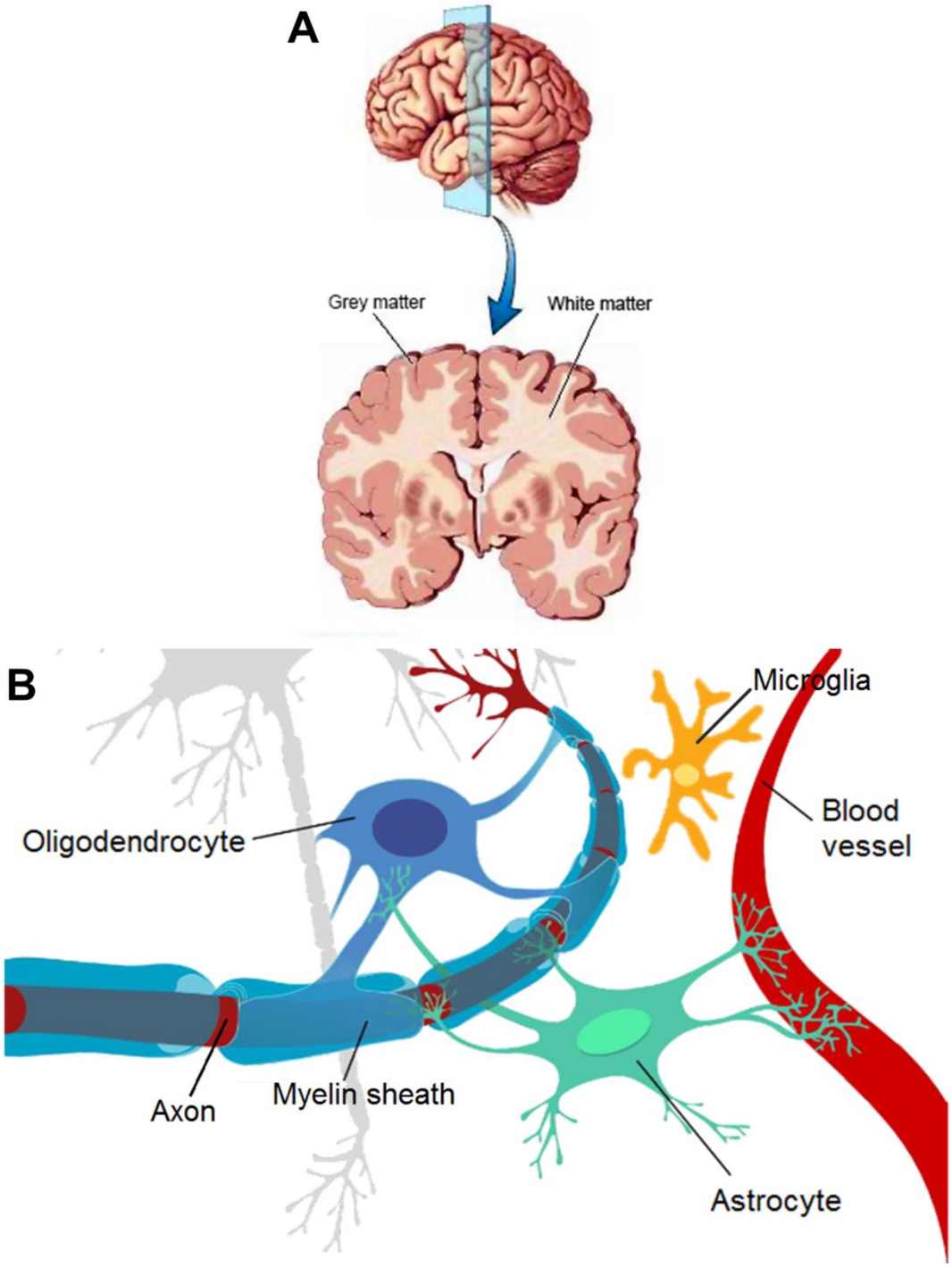

Figure 1.1 ***White matter and its components*****.** [A] Schematic of a coronal section of the human brain showing areas of grey and white matter tissue (Bear et al., 2007). [B] White matter consists of blood vessels, astrocytes, microglia, oligodendrocytes and axons (image adapted from http://en.wikipedia.org/).

1.1.1.1 Astrocytes

Astrocytes are the most numerous cell types in the CNS and second most abundant in white matter. Astrocytes serve multiple roles; their function has been implicated in the maintenance of synapses (Allen and Barres, 2005), the homeostasis of extracellular ions (Laming et al., 2000), the function of the vasculature (Mulligan and MacVicar, 2004), the regulation of signaling (McIver et al., 2013), the trophic support of the oligodendrocytes (Paspalas and Papadopoulos, 1998) and the initiation of the myelination (Franklin and Ffrench-Constant, 2008).

1.1.1.3 Oligodendrocytes

The oligodendrocytes are the most prevalent cell type in the white matter. They are the cells that produce myelin, a substance comprised of 70% lipids and 30% proteins (Raine, 1984). They extend processes that wrap around axons in a process known as myelination. The nature of myelination is segmented, with the myelin segments being interrupted by gaps of unmyelinated axon known as nodes of Ranvier (Figure 1.2). One oligodendrocyte may ensheath multiple surrounding axons and different segments of myelin on the same axon may originate from different oligodendrocytes. Myelination acts as insulation proving higher conduction velocity of the electric impulses along the axons. It has been shown that conduction velocity increases up to 100 times in the myelinated axons in comparison with the unmyelinated ones (Fields, 2008). The presence of the myelin sheath is advantageous because it offers secure

signal transduction between the different brain regions and high speed conduction of the electric impulses by saving energy and space (Quarles et al., 2006).

The myelinating oligodendrocytes originate from oligodendrocyte precursor cells (OPCs) and they are the product of a precise developmental program (Bradl and Lassmann, 2010). This includes the differentiation of the OPCs to pre-/immature oligodendrocytes which then differentiate into mature myelinating oligodendrocytes expressing multiple myelin-specific proteins (detailed later in chapter 1.1.2.1). The oligodendrocytes insulate the axons with myelin and have multiple other roles. For example, they are responsible for the clustering of sodium channels at the nodes of Ranvier which is necessary for saltatory conduction (Kaplan et al., 1997; Kaplan et al., 2001). In addition, they are necessary for axonal survival (Uschkureit et al., 2000; Garbern et al., 2002) and fast axonal transport (Edgar et al., 2004) and they also provide trophic support to the neurons with the production of neurotrophic factors such as glial cell line-derived neurotrophic factor (GDNF), brain-derived neurotrophic factor (BDNF), or insulin-like growth factor-1 (IGF-1) (Du and Dreyfus, 2002).

The formation of the myelin sheath is a long process that proceeds from the caudal to the most rostral regions of the brain (Baumann and Pham-Dinh, 2001) and in some regions can form even during the sixth decade of life (Benes et al., 1994). However, myelination and the support of the myelin sheaths by the oligodendrocytes is extremely energy demanding and requires high amounts of oxygen and ATP (McTigue and Tripathi, 2008). The high metabolic rate of the oligodendrocytes produces toxic hydrogen peroxide and reactive oxygen species that need to be

metabolised (McTigue and Tripathi, 2008). In addition, the oligodendrocytes have high content in iron and low concentration in the anti-oxidative enzyme glutathione (Thorburne and Juurlink, 1996) which combined with the toxic byproducts of the metabolism makes them susceptible to oxidative damage.

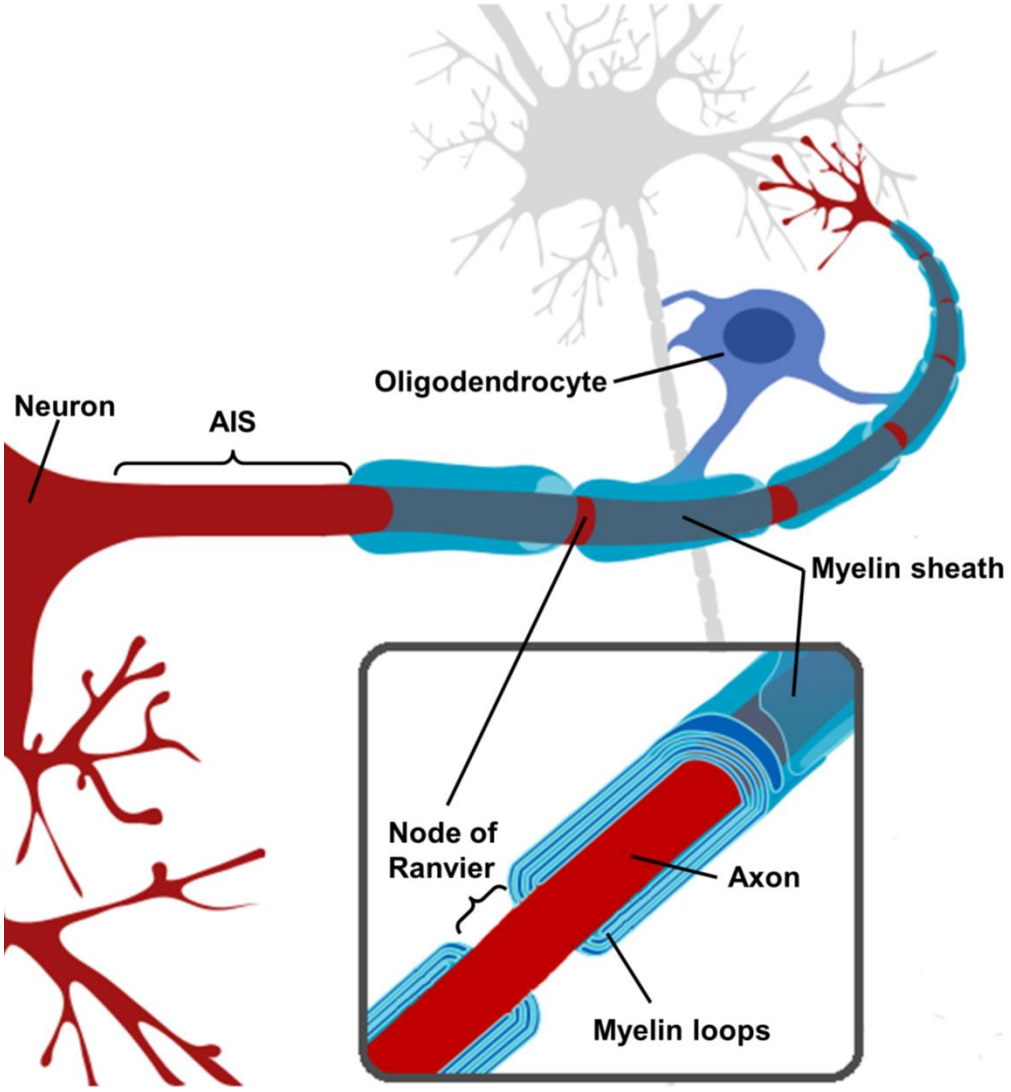

Figure 1.2 ***The myelinating oligodendrocytes***. Oligodendrocytes produce myelin and extend processes that wrap around the axon. The nature of myelination is segmented, with the myelin segments being interrupted by gaps of unmyelinated axon known as nodes of Ranvier (image adapted from http://en.wikipedia.org/).

1.1.1.4 Blood vessels

Blood supply to the white matter is mediated by a vascular network delivering oxygen, glucose and nutrients necessary for the cellular metabolism. From the pial network running on the surface of the brain, smaller arteries branch out and penetrate into the brain tissue (Cipolla, 2009). The penetrating arterioles further branch out at different directions going thought the cortex to the sub-cortical white matter. These arteries terminate in the capillary bed which is characterised by small branched vessels that supply distinct areas of white matter with blood (Lierse and Horstmann, 1965). This places the white matter at the end of the blood supply route (Pantoni, 2002) and it may be more vulnerable to cerebral blood flow (CBF) fluctuations (Pantoni and Garcia, 1997). This will be outlined in further detail in chapter 1.3.2.

1.1.2 The myelinated axon

Ramon Y Cajal was the first to introduce the concept of directionality for signal transmission and neuronal communication (Llinas, 2003). As mentioned earlier, the myelin sheaths insulate the axons and subsequently increase the velocity of the electric impulses along the axons by increasing the electrical resistance and decreasing the capacitance of the axonal membrane. The electric impulses are called action potentials (AP) and result from information processing of excitatory and inhibitory signals which converge at the neuron for the generation of an all-or-nothing response. The segmented nature of myelination allows salutatory conduction of the action potentials. Action potential initiation and propagation is mediated by

molecular domains of the myelinated axon with unique morphological and functional characteristics. These domains are: (1) the axon initial segment (AIS) which is a region of unmyelinated axon located close to the soma just before the first myelin segment and is where the action potential is generated, (2) the node of Ranvier which is a region of unmyelinated axon found between neighbouring myelin segments and is rich in voltage-gated sodium (Na^+) channels, (3) the paranode, the region where the myelin loops contact the axonal membrane, (4) the juxtaparanode, a region rich in potassium (K^+) channels and (5) the internode, where the myelin is compactly wrapped (Figure 1.3).

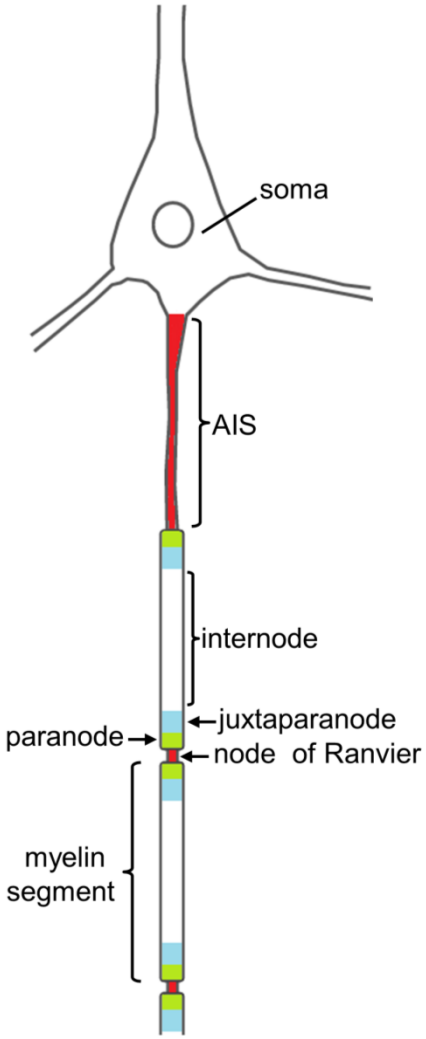

Figure 1.3 ***Molecular domains of the myelinated axon***. Schematic representation of a pyramidal neuron showing the localisation of the axon initial segment (AIS), the nodes of Ranvier, the paranodes, the juxtaparanodes and the internodes on the axon. Image adapted by Kole and Stuart (2012).

1.1.2.1 Myelin specific proteins

Myelin has a unique composition which facilitates its insulating properties. It has a low content of water (40%) and its dry weight is comprised by high content in lipids (70-85%) and low content in protein (15-30%) (Quarles et al., 2006). The proteins and the lipids are produced by the oligodendrocytes. In the CNS the major protein components of myelin are oligodendrocytes-specific and almost 80% of myelin's protein load is comprised by two proteins, the myelin basic protein (MBP) and the proteolipid protein (PLP). Other abundant proteins are the 2',3'- Cyclic Nucleotide 3'- Phosphodiesterase (CNPase), the myelin associated glycoprotein (MAG) the myelin oligodendrocyte glycoptotein (MOG) and the oligodendrocyte-myelin glycoprotein (OMgp).

MBP is a family of membrane proteins located exclusively on the cytoplasmic surface. The family includes different isoforms differentially expressed in the various stages of oligodendrocyte maturation and their role is to facilitate compaction of the appositional cytoplasmic surfaces (Omlin et al., 1982; Roach et al., 1985). In humans there are four isoforms of different molecular weight (21.5, 20.2, 18.5 and 17.2kDa), with the 18.5 and 17.2kDa isoforms being the most abundant. In mice there are also four isoforms (21.5, 18.5, 17 and 14kDa), with the 18.5 and 14kDa being the most abundant (Campagnoni and Macklin, 1988; Staugaitis et al., 1990). PLP is a 30 kDa transmembrane protein with both the N- and C- terminals at the cytoplasmic side and second most abundant myelin protein. Its role is the compaction and stabilization of the myelin sheath (Nadon and West, 1998). CNPase is another myelin protein; it can be found in two isoforms (CNP1 and CNP2) and has a 2',3'- Cyclic Nucleotide 3'-

Phosphodiesterase enzymatic activity (Lazzarini, 2004). MAG is a 100 kDa protein found on the oligodendroglial membranes of the myelin sheath that surround the axons and is involved in signalling mechanisms between the oligodendrocytes and the axons (Quarles, 2007). Other myelin proteins are MOG, which is a 26 KDa protein found on the outer surface of the myelin sheaths, and OMgp which is a 120 kDa expressed by both oligodendrocytes and neurons (Quarles, 2002).

1.1.2.2 Axonal cytoskeleton

The axonal cytoskeleton is a three dimensional structure contributing to the structural architecture of the axon as well as to axonal transport. It comprises of three different filament components namely microtubules, neurofilaments and microfilaments. The core structural protein of microtubules is tubulin, which comprise of α- and β-tubulin heterodimers which polymerize and align in such way for the formation of a 25 nm hollow tube. In addition, microtubules interact with multiple microtubule-associated proteins. Multiple roles have been attributed to microtubules including organelle transport, neuritic extension during development and maintenance of intracellular compartmentalisation. The second type of filaments, are neurofilaments, a rope-like structure of 8-10 nm diameter with projecting side arms. Neurofilaments are formed by three subunits; the light (60-70 kDa, NF-L), medium (130-170 kDa, NF-M) and heavy (180-200 kDa, NF-H) chain. In addition α-internexin and peripherin may interact with neurofilaments. Neurofilaments are important for maintaining the morphology of the axons and axonal transport. Alterations in the levels and the phosphorylation of neurofilaments have been linked to neurological

diseases such as AD, motorneuron disease, Parkinson's disease and others (Al-Chalabi and Miller, 2003). Finally, the third type of filaments are microfilaments which comprise of polymerized actin (43-kDa). The actin cytoskeleton has multiple roles including cell migration and adhesion, distribution of the proteins at the plasma membrane and their restriction at respective compartments.

1.1.2.3 Nodes of Ranvier

Myelin sheaths throughout axons are segmented and interrupted by gaps of unmyelinated axon, the nodes of Ranvier, which serve the long distance rapid saltatory propagation of the action potentials. Action potentials are all-or-nothing responses initiated by the rapid influx of Na^+ via voltage-gated sodium channels such as Na_v, Na+/K+ ATPases and Na+/Ca+ antiporters which are accumulated at the nodes of Ranvier (Duflocq et al., 2008; Pan et al., 2006). There are different subtypes of Na_v channels with $Na_v1.6$ being the most abundant in the adult CNS and $Na_v1.2$ being expressed during development (Boiko et al., 2001; Kaplan et al., 2001). The Na_v channels are comprised of an α subunit forming a pore through the axolemma and two β subunits interacting with cell adhesion molecules, extracellular matrix molecules and cytoskeletal scaffolds (Rasband, 2011). Targeting of Na_v channels at the membrane of the nodes of Ranvier is controlled by the oligodendrocytes and includes the formation of a macro-molecular complex of multiple interacting proteins such as the cytoskeletal adaptor protein ankyrin G (AnkG), the actin binding protein βIV-spectrin, as well as the cell-adhesion molecules neurofascin 186 KDa isoform (NF186) and NrCAM (Rasband, 2011) (Figure 1.4A). Clustering of the Na_v channels

at the nodes of Ranvier appears to be dependent on AnkG (Zhou et al., 1998; Pan et al., 2006; Dzhashiashvili et al., 2007). The neuron specific NF186 is responsible for AnkG recruitment at the node while AnkG is responsible for βIV-spectrin recruitment at the node (Dzhashiashvili et al., 2007; Susuki and Rasband, 2008b; Lacas-Gervais et al., 2004).

1.1.2.4 Paranodes

The paranodes are the principal site of axon-glial contact and serve as a diffusion barrier for the ion channels accumulated on either side of the paranode at the nodes of Ranvier and the juxtaparanodes (Figure 1.4A). This is achieved by the formation of septate-like junctions between the myelin loops of the oligodendrocytes and the axon membrane. The septate-like junctions have been thoroughly studied and it has been shown that a heterotrimeric molecular complex formed by contactin associated protein (Caspr) and contactin located on the axolemma and glial 155 KDa neurofascin isoform (NF155), is necessary for the axon-glial interaction. When any of the three members of the complex is absent, paranodal disruption and impaired signal propagation is observed (Bhat et al., 2001; Boyle et al., 2001; Pillai et al., 2009; Sherman et al., 2005). Moreover, if the paranodal formation is disrupted, this subsequently influences the voltage gated sodium channels clustering at the nodes of Ranvier (Rios et al., 2003). It is proposed that Caspr is recruited at the paranodal region before myelination at the time of the first axon-glial interaction and Caspr and NF155 extracellular interaction is also necessary for Caspr recruitment at the paranodes (Eisenbach et al., 2009; Pedraza et al., 2009). Finally, the paranodal

complex interacts with the cytoskeletal adaptor protein 4.1B, which can be found in paranodes and juxtaparanodes, via the intracellular domain of Caspr. The 4.1B protein is in turn linked to the actin cytoskeleton (Denisenko-Nehrbass et al., 2003).

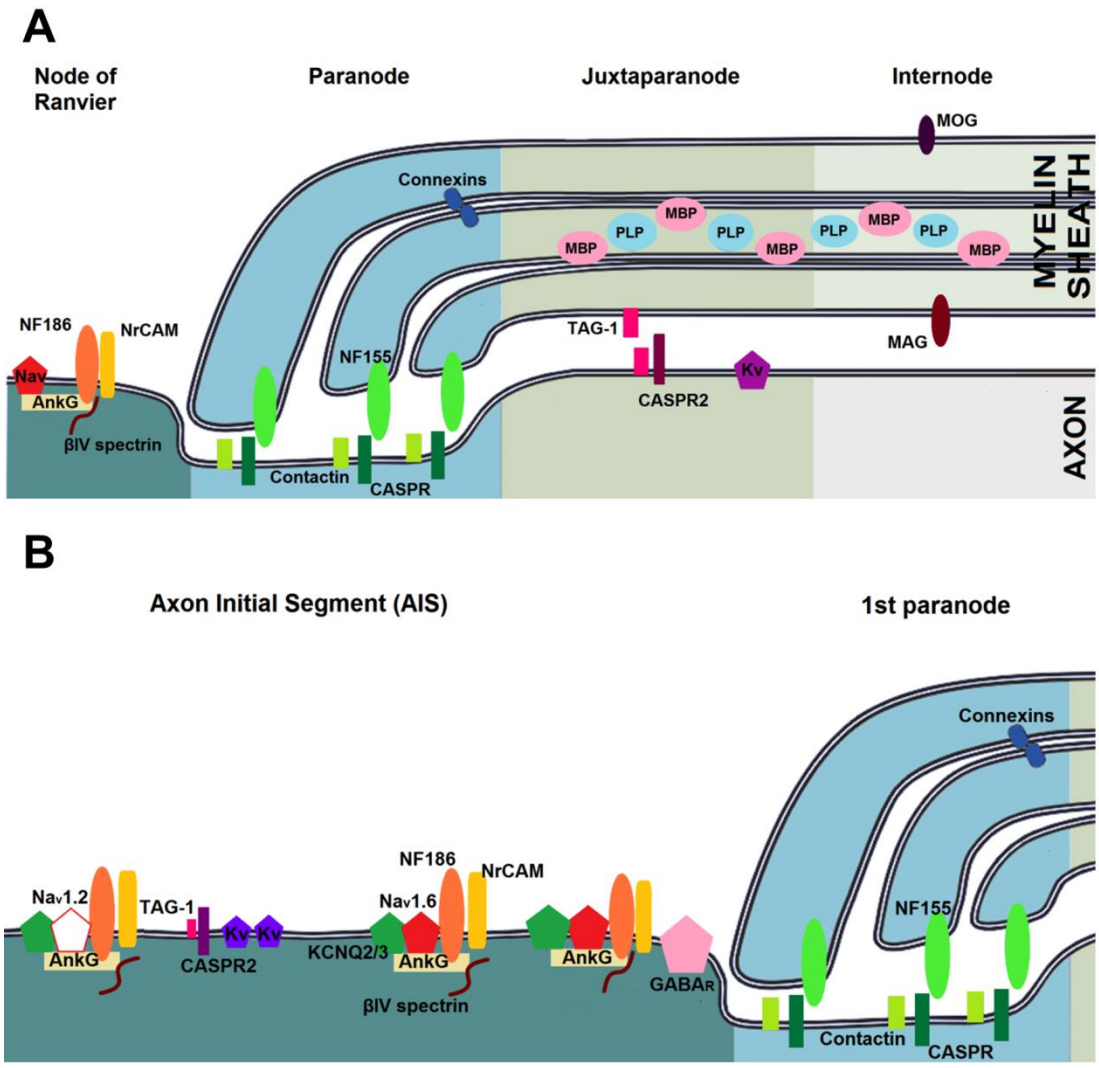

Figure 1.4. ***Protein architecture of molecular domains of the myelinated axon*****.** [A] The nodes of Ranvier are populated with voltage gated sodium channels (Na_v), they are stabilised at the axonal membrane via interaction with NF186, NrCAM and AnkG. AnkG is a scaffold protein which binds on βIV spectrin to stabilize the nodal complex on the actin cytoskeleton. The paranodes are the principal site of axon-glial contact. Contactin, NF155 and Caspr interact to form septate-like junctions between the axonal membrane and the paranodal loops. The juxtaparanodes are rich in potassium channels (K_v). [B] The AIS is a region of unmyelinated axon located close to the soma before the first myelin segment with the nodes of Ranvier. It is rich in Na_v channels ($Na_v1.6$, 1.2 and 1.1) and in potassium channels. The AIS is also a post-synaptic site for axo-axonic synapses and the γ-aminobutyric acid (GABA) receptor is expressed at the AIS plasma membrane. Image adapted from Mayer and Meinl (2012).

1.1.2.5 Juxtaparanodes

The juxtaparanodes are found adjacent to the paranodes and are characterised by accumulation of Shaker-type potassium channels (K_v) on the axonal membrane (Figure 1.4A). Their formation is controlled by a diffusion barrier formed by the septate-like junctions of the paranodes and the assembly of the juxtapanodal complex from axonal and glial interacting proteins that anchors on the cytoskeleton (Susuki and Rasband, 2008a). The juxtaparanodal complex is a heterotrimeric complex formed by TAG-1 (contactin-2) which is a cell adhesion molecule expressed on glial and axonal membranes, Caspr2 which is a second member of the Caspr family and the K_v channels (Poliak et al., 1999; Traka et al., 2003). Similar to the paranodal complex, Caspr2 of the juxtaparanodal complex interacts with 4.1B that anchors the whole complex on the actin cytoskeleton. TAG-1 is essential for juxtaparanodal organisation and K_v clustering (Savvaki et al., 2008).

1.1.2.6 Internodes

The internodes are the part of the myelinated axon found between neighbouring nodes of Ranvier and are characterized by compact myelin (Figure 1.4A). Typical myelin proteins such as MAG and MOG are expressed on the glial membranes of the internodes. MAG is expressed on the glial membrane most proximal to the axon while MOG is located on the outmost glial membrane. MBP and PLP are also expressed at the internodes. Moreover, the length of internodes is important for the

velocity and the configuration of action potential during saltatory conduction (Brill et al., 1977).

1.1.2.7 Axon Initial Segment

The axon initial segment (AIS) is a region of unmyelinated axon located close to the neuronal soma before the first myelin segment (Figure 1.4B). It has a role in action potential generation, configuration and propagation (Buffington and Rasband, 2011). The AIS shares some remarkable similarities in protein architecture with the nodes of Ranvier. It is highly rich in voltage-gated sodium channels (Na_v), $Na_v1.6$ is the abudant type (Caldwell et al., 2000) but $Na_v1.2$ and $Na_v1.1$ can also be found on the axonal membrane of the AIS (Buffington and Rasband, 2011). Similar to the nodes of Ranvier, during development $Na_v1.2$ is replaced by $Na_v1.6$. However, in the AIS, $Na_v1.2$ instead of being completed ablated it is restricted to proximal part of the AIS (Boiko et al., 2003; Hu et al., 2009). These channels provide the influx of Na+ necessary for action potential initiation (Peles and Salzer, 2000). Na_v channels together with axon specific proteins NF186 and NrCAM interact with AnkG, the cytoskeletal scaffolding protein. AnkG interacts with spectin βIV to provide stabilisation to the actin cytoskeleton of the axon (Berghs et al., 2000; Buffington and Rasband, 2011). In the AIS, axon-glial interaction is not necessary for Na_v channel recruitment at the axonal membrane (Bennett and Baines, 2001) which is in contrast to the glial-dependent mechanism at nodes. AnkG appears to be essential for Na_v channel targeting at the AIS and when it is ablated the formation of the AIS protein complexes fails (Hedstrom et al., 2008). Moreover, NF186 has been shown to

be responsible for AIS maturation leading to the switch from $Na_v1.2$ to $Na_v1.6$ expression (Buttermore et al., 2012).

The plasma membrane of the AIS is enriched with potassium channels (Pan et al., 2006). The K_v1 subtype interacts with Caspr2 at the AIS but the exact mechanism for AIS targeting is not known (Horresh et al., 2008; Ogawa et al., 2008; Ogawa et al., 2010). In contrast, the K_v7 subtype, KCNQ2 and KCNQ3 interact with AnkG which targets and stabilises the channels at the AIS plasma membrane (Pan et al., 2006).

The AIS also acts as a post-synaptic site for what is known as "axo-axonic" synapses (Huang et al., 2007). These synapses are implicated in synaptic integration and action potential generation. The GABA receptor is expressed on the AIS postsynaptic membrane and there is evidence that NF186 modulates the assembly of GABAergic synapses (Ango et al., 2004; Burkarth et al., 2007). Moreover, a few studies have shown that the AIS structure shows remarkable levels of activity-dependent plasticity and has the ability to change its size or location on the axon in response to altered electrical activity or synaptic input (Kuba et al., 2010; Grubb and Burrone, 2010a).

1.1.1.2 Microglia

Microglia are the main immune cells of CNS. Microglial cells are differentiated macrophages residing in the brain with an important role in brain injury and inflammation. Under normal conditions, in the healthy brain, they can be found in their "resting" ramified state, which is characterized by small soma and fine short processes and they are constantly surveying their environment. Any type of insult,

infection or disease which disrupts or alters brain homeostasis and potentially could be a danger to the brain results in what is known as “microglial activation” (Kettenmann, 2006). When activated, microglial cells lose their morphological complexity acquiring an amoeboid appearance. `Activated microglia are recruited at the site of the insult and are implicated with increased proliferation and migration of more activated microglial cells to the site of injury, phagocytosis of tissue debris, damaged cells or pathogens, release of chemotactic molecules which recruit immune cells to the CNS, antigen presentation and regulation of the extent of the immune response. In the aged brain as well as in many neurodegenerative diseases such as multiple sclerosis, Alzheimer’s disease (AD) and Parkinson’s disease, increased microglial activation is a common feature (von Bernhardi et al., 2010; Tambuyzer et al., 2009). In AD, in particular, microglial activation is well described and has been associated with the deposits of pathological proteins (amyloid-β, Aβ) to the brain parenchyma (Wisniewski et al., 1989).

1.2 The ageing brain

Age has been highlighted as the most important risk factor for white matter attenuation and cognitive decline in healthy individuals. Studies in healthy individuals have suggested that, with ageing, there is a decline of cognitive processes such as the recall of verbal information, working memory, short-term recall and the speed of processing information (Craik et al., 1994; McDonald-Miszczak et al., 1995; Petersen et al., 1992; Zelinski and Burnight, 1997). White matter mediates the communication of distinct brain regions and its properties that have been described earlier confer the speed of processing and conduction of information that is essential for higher cognitive functions (Bartzokis et al., 2004). Thus deterioration of myelin integrity disrupts signal conduction and communication between the different brain regions and subsequently may alter cognitive functions.

Numerous studies using both histopathological and neuroimaging techniques have provided evidence about the nature of changes in white matter integrity that may contribute to the decline of the cognitive performance. For example, histopathological studies in humans have shown that the length of myelinated axons is decreased by approximately 45% between 20 and 80 years of age, reducing by 10% every decade (Marner et al., 2003). Tang et al. (1997) also observed a significant reduction in myelinated fiber length and reported a loss in small caliber fiber with age. Other age-related changes in white matter include the decrease in the total number of the myelinated fibers (Meier-Ruge et al., 1992; Marner et al., 2003) and loss of myelin staining (Kemper, 1994; Lintl and Braak, 1983). There is also evidence that late-life myelinated fibers are more sensitive and the first lost in the

ageing brain (Bartzokis et al., 2003) In support of this data, detailed electron microscopy studies in aged non-human primates have shown the formation of splits and cavities ("balloons") within the lamellae of the myelin sheath (Peters and Sethares, 2002; Peters et al., 2000; Feldman and Peters, 1998). In addition, evidence from non-human primates studies show a direct association between the percentage of fibers with age-related alterations and the level of cognitive impairment (Peters et al., 2001).

There are a few studies in monkeys and rodents showing age-related changes in the excitable domains of the myelinated axons. For example, Hinman et al. (2006) showed an increased number of axons with the $K_v1.2$ channel abnormally localized within the paranodal region in aged monkeys and rats. Moreover, examination of the paranodal region with electron microscopy in aged mice showed paranodal disruption as indicated by the pilling of the paranodal loops and loss of transverse bands (Shepherd et al., 2012).

Neuroimaging studies have also provided strong evidence connecting white matter alterations and normal ageing. A dominant feature of ageing is the reduction of total brain volume which accelerates after 50 years of age (Raz and Rodrigue, 2006). A number of studies have shown that white matter loss is more prominent than grey matter loss in aged individuals (Allen et al., 2005; Bartzokis et al., 2003; Jernigan et al., 2001). In addition, the presence of white matter lesions which appear as areas of increased signal (hyperintensities, Figure 1.5) on T2-weighted images of magnetic resonance imaging (MRI) scans is a well-established observation in the aged white matter. These hyperintensities are present in more than half of the individuals over

65 years of age (Enzinger et al., 2006) and their number correlates with the level of cognitive decline (Bunce et al., 2007; DeCarli et al., 1995; Hedden et al., 2012). Diffusion tensor imaging (DTI) has also been used to examine microstructural myelin integrity by measuring fraction anisotropy (FA) which is a measure of the anisotropy of diffusion of water in the brain based on its tendency to diffuse along the length of the myelinated fibers. FA studies have shown alterations in white matter integrity with increasing age in regions of the prefrontal cortex, the striatum and the corpus callosum (Gunning-Dixon et al., 2009; Janowsky et al., 1996; Salat et al., 2005; Sullivan et al., 2001). Moreover, there is evidence that deterioration of white matter integrity examined with DTI is associated with poor cognitive performance (Bucur et al., 2008; Deary et al., 2006; Kennedy and Raz, 2009; Jacobs et al., 2013; Kerchner et al., 2012; Papp et al., 2013).

In addition to white matter alterations, the ageing brain is also characterised by a decrease in synaptic density which has also been suggested to be a contributing factor to age-related cognitive decline (Dickson et al., 1995; Scheff et al., 2006; VanGuilder et al., 2011). Synapses form between presynaptic boutons of the axons and the post-synaptic dendritic spines. A decrease in synaptic density has been observed in the brain of aged humans, primates and rodents (Geinisman et al., 1986; Bourgeois and Rakic, 1996; Liu et al., 1996). In addition there is evidence from studies in aged rats that the excitatory synaptic transmission changes with ageing (Burke and Barnes, 2010). Such alterations in synaptic transmission combined with alterations in myelin integrity that is essential for effective signal conduction could potentially result in perturbations synaptic plasticity and subsequently long term

potentiation (LTP) which is indicative of how the memory mechanisms function (Kumar and Foster, 2007).

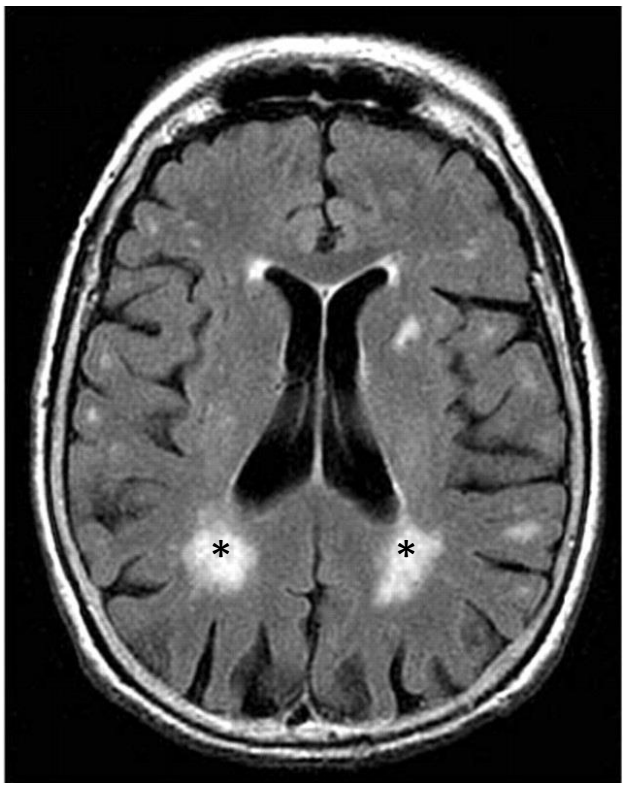

Figure 1.5 ***White matter hyperintensities***. Image of a MRI scan from an 80 year old individual, white matter lesions are showing as hypersintensities (asterisks). Image reproduced from Debette and Markus (2010).

1.3 Chronic cerebral hypoperfusion

1.3.1 Cerebral blood flow and metabolism

Cerebral blood flow (CBF) supplies the brain with glucose and oxygen necessary for its function. In humans, almost 80% of cerebral perfusion is supplied by the carotid while the two vertebra arteries, which join together to create the basilar artery, contribute to the remaining 20%. The brain, which is only 2% of the total body weight, receives 15% of the cardiac blood flow output and uses for its normal function 20% and 25% of the total body oxygen and glucose respectively (Zauner and Muizelaar, 1997). The neurons use almost 75% of the oxygen supply and almost 80% of the energy produced is used for the maintenance of the ionic gradients necessary for action potential generation and propagation (Zauner and Muizelaar, 1997). Thus, reduction or ablation of CBF may have severe effects on normal brain function.

1.3.2 Chronic cerebral hypoperfusion in normal ageing

Chronic cerebral hypoperfusion, or reductions in CBF, occurs in the normal ageing brain CBF is reduced gradually and continuously over time and during the eighth decade CBF is 20-25% lower than that of the third decade (Buijs et al., 1998; Stoquart-ElSankari et al., 2007). Total blood volume that flows into the brain, as well as oxygen consumption reduce by approximately 0.5% every year from the third to the eighth decade (Leenders et al., 1990). Morphological alterations in vasculature and particularly in the microvasculature have been reported including thickening of

the vascular wall, arteriosclerosis, and increase in arteriolar tortuosity, capillary loss and lipohyalinosis, (Brown and Thore, 2011; Farkas and Luiten, 2001; Kalaria, 1996). These types of cerebrovascular pathologies have been linked with CBF reduction, impairment of white matter integrity and cognitive decline both in humans and in animal models (Appelman et al., 2010; Breteler et al., 1994; Farkas et al., 2007; Pantoni and Garcia, 1997; Sekhon et al., 1994; Shibata et al., 2004).

The exact mechanism that links the chronic cerebral hypoperfusion and white matter alterations is unclear. In the elderly, as indicated earlier, CBF is approximately 20-25% lower to that of young individuals (Buijs et al., 1998; Stoquart-ElSankari et al., 2007). Moreover, the brain regions with lower CBF such as the white matter appear to be more vulnerable to CBF fluctuations (Pantoni and Garcia, 1997). A likely explanation could be that, as described in chapter 1.1.1.4, white matter is at the end of blood supply with each penetrating arteriole providing blood to distinct white matter regions. Thus any reduction in CBF cannot be compensated by surrounding vessels because it is at a vascular end-zone (Borch et al., 2010; Rowbotham and Little, 1965).

In addition, cerebral hypoperfusion in the human ageing brain may be caused by a large variety of vascular risk factors such as hypotension, hypertension, diabetes mellitus, atherosclerosis and cardiovascular disease (de la Torre, 2010). This makes it difficult to determine the exact cause of cerebral hypoperfusion and white matter pathology. Therefore, the development of animal models simulating cerebral chronic hypoperfusion alone is highly important because it could possibly unravel the

mechanisms by which hypoperfusion affects white matter integrity and cognitive performance.

1.3.3 Models of chronic cerebral hypoperfusion

Investigation, in isolation, of the effects of hypoperfusion on white matter integrity and cognition is possible with the development of animal models. The model that is used most often is the permanent bilateral common carotid artery occlusion (BCCAO) or 2 vessel occlusion (2VO) in the rat. In this model, hypoperfusion is induced with a surgical procedure by ligating the two common carotid arteries. Shortly after surgery, a significant reduction in CBF is observed which appears to be more severe in the cortex and in white matter areas (~35-45% of the baseline) than in the hippocampus (~65% of the baseline) (Choy et al., 2006; Ohta et al., 1997; Otori et al., 2003; Tomimoto et al., 2003; Tsuchiya et al., 1992). After one week there are signs of recovery but the CBF remains significantly lower than the baseline up to 4 weeks after surgery (Otori et al., 2003; Tomimoto et al., 2003; Tsuchiya et al., 1992). Only after 8 weeks or longer is there complete recovery of CBF in some areas and signs of vascular remodeling (Choy et al., 2006; Otori et al., 2003).

Induction of hypoperfusion with 2VO results in neuropathological changes such as neuronal cell death, synaptic loss, microglial activation and white matter alterations. Increased neuronal cell loss is observed in the hippocampus, particularly in the CA1 region after one week (Farkas et al., 2006; Schmidt-Kastner et al., 2001), and is further increased over time (Farkas et al., 2004; Liu et al., 2006). Synaptic loss has

also been reported and associated with cognitive decline (Liu et al., 2005). In addition white matter integrity is disrupted after the onset of hypoperfusion. The optic tract is particularly sensitive in this model due to its direct supply with blood from the internal carotid artery (Ohta et al., 1997; Takizawa et al., 2003; Wakita et al., 2002) but the corpus callosum is also affected. A variety of white matter pathologies are observed including white matter rarefaction and vacuolation (Ohta et al., 1997; Wakita et al., 2002), disruption of the myelin sheaths (Farkas et al., 2004) and oligodendroglial and astrocytic cell death (Lee et al., 2006; Tomimoto et al., 2003). Cognitive testing of the rats showed deficits in spatial and non-spatial memory and in anxiety-related tasks after the onset of 2VO (Farkas et al., 2007). However, in this model it could not be established whether neuronal cell loss or white matter alterations are driving the observed poor cognitive performance in the behavioural tests. At the same time in this model the visual system is severely compromised that could affect performance in cognitive tests using visual cues (Farkas et al., 2007).

A second model that has been used to investigate the effects of hypoperfusion is a model of bilateral common carotid artery stenosis to the Mongolian gerbil. In this model, stenosis of arteries is achieved with the surgical application of wire coils (microcoils) of known diameter around the common carotid arteries inducing modest reduction to the blood flow. Stenosis with a 0.2-0.3 mm diameter microil showed grey matter damage as early as one week after the induction of hypoperfusion whilst white matter lesions (Hattori et al., 1992) develop after 8 weeks. In addition, after 2 months of hypoperfusion axonal changes are observed (Kurumatani et al., 1998)

whilst impairment in cognitive performance is reported 3 months after the induction of hypoperfusion (Kudo et al., 1993).

In 2004, Shibata et al adapted the bilateral common carotid artery stenosis model to the mouse. Application of microcoils with different diameter induces different levels of blood flow reduction after surgery. The 0.16 mm diameter microcoil reduces CBF to ~50% of the baseline 2 hours after surgery which gradually recovers to ~80% of the baseline after 1month. Using the 0.18mm diameter microcoil decreases CBF to ~70% of the baseline 2 hours after hypoperfusion induction which also recovers to nearly 85% after one month.

The use of the 0.18 mm microcoil in the common carotid artery model results in the development of diffuse white matter pathology (Holland et al., 2011; Shibata et al., 2004). The initial study on this model by Shibata et al. (2004), using the 0.18 mm microcoil, reports that some white matter lesions first appear after 14 days in the corpus callosum, the caudate and the internal capsule; however, after 30 days from the onset of hypoperfusion there is severe white matter pathology in the same regions. Moreover, some damage in the optic tract is also observed but there is no evidence of any ischemic damage (Shibata et al 2004). In a later study, Shibata et al. (2007) show that 8 weeks after the induction of hypoperfusion, the hypoperfused animals performed poorly compared to controls in the 8-arm radial arm maze paradigm, which tests spatial working memory. In our lab, the 0.18 mm microcoil has also been used to investigate the integrity of white matter components (Coltman et al., 2011; Reimer et al., 2011) and cognitive performance in response to cerebral hypoperfusion (Coltman et al., 2011). For example, Coltman et al. (2011) investigate

white matter integrity in parallel with cognitive performance and it is demonstrated that in the absence of any grey matter pathology spatial working memory deficits are linked with disruption in myelinated fibers detected with antibodies against MAG and degraded MBP. However, in other tests of spatial memory such as the spatial reference memory in Morris water maze, no defect in the hypoperfused animals is observed one month after hypoperfusion (Coltman et al., 2011). In addition, in some hypoperfused animals some ischemic neurons are observed (Coltman et al., 2011). Moreover, detailed investigation of the myelinated axons showed that the nodes of Ranvier and the paranodes are vulnerable to the effects of hypoperfusion (Reimer et al., 2011). For example, as early as three days from the induction of hypoperfusion the length of $Na_v1.6$ positive nodes of Ranvier was increased, an effect that persisted at one month. Moreover, investigation of paranodal integrity showed a loss of the paranodal NF155 from the paranodal region as early as 3 days after hypoperfusion whilst examination of the paranodal region with electron microscopy showed loss of the paranodal septate-like junctions after one month from the induction of hypoperfusion (Reimer et al., 2011).

The common carotid artery stenosis mouse model is a very good tool for investigating the effects of hypoperfusion on white matter. It is well described that bilateral carotid stenosis (using microcoils of 0.18 mm diameter) induces diffuse white matter alterations which in turn are associated with specific cognitive impairment. Moreover, it can be useful for studying mechanisms implicated in AD since cerebral hypoperfusion is known to be an early feature of AD occurring prior to the onset of clinical symptoms (described in detail in chapter 1.4.4). This model will

be used in the thesis to study the effects of hypoperfusion on myelinated axon integrity and cognition in a mouse model of AD (Chapter 4).

1.4 Alzheimer's disease

Alzheimer's disease (AD) is a highly heterogeneous and multifactorial neurodegenerative disorder characterized by progressive cognitive decline accounting for 50-75% of dementia cases worldwide. It is estimated that there are 36 million patients worldwide. Over the next decades this figure is estimated to rise to 66 million by year 2030 and 115 million by 2050 (World Alzheimer Reports 2010, http://www.alz.co.uk). In the United Kingdom the number of AD patients is estimated at 800,000 and expected to rise to 1 million by 2021 (http://www.alzheimers.org.uk). AD comes third, after cardiovascular disease and depression, in the healthcare costs worldwide. In 2012, dementia related costs accumulated to £23 billion in the UK.

1.4.1 Pathology of Alzheimer's disease

AD was named after the German psychiatrist and neuropathologist Alois Alzheimer who was the first to describe the clinical and pathological symptoms of the disease in 1907 (Alzheimer, 1907). AD is characterized by the progressive deterioration of cognitive functions, the accumulation of β-amyloid (Aβ) in extracellular insoluble neuritic plaques and blood vessels, and the formation of intraneuronal neurofibrillary tangles (NFT) containing hyperphosphorylated tau protein. There is evidence that Aβ deposits (plaques) and NTF are present in the brain even at the early pre-clinical stages of the disease (Braak and Braak, 1997). The brain areas mostly affected are the cortex, hippocampus, entorhinal cortex and amygdala (Wenk, 2003) known to have an important role in higher cognitive functions such as learning and memory.

Severe brain atrophy and neuronal loss are also observed (Castellani et al., 2010). Definite diagnosis for AD can only be done *post-mortem* with the detection of Aβ plaques and NFT in the brain of the patients. However, the recently developed methods for *in vivo* imaging of Aβ are promising for the development of a tool to aid AD diagnosis (McKhann et al., 2011; Morris et al., 2009; Roe et al., 2013).

The reason for the development of AD remains unknown. However, there is a very small proportion (~1%) of familial AD cases (Hardy, 2009), early-onset, that can be attributed to the presence of dominant hereditary genetic mutations. These mutations are located at genes responsible for amyloid precursor protein (APP) or presenilins 1 (PS1) and presenilin 2 (PS2) which are components of the γ-secretase enzymatic complex (Seiffert et al., 2000). So far more than 20 mutations in the APP gene and approximately 200 mutations in the presenilin genes have been identified (Kitazawa et al., 2012). These genes encode for proteins responsible for Aβ generation and affect Aβ production by increasing the levels of total Aβ or of specific Aβ species (Aβ40 and Aβ42) altering the ratio of Aβ42 to Aβ40 (Chartier-Harlin et al., 1991; Chui et al., 1999; Mullan et al., 1992). For the rest of late-onset or sporadic AD cases, there are numerous epidemiological studies highlighting a variety of risk factors. Age has been one of the most prominent factors as the prevalence of AD is doubled every 5 years after the age of 60 (Jorm et al., 1987).

Amyloid-β deposition is a pathophysiological hallmark of AD. Aβ is a 4 kDa peptide (Glenner et al., 1984), 39-43 amino acids in length, which derives from the abnormal processing of APP. APP is a transmembrane protein expressed in abundance in the human brain. Its normal function has not yet been fully defined, however it has been reported that APP is implicated in synaptic transmission, axonal transport, cell

adhesion, cholesterol metabolism (Turner et al., 2003; Zheng and Koo, 2006). APP is proteolyticaly processed by at least 3 different proteases namely α-, β- and γ-secretases via two different pathways; the non-amyloidogenic and the amyloidogenic which leads to the generation of Aβ protein (Nunan and Small, 2000) (Figure 1.6A). In the non-amyloidogenic pathway, APP is initially cleaved by α-secretase inside β-amyloid domain producing a large soluble N-terminal fragment (sAPP-α), believed to be neuroprotective (Furukawa et al., 1996), and C-terminal fragment (C83). The C83 fragment is subsequently cleaved by the γ-secretase enzymatic complex producing a 3 KDa fragment known as p3 (Cole and Vassar, 2007). During the amyloidogenic pathway APP is processed by β-secretase (β-amyloid cleaving enzyme, BACE) for the generation of a secreted sAPP-β fragment and a C-terminal (C99) fragment which remains anchored on the plasma membrane. The C99 fragment is subsequently cleaved by the γ-secretase enzymatic complex producing the Aβ peptides (Nunan and Small, 2000). The main products from amyloidogenic processing of APP are the 40 amino acids long Aβ40 and the 42 amino acids long Aβ42. In the early-onset AD the genetic mutations in APP, PS1 or PS2 genes dramatically increase Aβ42 production which highlights the key role of Aβ in the pathogenesis of AD. Aβ peptides are prone to polymerarization and form fibrils (Figure 1.6B) that aggregate in the vessels (cerebral amyloid angiopathy, CAA) or extracellularly in the brain forming Aβ plaques. Aβ42 is more hydrophobic and likely to form insoluble fibrils and is found in the extracellular plaques whilst Aβ40 is primarily found in vasculature and associated with CAA (Jarrett et al., 1993).

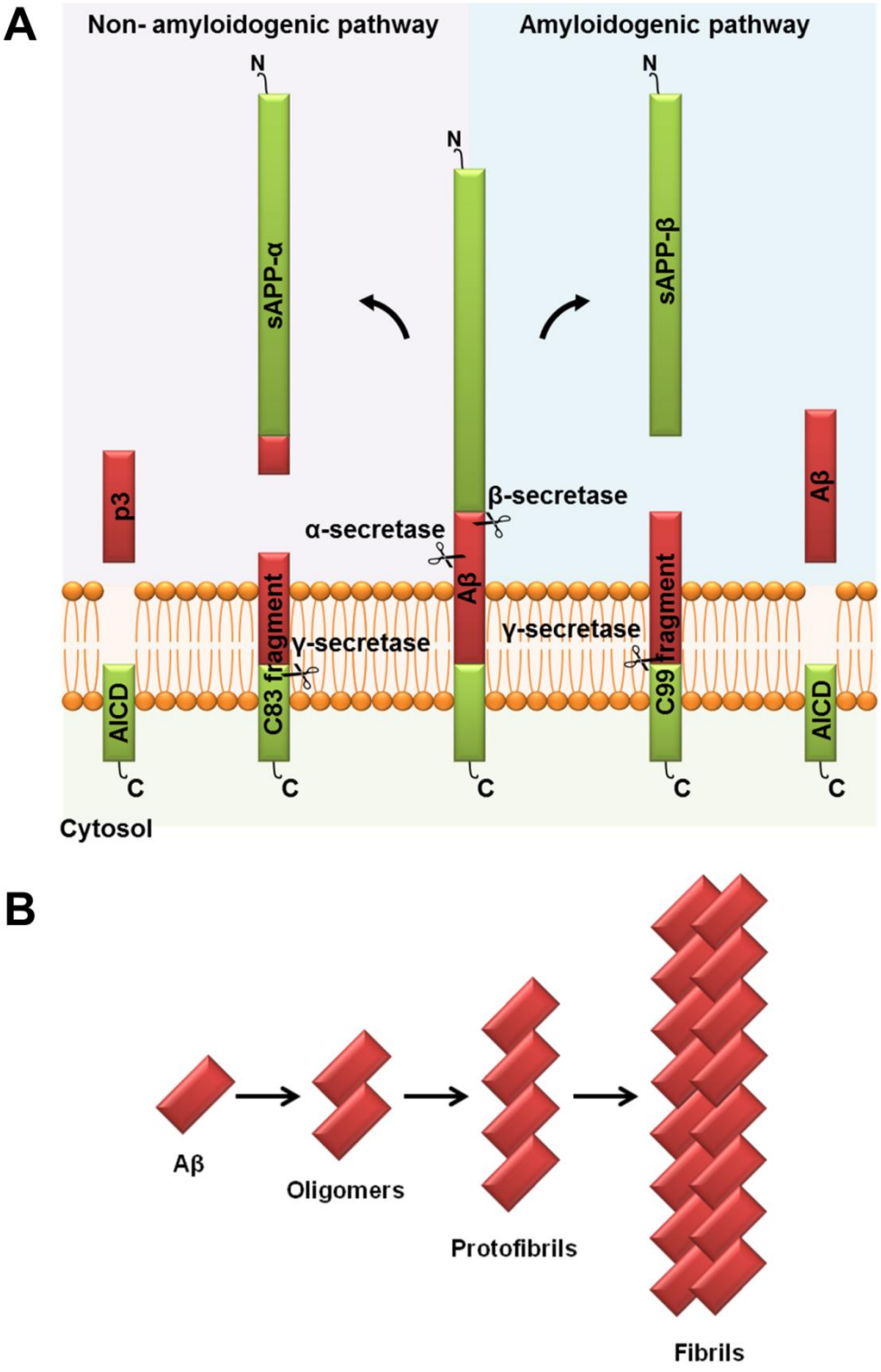

Figure 1.6 ***Processing of APP and Aβ polymerization***. [A] APP is proteolytically processed by α-, β- and γ-secretases via two different pathways; the non-amyloidogenic and the amyloidogenic with leads to the generation of Aβ protein. [B] Aβ is prone to polymerization; it forms oligomers, then protofibrils and then fibrils that aggregate to form Aβ deposits.

The discovery the Aβ peptide which is the primary component of the amyloid plaques, a pathological feature of AD, together with the identification of the mutations in the APP gene responsible for early-onset AD lead to the hypothesis that Aβ deposition, which is an early event in AD, is the cause of AD pathology and all the other pathologies (NFT, neuronal loss and dementia) observed are driven by Aβ production and imbalanced clearance (Hardy and Selkoe, 2002; Hardy and Higgins, 1992). This is now known as the amyloid cascade hypothesis.

In support of the amyloid cascade hypothesis there is evidence for the neurotoxic properties of Aβ. The soluble oligomeric forms of Aβ have been shown to be highly neurotoxic compared to the insoluble Aβ species (Lesne et al., 2006; Shankar et al., 2008) and proposed to damage synapses (Lambert et al., 1998). Moreover, the oligomeric Aβ levels and not the total burden of amyloid plaques correlate with cognitive deficits (LaFerla et al., 2007; Giannakopoulos et al., 2003) while the Aβ42 type is suspected to be more toxic than the Aβ40 (Findeis, 2007). However, in contrast to what was predicted by the amyloid hypothesis, in clinical trials of immunization against Aβ, despite removing the Aβ plaques no concomitant improvement in AD symptoms was observed (Holmes et al., 2008). Additionally, there is evidence of amyloid plaque deposition in the brains of healthy non-demented individuals (Becker et al., 2011). The amyloid cascade hypothesis however does not give a satisfactory explanation for the early-events in AD progression occurring prior to Aβ deposition which may trigger Aβ pathology. Therefore, in an effort to formulate a hypothesis that better accounts for the data in AD research, Hardy (2009) updated the amyloid hypothesis by introducing the concept of vascular damage as a

contributing factor in AD neurodegeneration which may both induce Aβ damage or be the result of Aβ deposition.

1.4.2 Risk factors for the development of Alzheimer's disease

Over the last decades several risk factors have been highlighted to play a role in the development of sporadic AD. Age is shown to be the single most important risk factor for the development of AD (Bartzokis, 2004). It appears that the incidence rate of AD is lower than 1% at the age of 65 years whereas it rises to over 25% at the age of 85 years (Breteler, 2000). Other factors associated with the development of AD include traumatic brain injury (Heyman et al., 1984), and vascular risk factors such as diabetes mellitus, cerebral ischemia, atherosclerosis, arteriosclerosis, hypertension, hypercholesterolemia, cardiovascular disease and cerebrovascular disease (de la Torre, 2010).

In addition, the APOEε4 allele was the first genetic variation found to influence the risk for AD development; with abundance rate in the general population around 14% APOEε4 increases the risk for AD 3-4 times in the heterozygous carriers (APOEε2/ε4 or APOEε3/ε4) and more than 10 times in the homozygous (Farrer et al., 1997). Over the last years more genes associated with sporadic AD have been highlighted including genes encoding for sortilin-related receptor 1 (SORL1) (Rogaeva et al., 2007), clusterin (CLU) (Harold et al., 2009; Lambert et al., 2009), phosphatidylinositol-binding clathrin assembly protein gene (PICALM) (Harold et al., 2009; Lambert et al., 2009), triggering receptor expressed on myeloid cells 2

protein (TREM2) (Guerreiro et al., 2013), bridging Integrator 1 BIN1 (Seshadri et al., 2010), protein phosphatase 1, regulatory subunit 3B PPP1R3B (Kamboh et al., 2012), complement receptor 1 (CR1) ATP-binding cassette sub-family A, member 7 (ABCA7), membrane-spanning 4 subfamily A (MS4A4E/MS4A6E), ephrin receptor A1 (EPHA1), CD33 and CD2-associated protein (CD2AP) (Hollingworth et al., 2012). Thus a number of genes have now been identified that can modify risk of development of AD.

The numerous risk factors for AD indicate that it is a highly complicated disease affecting an increasing number of individuals. Therefore, the development over almost the last 20 years of multiple mouse models featuring aspects of AD-related pathologies has been helpful in the investigation of how these may affect brain function and has increased the understanding of the mechanisms underlying the disease.

1.4.3 Models of Alzheimer's disease

The identification of specific genetic mutations responsible for early-onset familial AD was crucial for the generation of transgenic AD mouse models. Mice do not naturally develop age-related Aβ aggregation and deposition possibly because the mouse APP protein differs from human APP by three amino acids (De Strooper et al., 1995). Therefore, the most popular strategy for transgenic AD mouse models generation is the overexpression of one or more familial AD associated mutated genes.

So far more than 50 different transgenic models have been described, overexpressing human wild-type or mutant APP (www.alzforum.org/res/com/tra/app/default.asp). Introducing one or more human APP mutations into the mouse genome usually results in the recapitulation of some features of AD pathology such as age dependent Aβ deposition and cognitive decline. Other pathophysiological features of AD observed in the mouse models include astrocytic reactivity, microglial activation, dystrophic neurons, synaptic loss and disrupted electrophysiology, however just the expression of mutated APP alone does not appear to induce the NFT pathology or severe neuronal loss observed in AD (Borchelt et al., 1996; Games et al., 1995; Hsiao et al., 1996; Mucke et al., 2000; Sturchler-Pierrat et al., 1997; Kitazawa et al., 2012).

The extent and the age of onset of Aβ pathology is related to the type of mutations expressed and the type of promoters used to drive transgene expression. The first model that was developed was the PDAPP, which expresses the human Indiana nutation (APPInd, V717F) driven by the platelet derived growth factor (PDGF) promoter. Aβ pathology is first observed at 6-9 months of age and is further progressed with advancing age (Games et al., 1995). Astrocytic reactivity is also observed adjacent to the Aβ deposits together with synaptic loss (Games et al., 1995). Some studies report a 12-30% decrease in the volume of the hippocampus and the dentate gyrus (Redwine et al., 2003; Wu et al., 2004a). Cognitive performance is affected in PDAPP mice as young as 3 months old; they have impaired recognition and episodic memory that further deteriorates with age (Chen et al., 2000; Dodart et al., 1999). Moreover, incorporation of the same APP mutant transgene in another model (H6) was accompanied with hippocampal synaptic loss and neurodegeneration

which was not associated with Aβ deposition in the brain suggesting that soluble Aβ may lead to neurodegeneration (Hsia et al., 1999).

An APP mutation that has been broadly used in AD mouse models is the Swedish double mutation (K670N/M671L, APPSwe). A popular model is the Tg2576 mouse that expresses the APPSwe mutation under the control of hamster prion promoter that drives expression at the spinal cord and areas of the forebrain (Hsiao et al., 1996). This transgenic mouse model develops dense Aβ plaques at 10-12 months of age. Cognitive deficits however, are reported as early as six months of age prior to any Aβ plaque pathology implicating oligomeric Aβ-mediated toxicity (Alpar et al., 2006). Other AD-related pathological features observed in this model are synaptic loss at the entorhinal cortex as well as dendritic spine loss (Dong et al., 2007). However, no significant loss of neurons was reported in the Aβ affected areas in the Tg2576 model (Irizarry et al., 1997). A second model that expresses the APPSwe mutation but under the control of a different promoter (Thy-1.2) is the APP23. In this model, Aβ plaques are reported at the age 6 months and are exacerbated with age. Moreover, there is extensive activation of microglia adjacent to the Aβ plaques and evidence of phosphorylated tau (Sturchler-Pierrat et al., 1997). Hippocampal neuronal loss is also observed at 14-18 months old animals particularly at the CA1 area (Calhoun et al., 1998).

Studies of mouse models that express single APP mutations indicate that the temporal and regional profile of the development of Aβ pathology and the development of cognitive deficits or other AD-related pathologies is dependant on the mutation that is expressed. For that reason, a strategy that is used for the development of AD models is the introduction of more than one APP mutation in a

single APP transgene in an effort to accelerate Aβ pathology. For instance, there are two lines (J20 and J9 line) with the Swedish and the Indiana mutation incorporated on the same APP transgene (APPSw,Ind) under the PDGF promoter. However, the relative levels of the APPSw,Ind transgene expression in the J9 line is almost half of that of the J20 line animals (Mucke et al., 2000). The temporal profile and the severity of Aβ pathology are different as well. For example both lines develop Aβ deposition by 5-7 months of age, in the J20 line, however, there is rapid Aβ pathology up to 8-10 months of age while in the J9 line Aβ deposition is a slower process that continues up to 21-25 months of age (Mucke et al., 2000). In addition, comparison between J9 and J20 animals of the same age shows more severe Aβ pathology in the J20 animals (Mucke et al., 2000). Interestingly, the synaptic loss is observed in both lines by 2-4 months of age before any Aβ deposition, which correlates with Aβ levels but not with the Aβ plaque load (Mucke et al., 2000). Additionally, in both lines impaired synaptic transmission is observed by 2-4 months of age (Harris et al., 2010; Hsia et al., 1999) and long-term potentiation (LTP) deficits are observed in animals from 2-22 months of age (Dziewczapolski et al., 2009; Harris et al., 2010). Behavioural deficits have also been described in these two lines. J9 mice perform poorly in tasks testing spatial learning and memory (Raber et al., 2000; Dziewczapolski et al., 2009) as early as 6 months on age (Raber et al., 2000) whereas the J20 mice are reported to have impaired cognitive performance in spatial and non-spatial learning and memory and anxiety-related tasks by 2-3 months of age (Harris et al., 2010).

Moreover, introduction to the mouse genome of multiple transgenes alters the temporal and regional profile of Aβ pathology. For example expression of both

mutant *presenilin* and mutant APP transgenes accelerates Aβ deposition and cognitive impairment in comparison with lines expressing a single APP mutant transgene (Borchelt et al., 1997). In addition, expression of mutant *presenilin* transgene alone results in high levels of Aβ42 (Duff et al., 1996).

One pathological hallmark of AD that the APP and/or presenilin transgenic mouse models do not develop is the neurofibrillary tangles (NFT). Moreover, there are not any AD-related mutations in tau therefore in order to develop mouse models with tau pathology it was necessary to use transgenes that drive the expression of human mutant tau (P301L) responsible for frontotemporal dementia and Parkinsonism (Hutton et al., 1998). Overexpression of human mutant tau (P301L) in mice results in widespread tau pathology in the brain, neuronal loss, cognitive impairment and motor deficits (Lewis et al., 2000). In an effort to model both Aβ and NFT pathology observed in AD, the 3xTg-AD mouse model that expresses mutant APP (APPSwe), presenilin 1 (M146V) and tau (P301L) was developed (Oddo et al., 2003). In this, Aβ pathology in the form of intracellular deposits is observed at 3 months whilst Aβ plaques are reported at 6 months. NTFs are observed at 12 months of age. Moreover, synaptic transmission and LTP impairment is observed at 6 months (Oddo et al., 2003). Cognition is also impaired in the 3xTg-AD mice and is reported as a deterioration of long-term retention at 4 months (Billings et al., 2005).

The AD transgenic models have uncovered key mechanisms underlying AD neuropathology. There are, however, fundamental differences between human AD and how features of AD are recapitulated in mouse models that highlight the need for careful interpretation of the acquired data. For example, the mutations expressed in the AD models are associated with early onset familial AD that accounts for only a

small proportion of AD patients. Moreover, in contrast with humans, the appearance of Aβ deposition in the majority of AD models normally requires higher levels of APP expression. A possible explanation is that in humans the AD pathology develops over decades and in the mouse models this pathology is concentrated in the shorter life span of the mice. There are however some species such as the rhesus macaque, the cat and the dog that normally develop age related Aβ pathology and cognitive impairment (Gunn-Moore et al., 2007; Head, 2011; Ichinohe et al., 2009). Despite the fact that the pathology in these models has similarities with sporadic AD, the time needed for the appearance of the pathology, the ethical implications and the high cost are restrictive factors for their broader use. Thus mice are the most common model of choice for investigating AD due to ease of manipulation and maintenance, low cost and a short breeding cycle.

1.4.4 Cerebral hypoperfusion and Alzheimer's disease

Regional reductions in cerebral blood flow are a feature of AD which can be observed from early preclinical stages of the disease and persist over disease progression (de la Torre, 2009). Early studies investigating cerebral blood flow in AD patients using inhalation or intravenous injection of a radioactive tracer e.g. ^{133}Xenon and computed tomography (CT), single photon emission computed tomography (SPECT) or 2-deoxy-2-[F-18]fluoro-D-glucose (FDG-PET) imaging highlighted that CBF is significantly decreased in the temporoparietal cortex of AD patients compared to age-matched healthy individuals(Komatani et al., 1988). These findings have been further confirmed by more sophisticated and higher resolution

perfusion weighted magnetic resonance imaging (PW-MRI) techniques such as arterial spin labeling (ASL) MRI. It was shown using ASL-MRI that there is a ~40% overall reduction in CBF in the AD patients compared to age-matched healthy individuals (Asllani et al., 2008), there are, however, some specific regional patterns with regions such as the posterior cingulate and the lateral parietal cortex consistently affected (Austin et al., 2011). Moreover, the level of CBF reduction has been associated with the severity of cognitive impairment (Roher et al., 2012). Studies investigating blood perfusion in healthy ageing, AD, and mild cognitive impairment (MCI) which is considered to be a prodromal state of AD have shown that in both AD and MCI the CBF is significantly reduced compared to the healthy aged individuals but exacerbated in AD compared to MCI cases (Rombouts et al., 2005). In addition, functional MRI (fMRI) studies have been a useful tool investigating functional connectivity namely the interregional synchronization of blood flow fluctuations (increases or decreases) in response to neuronal activity. These studies have shown that functional connectivity is disrupted in AD and progressively deteriorates in parallel with disease pathology (Zhang et al., 2010b). Moreover, during episodic memory and working memory tests, blood flow fluctuations in the MCI and AD patients is reduced in comparison with the healthy individuals. They are, however, more prominent in the AD cases (Rombouts et al., 2005). These findings imply that CBF reduction is an early event in disease progression.

Cerebrovascular pathology, observed in up to 90% of AD patients, has been proposed to underlie CBF reductions. This is suggested to result in energy, oxygen and nutrient deficiency in the brain while promoting disease progression and occurs

even prior to any overt neuronal of cognitive damage (Jellinger, 2002; de la Torre, 2002). Cerebrovascular pathologies linked with AD include CAA, microvascular and blood-brain barrier (BBB) disruption, microinfarctions, cerebral hemorrhages and other vascular lesions (Jellinger, 2010). In addition, studies in animal models have linked cerebrovascular dysfunction with BBB dysfunction which is suggested to impair clearance of Aβ from the brain and promote accumulation in the brain and/or the blood vessels (Deane et al., 2008; Deane et al., 2004; Eisele et al., 2010; Zlokovic et al., 2010; Zlokovic, 2005). Increasing Aβ levels further may impede cerebrovascular integrity (Bell et al., 2009; Deane et al., 2004). CAA is observed in more than 80% of AD patients (Jellinger, 2010; Bell and Zlokovic, 2009) and is linked with microvascular damage (Kalaria, 2002). SPECT imaging has shown that CBF is significantly reduced in AD patients in regions where CAA pathology is observed (Chung et al., 2009). In addition, CAA pathology increases the risk of cerebral haemorrhages while the prevalence of vascular lesions is associated with the CAA (Olichney et al., 1997) and cognitive impairment (Cordonnier, 2011).

The use of animal models has been helpful in further understanding the relationship between the cerebral hypoperfusion and vascular disturbances with AD-related pathology. For example, it was demonstrated that Aβ40 has vasoconstrictive properties and induced endothelial cell damage by excess production of free radicals (Thomas et al., 1996). Moreover, Niwa et al. (2002b) showed that in a transgenic model that develops aspects of AD (Tg2576) CBF and glucose utilization is reduced prior to the development of Aβ deposits. This is further confirmed by several studies in multiple APP mutant mice that have shown regional or full-brain decreases in blood flow (Hebert et al., 2013; Weidensteiner et al., 2009; Badea et al., 2010;

Delatour et al., 2006; Wu et al., 2004b) It has also been demonstrated that vascular dilatory responses (Iadecola et al., 1999; Park et al., 2004) and vascular autoregulation which is the ability to control CBF, is impaired in APP mutant mice (Iadecola et al., 1999; Niwa et al., 2002a; Niwa et al., 2000). Moreover, there is evidence that surgically induced hypoperfusion in APP mutant mice may increase Aβ levels (Kitaguchi et al., 2009; Yamada et al., 2011; Koike et al., 2010).

1.4.5 White matter alterations and Alzheimer's disease

In addition to the alterations in CBF, a large number of studies has highlighted the involvement of white matter pathology in the development of AD (Brun and Englund, 1986b; Englund et al., 1988; Bartzokis et al., 2000; Braak et al., 2000; Bartzokis et al., 2003). Alterations in white matter integrity are observed early in disease development even before any clinical symptoms (Bartzokis et al., 2003; Douaud et al., 2013; Stokin et al., 2005) and studies in both humans and animal models have indicated that they could occur prior to any Aβ or NFT pathology (Desai et al., 2010; Desai et al., 2009; deToledo-Morrell et al., 2007; Redwine et al., 2003; Stokin et al., 2005). *Post-mortem* examination of AD brains has shown that in ~65% of the cases white matter pathology in combination with AD pathology is observed (Roher et al., 2002).

White matter pathology that has been described in *post-mortem* brains of AD patients includes myelin damage, astrogliosis, microglial activation, axonal loss and reduction in the number of oligodendrocytes (Brun and Englund, 1986a; Brun and Englund, 1986b; Brun and Englund, 1981; Englund et al., 1988). In addition,

multiple MRI studies have provided evidence of changes in white matter volume (Balthazar et al., 2009; Li et al., 2008) and white matter hyperintensities (Gouw et al., 2008; Yoshita et al., 2006) in AD and during the progression of the disease. As described in chapter 1.2.1 alterations in white matter integrity can be observed in healthy aged individuals and there is evidence that white matter hyperintensities detected with MRI (T2 weighted) can be detected even 10 years before MCI (Silbert et al., 2012). MCI is considered to be prodromal to AD (Lonie et al., 2010) with 10% of MCI patients progressing to AD every year (Petersen, 2004). DTI studies have shown that in comparison with non-demented age-matched individuals, white matter integrity is compromised in MCI but this occurs to a greater extent in the brain of AD (O'Dwyer et al., 2011; Bosch et al., 2012). This finding suggests that there is a relationship between white matter integrity and cognitive performance (Douaud et al., 2013; Zhang et al., 2013). Regions that are affected in AD are located in both the posterior and anterior cerebral white matter (Chen et al., 2009; Mielke et al., 2009) whilst regions which are myelinated later in life appear to be more susceptible to myelin break-down (Bartzokis et al., 2004).

Although there is compelling evidence supporting white matter alterations in AD, studies in APP mutant mouse models have provided information about the nature of these alterations and which components of white matter are particularly vulnerable. For example, Desai et al. (2009) showed, in the 3xTg-AD mice, myelin disruption and decrease in the expression of myelin marker such as MBP and CNPase in the hippocampus and entorhinal cortex before the onset of Aβ or NFT pathology. In addition, impairment in the expression of $Na_v1.6$ channels, loss of oligodendrocytes and changes in axonal morphology is reported (Desai et al., 2010; Desai et al., 2009).

Similarly, in another AD mouse model (APP/PS1) axonopathy, that develops in an age-related manner (Wirths et al., 2007), and fibre tract atrophy (Chen et al., 2011; Delatour et al., 2006) have been reported. Neuroimaging studies using DTI in mice expressing APP transgene have shown axonal and myelin damage (Song et al, 2004; Sun et al, 2005).

White matter alterations are considered to be linked with cerebrovascular pathology (Pantoni, 2002) which is driven by the deterioration in vascular integrity and disruption of BBB (Young et al., 2008). Therefore it is not surprising that white matter alterations have been linked with hypoperfusion (Fernando et al., 2006; Ruitenberg et al., 2005). For example, Fernando et al. (2006) showed in *post-mortem* tissue that at regions of white matter damage, identified as hyperintensities on MRI, the vascular morphology is altered and markers of ischemia are expressed which suggests that hypoperfusion may underlie the observed white matter alterations. In addition, Farkas and Luiten (2001) showed in patients with MCI that white matter damage and reductions in CBF coexist before the development of AD. Furthermore, evidence from animal models (described in chapter 1.3.3) suggest that cerebral hypoperfusion induces selective white matter damage that may be associated with cognitive impairment (Coltman et al., 2011; Holland et al., 2011; Shibata et al., 2004; Shibata et al., 2007).

Although white matter damage occurs in both normal ageing and AD, the reason for which it is exacerbated in AD is not clear. There is some evidence that the Aβ oligomers are toxic to myelin and the oligodendrocytes (Torp et al., 2000; Xu et al., 2001). In addition, Aβ may promote oligodendroglial cell death by inducing of oxidative stress and mitochondrial dysfunction (Castellani et al., 2002; Juurlink et al.,

1998; Schapira, 1996; Dragicevic et al., 2010). However, Bartzokis (2011) suggested that white matter attenuation is a primary event in AD development and suggests that ageing disrupts the homeostasis of oligodendrocytes resulting in a failure of repair mechanisms, Aβ deposition and subsequent signal transduction failure and cognition impairment. Although the myelin model explains some features of AD, this needs further validation by studies in animal models.

1.5 Hypotheses and aims of the thesis

The general aim of the thesis is to investigate the structure of myelinated axons and in particular their excitable regions (nodes of Ranvier, axon initial segment) and their susceptibility to the effects of normal ageing, cerebral hypoperfusion and increasing levels of Aβ.

It was hypothesized that the AIS and nodes of Ranvier would be altered in ageing and that these effects would be exacerbated in the presence of increased levels of Aβ and that would be associated with impairment in learning and memory. Additionally it was hypothesised that altered synaptic input would play a role in AIS alterations given its activity-dependent plasticity. To address this, the effects of normal ageing on the integrity of the AIS, nodes of Ranvier, myelin, axons and synapses as well as on spatial working memory were examined in young and aged wild-type and TgAPPSw,Ind mice (Chapter 3).

In addition, it was hypothesised that the integrity of the nodes of Ranvier and the paranodes would be altered in response to hypoperfusion and that these effects would be exacerbated in the presence of increased levels of Aβ and associated with working memory deficits in young and aged mice. To address this, the effects of cerebral hypoperfusion on the integrity of the nodes of Ranvier, paranodes, myelin and axons and on spatial working memory performance was investigated in young and aged wild-type and TgAPPSw,Ind mice (Chapter 4).

Chapter 2

Materials and Methods

2.1 Animals

All animals in the studies described in the present thesis were housed at 22°C with 12h light/dark intervals. Food and water were freely available throughout the duration of the experiments except during testing at the radial arm maze where food intake and body weight of the animals was closely monitored. All experiments were carried out under the appropriate personal and project UK Home Office licenses and in accordance with the Animals (Scientific Procedures) Act (1986).

The effects of ageing and hypoperfusion on white matter in relation to Alzheimer's disease were investigated in a transgenic mouse model harbouring the familial Alzheimer's disease linked mutations K670N/M671L and V717F (APPSw,Ind; J9a line) where expression of the transgene is regulated by the platelet-derived growth factor (PDGF) promoter. As described by Hsia et al. (1999) the line was originally derived by microinjection of the PDGF-APPSw,Ind transgene into (C57BL/6 × DBA/2) F2 single-cell embryos. The line was obtained via Professor L. Mucke at Gladstone Institute and bred in house at the University of Edinburgh. Maintenance of the line was achieved by crossing heterozygous TgAPPSw,Ind transgenic animals with non-transgenic (C57Bl/6J, Charles River, UK) resulting in the generation of TgAPPSw,Ind mice heterozygous for the APP transgene and wild-type littermates.

2.2 Chronic cerebral hypoperfusion surgery

The induction of chronic cerebral hypoperfusion was performed as previously described (Shibata et al., 2004); surgeries were undertaken by Dr. Catherine Gliddon or Dr. Philip Holland. Animals were initially anaesthetized in a perspex box with 5% isoflurane. They were then transferred to a face mask and maintained under anaesthesia with 1.5% isoflurane. After a midline cervical incision, the common carotid arteries (CCA) were exposed and 0.18 mm diameter microcoils (Sawane Spring Co., Hamamatsu, Japan) were applied to each CCA. Between the application of the first and the second microcoil there was a 30 min interval. In the sham animals the same surgical procedure as in the hypoperfused was followed with the exception of microcoil application. Core body temperature was maintained at 37˚C. Finally, the cervical incision was closed with sutures. Following surgery the animals were given mashed food and were closely monitored for indications of poor recovery such as overt body weight loss. Animals that lost more than 20% of their pre-surgical weight or had poor recovery were culled.

2.3 Behavioural testing

Prior to any behavioural testing the animals selected for the studies were handled for 5 minutes over a period of 5 days in order to decrease stress due to handling during the experiments.

2.3.1 Spatial working memory assessment in the eight-arm radial maze

The eight-arm radial maze apparatus and its dimensions are shown in Figure 2.1. The radial arm maze (Stoelting Co. Europe, Dublin, Ireland) consisted of an octagonal central platform (20 cm diameter) with 8 equally spaced arms (47 cm length) radiating from it, each containing a small well at the distal end with a food pellet, confined by a 20 cm high transparent plastic wall and with a computer operated door at the entrance. The maze was placed in a well-lit room 1 m above the floor on a stable base with several extramaze two and three dimensional brightly coloured cues. The computer operated doors were controlled remotely by Any-Maze software (Stoelting Co. Europe, Dublin, Ireland), and the researcher could control their opening/closing. A camera attached to the ceiling, directly above the maze, tracked the animals' movements and video recordings of the trials detailing the behaviour and position of the animals during each task were produced by AnyMaze software (Stoelting Co. Europe, Dublin, Ireland).

One week prior to testing, mice were individually housed and subjected to food deprivation resulting in a reduction of body weight by 10–15%, which was maintained throughout the behavioural testing. Two pretraining days preceded the

actual task. On the first pretraining day all doors were open and food pellets (Bio-Serv, USA) were scattered all over the maze and animals were free to explore for 5 minutes. During the second pretraining day, each animal was placed at the entrance of an arm and monitored until having successfully retrieved a food pellet from the well at the distal end of the arm; this was repeated for all eight arms. Following pretraining, animals were trained over 16 days; for each daily testing session each arm was baited with a single food pellet or reward. Each session was initiated by placing the animal in the central area of the maze with all the doors closed. Once the animal was recognised by the software all doors opened and the animal was allowed to explore the maze and make an arm choice. The moment the body of the animal fully entered an arm the doors for the other seven arms closed and that was recorded as the first arm entry. The animal was monitored until found in the central area again; at that point the researcher confined the animal to the central platform for 5 seconds by remotely closing all doors. After the 5 second delay all doors opened and the animal was free to make another choice. This was repeated until all arms were entered or the maximum testing time (25 minutes) had elapsed. The number of novel (correct) entries in the first eight arm entries, the number of total arm entries, the number of revisiting errors and the duration of the task for all trials were recorded.

2.3.2. Exclusion criteria

Animals that were unable to perform in the eight-arm radial arm maze due to seizing behaviour during testing were excluded from further analysis

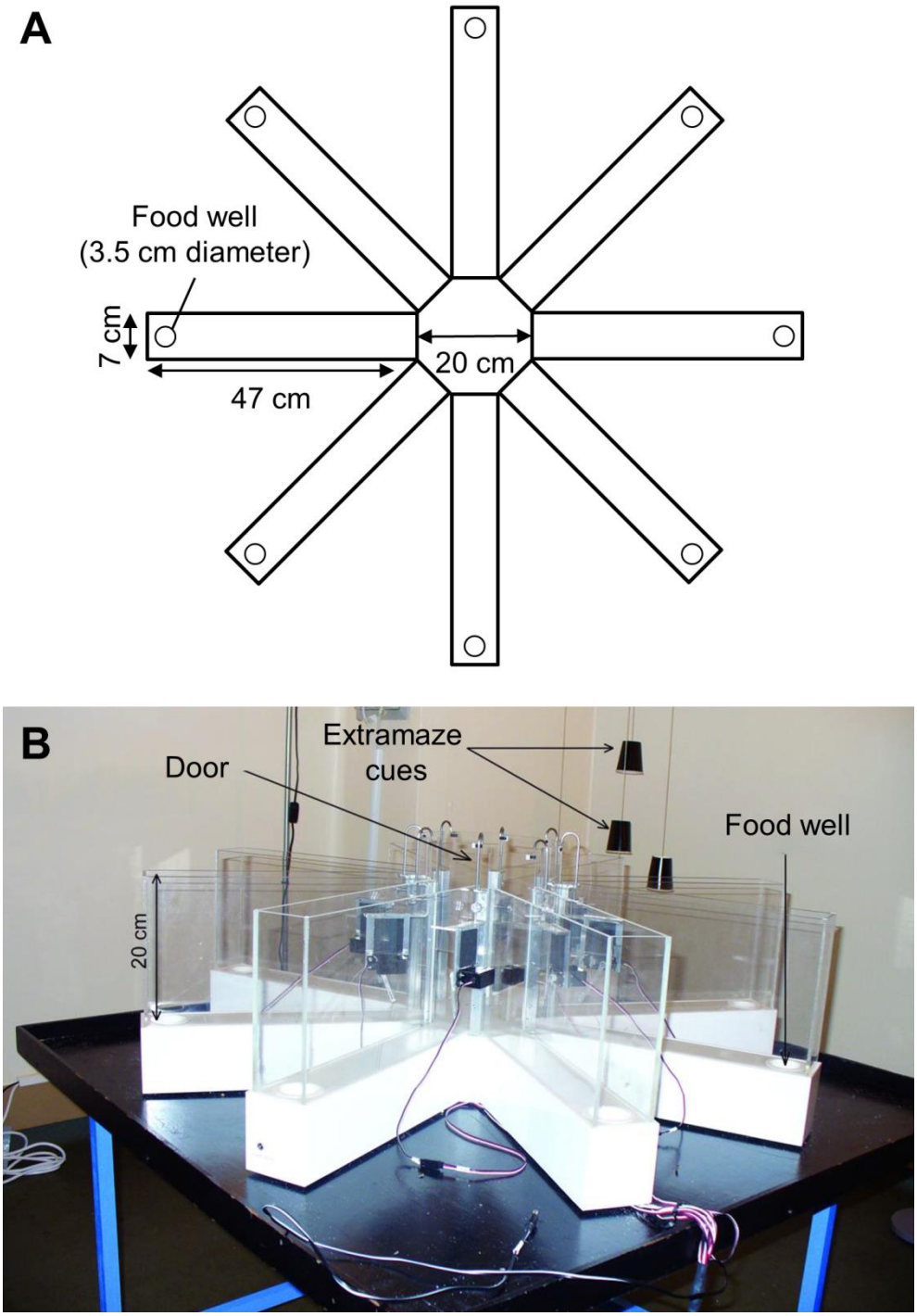

Figure 2.1 ***Eight-arm radial arm maze apparatus***. [A] Schematic representation and dimensions of the eight-arm maze apparatus used for testing working memory performance. The central platform is 20 cm in diameter, each arm is 47 cm long and 7cm wide and at the end of each arm a 3.5 cm diameter food well is found [B] Photograph of the eight-arm radial arm maze apparatus used for all experiments. The maze is placed 1 m above ground and extramaze cues surround the maze for spatial navigation

2.4 Perfusion and tissue preparation

2.4.1 Perfusion for immunohistochemistry and biochemistry

Animals selected for biochemical and immunohistochemical analysis were transcardially perfused. Animals were anaesthetized in 5% isoflurane in a Perspex box. The depth of the anaesthesia was evaluated by the presence of a hind-paw pinch reflex. Once it was confirmed that this reflex was absent the animal was transferred to a face mask on its back and kept under anesthesia for the whole procedure. The skin was cut to expose the thoracic cavity and the diaphragm was carefully cut. Then the ribs were cut through bilaterally with care not to damage the lungs and bent backwards and fixed to place for the heart to be exposed which was very carefully cleared from the surrounding connective tissue. A needle was placed into the left ventricle and fixed with a haemostat and then the left atrium was snipped. Through the clamped needle, 20 mL of 0.9% heparinised saline in phosphate buffer was administered at a rate of 2mL/min. After perfusion the animals were immediately decapitated and the brains were dissected from the skull and bisected across midline. The left hemibrains was post-fixed for 24 hours at 4˚C in 20 mL of 4% paraformaldehyde in phosphate buffer. From the right hemibrain a 2 mm hippocampal slice was coronally dissected using a mouse brain matrix as a guide [0.72mm to 2.74 mm interaural according to Franklin and Paxinos (1997)]. The hippocampal slice as well as the rest of the brain were placed in 1.5 mL Eppendorf tubes and instantly frozen in liquid nitrogen and stored at -80°C for biochemical analysis.

2.4.2 Tissue preparation and sectioning for immunohistochemistry

After 24 post-fixation in 4% paraformaldehyde the brains were attached to a tissue mount with super glue (Loctite, Henkel, Germany). After a few seconds while making sure that the glue was set, the tissue was submerged in a phosphate buffer (PB) bath at room temperature to avoid dehydration. The hemibrains were cut sagittaly into 50 μm sections in a PB bath at room temperature (RT) by a vibrating (frequency set at 60 Hz and amplitude at 0.9 mm) razor blade (Wilkinson Sword Ltd, UK) starting at lateral 2.40 ± 0.1 mm, according to Franklin and Paxinos (1997) using a vibratome (Hyrax V50, Zeiss, Germany). The vibratome was set at an optimal speed of 8 mm/s. All sections were stored free-floating in 1.5 mL of cryoprotective medium (30% glycerol/30% ethylene glycol in phosphate buffer) at -20˚C in 24-well plates for immunohistochemical staining.

2.5 Immunohistochemistry

Sections selected for immunohistochemical experiments were taken out of the -20˚C and allowed to adjust to room temperature and placed in 24-well plates with 1 mL of cryoprotective medium in each well. Cryoprotective medium was washed off with three 15 minutes washes with phosphate buffered saline (PBS, pH7.4), added in each well with a Pasteur pipette.

2.5.1 Fluorescent immunohistochemistry

At the onset, any trace of cryoprotective medium was removed by three 15 minute washes with PBS (pH7.4) containing 0.1% Triton-X100 (PBSTx). Antigen retrieval was performed as detailed in Table 2.1. Non-specific binding sites were blocked using 0.25 mL 3% normal serum of the appropriate species (depending on the species where the secondary antibodies used were produced) in PBSTx for 1 hour. Sections were then incubated overnight at 4^{o}C with 0.25 mL primary antibody or antibody cocktail at the optimal dilution (Table 2.1) in blocking solution. On the next day, sections were taken out of the cold room and allowed to reach room temperature. They were then washed three times for 15 minutes with PBSTx before adding 0.25 mL of secondary antibody or antibody cocktail in PBSTx and incubated overnight at 4ºC. The secondary antibodies used are detailed in Table 2.1 and were always against the species in which the primary antibodies were raised. Finally, after a series of washes with PBSTx (30 minutes), PBS (two washes for 15 minutes) and phosphate buffer (PB, pH7.4; 2 mL for 20 minutes) the sections were mounted onto

SuperFrost slides (WVR International, Lutterworth, UK) with Vectashield hard set mounting medium containing, if necessary, the nuclear stain 4',6-diamidino-2-phenylindole (DAPI) (H-1500, Vector Laboratories, U.S.A). All washes and antibody incubations were performed on a shaker at room temperature, unless it is otherwise stated.

2.5.2 Nissl neuronal cell body stain

Nissl neuronal cell body staining was performed after completion of fluorescent immunohistochemistry protocol if necessary. After the last two PBS washes (15 minutes) described above sections were incubated in 0.25 mL of fluorescent Nissl stain (1:20, NeuroTrace® 640⁄660 Deep-Red, Invitrogen, UK) solution for 20 minutes. Sections were then washed with PBSTx for 15 minutes followed by a 2 hour wash in PBS and a 20 minute wash in PB. Sections were then mounted onto SuperFrost slides (WVR International, Lutterworth, UK) with Vectashield hard set mounting medium. All washes and incubations were performed on a shaker at room temperature.

2.5.3 Chromogenic Immunohistochemistry

To ensure that every trace of cryoprotective medium was removed free-floating sections were washed 3 times with PB. The sections were mounted onto SuperFrost slides (WVR International, Lutterworth, UK) and air-dried for a minimum of 30

minutes. Sections were then rehydrated in phosphate buffer (PB, pH7.4). After rehydration of the sections, endogenous peroxidase was blocked by incubation for 30 min with 3% H_2O_2 in methanol at room temperature. Antigen retrieval was performed in 10mM citrate buffer (pH 6) in a pressure cooker (MenaPath AccessRetrieval Unit, Model MP-2002-CE, A. Menarini Diagnostics Ltd. UK) filled with 0.5 L of distilled water. The retrieval programme was run for 10 minutes with pressure at 100˚C with an additional 10 minutes of cooling time. Sections were then taken out of the pressure cooker and allowed to cool down to room temperature for an extra 10 minutes followed by a 2 minute wash with PBS. Then non-specific epitopes were blocked with 0.25 mL of 10% normal serum from the appropriate species and 0.5% bovine serum albumin for 60 minutes. Blocking solution was then drained from the slides and 0.25 mL of primary antibody (detailed in Table 2.1) in blocking solution was applied to the sections which were incubated overnight at 4°C in a cold room. The next day, the sections were taken out of the cold room and allowed to come to room temperature. They were then washed two times for 10 minutes by immersion in PBS followed by a 60 minute incubation with 0.25 mL of secondary antibody (against the species in which the primary antibody was raised) in PBS (1:100 dilution, Vector Laboratories, Burlingame, CA, USA). Another two 10 minutes washes in PBS followed. The ssignal was enhanced by applying 0.25 mL of Avidin-Biotinylated enzyme Complex (Elite ABC Kit, Vector Laboratories, Burlingame, CA, USA) for 60 minutes followed by two 10 minutes washes in PBS. Immunostaining was visualized (brown staining) by incubating the sections for three minutes in 3, 3´-diaminobenzidine (DAB kit, Vector Laboratories, Burlingame, CA, USA). The 3, 3´-diaminobenzidine was washed off in running water for 10 minutes.

The sections were then dehydrated with serial washes in graduated alcohol solutions and xylene as described in Table 2.2. The final step was mounting the sections in DPX mounting medium (Thermo Fisher, Loughborough, UK) and coverslipping.

2.5.4 Optimisation of antibodies

Before performing any immunohistochemical experiment the optimal dilution of each primary antibody and the optimal antigen retrieval method was determined. Optimal dilutions were determined with concentration-curve experiments where different dilutions of the primary antibodies were used on serial sections from the same animal. The dilution and the antigen retrieval method that gave the most specific cellular staining with the lowest background were chosen as optimal. Negative controls were used in all immunohistochemical experiments; they underwent identical treatment without primary antibody application and minimal staining was detected.

2.5.5 Exclusion criteria

After performing the immunohistochemical experiments the quality of immunostaining was examined. In some isolated cases the tissue at the region of interest was disrupted or the quality of immunostaining was poor (minimal staining) compared to all the other sections indicating technical issues. In these sections imaging was impossible and they were excluded from further analysis

Table 2.1 Information about the primary and secondary antibodies used in all immunohistochemical experiments, including details about working dilution, retrieval method and normal sera used

Primary antibody	Clone	Supplier	Dilution	Antigen retrieval	Normal serum	Secondary antibody	Supplier	Dilution
Anti-K_v1.2	K14/16	UC Davis, US	1:200	30 min in 0.1% PBSTx	Normal goat	AlexaFluor488 anti-mouse IgG2b	Life Technologies, CA	1:500
Anti-ankG	H-215	SantaCruz. US	1:5	30 min in 0.1% PBSTx	Normal goat	AlexaFluor546 anti-rabbit	Life Technologies, CA	1:500
Anti-SCN8A (Na_v1.6)	polyclonal	Millipore, UK	1:200	30 min in 0.1% PBSTx	Normal horse	anti-rabbit Cy3	Jackson ImmunoResearch Laboratories, US	1:200
Anti-Caspr	K65/35	UC Davis, US	1:50	30 min in 0.1% PBSTx	Normal goat	AlexaFluor647 anti-mouse IgG1(for AIS staining) OR AlexaFluor488 anti-mouse (for Nodes of Ranvier)	Life Technologies, CA	1:500
Anti-myelin basic protein (MBP)	12	Millipore, UK	1:200	30 min in 0.3% PBSTx	Normal horse	anti-rat Cy3	Jackson ImmunoResearch Laboratories, US	1:200
Anti-β amyloid	6E10	Covance, US	1:1000	citrate buffer	Normal horse	Biotinylated anti-mouse	Vector	1:100
Anti-pan Neurofilament	SMI312	Covance, US	1:100	30 min in 0.3% PBSTx	Normal horse	DyLight488 anti-mouse	Jackson ImmunoResearch Laboratories, US	1:200
Anti-synaptophysin	SVP-38	Sigma-Aldrich, UK	1:200	30 min in 0.1% PBSTx	Normal goat	AlexaFluor488 anti-mouse	Life Technologies, CA	1:500

Table 2.2 Dehydration sequence in graduated alcohol solutions and xylene

Solution	Time in solution
70% Ethanol in dH_2O	2 minutes
90% Ethanol in dH_2O	2 minutes
100% Ethanol	2 times for 5 minutes
Xylene	10 minutes

2.5.6. Regions of interest

The regions of interest examined in this thesis included the corpus callosum and regions within the hippocampus such as CA3 and the stratum lacunosum moleculare (Figure 2.2).

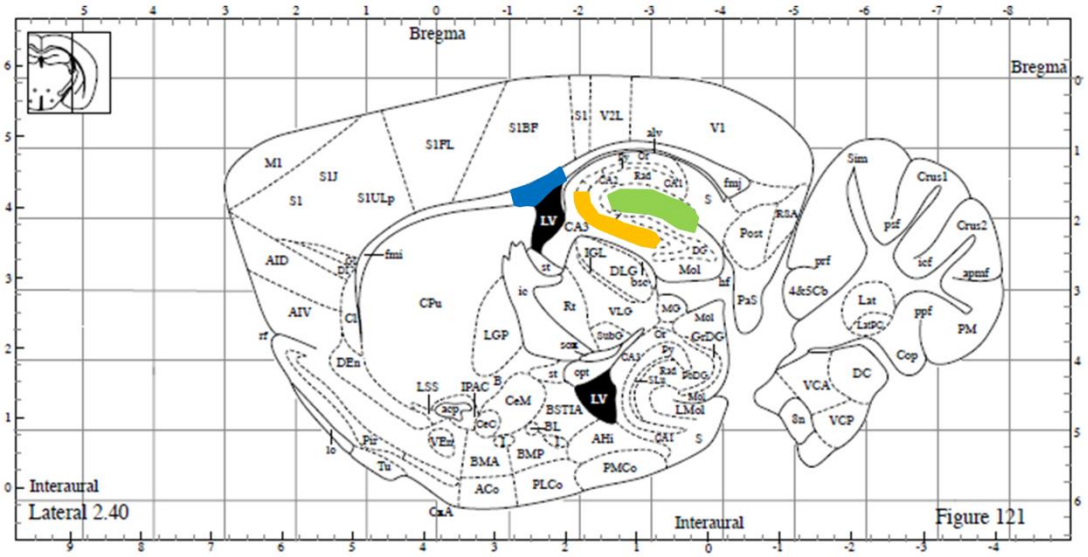

Figure 2.2 ***Regions of interest selected for examination***. Sagittal diagram of the mouse brain with highlighted regions of interest; corpus callosum in blue (■), CA3 in yellow (■) and stratum lacunosum moleculare in green (■). Image adapted from Franklin and Paxinos (1997).

2.6 Image acquisition and quantitative image analysis

Image acquisition and quantitative image analysis were performed by the author who was blind to the experimental conditions. To ensure reproducibility of the image analysis, images or image stacks acquired from three randomly selected animals were analysed accordingly for a minimum of three times. Reproducibility was achieved once there was less than a 10% difference of the three measurements from the median value.

2.6.1 Image acquisition

Before imaging sections that underwent fluorescent immunohistochemistry were screened at a fluorescent Leica DMR microscope (Leica Microsystems U.K.) to identify, by eye, the brightest stained section. This allowed determining the optimal imaging settings at the confocal and avoiding imaging at saturated levels of intensity. Then the sections were imaged with a Zeiss upright Axioskope LSM510 or with a Zeiss inverted AxioObserver LSM710 confocal laser scanning microscope using LSM software or ZEN software (ZEISS, Germany) respectively as the user interface at 1024x1024 pixels resolution. A pinhole of 1 Airy unit and identical confocal imaging settings for detector gain, digital offset, digital gain and laser power were used.

Chromogenic immunohistochemistry was imaged with an Olympus BX51 microscope (Olympus UK, Southendon-Sea, UK) using a QImaging MicroPublisher

3.3 camera (QImaging, Surrey, BC, CA) and QCapture Pro 7 software (QImaging, Surrey, BC, Canada) at 2048×1536 resolution.

2.6.2 Quantification of MBP and total neurofilament immunostaining

Fluorescently labelled sections with anti-MBP and anti-pan neurofilament (SMI312R) antibodies were imaged at the stratum lacunosum moleculare of the hippocampus and/or the corpus callosum with a confocal laser scanning microscope. Single optical images were acquired at a depth of 4 μm from the surface of the section and used to evaluate MBP and total neurofilament immunostaining. Images were opened using ImageJ as 8-bit colour images. Fluorescent intensity of all images was filtered with the application of a threshold that subtracts low intensity pixels due to non-specific/background staining. In order to determine the threshold value 5 grid boxes (20 x 20 pixels) per section were analysed in areas as good representation of the background intensity. From all the boxes, the average mean grey value (MGV) and standard deviation (SD) of the background was determined. The threshold was determined as the average mean grey value of the background plus three times its standard deviation (threshold = average MGV+3×SD). Background was subtracted consistently from all images. The percentage of the area (area fraction) occupied by MBP or SMI312R staining for each group and the fluorescent intensity (mean grey value) of MBP and SMI312R staining were determined and used for further analysis.

2.6.3 Quantification of myelin bulbs

Observation of MBP immunostaining staining from the stratum lacunosum-moleculare of the hippocampus revealed regional abnormalities of the myelin staining resembling bulbs on some myelinated fibres. These structures resemble in the myelin "balloons" observed with electron microscopy (Feldman and Peters, 1998). The number of these myelin sheath bulbs which were defined as any MBP-immunopositive formation that interrupts the continuity of the myelinated fibre, with a diameter 20% larger than the diameter of the fibre. The analysed image stacks were acquired with a Zeiss Axioskope LSM 510 confocal laser scanning microscope using a 40× oil-immersion objective (numeric aperture 1.3), from fluorescence labelled sections for MBP and total neurofilament. The corresponding Nyquist settings of 4.6× zoom and 0.16 μm z-steps were used to allow image deconvolution (Huygens Professional Deconvolution Software; SVI). After deconvolution, which produces 16-bit images, the images were transformed into 8-bit format. Before transformation the pixel intensities of 16-bit images were equalized across the full range of the histogram using ImageJ so that intensities at the 8-bit images are better distributed. Two adjacent confocal 40-slices stacks were acquired per animal where the average number of myelin sheath bulbs from two 76.8x76.8x10 μm^3 confocal stacks was determined and was used for further analysis.

2.6.4 Quantification of synaptophysin immunostaining

Presynaptic terminal density was assessed using an anti-synaptophysin antibody in the CA3 area of the hippocampus. Images were acquired with a Zeiss inverted AxioObserver LSM710 confocal laser scanning microscope using a 40× oil-immersion objective (numeric aperture 1.3). Two adjacent single optical images were acquired from the CA3 region of each animal at a depth of 4 μm from the surface of the section. Images were opened using ImageJ as 8-bit colour images As described in chapter 2.6.2 the background was subtracted consistently from all images and the percentage of the area (area fraction) occupied by presynaptic terminals was determined and values from the two images were averaged for each animal to be used for further analysis.

2.6.5 Nodes of Ranvier measurements

Images were acquired with a 63× oil-immersion objective (numerical aperture 1.4) from sections labelled with anti-$Na_v1.6$ channels and anti-Caspr antibodies. Nav1.6 staining and Caspr immunostaining were imaged on the red channel and the green channel respectively. The corresponding Nyquist settings, 3.1× zoom and 0.13 μm z-steps were used to allow image deconvolution (Huygens Professional Deconvolution Software; SVI). The 16-bit images produced after deconvolution, were transformed into 8-bit format. Before transformation the pixel intensities of 16-bit images were equalized across the full range of the histogram using ImageJ so that intensities at the 8-bit images were better distributed. The length and width of the $Na_v1.6$ positive

clusters as well the nodal gap length which is the space between two Caspr positive domains were measured in image stacks spanning 10 μm using the straight line tool on ImageJ. Having confirmed first that the gap is occupied by a $Na_v1.6$ cluster, the distance between the two closest points of the Caspr domains was measured (Figure 2.3 A). Only $Na_v1.6$ clusters found between two Caspr positive domains on either side were analysed and due to their irregular shape the maximum length and width were measured (Figure 2.3 B). Furthermore, by moving between the slices of the stack it was possible secure that the full length of the $Na_v1.6$ clusters or nodal gaps was measured in nodes imaged at an. Analysis was performed in the first 30 appearing nodes in the acquired 47 × 47 × 10 μm^3confocal stack for each animal.

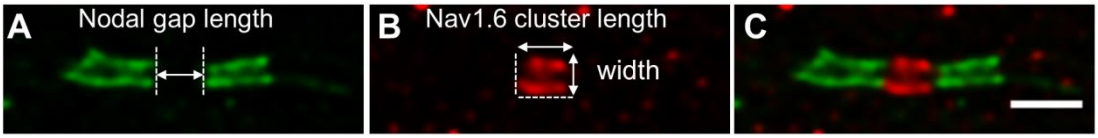

Figure 2.3 ***Measurements at the nodes of Ranvier***. Measuring the nodal gap length between two Caspr positive paranodes [A] and the $Na_v1.6$ cluster length and width [B]. Image of a complete node of Ranvier from the stratum lacunosum moleculare of the hippocampus [C]. Scale bar 2 μm.

2.6.6 Quantification of nodal density

The number of the nodes of Ranvier was determined on the same image stacks acquired for the nodal length measurements (described at chapter 2.6.5). The numerical density of the nodes was assessed in 47 × 47 × 10 μm^3 confocal stacks from the hippocampus or in 47 × 47 × 5 μm3 confocal stacks for the corpus

callosum. Only complete nodes namely $Na_v1.6$ clusters that were paired with Caspr immunolabelled paranodes on either side were counted in maximum intensity z-collapsed stacks. The original stacks were used at the side as a reference guide to secure that the overlapping nodes, which are difficult to separate within the collapsed stack, are counted. Nodes located on the first optical section and crossing the upper and the left edge of the stack were not counted.

2.6.7 Axon initial segment length measurements

Sections labelled with AnkG, Caspr and Nissl stain for neuronal cell bodies were imaged. Image stacks were acquired with a Zeiss inverted AxioObserver LSM710 confocal laser scanning microscope using a 40× oil-immersion objective (numeric aperture 1.3). Two adjacent image stacks 30 μm thick were acquired from the CA3 region of the hippocampus of each animal in order to ensure imaging of complete AIS. An AIS was considered complete when the neuronal cell body and the first paranode, labelled for Caspr, could be identified. Measurement of each AIS was achieved by isolating the mini-stacks that contained a complete AIS, collapsing the stack by using the z-collapse maximum intensity tool on ImageJ software and following the shape of the AIS from the cell body to the first paranode using the segmented line tool on ImageJ software. In total the length of 20 complete AIS labeled for ankG from each animal were measured.

2.6.8 Quantification of number of AIS

The number of the AIS was determined on the same image stacks acquired for the AIS length measurements (described at 2.6.7). The numbers of AIS were assessed in 212 × 212 × 10 μm^3 confocal stacks. AnkG positive structures with typical AIS morphology indicated by a length >5μm, a wide base and a tapered end were counted in maximum intensity z-collapsed stacks. The original stacks were used at the side as reference guide to secure that all AIS are counted in regions where multiple AIS were overlapping. AIS located on the first optical section and crossing the upper and the left edge of the stack were not counted.

2.6.9 Quantification of Kv1.2 immunostaining

Sections stained for K_v1.2 and Caspr were imaged at an inverted Zeiss Axioskope LSM 710 with a 63× oil-immersion objective (numerical aperture 1.4). The corresponding Nyquist settings, 3.1× zoom and 0.13 μm z-steps were used to allow image deconvolution (Huygens Professional Deconvolution Software; SVI). A 4 μm (30 slices) thick confocal stack was acquired from the corpus callosum. After deconvolution, which produces 16-bit images, the images were transformed into 8-bit format (as described in chapter 2.6.3). The background was subtracted consistently from all images by setting a common threshold for the red (K_v1.2) and the green (Caspr) channels (as described in chapter 2.6.2). For each slice of each stack the area occupied by Caspr staining and then the volume was calculated by multiplying with the z-step. Next the area occupied by both K_v1.2 and Caspr was

determined. This was achieved by subtracting from the area occupied by $K_v1.2$ positive staining the binary mask of the area that was not occupied by Caspr positive staining for each slice of each stack with the Math tool on ImageJ. Then the volume that was occupied by both $K_v1.2$ and Caspr staining was determined by multiplying with the z-step and expressed as a percentage of the total Caspr volume.

2.6.10 Quantification of amyloid-β immunostaining

Sections immunolabelled for Aβ with the 6E10 antibody were imaged at the stratum lacunosum moleculare of the hippocampus using a ×20 objective at an Olympus BX51 microscope. Images were opened with ImageJ and converted into greyscale. The background was subtracted consistently from all images by setting a common threshold (as described in chapter 2.6.2). The percentage of the area (area fraction) covered with amyloid deposits was determined and used for further analysis.

2.7 Biochemistry

2.7.1 Tissue homogenization

Tissue stored at -80˚C for biochemical analysis was homogenized in ice cold tissue homogenisation buffer containing sucrose (250mM), Tris Base (20mM), ethylenediaminetetraacetic acid (EDTA; 1mM) and ethyleneglycoltetraacetic acid (EGTA; 1mM). Protease (1:100 dilution; Merck Biosciences AG, Germany) and phosphatase inhibitors (1:50 dilution Merck Biosciences AG, Germany) were added to the buffer before use. Homogenisation was performed with a Dounce homogeniser on ice. Homogenised samples were centrifuged at rotor speed of 3000 rpm for 5 minutes at 4˚C with a Sigma 1-13 benchtop centrifuge (Sci Quip Ltd., Shrewsbury, UK). This short centrifugation allows the separation of the total homogenate from small pieces of non-homogenized tissue and facilitates the handling of the lysate in biochemistry experiments. Supernatant was carefully removed and was ready be used for assessing protein concentration.

2.7.2 Protein concentration assessment

Total protein concentration of each sample was determined with a BCA (bicinchoninic acid) protein assay (Thermo Fisher Scientific (Cramlington, UK). Working dilutions (1:10) in tissue homogenisation buffer (THB) of the homogenates and the standards were prepared and loaded in triplicate on to 96-well plates. Working reagent (solution of 4% cupric sulphate mixed 1:50 with a solution of sodium bicarbonate, bicinchoninic acid, sodium carbonate and sodium tartrate in

0.1M sodium hydroxide) was added to each well and incubated for 30 minutes at 37˚C. The plates were left to cool down to room temperature for a few minutes and then the absorbance at 562 nm was read with a Dynex MRX plate reader (Dynex Technologies Ltd., Worthing, UK). For each sample (homogenate or standard) three values were obtained and the average was calculated. The readings for the standard were used to produce a standard curve and subsequently calculate the protein concentration in each sample. Before use samples were stored at -20˚C in 5μL aliquots.

2.7.3 Enzyme-linked immunosorbent assay (ELISA)

Tissue homogenates (prepared as described in chapter 2.7.1) with known protein concentration (determined as described in chapter 2.7.2) were used to determine total human Aβ42 (hAβ42) concentration in TgAPPSw,Ind animals using a commercially available ELISA kit (Invitrogen, Camarillo, CA). On a 192-well ELISA kit 50μL of standards of hAβ42 peptide at different concentration (1000, 500, 250, 125, 62.5, 31.25, 15.63 and 0 pg/mL) or samples (in duplicate) diluted 2.5 times with Standard Diluent Buffer were loaded. One well was kept empty to serve as the chromogen blank. Then 50 μL of human Aβ42 detection antibody were loaded to each well except from the chromogen blank. After incubating for 3 hours at room temperature with shaking, liquid in the wells was aspirated and the wells were thoroughly washed 4 times with Wash Buffer. Next 100 μL of anti-rabbit IgG HRP. Working Solution was added to each well except from the blank followed by a 30 minute incubation at room temperature. After four thorough washes (Wash Buffer) 100μL of Stabilized

Chromogen was added to each well and the plate was incubated in the dark at room temperature for 30 minutes. Then 100μL of Stop Solution were gently mixed with the solution changing from blue to yellow. Absorbance was read for all wells at 450 nm with a plate reader blanked against the chromogen blank. Next the standard curve was produced and the concentration in human hAβ42 corrected for the sample dilution was determined by using the average reading of the duplicates of each sample. The experiment was run twice and the average hAβ42 concentration between the two experiments for each sample was calculated. The final hAβ42 concentration was expressed as pg of hAβ42 in mg of total protein.

2.7.4 Western blotting

Samples with 1 μg/μL or 4 μg/μL final protein concentrations were prepared using a 4x Laemelli buffer (1:4 dilution) and THB. Control sample from brain homogenate (prepared as described at chapter 2.7.1) from two 20 months old APPSw,Ind animals (perfused as described at chapter 2.4.1) was prepared in the same way.

The proteins were denaturated at 70˚C for 10 minutes in a water bath. The appropriate amount of sample protein (Table 2.3) was loaded on precast NuPAGE 4-12% Bis-Tris gels (Life Technologies, Carlsbad, CA) together with 5 μL of a molecular marker (LiCor Biosciences, Lincoln, Nebraska, USA). Control sample was also loaded on each gel. Samples were run with a 2-[N-morpholino] ethanesulfonic acid-sodiumdodecyl sulphate (MES-SDS) running buffer (Life Technologies, Carlsbad, CA) at 80V for approximately 90 minutes.

The proteins were then transferred to Amersham hybond-P polyvinylidene fluoride (PVDF) membrane at 30V for 2.5 hours in an XCell II™ Blot Module (Life Technologies, Carlsbad, CA). Successful transferring of the proteins onto the PVDF membrane was evaluated by staining gels in Coomasie Blue (Bio-Rad, Hemel Hempstead, UK) for one hour. Coomasie Blue detects proteins left on the gels and when these were strongly or unevenly stained, which is evidence of poor transfer or uneven loading, they were rerun. After transfer, PVDF membranes were rinsed in PBS and incubated for 1 hour on a shaker in Odyssey blocking buffer (1:1 in PBS, LiCor Biosciences, Lincoln, Nebraska, USA) in order to block non-reactive sites. Blocking buffer was then drained and the membranes were incubated overnight on a shaker at 4^{o}C with a cocktail of primary antibodies against the protein of interest (detailed in Table 2.3) and against Glyceraldehyde 3-phosphate dehydrogenase (1:100000 dilution, rabbit or mouse anti-GAPDH, Sigma-Aldrich Ltd., Poole, UK) made in Odyssey blocking buffer containing 0.1% Tween-20. The following day after six washes (for 5 minutes) with PBS-0.1% Tween-20, the membranes where incubated for 45 minutes at room temperature with the appropriate secondary antibodies (Table 2.3) (1:3000 dilution; LiCor Biosciences, Lincoln, Nebraska, USA) in Odyssey blocking buffer-0.1% Tween-20-0.01% SDS in light proof boxes and then washed again (6 times for 5 minutes) with PBS-0.01% Tween-20 before a final wash in PBS. The membranes were then left to dry protected from light before being imaged using the Odyssey infrared imaging system (LiCor Biosciences, Lincoln, Nebraska, USA).

Table 2.3 Information about the primary and secondary antibodies used in western blotting experiments, including details about working dilution and quantity of protein

Primary antibody	Clone	Supplier	Dilution	Secondary antibody	Protein amount
Anti APP	22C11	Millipore, UK	1:3000	Anti-mouse	10µg
Anti- APP C-terminal fragments	Polyclonal	Merck, UK	1:1000	Anti-rabbit	30µg
Anti-neurofilament (200 KDa)	Polyclonal	Sigma-Aldrich, UK	1:10000	Anti-rabbit	10 µg
anti-MBP	12	Millipore, UK	1:10000	Anti-rat	10 µg
Anti-pan Neurofilament	SMI312	Covance, US	1:10000	Anti-mouse	10 µg
Anti-Glyceraldehyde 3-phosphate dehydrogenase (GAPDH)	GAPDH-71.1	Sigma-Aldrich, UK	1:100000	Anti-mouse	N/A
Anti-Glyceraldehyde 3-phosphate dehydrogenase (GAPDH)	Polyclonal	Sigma-Aldrich, UK	1:100000	Anti-rabbit	N/A

2.7.5 Quantification of protein levels

Scanned images of western and dot blot membranes were analysed using Odyssey application software (version 3.0; Li-Cor, Cambridge, UK) in order to quantify the fluorescent intensity of the bands or dots of interest.

For each protein of interest, western blots were run in duplicate. Fluorescent intensity (in arbitrary units) for the band corresponding to the protein of interest was expressed as a ratio of the intensity of the GAPDH band from the same sample to normalise for loading variation. The average ratio value from the duplicates of each sample was used for analysis. Bands were excluded from analysis when there were bubbles or other noise that made intensity calculations impossible. Fluorescent intensity of the GAPDH bands from each sample was averaged between the duplicates and compared with an independent samples t-test between groups to confirm that GAPDH is an accurate loading control and was not changed between groups. The test was performed for every set of western blots. No difference between groups in GAPDH intensity was ever observed ($p > 0.05$). An example of this comparison is shown in Figure 2.4. Similarity of the images and of the values obtained between duplicates was used to confirm reproducibility of the blots.

In the dot blots, fluorescent intensity of each dot was quantified. Each sample was loaded in duplicate and the average intensity from each sample was expressed as a ratio of the average intensity value from the control sample. Any dot with evidence of noise was excluded from analysis.

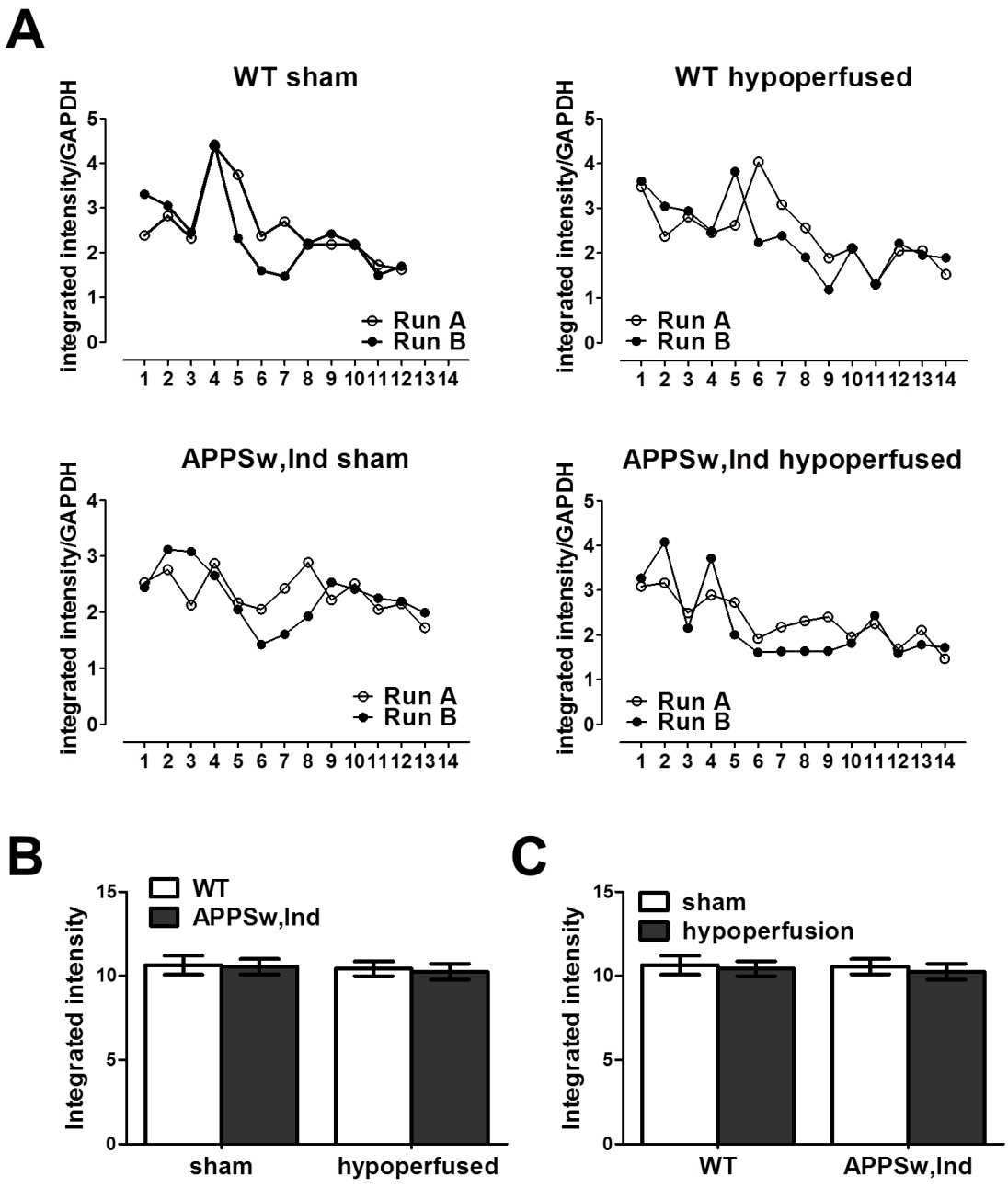

Figure 2.4 ***Western blot reproducibility*****.** [A] Similarity values obtained between duplicates (run A and B) was used to confirm reproducibility of the blots; shown here an example of data from total neurofilament (SMI312) blots [B & C] Integrated GAPDH intensity was used to normalise for loading variation. No differences were detected ($p > 0.05$) between the different groups. Here a representative example of young hypoperfused and sham WT and TgAPPSw,Ind animals where no effect of genotype or hypoperfusion is observed. WT sham: n=12, WT hypoperfused: n=14, TgAPPSw,Ind sham: n=13, TgAPPSw,Ind hypoperfused n=13. Graphs show mean ± SEM.

2.8 Statistical analysis

All experiments were performed blind with regard to conditions (genotype, age or surgery).

Behavioural performance in the 8-arm radial arm maze was analysed using SPSS v14.0 software (IBM, New York, USA). The number of novel (correct) entries in the first eight arm entries and the number of revisiting errors in the 8-arm radial arm maze task, expressed in two-trial blocks (average value of the measure for two consecutive days) were analysed. Difference of the means was assessed with two-way repeated measures ANOVA for the appropriate factors followed by Tukey's *post hoc* test if necessary. Additionally, the Greenhouse-Geiser correction was used when data violated sphericity ($p < 0.05$ at Mauchly's test). Difference of the means for number novel entries in the first eight arm entries from chance reported to be 5.3 entries (Olton and Samuelson, 1976) was analysed using student's unpaired t-test.

Cumulative frequency distribution of nodal length and AIS length measurements expressed as percentages were analysed with the two-sample Kolmogrov-Smirnov test. This analysis was performed with an open source statistics application developed by Kirkman (1996).

MBP, total neurofilament, Aβ and synaptophysin immunostaining, number of myelin bulbs, nodes of Ranvier and AIS, protein levels (except Aβ and hAPP) detected with western blot, and Kv1.2/Caspr colocalization were analysed using GraphPad Prism v5.0 (Graphpad Software Inc. El Camino Real, USA). Difference of the means was assessed with a two-way ANOVA for the appropriate factors followed by

Bonferroni's *post hoc* test if necessary. Difference of the means in Aβ42 concentration and Aβ and hAPP protein levels was analysed using the student's unpaired t-test. Association between means was analysed with the Spearman's correlation analysis.

All graphs were generated using GraphPad Prism v5.0 (Graphpad Software Inc. El Camino Real, USA). Statistical significance was established at $p < 0.05$. However, Bonferroni correction (Bland and Altman, 1995) was applied when multiple-comparisons were performed simultaneously using identical datasets. Significance ($p < 0.05$) was Bonferroni corrected by dividing with the number (n) of comparisons using the identical datasets ($p < 0.05/n$).

2.9 Sample size calculations

In order to secure that the studies are well-powered which means that if there is a difference between the investigated groups there is an increased chance of it to be detected, the adequate sample size for difference of the means was calculated were necessary. Firstly, the standardized difference (*d*) was calculated which equals to the target difference divided by the standard deviation. These values are not known in advance and are estimated based on the published literature of similar studies using similar methods. The sample size was then calculated with the formula $n = \frac{2}{d^2} \times c_{p,power}$ where n is the size of the group, d is the standardized difference and $c_{p,power}$ is a constant determined by the values of the chosen statistical significance (p) and power. The studies included in the thesis comprise of a maximum of four groups therefore the use of identical data for multiple comparisons and the need for Bonferroni correction (described above) is a possibility resulting in stricter criteria for the calculation of sample size. Here for the calculation of sample size a $p = 0.01$ and a power of 80% was used which makes $c_{0.01,80\%} = 11.7$ (Whitley and Ball, 2002).

Chapter 3

Age-related changes in myelinated axons and cognition in wild-type and TgAPPSw,Ind mice

3.1 Introduction

Myelin alterations are a key feature of the ageing brain and are exacerbated in AD, and have been linked with poor cognitive function (Bartzokis et al., 2003; Salat et al., 2005; Salat et al., 2009). Moreover, neuronal excitability is altered particularly within hippocampal networks (Disterhoft and Matthew Oh, 2003; Gleichmann and Mattson, 2010) in both normal ageing and AD. In view of the importance of the AIS and nodes of Ranvier in initiating and propagating action potentials, disruption of these regions could have a major impact on neuronal function in normal ageing and in AD. To date, there have been very few studies investigating the vulnerability of these regions and their structural integrity in normal ageing or AD.

From the limited studies in ageing, there is evidence that components of the nodes are disrupted in ageing rodents and in aged primates (Rios et al., 2003; Hinman et al., 2006; Shepherd et al., 2012). Moreover, in a transgenic mouse model featuring AD-related pathology there is evidence of changes in $Na_v1.6$ channel immunoreactivity (Desai et al., 2009). From studies using animal models of multiple sclerosis there is evidence that demyelination is the underlying mechanism for nodal disruption (Coman et al., 2006; Lasiene et al., 2008).

At the outset of the studies described in the thesis there were no studies which had investigated changes in AIS structure in normal ageing or AD. There was however some evidence that its integrity is challenged in response to other types of injury such as stroke (Schafer et al., 2009; Hinman et al., 2013) or brain trauma (Baalman et al., 2013) and a few studies have shown that AIS structure shows remarkable levels of activity-dependent plasticity in response to altered electrical activity or synaptic input (Kuba et al., 2010; Grubb and Burrone, 2010a). Synaptic loss has been described in aged non-demented individuals and is exacerbated in AD patients (Bertoni-Freddari et al., 1990) and correlates to cognitive impairment (Coleman and Yao, 2003). This is also supported by studies in aged rodents and AD mouse models where synaptic loss has been observed (Rutten et al., 2005; Geinisman et al., 1986; Landfield and Lynch, 1977).

3.1.1 Hypothesis and aims

Given the similar molecular architecture, it was hypothesised that the AIS and nodes of Ranvier would be altered in ageing and that these effects would be exacerbated in the presence of increased levels of Aβ. Additionally, it was hypothesised that altered synaptic input would play a role in AIS alterations given its activity-dependent plasticity. Moreover, alterations in these structures are hypothesised to be associated with impairment in learning and memory. To address this, the integrity of myelinated axons with a focus on the AIS and nodes of Ranvier, the synapses as well as cognitive performance were examined in young and aged wild-type and TgAPPSw,Ind mice which show increased amyloid levels with increasing age.

3.2 Materials & Methods

3.2.1 Animals

The transgenic mouse model used in this study is described in chapter 2.1. Experiments were performed in young (6 months old, n=14) and old (18-19 months old, n=15) TgAPPSw,Ind mice and compared to aged-matched wild-type C57Bl/6J control littermates (young n=14, old n=13).

3.2.2. Behavioural testing

Spatial working memory assessment for the animals was performed as described in chapter 2.3.1. The number of novel (correct) entries in the first eight arm entries, the number of total arm entries, the number of revisiting errors and the duration of the task for all trials were recorded

3.2.3 Neuropathological assessment

3.2.3.1 Perfusions and tissue preparation

Five days after completion of the behavioural experiments the animals were sacrificed for further immunohistochemical and biochemical analysis as described in chapter 2.4.1. Tissue was prepared for immunohistochemical and biochemical experiments as detailed in chapter 2.4.2.

3.2.3.2 Immunohistochemistry

Immunohistochemical experiments were performed on serial 50 μm sagittal sections starting at lateral 2.40 ± 0.1 mm, according to Franklin and Paxinos (1997). If necessary, exclusion criteria were applied after immunostaining as described in chapter 2.5.5. Immunohistochemisty for Aβ was performed as described in chapter 2.5.3 to detected Aβ deposition in the hippocampus. The integrity of the myelinated axons was examined using antibodies against myelin basic protein (MBP) and total neurofilament. Alterations in the length and the number of nodes of Ranvier were examined using antibodies against Caspr and $Na_v1.6$. In addition, the length of AIS was examined using antibodies against AnkG and Caspr combined with Neurotrace staining for the neuronal bodies. Moreover, synaptic integrity was investigated using an antibody against synaptophysin. The fluorescent immunochemistry and Neurotrace staining techniques used are described in chapters 2.5.1 and 2.5.3 respectively. The Aβ load was assessed in the hippocampus as described chapter 2.6.10 Myelin and axonal integrity was assessed in stratum lacunosum moleculare of the hippocampus in sections stained for MBP and total neurofilament as described in chapter 2.6.2. Myelin bulbs were also quantified at the same region as described in chapter 2.6.3. The length and the width of the $Na_v1.6$ clusters, the nodal gap length and the number of the nodes were examined in the stratum lacunosum moleculare of the hippocampus in sections stained for $Na_v1.6$ and Caspr as described in chapters 2.6.5 and 2.6.6. The length and the number of the AIS as well as synaptic integrity were examined in the CA3 region of the hippocampus as described in chapters 2.6.7,

2.6.8 and 2.6.4 respectively. In some animals imaging was impossible because of poor quality of staining and tissue (exclusion criteria described in chapter 2.5.5). The final analysis was conducted in group sizes detailed in table 3.1.

Table 3.1 Group sizes of the animals included in final analysis

Analysis	Groups size (*n*)			
	wild-type young	wild-type old	TgAPPSw,Ind young	TgAPPSw,Ind old
AIS length and number	14	12	14	15
Nodal length, width and number	11	12	14	15
MBP analysis	14	12	14	15
Total neurofilament analysis	13	12	14	15
Aβ deposition	13	12	13	15
Synaptophysin	14	13	14	15

3.2.4 Western blotting

Before proceeding to tissue homogenisation as described in chapter 2.7.1, the hippocampi from the 2mm hippocampal coronal slices of the right hemibrain (cohort 1) were dissected. The procedure was performed on a glass plate directly placed on ice. The hippocampi were then homogenized as described in chapter 2.7.1. Protein concentration was determined as described in chapter 2.7.2. MBP and pan neurofilament levels were determined using anti-MBP and anti-pan neurofilament antibodies whilst Aβ levels and human APP (hAPP) levels we determined with an anti Aβ antibody (clone 6E10). The details of the western blot technique and the antibodies used are described in chapter 2.7.4. Quantification of the protein levels for

MBP, total neurofilament, hAPP, monomeric Aβ and trimeric Aβ was performed as detailed in 2.7.5.

3.2.5 Statistical analysis

The AIS and nodal length measurements were analysed using the two-sample Kolmogrov-Smirnov test. The number of nodes and AIS, results for Aβ, MBP, total neurofilament and synaptophysin immunostaing and MBP and total neurofilament western blot analysis were analysed with 2-way-ANOVA with genotype and age as the factors followed by Bonferroni's *post hoc* test if necessary. Results for hAPP and amyloid-β western blot analysis were analysed using the student's unpaired t-test. Data acquired at the 8-arm radial arm maze was analysed with two-way (effect of age and genotype over training days) repeated measures ANOVA followed by Tukey's *post hoc* test. Spearman's correlation analysis was used to associate changes between the $Na_v1.6$ cluster and AIS length, Aβ levels and number of errors in the 8-arm radial arm maze. The software used for statistical analysis and graph generation is detailed in chapter 2.8. For all statistical tests significance was established at $p < 0.05$, except from the Kolmogrov-Smirnov test where the Bonferroni correction was applied adjusting significance at $p < 0.025$ as described in chapter 2.8 because identical datasets where used simultaneously twice.

3.3 Results

3.3.1 Decreased AIS length in response to ageing in wild-type animals and in young TgAPPSw,Ind compared to wild-type mice

The length of the AIS is proposed as a key mechanism to regulate neuronal excitability. The first aim of the study was to assess whether the length of the AIS may be altered in ageing and in response to increasing Aβ levels in CA3 pyramidal neurons of the hippocampus. The hippocampus is the primary region affected by Aβ deposition whilst the CA3 serves an important role in hippocampal circuitry. The AIS was immunolabeled for ankyrin-G and the length measured from the neuronal cells bodies identified by Neurotrace stain to the first paranode identified by Caspr immunolabelling (Figure 3.1 A). In general AIS were readily identifiable in all sections and there were no obvious morphological alterations in any of the individual mice. Quantification of the length of a number of AIS was undertaken in all cases. In the wild-type animals, the average length of AIS was found to be 49.2 ± 0.4 μm at a young age and 45.5 ± 0.4 μm in the older animals whilst in the young TgAPPSw,Ind average AIS length was 47.7 ± 0.4 μm and 46.8 ± 0.4 μm in the aged TgAPPSw,Ind. In the first instance the effect of age was studied in wild-type and TgAPPSw,Ind mice on AIS length. Notably, a significant decrease by 7.4 ± 1.2% in the length of the AIS was detected in aged wild-type when compared to young mice ($p < 0.001$, $D = 0.2343$; Figure 3.1 B and F). However, no significant change in the length of AIS was observed in the aged TgAPPSw,Ind when compared to younger animals ($p = 0.034$, $D = 0.1171$; Figure 3.1 C and G). Following on from this, it was determined whether the alterations in AIS length may be differentially affected in TgAPPSw,Ind

mice compared to wild-type littermates. At a young age, a significant decrease by 3 ± 1.2% in the length of AIS in young TgAPPSw,Ind mice when compared to wild-type animals of the same age ($p < 0.01$, $D = 0.1610$; Figure 3.1 D and H). However in the aged mice there was no difference in the AIS length between wild-type and TgAPPSw,Ind mice ($p = 0.311$, $D = 0.0825$; Figure 3.1 E and I).

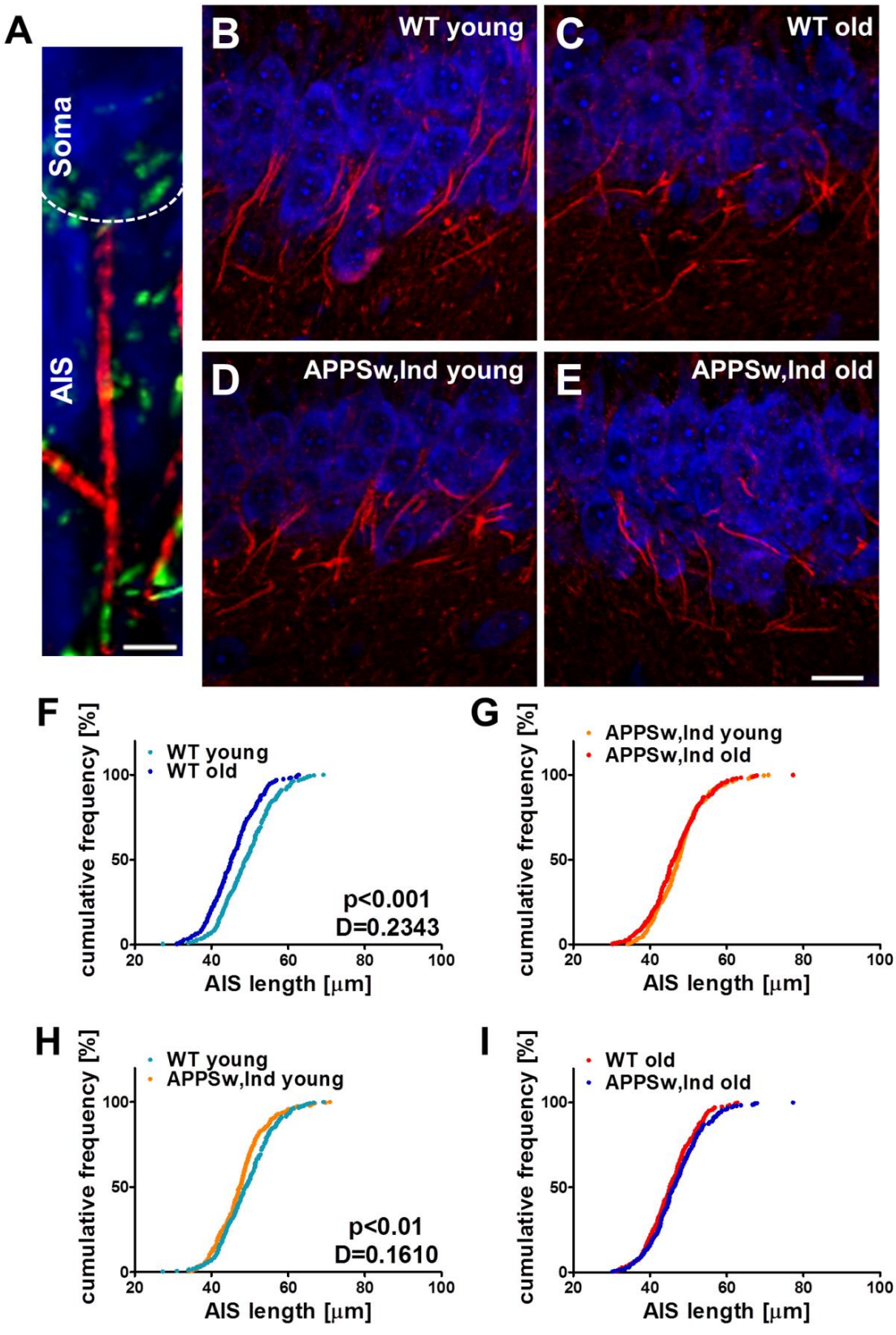

Figure 3.1 ***AIS shortens in response to normal ageing in the wild-type animals and in young TgAPPSw,Ind compared to wild-type mice at CA3 pyramidal neurons.***

The AIS [A] was immunolabeled for AnkG (red), the length was measured from the neuronal soma stained with Neurotrace stain (blue) to the first paranode labelled with Caspr (green). There was a significant age-dependent decrease ($p < 0.001$) of AIS length in the WT [B, C & F] but not in the TgAPPSw,Ind animals [D, E & G]. Young TgAPPSw,Ind animals had significantly ($p < 0.01$) shorter AIS than WT [B, D & H]. No significant change between aged animals of different genotypes was observed [C, E & I]. Twenty complete AIS arising from 20 pyramidal neurons of the CA3 were measured per animal. Length values were plotted as percentage of cumulative frequency distribution. WT young: n=14, WT old: n=12, TgAPPSw,Ind young: n=14, TgAPPSw,Ind old n=15. [A] Scale bar 5 μm. [B-E] Scale bar 20 μm.

3.3.2 Number of AIS unchanged with ageing in both wild-type and TgAPPSw,Ind animals

Next it was determined whether the overall number of AIS changed with age or between genotypes by stereologically counting the number of AIS structures in the same confocal stacks used for AIS length measurements (Figure 3.2 A-D). The number of AIS was found to be unchanged by either age ($F_{(1-51)} = 0.1382$, $p = 0.7116$) or genotype ($F_{(1-51)} = 0.9817$, $p = 0.3265$) and there was no interaction between age and genotype ($F_{(1-51)} = 3.391$, $p = 0.0714$) (Figure 3.2 E). These findings combined with those described in chapter 3.1 suggest that although ageing and genotype may have an impact on the size of AIS, this does not result in a change in the number.

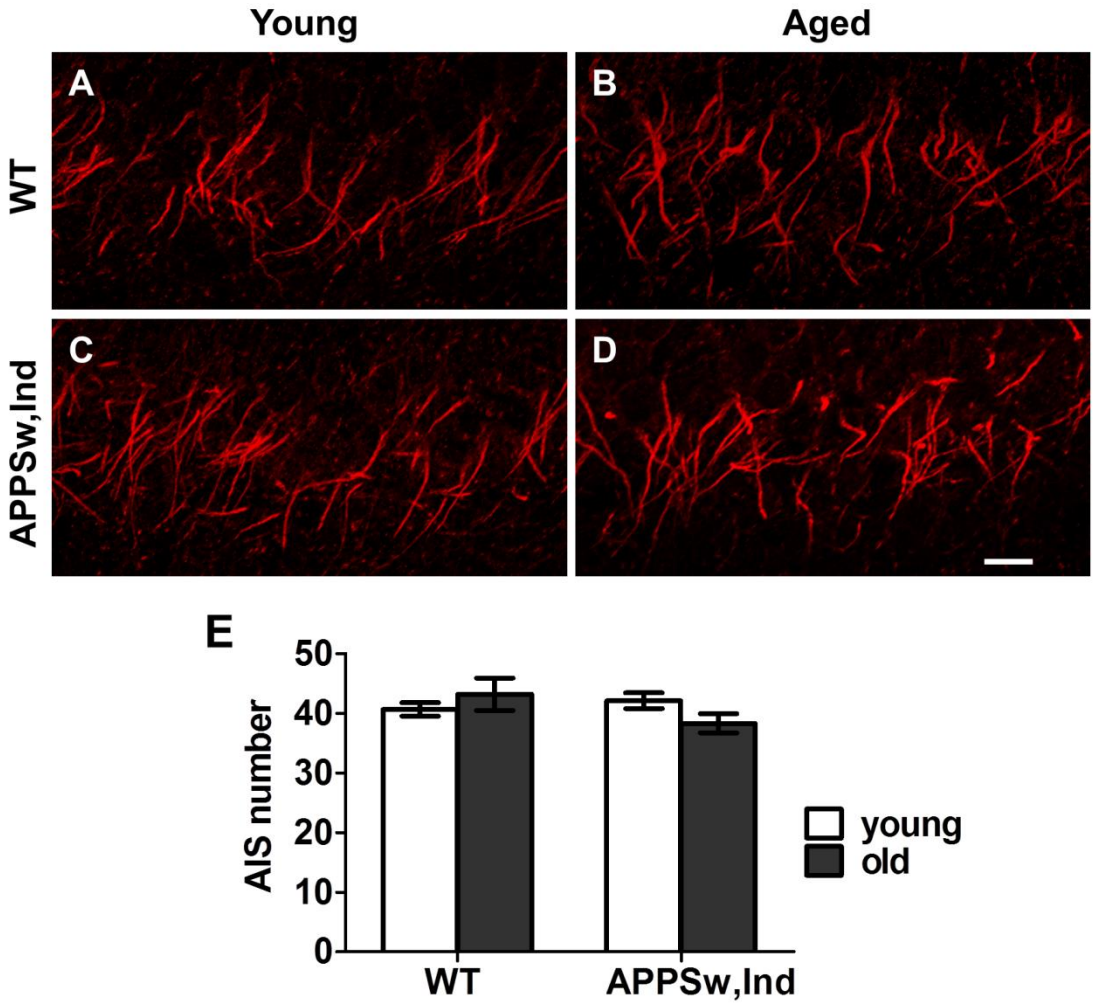

Figure 3.2 ***Number of AIS remains unchanged with ageing in both wild-type and TgAPPSw,Ind mice.*** The number of nodes was counted in 212x212x10 μm^3 confocal stacks at the CA3 region of the hippocampus immunolabeled with AnkG [A-D]. Two-way ANOVA for age and genotype did not show any significant effect of genotype or age in the number of AIS ($p > 0.05$) [E]. WT young: n=14, WT old: n=12, TgAPPSw,Ind young: n=14, TgAPPSw,Ind old n=15. Scale bar 20 μm. Graphs show mean ± SEM.

3.3.3 Changes in nodal size in response to ageing in both wild-type and TgAPPSw,Ind animals

Since the nodes of Ranvier share a similar molecular architecture to the AIS, it was predicted that alterations similar to those found at the AIS occur at the nodes of Ranvier with ageing and with Aβ. Nodal changes were examined in the stratum lacunosum moleculare of the hippocampus that contains fibres arising from the CA3 where the alterations in AIS length were observed. In general, the nodes were readily identifiable ($Na_v1.6$ immunopositive clusters bounded by pairs of Caspr immunopositive domains) in all sections and there were no obvious morphological alterations between the individual mice. The size of the nodes of Ranvier was investigated by measuring the length and the width of $Na_v1.6$ clusters (Figure 3.3). In the wild-type animals, the average length of $Na_v1.6$ cluster was found to be 1.40 ± 0.03 μm at a young age and 1.23 ± 0.03 μm in the older animals whilst in the young TgAPPSw,Ind average $Na_v1.6$ cluster length was 1.39 ± 0.03 μm and 1.21 ± 0.03 μm in the aged TgAPPSw,Ind. There was a significant reduction in the length of $Na_v1.6$ cluster in aged wild-type ($p < 0.001$, $D = 0.1806$, Figure 3.3 B) and TgAPPSw,Ind animals ($p < 0.001$, $D = 0.1931$, Figure 3.3 C) by 12.4 ± 2.8% and 13.1 ± 3.2% respectively when compared to young animals of the same genotypes. However, there was no significant effect of genotype on $Na_v1.6$ cluster length; TgAPPSw,Ind mice had similar nodal lengths when compared to wild-type mice at both a young ($p = 0.539$, $D = 0.0571$, Figure 3.3 D) and old age ($p = 0.273$, $D = 0.0753$, Figure 3.3 E).

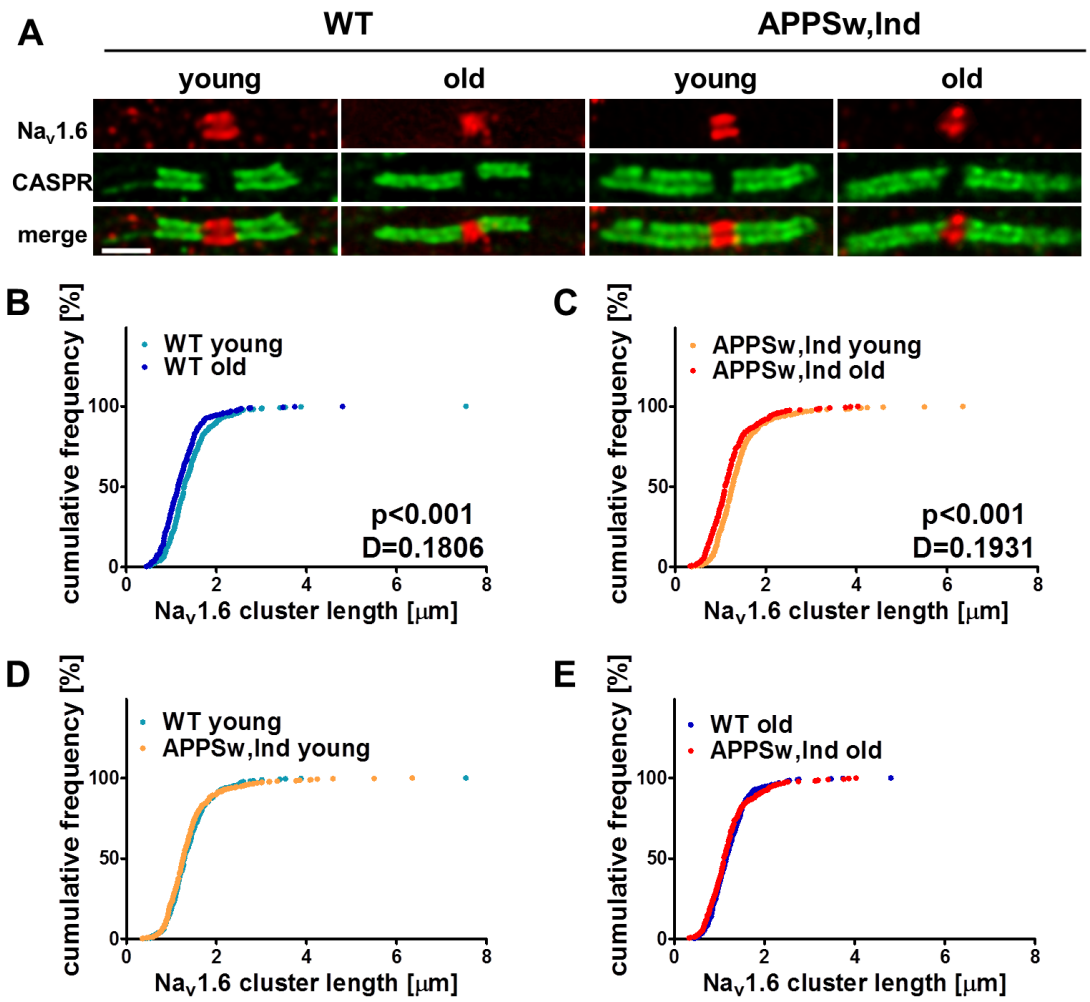

Figure 3.3 ***$Na_v1.6$ cluster length is decreased with normal ageing in wild-type and TgAPPSw,Ind mice in the stratum lacunosum moleculare of the hippocampus***. $Na_v1.6$ sodium channels (red) clusters bounded by the paranodal protein Caspr (green) outline the node of Ranvier [A]. There is a significant age-dependent decrease ($p < 0.001$) in the length [B & C] of the $Na_v1.6$ clusters in both WT and TgAPPSw,Ind animals. No effect ($p > 0.05$) of genotype was observed in either young or aged TgAPPSw,Ind animals [D & E]. The lengths of thirty $Na_v1.6$ clusters per animal were analysed and plotted as percentage of cumulative frequency distribution. WT young: n=11, WT old: n=12, TgAPPSw,Ind young: n=14, TgAPPSw,Ind old n=15. Scale bar 2 μm.

A similar pattern of changes was observed in the width of $Na_v1.6$ clusters. In the wild-type animals, the average width of $Na_v1.6$ cluster was found to be 0.91 ± 0.01 μm at a young age and 0.87 ± 0.01 μm in the older animals whilst in the young TgAPPSw,Ind average $Na_v1.6$ cluster width was 0.94 ± 0.01 μm and 0.89 ± 0.01 μm in the aged TgAPPSw,Ind. The width of the $Na_v1.6$ domain was significantly reduced in the aged wild-type ($p < 0.01$; $D = 0.1280$ Figure 3.4 A) by 4.3 ± 2.1% but not in the aged TgAPPSw,Ind animals ($p = 0.043$, $D = 0.1038$, Figure 3.4 B) when compared to the young animals of the same genotypes. Moreover, there was no significant effect of genotype on $Na_v1.6$ clusters width; TgAPPSw,Ind mice had similar $Na_v1.6$ clusters width when compared to wild-type mice at both a young ($p = 0.181$, $D = 0.0799$, Figure 3.4 C) and old age ($p = 0.257$, $D = 0.0783$, Figure 3.6 D).

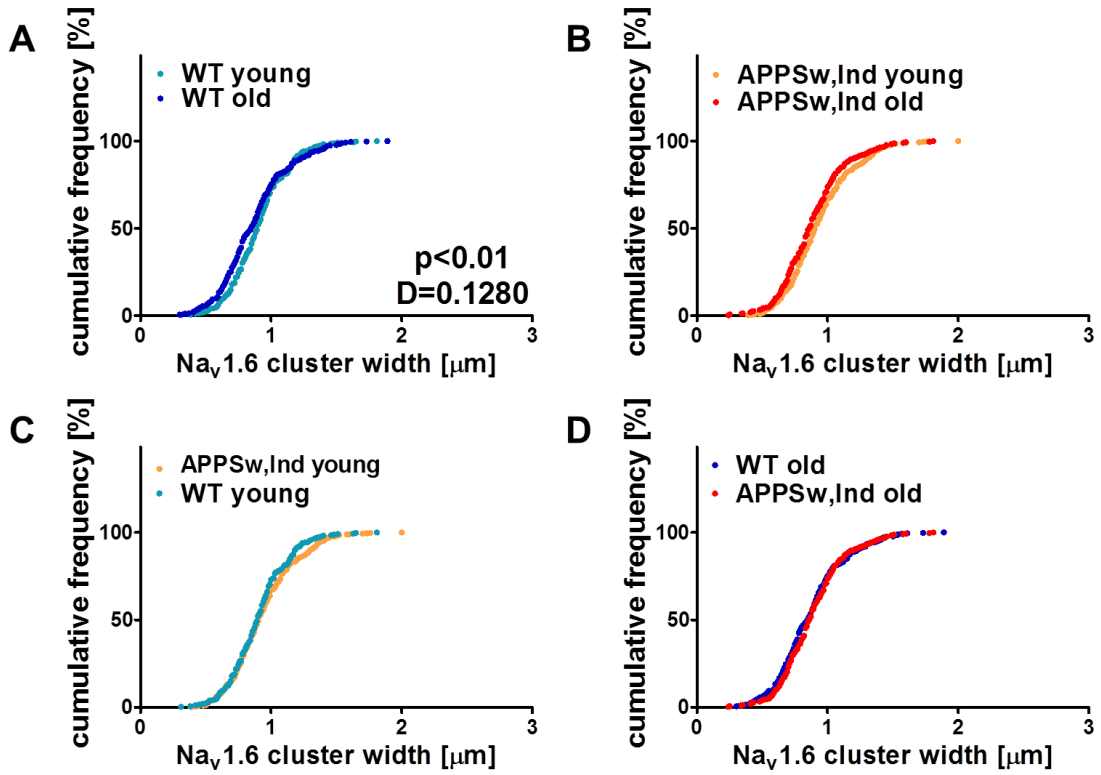

Figure 3.4 ***Na$_v$1.6 cluster width is decreased with normal ageing in wild-type mice in the stratum lacunosum moleculare of the hippocampus.*** There is a significant age-dependent decrease ($p < 0.01$) in the width of the Na$_v$1.6 clusters in WT [A] but not in TgAPPSw,Ind animals [B]. No difference ($p > 0.05$) was observed between WT and TgAPPSw,Ind either at a young [C] or old age [D]. The widths of thirty Na$_v$1.6 clusters per animal were analysed and plotted as percentage of cumulative frequency distribution. WT young: n=11, WT old: n=12, TgAPPSw,Ind young: n=14, TgAPPSw,Ind old n=15.

Since a decrease in the $Na_v1.6$ cluster length was observed in the aged animals, it was then investigated whether the paranodes were similarly altered. In the wild-type animals, the average nodal gap length was found to be 1.07 ± 0.03 μm at a young age and 0.95 ± 0.02 μm in the older animals whilst in the young TgAPPSw,Ind average nodal gap length was 1.08 ± 0.03 μm and 0.98 ± 0.02 μm in the aged TgAPPSw,Ind. It was shown that the nodal changes in $Na_v1.6$ length were mirrored in those seen with Caspr immunolabelling. Nodal gap was shown to be reduced in both the aged wild-types ($p < 0.01$, $D = 0.1528$, Figure 3.5 A) and the aged TgAPPSw,Ind ($p < 0.01$, $D = 0.1385$, Figure 3.5 B) by 11.1 ± 3.2% and 9.5 ± 3.4% respectively when compared to the young animals of the same genotypes. However, there was no significant effect of genotype on nodal gap length; TgAPPSw,Ind mice had similar nodal gap lengths when compared to wild-type mice at both a young ($p = 0.890$; $D = 0.0441$, Figure 3.5 C) and old age ($p = 0.560$, $D = 0.0583$, Figure 3. D).

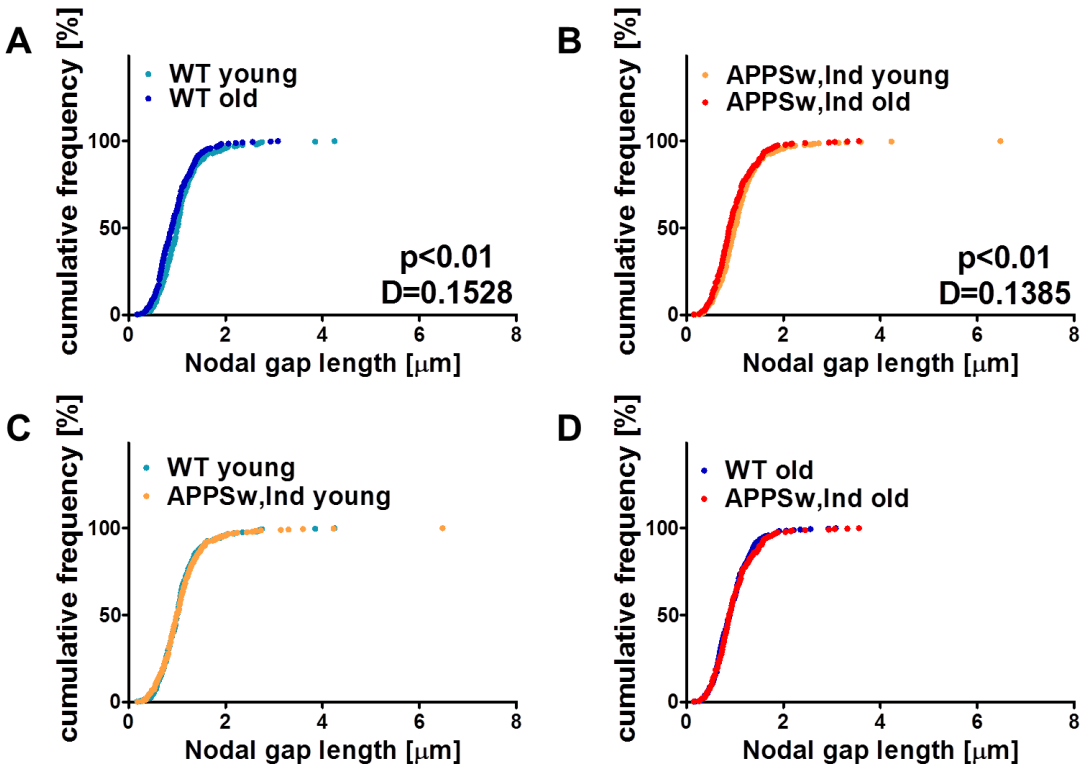

Figure 3.5 ***Nodal gap decreased with normal ageing in wild-type and TgAPPSw,Ind mice in the stratum lacunosum moleculare of the hippocampus.*** There is a significant age-dependent decrease ($p < 0.01$) in the nodal gap [A-B] in both WT and TgAPPSw,Ind animals. No difference ($p > 0.05$) was observed between WT and TgAPPSw,Ind animals either at a young [C] or old age [D]. The nodal gap of thirty nodes per animal were analysed and plotted as percentage of cumulative frequency distribution. WT young: n=11, WT old: n=12, TgAPPSw,Ind young: n=14, TgAPPSw,Ind old n=15

3.3.4 Reduction in nodal length was not associated with reduction in AIS length

To investigate whether the nodal length was associated with AIS length, for each animal the average $Na_v1.6$ cluster length was plotted against the average AIS length. There was no significant correlation between AIS and $Na_v1.6$ cluster length (Figure 3.6, $p = 0.1056$, r = 0.227). These findings suggest that the changes in the length of AIS are not associated with the changes in nodal length.

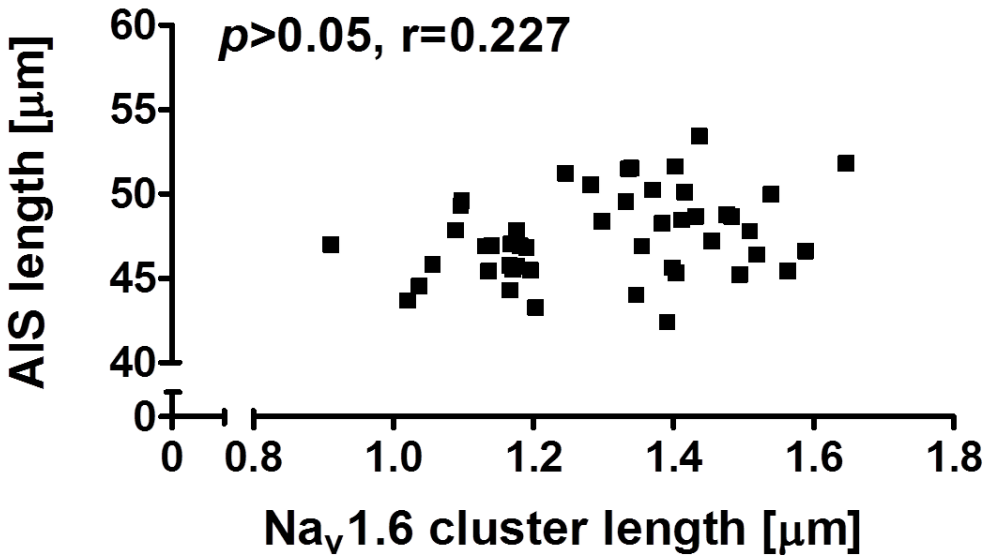

Figure 3.6 ***No association between the nodal and AIS length***. Plotting the means of $Na_v1.6$ cluster length together with the means of AIS length showed no significant association between with $Na_v1.6$ cluster length and AIS length ($p > 0.05$, Spearman's correlation analysis).

3.3.5 Number of nodes unchanged with ageing in both wild-type and TgAPPSw,Ind animals

We next determined whether the overall number of nodes of Ranvier may be changed with age or between genotypes by stereologically counting the number of nodes in confocal stacks used for nodal measurements (Figure 3.7). The number of nodes was found to be unaffected by either age ($F_{(1-48)} = 0.4556$, $p = 0.5033$) or genotype ($F_{(1-48)} = 2.368$, $p = 0.1311$) and there was no interaction between age and genotype ($F_{(1-48)} = 1.036$, $p = 0.3145$). These findings suggest that ageing or genotype whilst modifying the size of the nodes, do not result in an increase in the number.

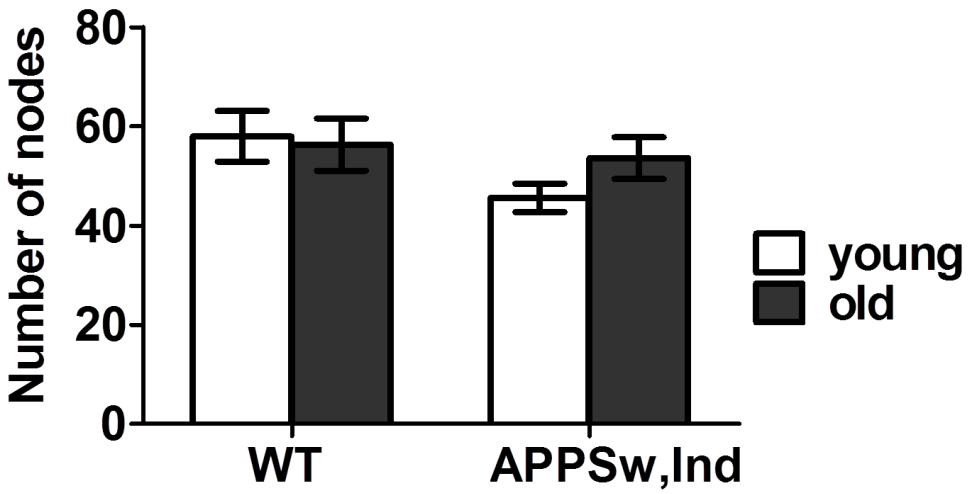

Figure 3.7 ***Number of nodes of Ranvier remains unchanged with ageing in the stratum lacunosum moleculare of the hippocampus.*** The number of nodes was stereologically counted in 47x47x10 μm^3 confocal stacks of stratum lacunosum molecular of the hippocampus Two-way ANOVA for age and genotype did not show any significant effect of genotype or age in the number of nodes ($p > 0.05$). WT young: n=11, WT old: n=12, TgAPPSw,Ind young: n=14, TgAPPSw,Ind old n=15. Graphs show mean ± SEM.

3.3.6 Myelin alterations with normal ageing in the hippocampus

Since myelin loss has been a feature of ageing and AD and myelin sheath alterations have been proposed to play a role in nodal disruption the integrity of myelin was next investigated in the stratum lacunosum moleculare; the same region where age-related decrease of nodal length was observed. This was achieved with immunolabelling for myelin basic protein (MBP) (Figure 3.8 A-D). Both the percentage area occupied by MBP as a measure for the myelinated fibers population and the intensity of MBP staining as a measure for the MBP content in the myelinated fibers were assessed in young (n=14) and old (n=12) wild-type mice and in young (n=14) and old (n=15) TgAPPSw,Ind mice. Notably, the area occupied by MBP staining was found to be reduced by age (p = 0.0234, $F_{(1-51)}$ = 5.463, Figure 3.8 E) but it was not affected by genotype (p = 0.1300, $F_{(1-51)}$ = 2.369) and there was not a significant overall interaction between age and genotype (p = 0.1741, $F_{(1-51)}$ = 1.900). *Post-hoc* analysis showed that there is a significant decrease in the percentage area occupied by MBP in the aged wild-type ($p < 0.05$, $|t| = 2.559$) but not in the aged TgAPPSw,Ind ($p > 0.05$, $|t| = 0.6969$) when compared to younger animals. Moreover, there was no significant difference between wild-types and TgAPPSw,Ind either at a young ($p > 0.05$, $|t| = 2.046$) or old age ($p > 0.05$, $|t| = 0.1145$).

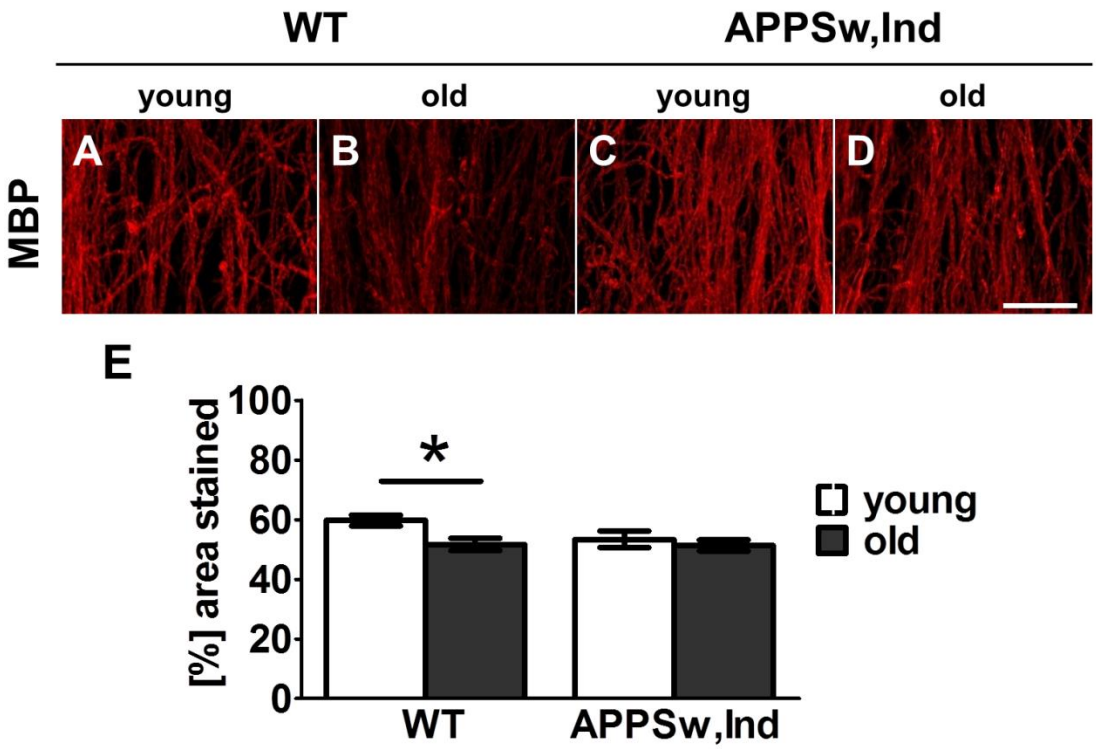

Figure 3.8 ***Alterations of myelin integrity in response to ageing in the stratum lacunosum moleculare of the hippocampus***. Myelin integrity was assessed in the stratum lacunosum moleculare of the hippocampus using myelin basic protein (MBP) immunostaining [A-D]. There was a significant overall effect of age in percentage area occupied by MBP ($p < 0.05$). *Post-hoc* testing showed that myelin density was significantly reduced ($p < 0.05$) in aged WT when compared to young WT mice. There was no significant difference ($p > 0.05$) in myelin density with increased Aβ in old TgAPPSw,Ind as compared to young TgAPPSw,Ind [I]. WT young: n=14, WT old: n=12, TgAPPSw,Ind young: n=14, TgAPPSw,Ind old n=15. *: $p < 0.05$. Graphs show mean ± SEM. Scale bar 20μm.

Similarly, the intensity of MBP staining was significantly reduced by age (p = 0.0124, $F_{(1-51)}$ = 6.717) but not by genotype (p = 0.5329, $F_{(1-51)}$ = 0.3942) and no significant interaction between age and genotype (p = 0.2760, $F_{(1-51)}$ = 1.213) was observed (Appendix A1 A). *Post-hoc* analysis showed that a significant age-related decrease in the intensity of MBP staining in the wild-type animals ($p < 0.05$, $|t| = 2.54$) but not in the TgAPPSw,Ind ($p > 0.05$, $|t| = 1.084$). Moreover, there was no significant difference between wild-types and TgAPPSw,Ind either at a young ($p > 0.05$, $|t| = 1.213$) or old age ($p > 0.05$, $|t| = 0.0337$).

Detailed observation of MBP staining revealed morphological alterations in the form of myelin bulbs that share similarities with the myelin sheath balloons observed in normal ageing. The number of myelin bulbs was stereologically counted in the same confocal stacks used for MBP measurements (Figure 3.9 A-D). Data showed a significant increase in the number of myelin bulbs in the aged animals (p = 0.0071, $F_{(1-51)}$ = 7.870) an effect which was independent of genotype ($F_{(1-51)}$ = 0.6524, p = 0.4229) whilst no significant interaction between age and genotype ($F_{(1-51)}$ = 0.1033, p = 0.7492) was observed (Figure 3.9 E). These findings suggest that ageing has an effect in myelin integrity and may drive structural alterations at the myelin sheath.

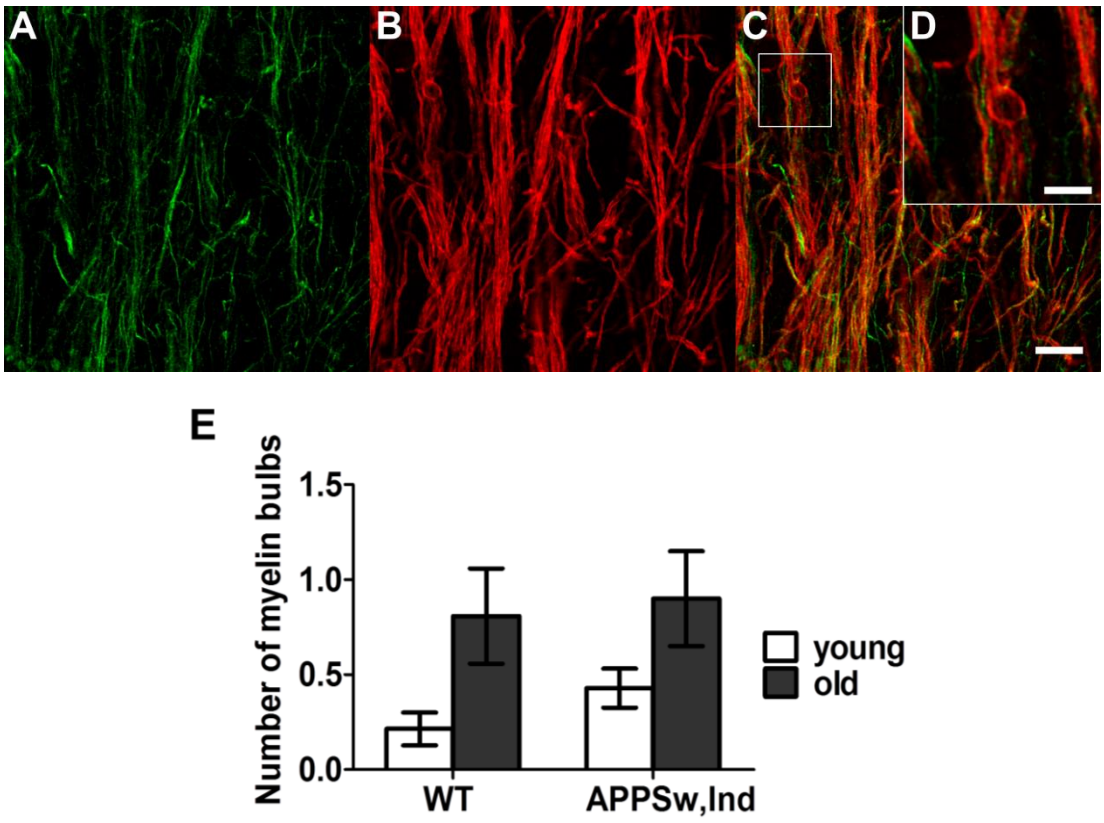

Figure 3.9 ***Number of myelin bulbs increased with age in the stratum lacunosum moleculare of the hippocampus.*** The number of myelin bulbs was stereologically determined in 76.8x76.8x10 μm^3 confocal stacks double stained for total neurofilament [A] and MBP [B] imaged at the stratum lacunosum moleculare of the hippocampus. There was a significant increase in the number of myelin bulbs [C & D] with age ($p < 0.05$) [E] but no significant difference between the genotypes was observed at any age. WT young: n=14, WT old: n=12, TgAPPSw,Ind young: n=14, TgAPPSw,Ind old n=15. [A-C] Scale bar 10 μm, [D] Scale bar 5 μm. Graphs show mean ± SEM.

3.3.7 No evidence of axonal damage with normal ageing in the hippocampus of both wild-type and TgAPPSw,Ind animals

Given that loss of axons may be responsible for the observed age-related myelin alteration, therefore the integrity of axons was examined in the same region. This was achieved with immunolabelling for total neurofilament (SMI312) (Figure 3.10 A-D). The percentage area occupied by total neurofilament and the intensity of SMI312 staining was assessed in young (n=13) and old (n=12) wild-type mice and in young (n=14) and old (n=15) TgAPPSw,Ind mice. It was shown that there was no significant effect of age (p = 0.4568, $F_{(1-50)}$ = 0.5624,) or of genotype (p = 0.3159, $F_{(1-50)}$ = 1.026) and no significant overall interaction between age and genotype (p = 0.9843, $F_{(1-50)}$ = 0.0004) was observed in the percentage area occupied by total neurofilament (Figure 3.10 E). Similarly, no significant effect of age (p = 0.276, $F_{(1-50)}$ = 1.212,) or of genotype (p = 0.8669, $F_{(1-50)}$ = 0.0284) and no significant overall interaction between age and genotype (p = 0.8158, $F_{(1-50)}$ = 0.0548) was observed in the intensity of SMI312 staining (Appendix A.1 B). This data suggests that although there is evidence of MBP staining loss in response to ageing this is not a result of axonal loss.

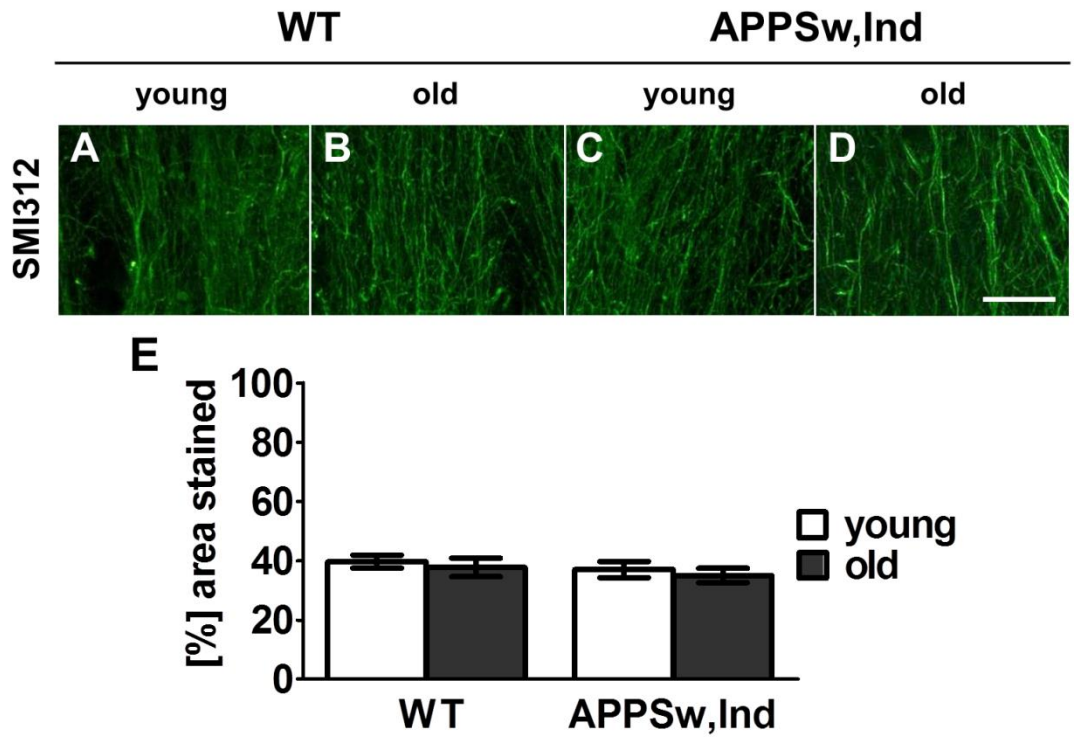

Figure 3.10 ***No alterations in axonal integrity in response to ageing in the stratum lacunosum moleculare of the hippocampus in both wild-type and TgAPPSw,Ind animals.*** Axonal integrity was assessed in the stratum lacunosum moleculare of the hippocampus using total neurofilament (SMI312) immunostaining [A-D]. Two-way ANOVA for age and genotype did not show any significant effect of genotype or age on percentage area occupied by total neurofilament ($p > 0.05$) [I]. WT young: n=13, WT old: n=12, TgAPPSw,Ind young: n=14, TgAPPSw,Ind old n=15. Graphs show mean ± SEM. Scale bar 20μm.

3.3.8 No change in levels of myelin basic protein and total neurofilament with ageing in both wild-type and TgAPPSw,Ind animals

Levels of myelin basic protein (MBP) and total neurofilament were also examined in tissue homogenates from the hippocampus to determine if there are changes in protein levels overall. Western blotting for MBP showed four bands at 21.5, 18.5, 17 and 14 KDa (Figure 3.11 A), all four bands were quantified. Western blotting for total neurofilament detected with the SMI312 antibody showed a band at 200 KDa (Figure 3.11 A), which was quantified. There was no significant effect of age (p = 0.995, $F_{(1-50)}$ = 0.00003) or genotype (p = 0.7337, $F_{(1-50)}$ = 0.1171) and no significant interaction between age and genotype (p = 0.2872, $F_{(1-50)}$ = 1.157) in the levels of MBP (Figure 3.11 B). Similarly, there was no significant effect of age (p = 0.5530, $F_{(1-50)}$ = 0.3567) or genotype (p = 0.2337, $F_{(1-50)}$ = 1.453) and no significant interaction between age and genotype ($F_{(1-50)}$ = 0.0015, p = 0.9694) in the levels of total neurofilament (Figure 3.11 C).

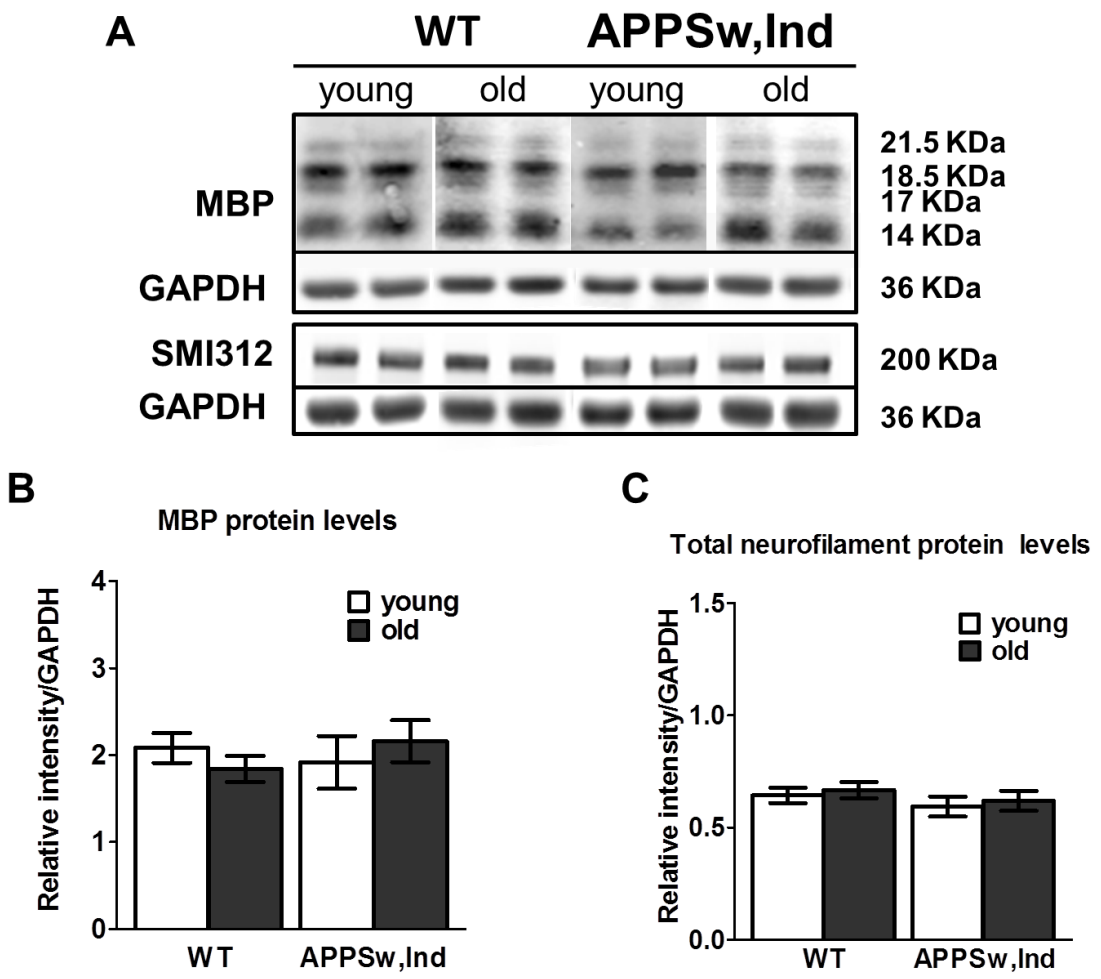

Figure 3.11 ***No change in levels of myelin basic protein and total neurofilament with ageing.*** Total levels of MBP and total neurofilament levels were assessed in tissue homogenates of the hippocampus using western blotting [A]. It was shown that there was no significant overall effect of age or genotype ($p > 0.05$) in the levels of MBP [B] or total neurofilament [C]. WT young: n=14, WT old: n=12, TgAPPSw,Ind young: n=13, TgAPPSw,Ind old n=15.Graphs show mean ± SEM.

3.3.9 Increased presynaptic terminal density in young TgAPPSw,Ind compared to wild-type mice and age-dependent decrease in TgAPPSw,Ind mice.

Synaptic loss is observed in both normal ageing and in AD. Synaptic input is proposed to play a role in the plasticity of AIS length, therefore presynaptic terminal density was assessed in the CA3 region of the hippocampus where the alterations in AIS length were found using immunolabelling for synaptophysin (Figure 3.12 A-D). The percentage area occupied by presynaptic terminals was assessed, as a measure of presynaptic terminal density, in young and old TgAPPSw,Ind and wild-type mice. There was a significant effect of age ($p = 0.0227$, $F_{(1-52)} = 5.514$) and of genotype ($p = 0.0135$, $F_{(1-52)} = 6.541$) in the density of presynaptic terminals. There was however no interaction between age and genotype ($p = 0.0227$, $F_{(1-52)} = 5.514$). Notably, *post-hoc* analysis showed that there is a significant decrease postsynaptic terminal density in the aged TgAPPSw,Ind mice ($p < 0.05$, $|t| = 2.701$) but not in wild-types ($p > 0.05$, $|t| = 0.9484$) when compared to young animals of the same genotype (Figure 3.12 E). Moreover, there was a significant increase in presynaptic terminal density in the young ($p < 0.05$, $|t| = 2.507$) but not in the aged ($p > 0.05$, $|t| = 0.8161$) TgAPPSw,Ind mice when compared to wild-type animals of the same age (Figure 3.12 E). These findings suggest that synaptic density is different between the wild-types and the TgAPPSw,Ind and that is reduced in response to ageing.

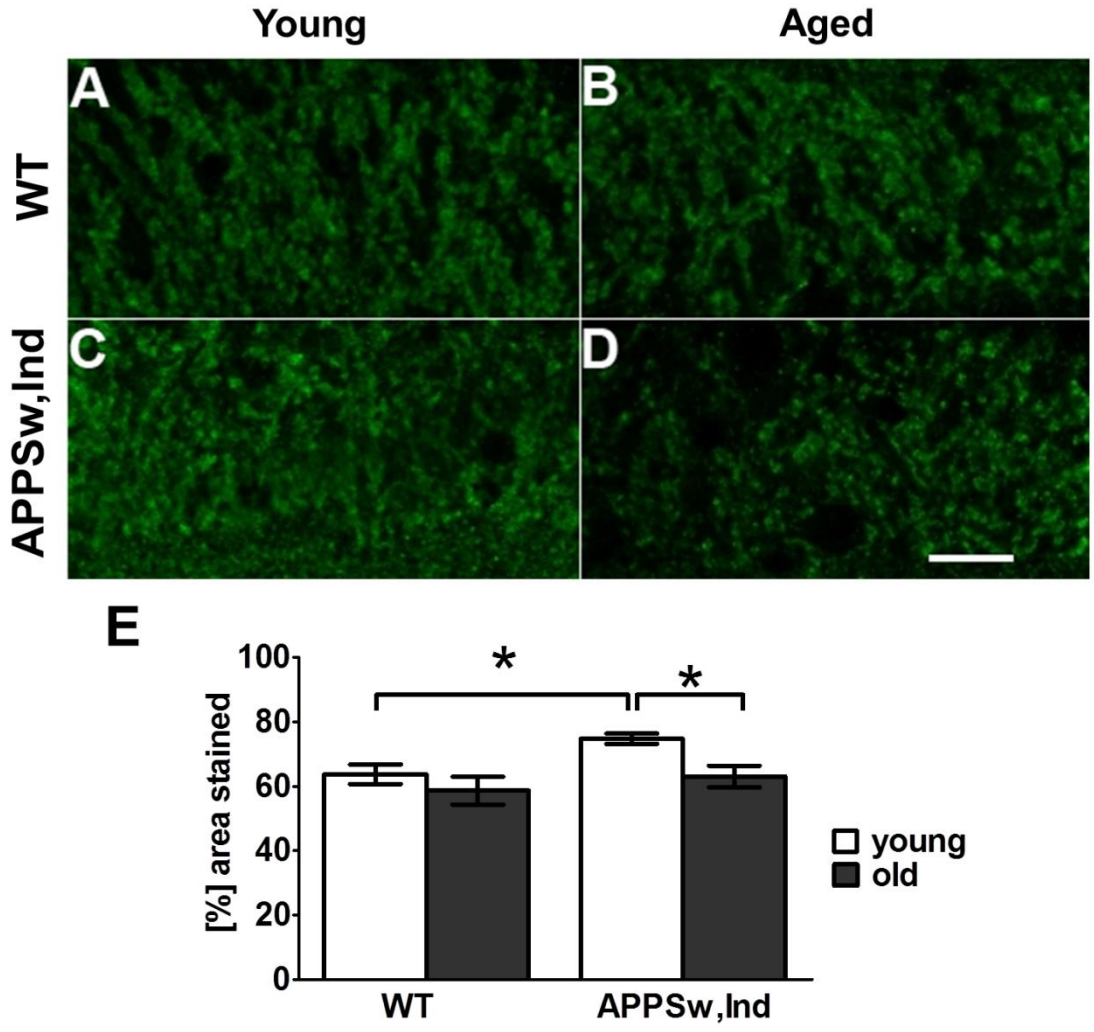

Figure 3.12 ***Increased presynaptic terminal density in young TgAPPSw,Ind compared to wild-type mice and age-dependent decrease in TgAPPSw,Ind mice.*** Presynaptic terminal density was assessed in the CA3 region of the hippocampus using immunolabelling for synaptophysin [A-D]. There was a significant effect ($p < 0.05$) of age and genotype in the area occupied by presynaptic terminals [E]. The young TgAPPSw,Ind mice have more presynaptic terminals when compared to WT of the same age ($p < 0.05$) while the density of presynaptic terminals in the aged TgAPPSw,Ind mice is significantly reduced in comparison with young animal of the same genotype ($p < 0.05$). WT young: n=14, WT old: n=13, TgAPPSw,Ind young: n=14, TgAPPSw,Ind old n=15. *: $p < 0.05$. Graphs show mean ± SEM. Scale bar 20μm.

3.3.10 Increased Aβ deposition in the stratum lacunosum moleculare of the hippocampus of aged TgAPPSw,Ind mice.

Aβ deposition at the hippocampus was also examined in the animals included in the study in order to confirm the Aβ load since the collected data so far did not show and difference between the aged wild-type and TgAPPSw,Ind animals. Deposition of β-amyloid was localised to the hippocampus and particularly in the stratum lacunosum moleculare of TgAPPSw,Ind mice where it was analysed (Appendix A2 A-D). There was no Aβ deposition in the wild-type animals. The extent of Aβ immunostaining was significantly increased in the TgAPPSw,Ind animals (Appendix A2 E) compared to the wild-types ($p = 0.0007$, $F_{(1-50)} = 13.17$). Moreover, the extent of Aβ load in the stratum lacunosum was significantly increased with age ($p = 0.0258$, $F_{(1-50)} = 5.28$). There was also a significant interaction between age and genotype ($p = 0.0239$, $F_{(1-50)} = 5.42$). *Post-hoc* analysis showed that the aged APPSw,Ind have a greater extent of Aβ in the stratum lacunosum moleculare occupied by β-amyloid when compared to young TgAPPSw,Ind ($p < 0.01$, $|t| = 3.401$) and aged wild-types ($p < 0.001$, $|t| = 4.201$). There was no significant difference between young and aged wild-type mice ($p > 0.05$, $|t| = 0.02902$) or young wild-type and young TgAPPSw,Ind mice ($p > 0.05$, $|t| = 0.922$). These findings confirm the aged dependent nature of Aβ deposition in the TgAPPSw,Ind mice.

3.3.11 Increased human amyloid precursor protein (hAPP) and monomeric Aβ levels in the hippocampus of aged TgAPPSw,Ind mice.

Total levels of human amyloid precursor protein (hAPP) and levels Aβ species were also assessed in tissue homogenates to determine whether they are increased with age. Human APP, β-amyloid trimer and Aβ monomer were detected only in the TgAPPSw,Ind mice and not in wild-type mice. Western blotting for hAPP, β-amyloid trimer and Aβ monomer showed bands at 100, 12 and 4 KDa respectively (Figure 3.13 A). Human APP levels were significantly increased in the ages TgAPPSw,Ind mice compared to the young (Figure 3.13 B, $p = 0.0016$, $|t| = 3.567$). Aβ trimer levels were unchanged in the aged TgAPPSw,Ind mice compared to the young (Figure 3.13 B, $p = 0.2519$, $|t| = 1.174$). Monomeric β-amyloid levels were significantly increased in the aged TgAPPSw,Ind mice when compared to young animals (Figure 3.13 B, $p = 0.0343$, $|t| = 2.245$). These findings show that both the expression of the hAPP and monomeric Aβ are elevated in the aged TgAPPSw,Ind mice. Thus the work indicates that despite the elevated levels of hAPP and Aβ in the aged TgAPPSw,Ind mice and their absence from the wild-type animals there is minimal effect of TgAPPSw,Ind genotype on nodal and AIS length, and gross myelin and axonal integrity.

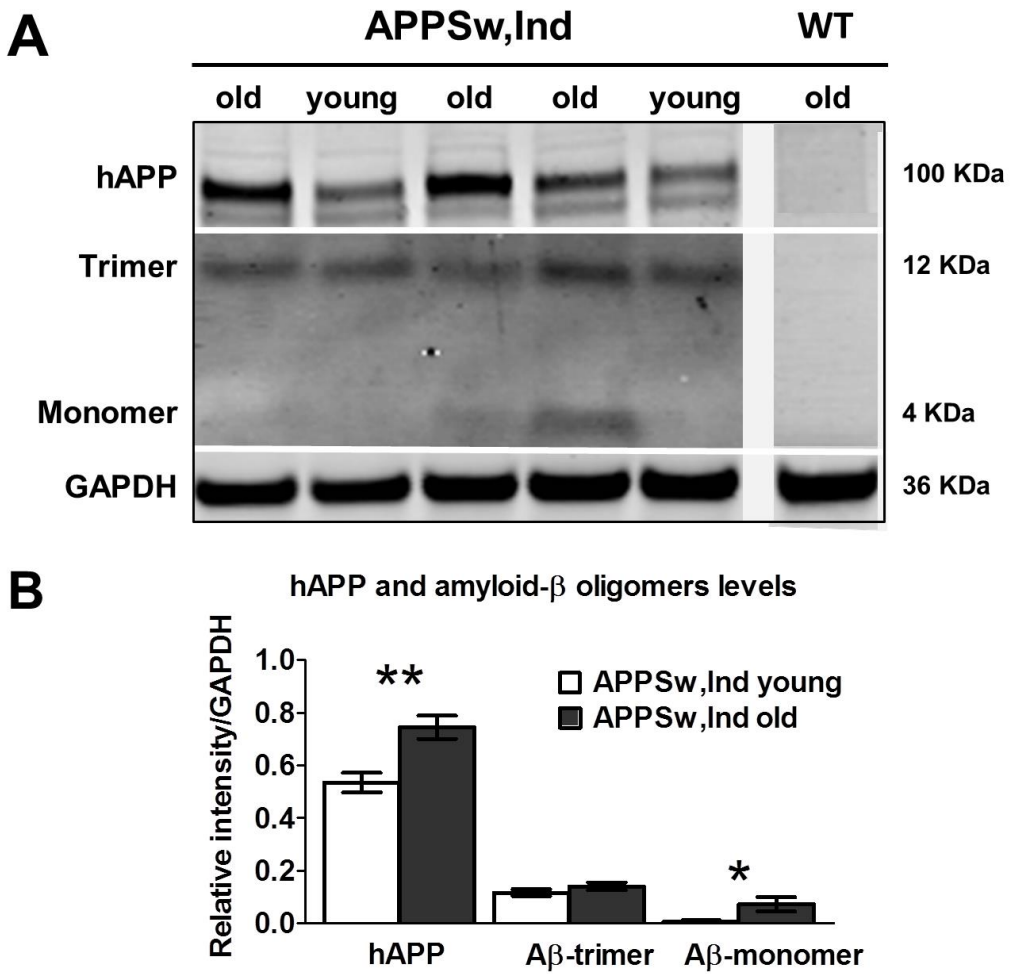

Figure 3.13 ***Increased hAPP and monomeric β-amyloid levels in aged TgAPPSw,Ind mice.*** Human amyloid precursor protein (hAPP) and monomeric amyloid levels where assessed in tissue homogenates of the hippocampus using western blots [A]. In the TgAPPSw,Ind there was a significant increase of hAPP ($p < 0.01$) and monomeric Aβ ($p < 0.05$) with ageing. Aβ trimer levels were unchanged. TgAPPSw,Ind young: n=12, TgAPPSw,Ind old: n=14. **: $p < 0.01$, *: $p < 0.05$. Graphs show mean ± SEM.

3.3.12 Working memory is not affected in aged wild-type or TgAPPSw,Ind mutant animals

Since the AIS and the nodes of Ranvier have an important role in neuronal function it was predicted that the alterations observed in these structures would have a functional impact on spatial working memory performance. Spatial working memory performance of young and old TgAPPSw,Ind mutant and wild-type mice was examined in the eight-arm radial arm maze task. Data for number of novel arm entries in the first eight entries, number of errors were analysed.

All groups significantly increased the number of novel arm entries in the first eight entries across the training period ($p < 0.0001$, $F_{(7-364)} = 33.987$, Figure 3.14 A-D) and by block 5 (a trial block is two days) performed significantly better (WT young, $p = 0.0012$; WT old, $p = 0.0025$; TgAPPSw,Ind young, $p = 0.0004$; TgAPPSw,Ind, $p = 0.0292$) than chance (5.3 entries) suggesting that all groups learn the task. However, there was no significant effect of age ($p = 0.609$, $F_{(1-52)} = 0.265$, Figure 3.14 A and B) or genotype ($p = 0.080$, $F_{(1-52)} = 3.180$, Figure 3.14 C and D) and no significant interaction between age and genotype ($p = 0.129$, $F_{(1-52)} = 2.376$) observed in the number of novel arm entries in the first eight entries. Similarly, the number of errors was significantly decreased across the training trials in all groups period ($p < 0.0001$, $F_{(7-364)} = 24.137$, Figure 3.15 A-D). Similar to the novel arm entries results, it was shown that there was no significant difference between the different age groups ($p = 0.716$, $F_{(1-52)} = 0.133$, Figure 3.15 A and B) or between the different genotypes ($p = 0.781$, $F_{(1-52)} = 0.078$, Figure 3.15 C and D) and no significant interaction between age and genotype ($p = 0.781$, $F_{(1-52)} = 0.078$) was observed in the number of errors.

These findings suggest that despite the observed alterations in the AIS and the nodes of Ranvier described earlier in this chapter in response to ageing or genotype, spatial working memory performance is not affected.

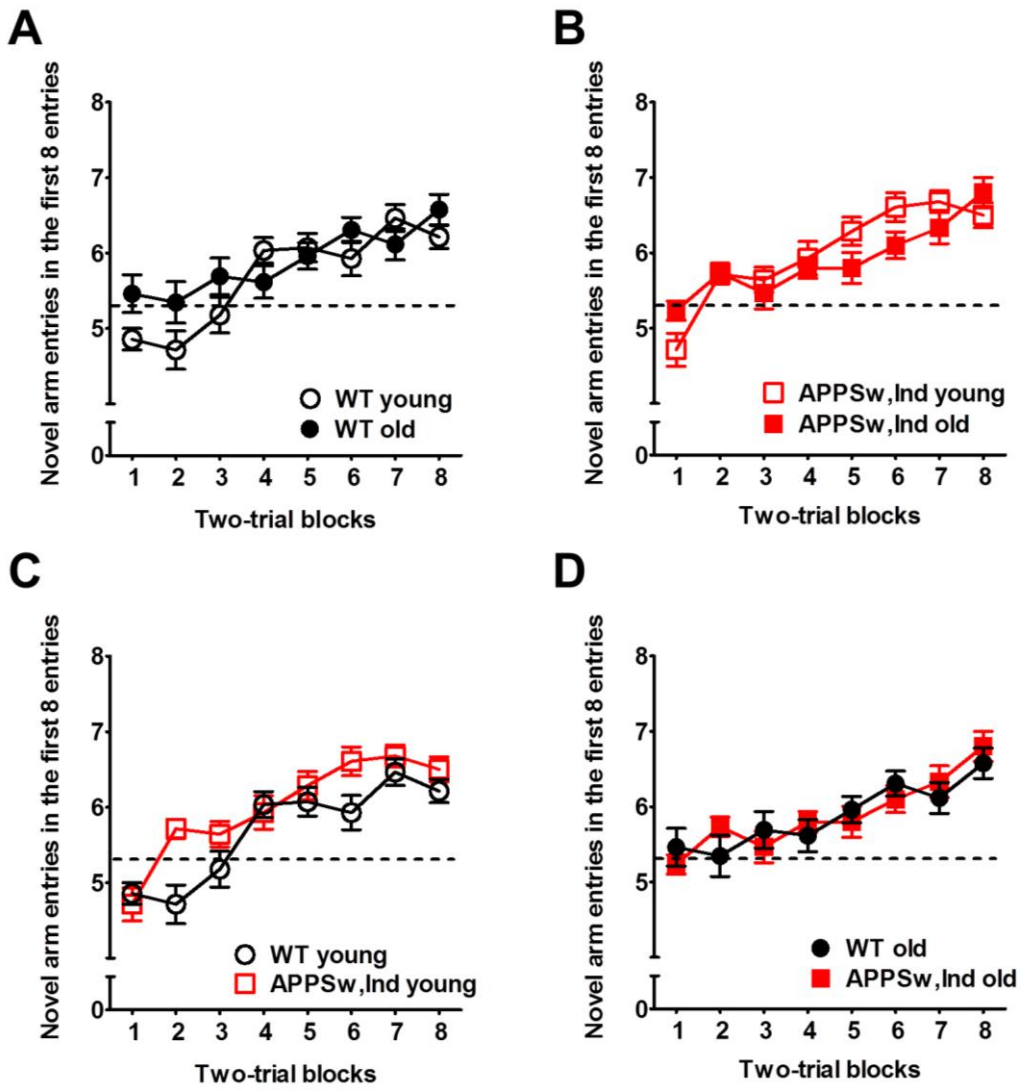

Figure 3.14 ***Number of novel arm entries is not changed in aged TgAPPSw,Ind and wild-type mice.*** All groups significantly increased ($p < 0.05$) the number of novel arm entries in the first eight entries across the training period of 16 days (a trial block is two days). By trial-block 4 the mice have learned the task and perform above chance (5.3 entries, dash line). Overall the aged WT [A] and TgAPPSw,Ind animals [B] make the same number of novel entries when compared to young animals of the same genotype ($p > 0.05$). Moreover, there was no significant difference ($p > 0.05$) in the number of novel arm entries between WT and TgAPPSw,Ind mice at either age [C & D]. WT young: n=14, WT old: n=13, TgAPPSw,Ind young: n=14, TgAPPSw,Ind old: n=15.Graphs show mean ± SEM.

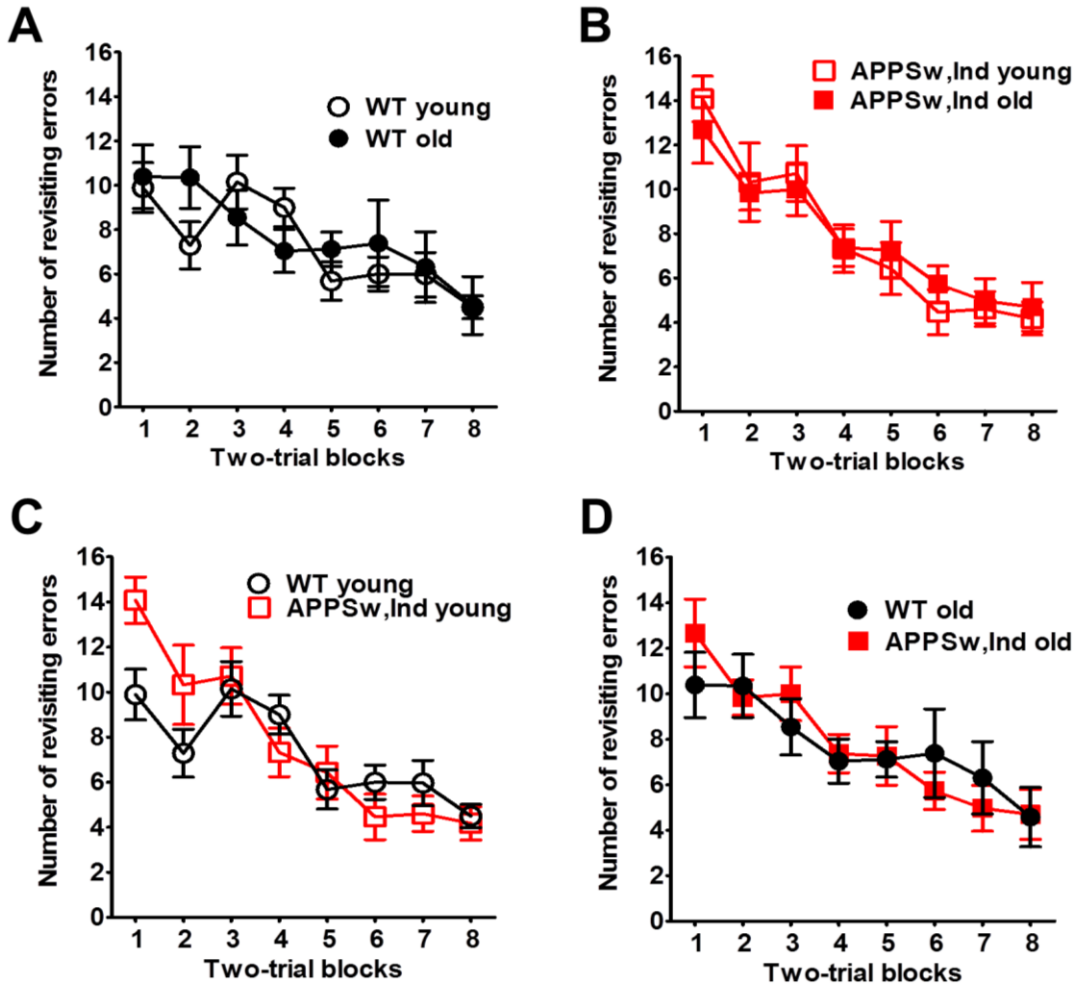

Figure 3.15 ***Number of revisiting errors is not changed in aged TgAPPSw,Ind and wild-type mice.*** All groups significantly decreased ($p < 0.05$) the number of revisiting errors across the training period of 16 days (a trial block is two days). Overall the aged WT [A] and TgAPPSw,Ind animals [B] make the same number of errors when compared to young animals of the same genotype ($p > 0.05$). Moreover, there was no significant difference ($p > 0.05$) in the number of errors between WT and TgAPPSw,Ind mice at either age [C & D]. WT young: n=14, WT old: n=13, TgAPPSw,Ind young: n=13, TgAPPSw,Ind old: n=15.Graphs show mean ± SEM.

3.3.13 Working memory performance of young and aged wild-type and TgAPPSw,Ind animals in the 8-arm radial arm maze is not associated with the nodal or AIS length

In order to investigate whether the measures of nodal length and AIS length can be related to working memory performance in the 8-arm radial arm maze, for each animal the average $Na_v1.6$ cluster and AIS length was plotted against the number of revisiting errors at trial block 8 (Figure 3.16 A and B). There was no significant correlation between the number of revisiting errors and the $Na_v1.6$ cluster length (Figure 3.16 A, p = 0.9467, r = 0.009909) or the AIS length (Figure 3.16 A, p = 0.3862, r = 0.1192). These findings suggest that the observed changes in the length of the AIS or the nodes may not be directly related to the working memory performance.

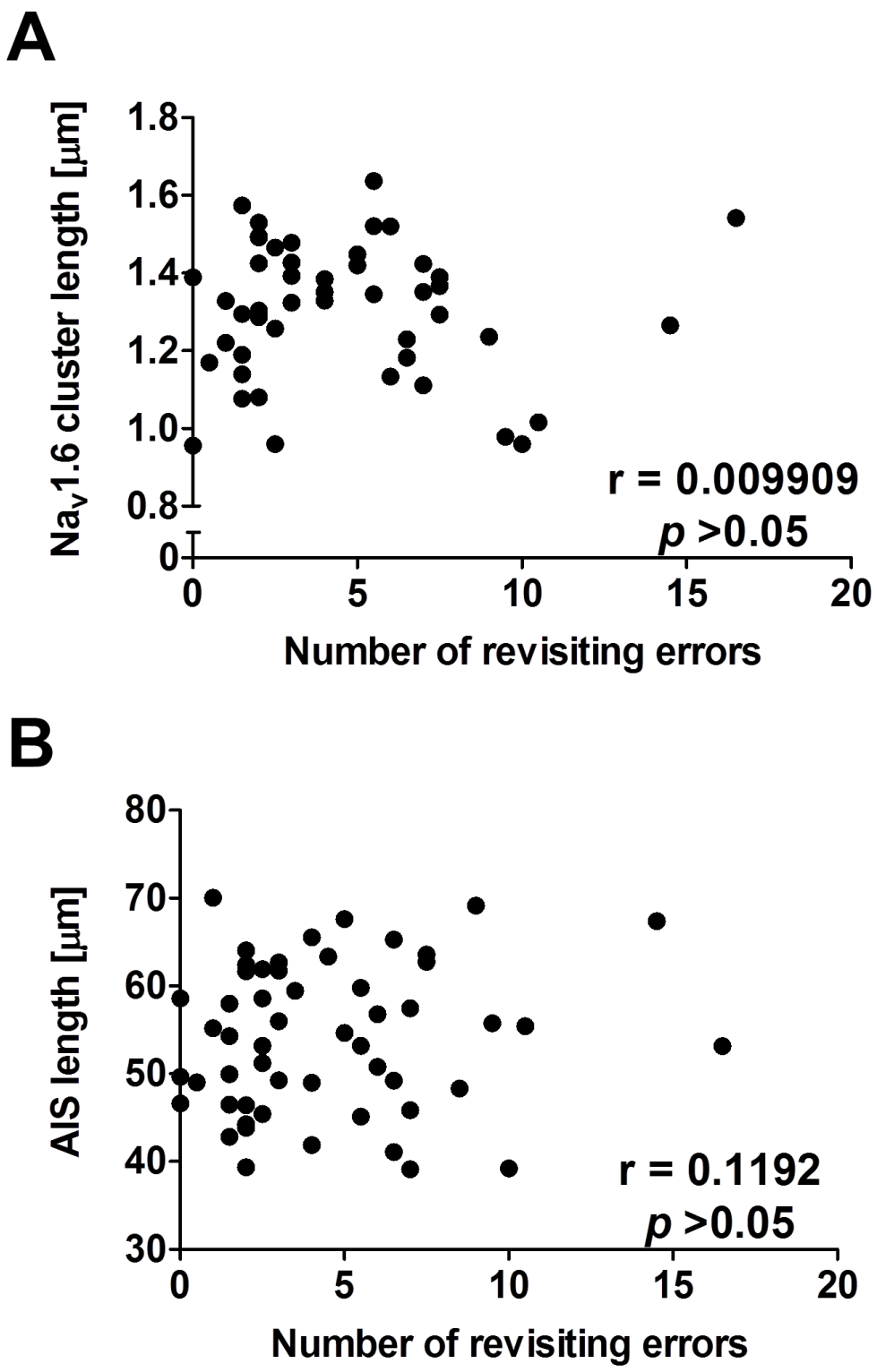

Figure 3.16 ***Working memory performance in the 8-arm radial arm maze is not associated with the nodal or AIS length.*** Plotting the number of revisiting errors (trial block 8) together with the means of $Na_v1.6$ cluster length [A] and AIS length [B} showed no significant association ($p > 0.05$, Spearman's correlation analysis).

3.3.14 Working memory performance of young and aged TgAPPSw,Ind animals in the 8-arm radial arm maze is not associated the hippocampal load of monomeric Aβ

In order to investigate working memory performance in the 8-arm radial arm maze is related to the levels of Aβ in the hippocampus of the TgAPPSw,Ind mice for each animal the protein level of monomeric Aβ was plotted against the number of revisiting errors at trial block 8 (Figure 3.17). There was no significant correlation between the number of revisiting errors and the monomeric Aβ protein levels (p = 0.5337, r = 0.1278). This data suggests there might not be a relation between Aβ load and working memory performance in the 8-arm radial arm maze.to the working memory performance.

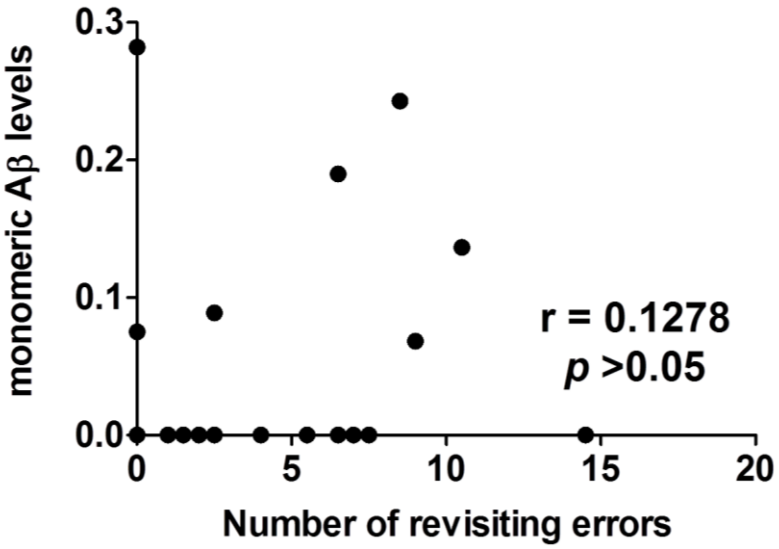

Figure 3.17 ***Working memory performance in the 8-arm radial arm maze is not associated with Aβ levels in the TgAPPSw,Ind mice.*** Plotting the number of revisiting errors (trial block 8) together with the levels of monomeric showed no significant association (p > 0.05, Spearman's correlation analysis).

3.3.15 Summary of results

The following table (Table 3.3) summarises the findings described in the present chapter.

Table 3.2 Summary of results

Feature examined	Findings
AIS length	↓ in aged WT compared to young ↓ in young APPSw,Ind compared to WT
AIS number	↔
$Na_v1.6$ cluster length	↓ in aged WT and APPSw,Ind compared to young of the same genotype
$Na_v1.6$ cluster width	↓ in aged WT compared to young
Nodal gap length	↓ in aged WT and APPSw,Ind compared to young of the same genotype
Nodal number	↔
MBP (% area)	↓ in aged WT compared to young
Number of myelin bulbs	↑ in aged animals compared to young
SMI312 (% area)	↔
MBP and SMI312 protein levels	↔
Synaptophysin (% area)	↑ increased in young APPSw,Ind compared to WT ↓ decrease in aged APPSw,Ind compared to young
Aβ deposition	↑ increased in aged APPSw,Ind compared to young
hAPP levels	↑ increased in aged APPSw,Ind compared to young
Aβ monomer levels	↑ increased in aged APPSw,Ind compared to young
Novel arm entries in the first 8 entries & number of revisiting errors *(Working memory)*	↔

Note: ↑ increase, ↓ decrease, ↔ unchanged

3.4 Discussion

It is known that with both normal ageing and AD neuronal networks are compromised particularly within the hippocampus and this has been linked with cognitive decline (Rosenzweig and Barnes, 2003; Geula, 1998; Celone et al., 2006; Kanak et al., 2013). The AIS and the nodes of Ranvier are specialized regions within the myelinated axons responsible for action potential initiation and propagation. Disruption to the AIS and nodes of Ranvier integrity could have critical effects on nervous system function. This study demonstrates that the structure of the AIS and nodes of Ranvier are markedly affected with age. A significant reduction in the length of nodes of Ranvier was demonstrated in aged wild-type and TgAPPSw,Ind mice. In addition, the length of AIS was significantly reduced in the aged wild-type animals while the young TgAPPSw,Ind had significantly shorter AIS than the wild-type mice of the same age. In contrast to the original hypothesis these effects on the nodes and AIS were not influenced by the presence of amyloid-β.

It has previously been shown that both the AIS and nodes of Ranvier are sensitive to different types of brain injury (Schafer et al., 2009; Hinman et al., 2006; Hinman et al., 2013; Reimer et al., 2011). Thus it was hypothesised that ageing would also have an effect on these structures. In support of this hypothesis marked alterations in AIS length and nodes of Ranvier were demonstrated, although there were no changes in their number. Ageing appears to reduce the AIS length by 7.4% in the wild-type mice. Here, the changes in AIS length are observed in the CA3 of the hippocampus, a region that which plays an important role in hippocampal circuitry as it is suggested that information enters the hippocampus via projections of the entorhinal

cortex to the dentate gyrus that in turn projects on the CA3 (Gilbert and Brushfield, 2009). Similar findings come from a rat model of mild traumatic brain injury (mTBI) induced by a blast wave where there was a 1-4% decrease in AIS length in the hippocampus of the injured animals associated with long-lasting memory impairment (Baalman et al., 2013). In animal models of stroke however the proximity to the infarct area has a differential effect on AIS alterations. For example, middle cerebral artery occlusion induced stroke leads to proteolytic ablation of proteins such as AnkG and βIV spectrin and no AIS structures could be identified within the infarct area (Schafer et al., 2009). Furthermore, in a mouse model of photothrombotic stroke of the motor cortex where focal ischaemic lesions are induced with retrograde neuronal tracing, it was demonstrated that in the peri-infarct region AIS morphology and length changes; with the AIS in the injured animals decreased by 14%, almost double the level of change observed in our aged wild-type animals (Hinman et al., 2013). The number of AIS was also examined and found to be unchanged in response to ageing. Given that alterations in AIS number have been observed after ischemic insults where cell death is occurring (Hinman et al., 2013; Schafer et al., 2009), it could be suggested that here the number of neurons in the CA3 is preserved in response to ageing which is consistent with multiple studies both in aged humans and rodents (Rapp and Gallagher, 1996; Rasmussen et al., 1996; West, 1993).

Although, the observations in the present study are limited to alterations of the AIS length, over the last few years a number of studies have suggested that a mechanism for regulating neuronal excitability is alteration of AIS length. For example, in the chick it was shown that auditory synaptic deprivation results in elongation of AIS and decrease of excitation threshold thus increasing neuronal excitability (Kuba et

al., 2010). Moreover, in mouse model of Angleman syndrome, elongation of the AIS was observed in hippocampal pyramidal neurons and paired with increased action potential amplitude and rate of rise as well as decreased action potential threshold and this was associated with increased expression of AnkG (Kaphzan et al., 2011). In contrast, when reduction of AIS length was simulated in a computational model of pyramidal neurons, an increase in the threshold and the interspike interval of neurons fired repeatedly was observed (Baalman et al., 2013).

Similar to the AIS, the length of the nodes of Ranvier was markedly reduced in response to ageing in the wild-type animals. The reduction of nodal length was observed in the stratum lacunosum moleculare which contains fibres that arise from pyramidal neurons in the CA3 and project onto the CA1 (Gilbert and Brushfield, 2009). The observed reduction in nodal length is consistent with a number of studies that have reported age-related changes at the nodes of Ranvier and the surrounding regions such as the paranodes and the juxtaparanodes both in rodents and non-human primates. For example, a decrease, of the same magnitude, in the length of Na_v cluster at the nodes of has been previously observed in the optic nerve of 2 years old wild-type mice (Rios et al., 2003). In the same study, it was suggested that the paranodal interactions play a key role in Na_v channel distribution at the node of Ranvier as they act as a diffusion barrier for Na_v clustering. Furthermore, the paranodes have been shown to be disrupted in normal ageing. In aged rats it was shown that piling of the myelin sheath paranodal loops are a feature of ageing. Furthermore not all the paranodal loops were in contact with the axon and there was loss of transverse bands (Shepherd et al., 2012). At a molecular level, Hinman et al. (2006) have shown alterations in the molecular architecture of the paranodes and the

juxtaparanodes with ageing. For example, they observed reduced expression of $K_v1.2$ channels which were also mislocalized in the Caspr positive paranodal region. Moreover, in a mouse model, where oligodendrocyte-myelin glycoprotein (OMGp) was ablated, disorganized paranodal loops and a reduction of the nodal length as seen here were observed and there was also significant reduction of conduction velocity (Nie et al., 2006). These findings combined with our data indicate that ageing is responsible for alterations in nodes of Ranvier architecture. Our study is limited to the structural observation of the nodes of Ranvier but there is evidence that both the paranodes and the juxtaparanodes are affected by ageing. To assess paranodal disruption examination of the septate-like junctions with electron microscopy or $K_v1.2$ distribution at the paranodes would be necessary.

The nodes of Ranvier and the AIS have similar molecular composition and it was hypothesised that the observed decrease in their length may be associated. In contrast with what was hypothesised no association was found between the length of the AIS and the nodes. A possible explanation is that two different markers were used to evaluate the length of these structures which may not be directly comparable. However, in both regions, the $Na_v1.6$ channels are anchored in high concentrations, by direct interaction with the scaffolding protein AnkG. In the AIS, AnkG has the main role for organization of the AIS components as it was shown that in neurons lacking AnkG no $Na_v1.6$ clustering was observed at the AIS (Hedstrom et al., 2008; Rasband, 2010). Hence the close relation between AnkG and $Na_v1.6$ targeting at AIS may suggest that the decrease of AIS length detected with AnkG observed in the present study could suggest loss of $Na_v1.6$ channels from that region. Hinman et al. (2013) have shown, that in a stroke mouse model, in the peri-infarct area where

decrease of AIS length was shown by AnkG there was no change in AnkG to $Na_v1.6$ length ratio suggesting that there is loss of $Na_v1.6$ channels from the AIS. Additionally, the observed decrease in nodal length could suggest that there is loss of $Na_v1.6$ channels from the nodes of Ranvier as well. Notably, Nie et al. (2006) in an OMGp-null mouse model, observed reduced nodal length together with decreased Na_v subunit α levels. Moreover, studies in $Na_v1.6$-null mouse models have shown that neurons lacking $Na_v1.6$ channels have reduced spike frequency (Van Wart and Matthews, 2006) and increased threshold for spike initiation (Royeck et al., 2008) highlighting the importance of these channels for neuronal excitability. Assessment of $Na_v1.6$ channel levels would determine whether these channels are altered in response to ageing both in the nodes and the AIS Moreover, in order to further investigate the effect of reduced AIS and nodal length on the neuronal excitability in aged animals, electrophysiological approaches or computational modeling of the changes would be necessary.

The next aim of the study was to examine myelin and axonal integrity. Here it was demonstrated that there is age-dependent loss of MBP immunostaining in the wild-type animals and an overall increased number of myelin bulbs in the stratum lacunosum moleculare. The decrease in MBP staining is in accordance with published data from studies in human and non-human primates that have reported a loss of white matter volume as well as ultrastructural alterations of splits and cavities (“balloons”) within the lamellae of the myelin sheath (Bartzokis et al., 2003; Feldman and Peters, 1998; Peters, 2002). Studies in other species has shown reduced myelin staining in response to ageing has been observed in canines (Chambers et al., 2012) whereas in aged primates both loss of myelin staining (Sloane et al., 2003) and

thinner myelin sheaths (Bowley et al., 2010) have been observed. The structural alterations in the myelin sheath (myelin bulbs) observed here in the aged animals have similarities to the ultrastructural changes to the myelin sheath (myelin balloons) reported both in aged rodents and non-human primates (Bowley et al., 2010; Luebke et al., 2010; Peters, 2009; Sugiyama et al., 2002; Shepherd et al., 2012). These structures are suggested to be indicative of neurodegeneration (Peters, 2009) and have also been observed during demyelination (Summers and Appel, 1987; Ludwin, 1978). Further ultrastructural analysis of these structures in ageing and TgAPPSw,Ind mice would be required.

In the present study there were no alterations in axons as assessed by total neurofilament in the stratum lacunosum moleculare. This finding is similar to other studies which show myelin alterations precede axonal degeneration (Sandell and Peters, 2003; Desai et al., 2009). Western blot analysis of MBP and total neurofilament levels in tissue homogenates of the hippocampus indicated that the levels were not changed in response to ageing. The discrepancy between MBP immunostaining and western blotting data may be due to the sensitivity of the two methods to detect differences. Immunostaining allows the identification of specific regional alterations whereas western blotting can only detect gross changes in protein levels. For example, Desai et al. (2009) show regional changes in MBP immunostaining within the hippocampus of aged 3xTg animals but when MBP levels are examined in hippocampal homogenates no change was found.

Myelin integrity has been hypothesised to play an important role in nodal structure and has been closely investigated in demyelinated diseases or injury both in the CNS

and the PNS. For example, in PNS remyelination after nerve injury thinner myelin and shorter nodes are observed (Gaudet et al., 2011). In addition, a key feature of remyelinated axons is the decreased length of internodes (Powers et al., 2012; Lasiene et al., 2008) which subsequently increases the number of nodes (Black et al., 2006). Ageing, however, did not appear to have an effect on the number of nodes. This is in accordance with another study where the number of nodes was examined by assessing the number of Caspr positive paranodal pairs in aged (17-22 months) wild-type mice (Shepherd et al., 2012). However, the decrease in nodal length without any changes in the number of nodes may be reflecting reduction in hippocampal fibre length which has been reported by studies in aged humans, non-human primates and rodents (Marner et al., 2003; Calhoun et al., 2004; Ypsilanti et al., 2008). In addition, in multiple sclerosis diffusion of Na_v channels along axons has been observed which has been attributed to profound demyelination, a hallmark of the disease (Coman et al., 2006; Smith, 2007). Although the changes in the nodes of Ranvier that have been observed here with normal ageing cannot be compared to the severity of those observed in demyelinating diseases such as multiple sclerosis, it becomes evident that the integrity of axon-glial crosstalk plays an important role. The assembly of the macromolecular complex required for Na_v targeting at the AIS and the nodes of Ranvier requires cytoskeletal integrity (Susuki and Rasband, 2008b). However, there is some evidence that some components of cytoskeleton such as αII spectrin are compromised with normal ageing, for example in aged rats it has been shown that there are elevated products of cytoskeletal breakdown mediated by calpain (Bernath et al., 2006). Moreover, in aged rhesus monkeys it was shown that there is an increase in calpain-mediated proteolysis of oligodendrocyte proteins

(Sloane et al., 2003). Calpain has also been pointed out as a key mechanism for AIS remodelling after stroke, Schafer et al. (2009) have shown elevation of the βIV spectrin and AnkG calpain-mediated proteolytic products. Although, cytoskeletal integrity examined with an anti-total neurofilament antibody was found to be intact in the aged animals, it cannot be rejected that other cytoskeletal components, such as βIV spectrin, may be affected. Further investigation for calpain-mediated proteolytic products in hippocampal tissue homogenates of aged animals would be necessary to confirm age-dependent calpain activation.

In addition, normal ageing is characterized by increased mitochondrial dysfunction, oxidative stress and neuroinflammation which are processes that have been linked with the integrity of the nodes of Ranvier (Bagh et al., 2011; Boumezbeur et al., 2010; Stichel and Luebbert, 2007). The mitochondria are subcellular structures essential for energy production in the cell. In the normal ageing brain, there is evidence that the mitochondria accumulate mutations resulting in reduced cytochrome oxidase activity (Lin et al., 2002) and have reduced respiratory rates making the brain more susceptible to oxidative stress (Boveris and Navarro, 2008; Chakrabarti et al., 2011). Moreover, they play an important role in nodal function as they provide the required energy for the maintenance of plasma membrane potential equilibrium (Chiu, 2011). There is some evidence that there is dysregulation of mitochondrial distribution when then the axon-glial junction is disrupted (Einheber et al., 2006) suggesting that local energy metabolism at the node of Ranvier is regulated by axon glial-integrity which may be disrupted in normal ageing. As mentioned earlier, mitochondrial dysfunction leads to oxidative stress in the ageing brain. Moreover, neuroinflammation has been described in the healthy aged brain of many

species (Luo et al., 2010). Both these processes (oxidative stress and neuroinflammation) have been shown to reduce the oligodendroglial population (Balabanov et al., 2007; Cammer and Zhang, 1999; Deng et al., 2004; French et al., 2009). Therefore, given that nodal assembly and maintenance is under glial control, alterations in the oligodendroglial cell number due to normal ageing could have an impact on nodal integrity.

The hippocampus is a region vulnerable to AD-related damage thus it was hypothesised that in a mouse model which develops age-related deposition of amyloid within the hippocampus, as seen here, alterations to AIS and nodes may be exacerbated. In the present study, there is a baseline difference in AIS length with the young APPSw,Ind animals having shorter AIS than the young wild-types. However, there was no difference in AIS length in the aged animals between TgAPPSw,Ind and wild-type animals. There are very few studies investigating the integrity of AIS in AD. Interestingly, there is some evidence that genetic polymorphisms of *ANK3* gene which encodes for AnkG have been linked with late-onset AD (Morgan et al., 2007). In addition, a recent study by Santuccione et al. (2013) showed in AD patients increased immunoreactivity against AnkG in their serum which reversely correlates with slower cognitive decline and altered distribution of AnkG and accumulation at the Aβ plaques. The integrity of AIS before the onset of Aβ pathology has never before been investigated and the reduction of AIS length measured by AnkG may also reflect loss of $Na_v1.6$ from the region. Indeed there is evidence that in 4-7 months old TgAPPSw,Ind (J20 line) mice that the expression of $Na_v1.6$ channels is reduced in the cortex (Verret et al., 2012). However, similar to the current study, when the integrity of AIS was examined proximal to Aβ deposits in another model

(AβPP/PS1) at 12 months of age, no change in AIS length between APP overexpressing animals and wild types was observed (Leon-Espinosa et al., 2012). These findings suggest Aβ may drive an initial decrease in AIS length at a young age which this in not further exacerbated by age but is comparable with the decrease induced by ageing in the wild-type animals.

Furthermore, in the aged APPSw,Ind mice nodal length was reduced but there was no evidence that this was different from the wild-type mice suggesting that this is not influenced by the presence of amyloid. The reduction in nodal length is similar to that observed in the wild-types here and in other studies (Rios et al., 2003). In contrast, a study in another AD model (3xTg) which develops overt amyloid pathology showed $Na_v1.6$ immunoreactivity was reduced in the mutant animals at 6 months of age (Desai et al., 2009). However, in that study the effect of ageing is not taken into account as young wild-type animals are used as controls. In the same study myelin disturbances where proposed to underlie the reduced in $Na_v1.6$ immunostaining. Here, in contrast to what was hypothesized, MBP and total neurofilament levels were unchanged in the aged TgAPPSw,Ind mice compared to young animals, there was however a significant overall increase in the number of myelin bulbs the aged animals. Myelin disruption has been described both in AD patients and other mutant APP models (Stokin et al., 2005; Desai et al., 2009) (deToledo-Morrell et al., 2007) and, similar to ageing, can occur prior to axonal damage (Bartzokis et al., 2003). However, there is evidence that alterations of myelin staining in the hippocampus of APP mutant animals are region-specific, with some regions such as the CA1 being affected while others such as the CA3 are not (Desai et al., 2009) which could explain the absence of myelin changes in the TgAPPSw,Ind

mice. Moreover, the current study is limited to the use of MBP and total neurofilament for the evaluation of myelin and axonal integrity. Examination of the myelinated axons at the stratum lacunosum moleculare with electron microscopy would provide evidence of myelin sheath and axonal disruption at an ultrastructural level. Axonal integrity could also be examined by investigating the level of neurofilament phosphorylation as there is evidence that it is increased in another AD model (Yang et al., 2009) whilst myelin integrity could be further investigated with the use of markers such as MAG which has been sensitive to axon glial disruption (Reimer et al., 2011).

A number of studies have shown that AIS structure is not stable and there are homeostatic changes in response to altered synaptic input leading to changes of AIS length or axonal position (Kuba, 2010; Kuba et al., 2010; Grubb and Burrone, 2010a; Grubb and Burrone, 2010b). In this study synaptic integrity was investigated with the presynaptic vesicle protein synaptophysin. Interestingly, it was observed that the young TgAPPSw,Ind mice have increased baseline synaptophysin staining. This could be attributed to the neurotrophic properties of the sAPPα (Furukawa et al., 1996) which is produced via the non-amyloidogenic processing of APP and may play a role in synaptic preservation (Bailey et al., 2011). In addition there are some evidence from animal models that in the early stages of Aβ pathology there is an increase in cholinergic, glutamatergic and GABAergic synaptic boutons (Bell et al., 2003; Hu et al., 2003). Nevertheless, in accordance with previous studies in the TgAPPSw,Ind mice that have shown a deficit in synaptic electrophysiology (Hsia et al., 1999) and with studies in multiple AD animal models (Hsia et al., 1999; Chapman et al., 1999; Auffret et al., 2010), data from this study showed an age-

dependent loss of synaptophysin positive presynaptic vesicles in the hippocampus. However, it remains unclear if these synaptic changes can be related with activity dependent changes in AIS structure. Loss directly associated with the AIS in GABAergic synapses has been demonstrated in an AD model (Leon-Espinosa et al., 2012). Moreover, loss of axoaxonic GABAergic synapses, which are thought to be inhibitory, has been concomitantly observed with a decrease in AIS length in an animal model of stroke (Hinman et al., 2013). It becomes evident that this study is limited to a gross evaluation of presynaptic boutons and further investigation of the types of synapses that might be affected by ageing and/or increased Aβ levels would provide further insight on whether synaptic input alters AIS structure.

The last aim of this study was to evaluate spatial working memory at the eight arm radial arm maze in aged wild-type and TgAPPSw,Ind mice. It was hypothesised that the observed alterations at the AIS and the nodes of Ranvier would have an effect on spatial working memory. However it was shown that spatial working memory was not impaired with ageing in either the wild-type or the TgAPPSw,Ind animals. Moreover the length of the nodes and the AIS was not associated with the performance (number of revisiting errors) in the 8-arm radial arm maze. This data suggests that the observed changes in the AIS and the nodes of Ranvier are not of enough magnitude to cause working memory impairment. This 8-arm arm radial arm maze test was chosen due to previous evidence that white matter disruption may result in poor working memory performance in the 8-arm radial arm maze (Coltman et al., 2011). Moreover, it is well established that spatial working memory impairment may be detected by the eight-arm radial maze test in aged rodents (Barnes et al., 1980; de Toledo-Morrell et al., 1984; Beatty et al., 1987; Caprioli et

al., 1991; Mizumori et al., 1996). However, the aged mice have inherent cognitive variability; for example, in a study where spatial working memory performance was examined in young (4 months old) and aged (18 months), the old animals were divided into good performers and bad performers based on the number of errors and only the bad performers showed slower improvement in learning the task (Ikegami, 1994). Moreover, in the same study, by baiting with food pellets only four arms which made the task more difficult as it decreased chance for "correct" choices both subgroups of aged animals made more errors than the young animals. Furthermore, in a study where spatial working memory was examined at a later age (24 months old) with a delayed matching to place protocol at the eight-radial arm maze severe cognitive performance was impaired (Lebrun et al., 1990). From these studies it could be suggested that detection of spatial working memory deficits in the radial arm maze is dependent on the difficulty of the behavioural protocol used which might not have been sensitive enough to decipher differences between groups in the present study. Although, the data presented here does not suggest spatial working memory performance being related to Aβ load, there is evidence that memory is challenged in response to ageing both in the wild-type and TgAPPSw,Ind mice in hippocampus-specific tasks. For example, the 6-month old TgAPPSw,Ind mice show learning and memory deficits in Morris water maze (Valero et al., 2011) whilst aged wild-types show impaired spatial memory at 12 months old in Barnes maze (Bach et al., 1999). In addition, the eight-arm radial arm maze has two limitations, the presence of odours and the need for food deprivation. Odours from the food pellet placed at the end of each arm or from previously tested animals that might have remained, despite the thorough cleaning of the maze after each test, and facilitate

navigation. Further electrophysiological investigation would be necessary to establish the functional impact of the observed changes at the nodes of Ranvier and the AIS. For example, electrophysiological measurements (whole cell patch-clamp) form the CA3 region on hippocampal slices may give information for the way action potential amplitude or threshold changes when the AIS are shorter within that region.

Overall, it has been demonstrated that ageing has direct effects on AIS and nodes of Ranvier structure. Both the AIS and the nodes of Ranvier appear to be sensitive in cerebral blood flow reduction. For example, after a stroke there is a pronounced disruption of the ablation of the AIS structure (Schafer et al., 2009) in the infarct area whilst in the perinfarct area reduction of the AIS length is observed (Hinman et al., 2013). More modest reductions in cerebral blood flow can also cause rapid changes in axon-glial integrity and disruption of $Na_v1.6$ within the nodes of Ranvier (Reimer et al., 2011). Given that hypoperfusion and cerebrovascular pathologies have been observed in normal ageing and AD both in humans and animal models (Stoquart-ElSankari et al., 2007; de la Torre, 2009), it could be suggested that it is driving the observed changes. Additionally, hypoperfusion has been associated with white matter disruption (Shibata et al., 2004; Appelman et al., 2010), whilst myelinated axon and axon-glial integrity are important for AIS and nodal structure (Coman et al., 2006; Reimer et al., 2011; Zonta et al., 2011). The potential implication of hypoperfusion in nodes of Ranvier disruption will be investigated in the following chapter.

To summarise, this is the first study demonstrating structural alterations in the AIS and/or the nodes in response to ageing and amyloid in the hippocampus. In the

future, it would be important to investigate the impact of these alterations on the electrophysiological properties of the neurons in the ageing brain. These alterations in the context of complex neuronal networks may play a role the breakdown of effective neuronal communication leading to age-related cognitive decline. Therefore it is essential to identify the mechanisms underlying the observed structural alterations and also to specify the implication of amyloid in these mechanisms.

Chapter 4

Effects of hypoperfusion on myelinated axon integrity and cognition in young and aged wild-type and TgAPPSw,Ind mice

4.1 Introduction

Alterations to myelinated axons is a key feature of the ageing brain (Peters, 2002; Peters, 2009) and these changes are exacerbated in AD (Salat et al., 2009). These changes are associated with impairments in cognitive ability. The previous chapter demonstrated alterations to the protein architecture of myelinated axons, specifically in the node of Ranvier and the AIS, with ageing and modulation by amyloid, a key feature of AD.

The mechanism responsible for alteration to myelinated axons in ageing and in AD is not clear. Cerebral hypoperfusion is a feature of normal ageing and is closely related with white matter changes. Modelling of cerebral hypoperfusion in rodents now permits the investigation of the effects of hypoperfusion in isolation which could provide a greater understanding of mechanisms underlying white matter alteration in response to hypoperfusion. Studies in this chapter build on previous work in a model of hypoperfusion where it was demonstrated that as early as three days after the induction of hypoperfusion the protein architecture of the nodes of Ranvier is changed and this change persists after one month in parallel with alterations at the paranodes (Reimer et al., 2011). In addition, other hypoperfusion studies in mice have provided evidence of widespread myelin damage and poor working memory

performance (Holland et al., 2011; Shibata et al., 2004). However, no previous studies have investigated the integrity of the nodes of Ranvier in response to hypoperfusion in relation with amyloid pathology and age.

4.1.1 Hypothesis and aims

It was hypothesised that the integrity of the myelinated axons and particularly the nodes of Ranvier and the paranodes would be altered in response to hypoperfusion and that these effects would be exacerbated in the presence of increased levels of Aβ and associated with working memory deficits in young and aged mice. In order to address this hypothesis the effects of surgically induced hypoperfusion on the integrity of the nodes of Ranvier, paranodes, myelin and axons and in working memory performance was investigated in young and aged wild-type and TgAPPSw,Ind mice which show increased amyloid levels with increasing age.

4.2 Materials & Methods

4.2.1 Animals

The transgenic mouse model used in this study is described in chapter 2.1. Animals were examined at 4 months and 16-17 months of age at the start of procedures in separated studies. Surgical procedures were performed Dr Cath Gliddon and Dr Philip Holland.

Young study: Behavioural performance was examined in hypoperfused (n=14) and sham operated (n=13) TgAPPSw,Ind and compared to aged-matched wild-type C57Bl/6J control littermates (sham n=14, hypoperfused n=13). During behavioural testing, some animals had seizures which lead to their exclusion from the study under the exclusion criteria described in chapter 2.3.2. The final group numbers were n=12 for the wild-type sham, n=12 for the WT hypoperfused, n=13 for the TgAPPSw,Ind sham and n=10 TgAPPSw,Ind hypoperfused. Tissue harvested from animals of this cohort was used for all biochemical experiments and for examining gross myelin and axonal integrity. Nodal and paranodal integrity was examined in a separate age-matched cohort. The size of the groups was n=9 for the TgAPPSw,Ind hypoperfused; n=9 for the wild-type hypoperfused; n=9 for the TgAPPSw,Ind sham and n=9 for wild-type sham. The use of a different cohort was necessary because tissue at the appropriate level from the behavioural cohort was in shortage.

Aged study: Behavioural performance was examined in hypoperfused (n=15) and sham operated (n=11) TgAPPSw,Ind and compared to aged-matched wild-type C57Bl/6J control littermates (sham n=14, hypoperfused n=12). All experiments were

performed on tissue harvested from animals of this cohort. However, nodal and paranodal integrity, in order to facilitate imaging and analysis, was examined in a subset of animals from each group with simple random sampling. For random sampling, the experimental numbers for each group were written on identical pieces of paper, folded and placed in a dark container, and then another researcher without direct visual contact with the container chose *n* number of papers. This was repeated for each group and the adjusted group sizes were n=9 for the TgAPPSw,Ind hypoperfused; n=9 for the wild-type hypoperfused; n=9 for the TgAPPSw,Ind sham and n=9 for wild-type sham.

For the nodal measurements sample size calculations at both ages were performed to determine that the study is adequately powered as described in chapter 2.9. From a previously published study on the same model and under similar conditions by Reimer et al. (2011), the target difference in the length of the nodes was 0.24 μm (approximately 10% difference) and the standard deviation 0.705 μm which makes the standardized difference (d) = 0.340. With the use of the formula described in chapter 2.9, the 202 nodes need to be measured for the study to be well-powered. If 30 nodes per animal are measured, each group should include a minimum of 7 animals. This criterion is met by both studies.

4.2.2. Behavioural testing

4.2.2.1 Spatial working memory assessment

Behavioural testing in the radial arm maze began 4 weeks after the induction of hypoperfusion. Spatial working memory assessment for the animals of the young and the aged cohort was performed as described in chapter 2.3.1. The number of novel (correct) entries in the first eight arm entries, the number of total arm entries, the number of revisiting errors and the duration of the task for all trials were recorded. The experiments were performed by the author and Dr Gillian Scullion.

4.2.3 Neuropathological assessment

4.2.3.1 Perfusions and tissue preparation

Mice were sacrificed 8 weeks after surgery as described in chapter 2.4.1. Tissue was harvested for immunohistochemical and biochemical analysis as described in chapter 2.4.2.

4.2.3.2 Immunohistochemistry

The integrity of myelinated axons was examined using antibodies against myelin basic protein (MBP) and total neurofilament. Alterations to the length and the number of nodes of Ranvier were examined using antibodies against Caspr and $Na_v1.6$ and paranodal integrity was examined with $K_v1.2$ and Caspr double labeling. The fluorescent immunochemistry techniques used are described in chapter 2.5.1. Myelin and axonal integrity was assessed on single confocal images acquired with a Zeiss Axioskope LSM 710 confocal laser scanning microscope using a 20× objective

(numeric aperture 0.8), a pinhole of 1 Airy unit and x1 zoom in the corpus callosum in sections stained for MBP and total neurofilament as described in chapter 2.6.2. The length, the nodal gap length and the number of the nodes were examined in the corpus callosum and stratum lacunosum moleculare of the hippocampus in sections stained for $Na_v1.6$ and Caspr as described in chapters 2.6.5 and 2.6.6. Colocalization of $K_v1.2$ and Caspr was examined at the corpus callosum as described in chapter 2.6.7. In some animals imaging was impossible because of poor quality of staining and tissue (exclusion criteria described in chapter 2.5.5). The final analysis was conducted in groups whose size is detailed in table 4.1 for the young study and in table 4.2 for the aged.

Table 4.1 Group sizes of the animals included in final analysis for the young study

Analysis (young study)	**Groups size (*n*)**			
	wild-type sham	wild-type hypoperfused	TgAPPSw,Ind sham	TgAPPSw,Ind hypoperfused
Nodal length, width and number	9	8	8	8
$K_v1.2$	9	9	8	9
MBP and total neurofilament analysis	10	12	13	10

Table 4.2 Group sizes of the animals included in final analysis for the aged study

Analysis (aged study)	**Groups size (*n*)**			
	wild-type sham	wild-type hypoperfused	TgAPPSw,Ind sham	TgAPPSw,Ind hypoperfused
Nodal length and number	8	8	9	8
$K_v1.2$	9	8	9	9
MBP and total neurofilament analysis	11	13	11	12

4.2.4 Biochemistry

The 2mm hippocampal coronal slices of the right hemibrain from the animals of the young and the aged were then homogenized as described in chapter 2.7.1. Protein concentration was determined as described in chapter 2.7.2. MBP, pan neurofilament, 200KDa neurofilament, APP and APP C-terminal fragments levels were determined using anti-MBP, anti-pan neurofilament, anti-neurofilament 200KDa, anti-APP and anti-APP C-terminal fragments antibodies respectively. Western blotting was performed as described in 2.7.4 by the author and Dr Gillian Scullion. Human Aβ42 levels were detected ELISA as described in chapter 2.7.3, the experiment was run by Mrs Natalia Salvadores. Quantification of MBP, pan neurofilament, 200KDa neurofilament, APP, C83 and C99 fragments and oligomeric amyloid levels performed as detailed in 2.7.5.

4.2.5 Statistical analysis

All nodal length measurements were analysed using the two-sample Kolmogrov-Smirnov test. Spearman's correlation test was used to associate changes between the $Na_v1.6$ cluster to nodal gap length ratio with working memory performance. The number of nodes, MBP and total-neurofilament intensity and area fraction, $K_v1.2$/Caspr colocalization and MBP, total neurofilament, NF200, APP and APP C-terminal fragments levels and the gradient of the line generated between the numbers of errors in block 1 to block 8 (8-arm radial arm mase) were analysed by 2-way-ANOVA with genotype and hypoperfusion as the factors, followed by Bonferroni's

post hoc test if necessary. Differences in the levels of oligomeric Aβ or hAβ42 concentration in sham and hypoperfused TgAPPSw,Ind mice were analysed using the student's unpaired t-test. Data acquired at the 8-arm radial arm maze was analysed with two-way (effect of hypoperfusion and genotype over training days) repeated measures ANOVA followed by Tukey's *post hoc* test. Additionally, the Greenhouse-Geiser correction was used when data violated sphericity ($p < 0.05$ at Mauchly's test). Software used for statistical analysis and the graph generation is detailed in 2.8. For all statistical tests ,significance was established at $p < 0.05$, except from the Kolmogrov-Smirnov test where the Bonferroni correction was applied adjusting significance at $p < 0.025$ as described in chapter 2.8 because identical datasets where used simultaneously twice.

4.3 Results

4.3.1 Hypoperfusion decreases $Na_v1.6$ cluster and nodal gap length in the nodes of Ranvier of the corpus callosum but not of the hippocampus in young animals

The nodes of Ranvier are important for action potential propagation and there is evidence that they are altered in length in response to cerebral hypoperfusion. The first aim of the study was to assess whether the integrity of the nodal domain may be altered in response to hypoperfusion and increased levels of Aβ in young animals. The myelinated axons were investigated in both the corpus callosum, known to be susceptible to the effects of hypoperfusion, and the hippocampus (stratum lacunosum moleculare) which is the primary site of age-dependent amyloid deposition in the TgAPPSw,Ind animals. In general the nodes were readily identifiable ($Na_v1.6$ immunopositive clusters bounded by pairs of Caspr immunopositive domains) in all sections and there were no obvious morphological alterations between the individual mice.

Examination of at the corpus callosum of young wild-type and TgAPPSw,Ind mice revealed alterations to the $Na_v1.6$ channel clusters size and the nodal gap in response to hypoperfusion (Figure 4.1 A). In the wild-type animals the average length of the $Na_v1.6$ cluster was found to be 2.32 ± 0.05 μm in the shams and 2.01 ± 0.05 μm in the hypoperfused animals whilst in the sham TgAPPSw,Ind the average $Na_v1.6$ cluster length was 2.22 ± 0.05 μm and 1.74 ± 0.04 μm in the hypoperfused TgAPPSw,Ind mice. There was a significant reduction in the length of Nav1.6 cluster length in the hypoperfused wild-types ($p < 0.0001$, $D = 0.2444$, Figure 4.1 B) and

TgAPPSw,Ind animals ($p < 0.0001$, $D = 0.2879$, Figure 4.1 C) by 13.6 ± 2.9% and 21.9 ± 3% respectively when compared to sham animals of the same genotype. Moreover, there was a significant difference (by 13 ± 3.1%) in the $Na_v1.6$ cluster length between hypoperfused wild-type and TgAPPSw,Ind animals ($p < 0.0001$, $D = 0.1851$, Figure 4.1 E), suggesting that hypoperfusion has an even greater effect in reducing the $Na_v1.6$ cluster length in the TgAPPSw,Ind mice. No difference was observed between sham wild-types and sham TgAPPSw,Ind ($p = 0.095$, $D = 0.1084$, Figure 4.3 D).

Since a decrease in the $Na_v1.6$ cluster length was observed in response to hypoperfusion, it was then investigated whether the paranodes were similarly altered. A decrease in the nodal gap length defined by pairs of Caspr immunopositive domains (Figure 4.1 A) was observed in the hypoperfused animals. In the sham wild-type animals the average nodal gap length was 1.27 ± 0.04 μm and 1.02 ± 0.04 μm in the hypoperfused wild-type animals whilst in the sham TgAPPSw,Ind the average nodal gap length was 1.27 ± 0.05 μm and 0.81 ± 0.03 μm in the hypoperfused TgAPPSw,Ind mice. When comparing sham and hypoperfused animals a significant reduction in nodal gap length both in the wild-type ($p < 0.0001$, $D = 0.2494$, Figure 4.2 A) and the TgAPPSw,Ind ($p < 0.0001$, $D = 0.3512$, Figure 4.2 B) mice by 20.1 ± 4.1% and 35.9 ± 4.3% respectively was found. Additionally, the nodal gap was significantly smaller by 20.1 ± 4.4% in the hypoperfused TgAPPSw,Ind mice compared to the wild-type animals ($p < 0.0001$, $D = 0.2232$, Figure 4.2 D). No difference was observed between sham wild-type and TgAPPSw,Ind animals ($p = 0.733$, $D = 0.0603$, Figure 4.2 C).

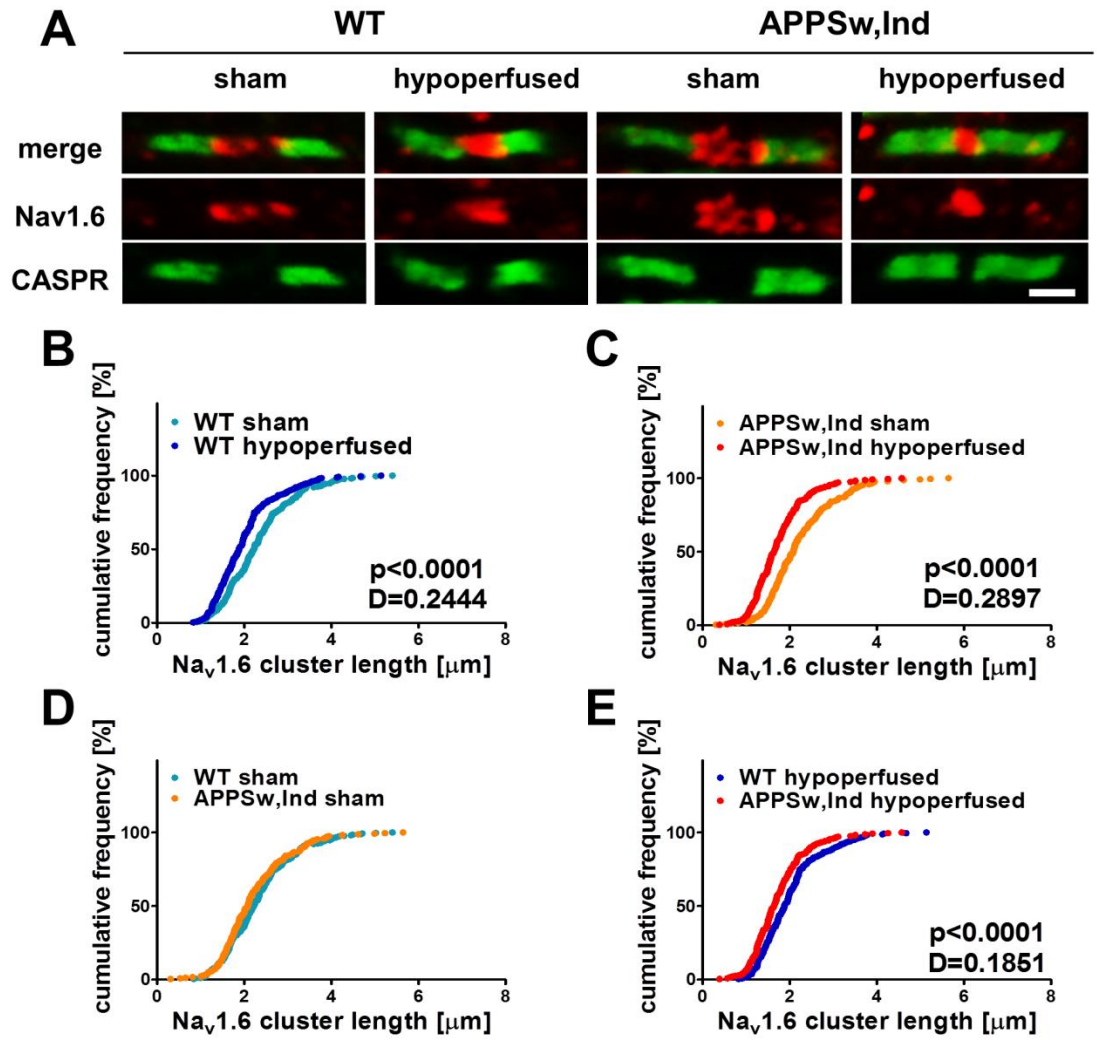

Figure 4.1 ***$Na_v1.6$ cluster length is decreased in the corpus callosum of young animals in response to hypoperfusion and this effect is exacerbated in TgAPPSw,Ind mice***. $Na_v1.6$ sodium channels clusters bounded by the paranodal protein Caspr outline the node of Ranvier [A]. There is a significant decrease ($p < 0.0001$) in the length [B & C] of the $Na_v1.6$ clusters in both WT and TgAPPSw,Ind hypoperfused animals, an effect that is exacerbated ($p < 0.0001$) in the TgAPPSw,Ind mice [E]. No difference ($p > 0.05$) was observed between sham animals of both genotypes [D]. The lengths of thirty $Na_v1.6$ clusters per animal were analysed and plotted as percentage of cumulative frequency distribution. WT sham: n=9, WT hypoperfused: n=8, TgAPPSw,Ind sham: n=8, TgAPPSw,Ind hypoperfused n=8. Scale bar 2 μm.

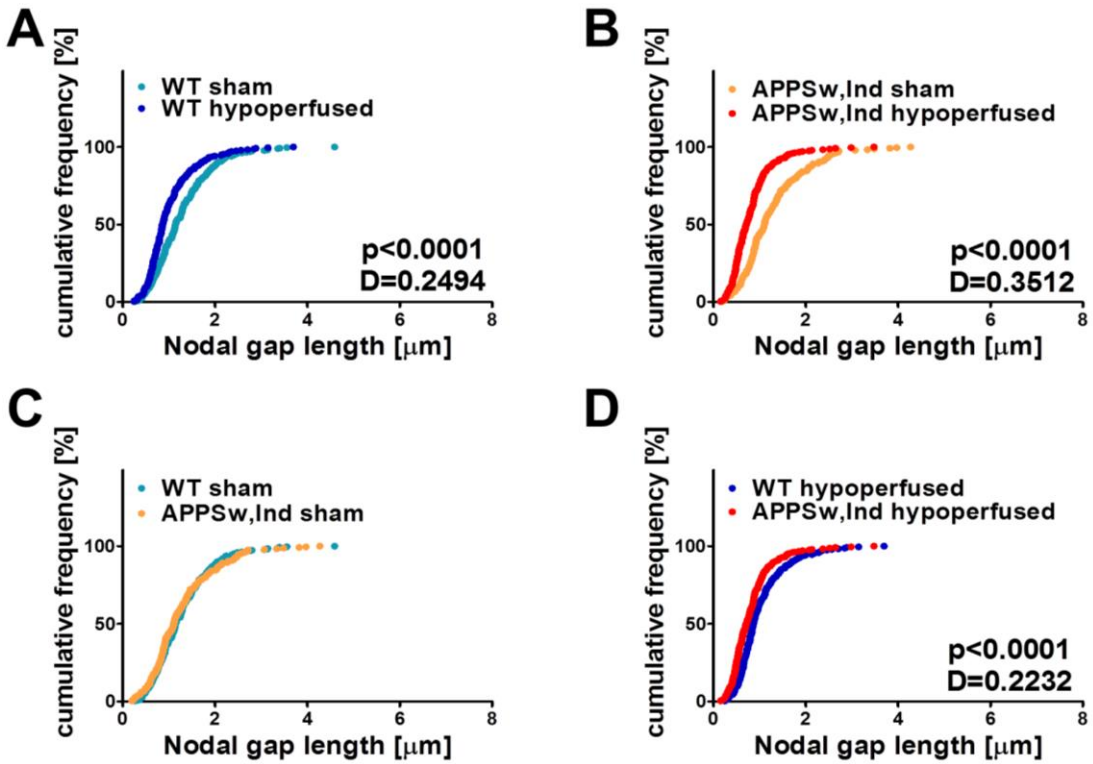

Figure 4.2 ***Nodal gap length is decreased in the corpus callosum of young animals in response to hypoperfusion and this effect is exacerbated in TgAPPSw,Ind mice***. There is a significant decrease ($p < 0.0001$) in nodal gap length [B-C] in both WT and TgAPPSw,Ind hypoperfused animals, an effect that is exacerbated ($p < 0.0001$) in the TgAPPSw,Ind mice [E]. No difference ($p > 0.05$) was observed between sham animals of both genotypes [D]. The nodal gap lengths of thirty nodes per animal were analysed and plotted as percentage of cumulative frequency distribution. WT sham: n=9, WT hypoperfused: n=8, TgAPPSw,Ind sham: n=8, TgAPPSw,Ind hypoperfused n=8.

The stratum lacunosum moleculare of the hippocampus was the second region that was examined and no change in the $Na_v1.6$ cluster or nodal gap length was observed in response to hypoperfusion (Figure 4.3 A). The length of the $Na_v1.6$ cluster was not different between hypoperfused wild-type (p = 0.501, D = 0.0704; Figure 4.3 B) or TgAPPSw,Ind mice (p = 0.354, D = 0.0815, Figure 4.3 C) when compared to sham animals of the same genotype. Moreover, no significant difference in the $Na_v1.6$ cluster length was observed between the two genotypes in the sham (p = 0.327, D = 0.0833, Figure 4.3 D) or the hypoperfused (p = 0.083, D = 0.1074, Figure 4.3 E) animals. Similarly, the nodal gap length was not different between hypoperfused wild-type (p = 0.225, D = 0.0889, Figure 4.4 A) or TgAPPSw,Ind (p = 0.882, D = 0.0514, Figure 4.4 B) animals when compared to sham animals of the same genotype. Moreover, no significant difference in nodal gap length was observed between wild-type and TgAPPSw,Ind in the sham (p = 0.907, D = 0.0495, Figure 4.4 C) or hypoperfused (p = 0.435, D = 0.0741, Figure 4.4 D) animals.

These findings suggest that in the corpus callosum of the young animals, hypoperfusion is causing a decrease to the size of the nodes of Ranvier and this effect is exacerbated in the TgAPPSw,Ind mice. However, this effect is region-specific as the nodes of Ranvier in the stratum lacunosum moleculare of the hippocampus are not altered by hypoperfusion.

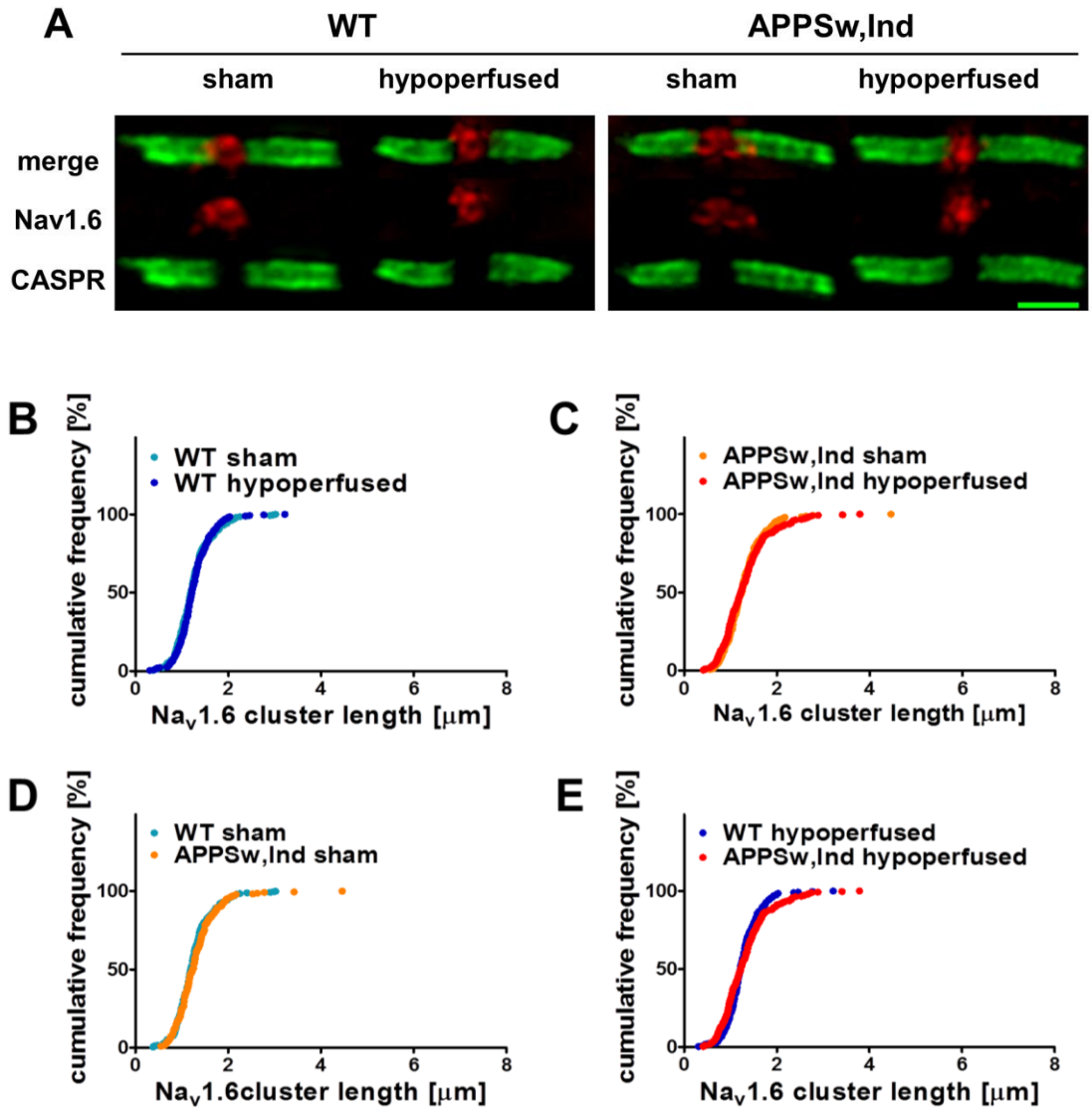

Figure 4.3 ***Na$_v$1.6 cluster is not altered in the hippocampus of young animals in response to hypoperfusion.*** Na$_v$1.6 clusters bounded by the paranodal protein Caspr outline the node of Ranvier [A]. No significant change ($p > 0.05$) in the length of the Na$_v$1.6 clusters in response to hypoperfusion was observed [B & C]. The Na$_v$1.6 clusters were not different ($p > 0.05$) between WT and TgAPPSw,Ind in the sham or the hypoperfused animals [D & E]. The Na$_v$1.6 cluster lengths of thirty nodes per animal were analysed and plotted as a percentage of cumulative frequency distribution. WT sham: n=9, WT hypoperfused: n=8, TgAPPSw,Ind sham: n=8, TgAPPSw,Ind hypoperfused n=8. Scale bar 2 μm.

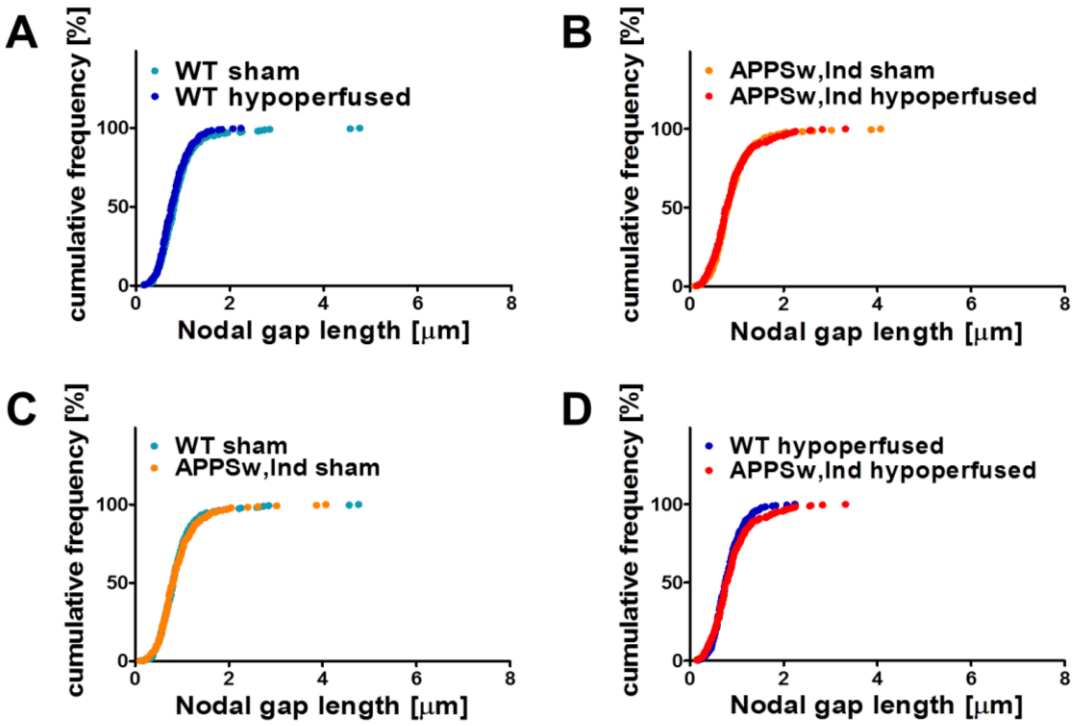

Figure 4.4 ***Nodal gap is not altered in the hippocampus of young animals in response to hypoperfusion.*** No significant change ($p > 0.05$) in nodal gap length in response to hypoperfusion was observed [A & B]. Nodal gap length was not different ($p > 0.05$) between WT and TgAPPSw,Ind in the sham or the hypoperfused animals [C & D]. The nodal gap lengths of thirty nodes per animal was analysed and plotted as percentage of cumulative frequency distribution. WT sham: n=9, WT hypoperfused: n=8, TgAPPSw,Ind sham: n=8, TgAPPSw,Ind hypoperfused n=8.

4.3.2 Hypoperfusion decreases $Na_v1.6$ cluster and nodal gap length in the nodes of Ranvier of the corpus callosum and the hippocampus of aged animals

The next aim of the study was to investigate whether the alterations to the nodal structure observed in response to hypoperfusion and increased Aβ levels in young mice would be exacerbated with ageing. Thus the same approaches to those used previously were employed to study nodes/paranodes in cohorts of aged wild-type and TgAPPSw,Ind mice.

In the aged cohort the $Na_v1.6$ cluster and nodal gap length were also analysed in the corpus callosum (Figure 4.5 A) and the stratum lacunosum moleculare of the hippocampus (Figure 4.7 A). In corpus callosum of wild-type animals the average length of the $Na_v1.6$ cluster was found to be 1.82 ± 0.05 μm in the shams and 1.65 ± 0.05 μm in the hypoperfused animals whilst in the sham TgAPPSw,Ind the average $Na_v1.6$ cluster length was 1.8 ± 0.05 μm and 1.52 ± 0.04 μm in the hypoperfused TgAPPSw,Ind mice. Similar to the young cohort in the corpus callosum there was a significant reduction in the length of $Na_v1.6$ positive domains in response to hypoperfusion both in wild-type ($p < 0.01$, $D = 0.1661$, Figure 4.5 B) and the TgAPPSw,Ind animals ($p < 0.0001$, $D = 0.1917$, Figure 4.5 C) by 9.7 ± 3.8% and 15.7 ± 3.4% respectively when compared to sham animals of the same genotype. However, no significant difference in the $Na_v1.6$ cluster length was observed between the two genotypes in the sham ($p = 0.948$, $D = 0.0458$, Figure 4.5 D,) or the hypoperfused ($p = 0.190$, $D = 0.1012$, Figure 4.6 E) animals.

Since a decrease in the $Na_v1.6$ cluster length was observed in response to hypoperfusion, whether the paranodes were similarly altered was then investigated. Indeed similar changes were observed in the nodal gap length at the corpus callosum. In the sham wild-type animals the average nodal gap length was 0.97 ± 0.04 μm and 0.72 ± 0.03 μm in the hypoperfused wild-type animals whilst in the sham TgAPPSw,Ind average nodal gap length was 0.92 ± 0.03 μm and 0.71 ± 0.03 μm in the hypoperfused TgAPPSw,Ind mice. Hypoperfusion significantly decreased the nodal gap length in both wild-type ($p < 0.0001$, $D = 0.2077$, Figure 4.6 A) and the TgAPPSw,Ind ($p < 0.0001$, $D = 0.1949$, Figure 4.6 B) animals by 25.3 ± 5.2% and 22.9 ± 4.7% respectively. No changes were observed between the two genotypes in the sham ($p = 0.498$, $D = 0.0727$, Figure 4.6 C) or the hypoperfused ($p = 0.839$, $D = 0.577$, Figure 4.6 D) animals.

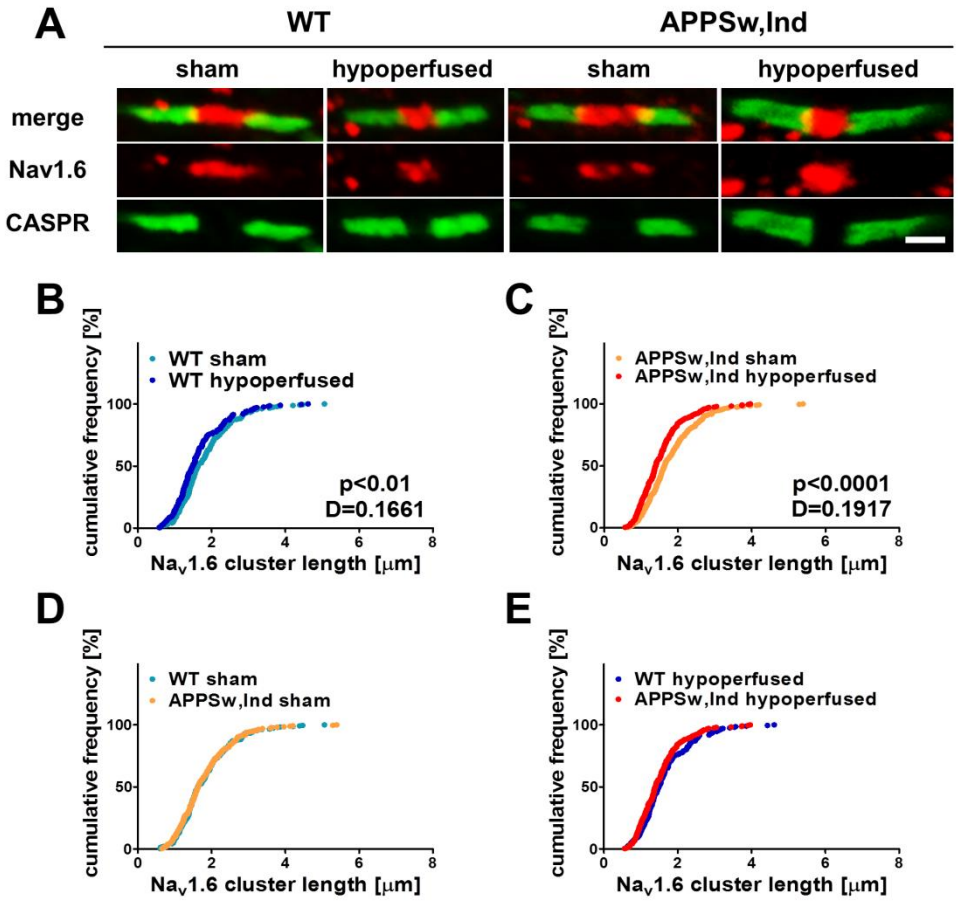

Figure 4.5 ***Na$_v$1.6 cluster length is decreased in the corpus callosum of aged animals in response to hypoperfusion***. Na$_v$1.6 clusters bounded by the paranodal protein Caspr outline the node of Ranvier [A]. There is a significant decrease in the length [B & C] of the Na$_v$1.6 clusters in both WT ($p < 0.01$) and TgAPPSw,Ind hypoperfused animals ($p < 0.0001$). No difference ($p > 0.05$) was observed between genotypes in the sham or the hypoperfused animals [D & E]. The lengths of thirty Na$_v$1.6 clusters per animal were analysed and plotted as percentage of cumulative frequency distribution. WT sham: n=8, WT hypoperfused: n=9, TgAPPSw,Ind sham: n=8, TgAPPSw,Ind hypoperfused n=8. Scale bar 2 μm.

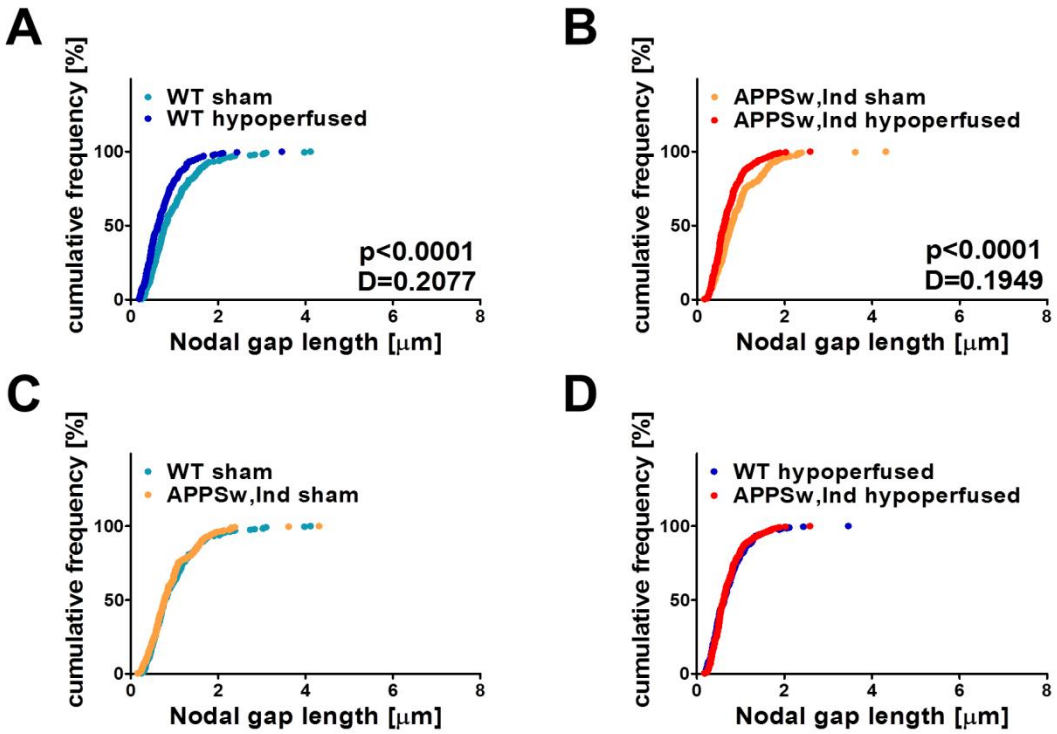

Figure 4.6 ***Nodal gap length is decreased in the corpus callosum of aged animals in response to hypoperfusion***. There is a significant ($p < 0.0001$) decrease in the nodal gap length [A & B] in response to hypoperfusion in both WT and TgAPPSw,Ind animals. No difference ($p > 0.05$) was observed between genotypes in the sham or the hypoperfused animals [C & D]. The nodal gap lengths of thirty nodes per animal were analysed and plotted as percentage of cumulative frequency distribution. WT sham: n=8, WT hypoperfused: n=9, TgAPPSw,Ind sham: n=8, TgAPPSw,Ind hypoperfused n=8.

In the aged cohort at the stratum lacunosum moleculare of the hippocampus, alterations to the $Na_v1.6$ cluster and nodal gap length were observed in response to hypoperfusion (Figure 4.7 A). The average length of the $Na_v1.6$ cluster was found to be 1.52 ± 0.04 μm in the shams and 1.40 ± 0.04 μm in the hypoperfused animals whilst in the sham TgAPPSw,Ind the average $Na_v1.6$ cluster length was 1.56 ± 0.04 μm and 1.38 ± 0.03 μm in the hypoperfused TgAPPSw,Ind mice. In hypoperfused wild-type the length of $Na_v1.6$ clusters ($p > 0.01$, $D = 0.1632$, Figure 4.7 B) and the nodal gap length ($p < 0.01$, $D = 0.1611$, Figure 4.8 A) were significantly reduced compared to sham by 7.9 ± 3.2% and 13.4 ± 4.4% respectively. In the hypoperfused TgAPPSw,Ind animals, only the $Na_v1.6$ cluster length was significantly decreased by 11.9 ± 3.3% ($p = 0.019$, $D = 0.1296$; Figure 4.7 C) but not the nodal gap ($p = 0.319$, $D = 0.0815$, Figure 4.8 B) when compared to sham animals of the same genotype. Moreover, there was no significant difference in the $Na_v1.6$ cluster length between the two genotypes in the sham ($p = 0.340$, $D = 0.0829$ Figure 4.7 D) or the hypoperfused animals ($p = 0.346$, $D = 0.0795$, Figure 4.7 E). Similarly, the nodal gap length was not different between wild-type and TgAPPSw,Ind either sham ($p = 0.041$, $D = 0.1224$, Figure 4.8 C) or hypoperfused animals ($p = 0.406$, $D = 0.0757$, Figure 4.8 D) compared to wild-type animals.

These findings suggest that similarly to the young animals, hypoperfusion causes a decrease in the size of the nodes of Ranvier in the corpus callosum of the aged animals. However, contrary to what is observed in the young mice, this effect was not exacerbated in the TgAPPSw,Ind mice. Additionally, ageing appears to increase susceptibility of the brain to hypoperfusion as the nodes of Ranvier in the hippocampus are also reduced in size.

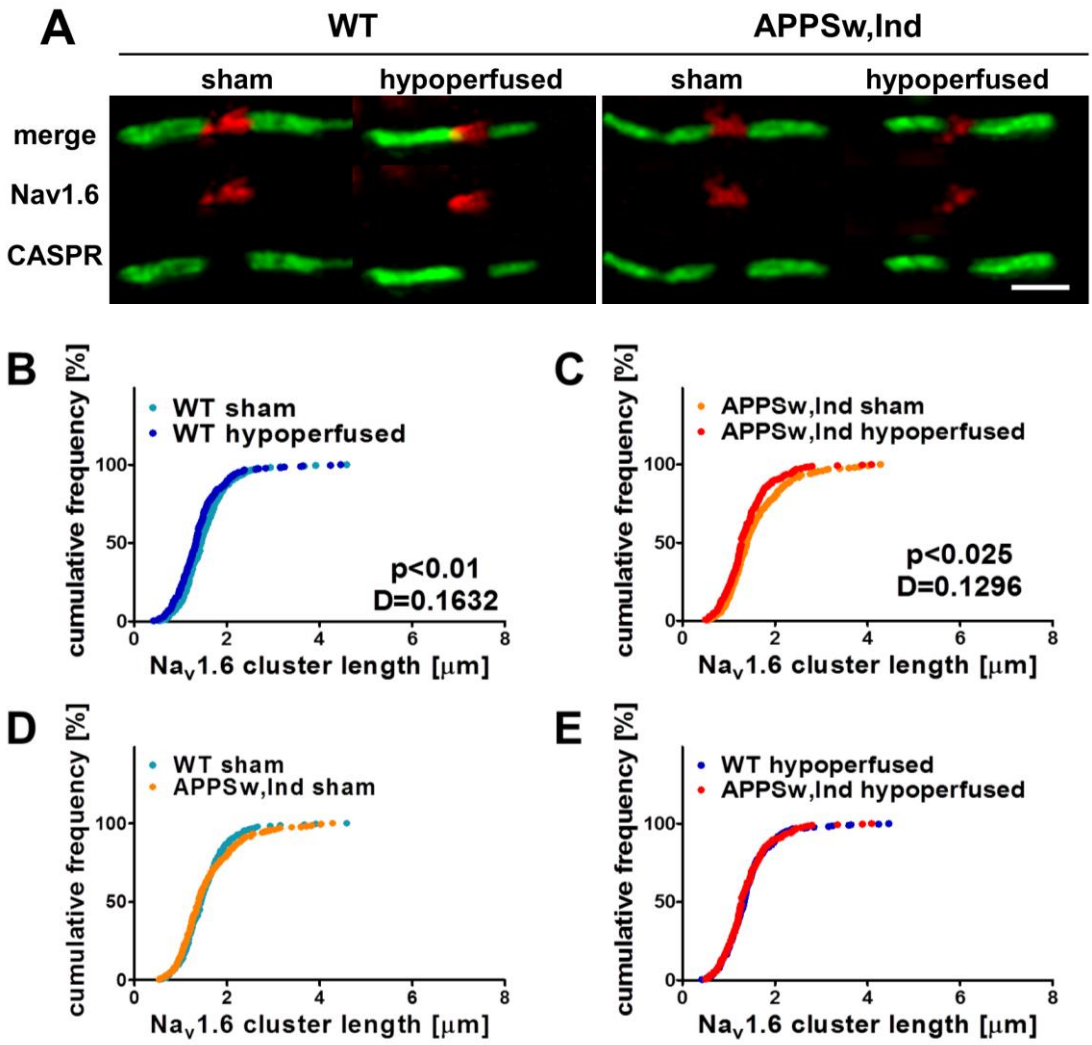

Figure 4.7 ***Na$_v$1.6 cluster length is decreased in hippocampus of aged animals in response to hypoperfusion***. Na$_v$1.6 clusters bounded by the paranodal protein Caspr outline the node of Ranvier [A]. There is a significant decrease in the length [B & C] of the Na$_v$1.6 clusters in both WT ($p < 0.01$) and TgAPPSw,Ind ($p < 0.025$) hypoperfused animals. No difference ($p > 0.05$) was observed between genotypes in the sham or the hypoperfused animals [D & E]. The lengths of thirty Na$_v$1.6 clusters per animal were analysed and plotted as percentage of cumulative frequency distribution. WT sham: n=8, WT hypoperfused: n=9, TgAPPSw,Ind sham: n=8, TgAPPSw,Ind hypoperfused n=8. Scale bar 2 μm.

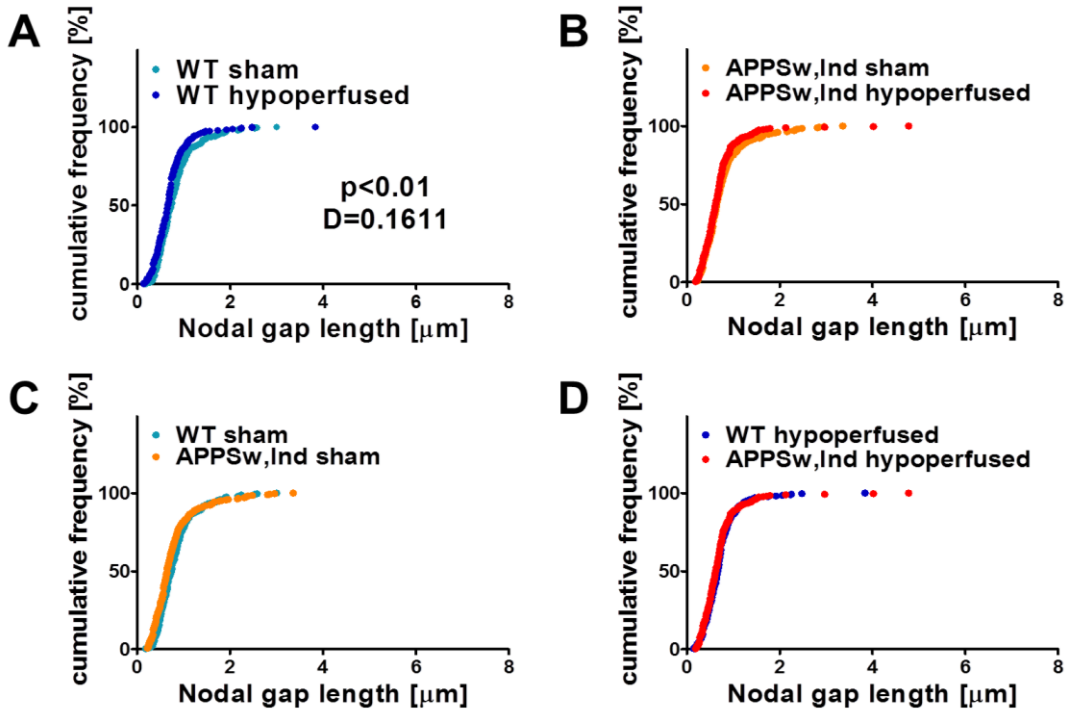

Figure 4.8 ***Nodal gap is decreased in the hippocampus of aged WT animals in response to hypoperfusion.*** A significant decrease ($p < 0.01$) in nodal gap length of WT animals in response to hypoperfusion was observed [A]. Nodal gap length was not different ($p > 0.05$) between sham and hypoperfused TgAPPSw,Ind animals [B] or between WT and TgAPPSw,Ind either in the sham or the hypoperfused animals [C & D]. The nodal gap lengths of thirty nodes per animal was analysed and plotted as percentage of cumulative frequency distribution. WT sham: n=8, WT hypoperfused: n=9, TgAPPSw,Ind sham: n=8, TgAPPSw,Ind hypoperfused n=8.

4.3.3 Number of nodes unchanged with hypoperfusion in the corpus callosum and the hippocampus of young and aged animals

It was next determined whether the overall number of nodes of Ranvier may be changed with hypoperfusion or between genotypes in young and aged animals in the same regions where the nodal size was measured by stereologically counting the number of nodes in the same confocal stacks used for nodal measurements.

In the young animals (Figure 4.9 A and B) there was no significant effect of genotype (corpus callosum: $p = 0.6824$, $F_{(1-29)} = 0.1708$; hippocampus: $p = 0.5931$, $F_{(1-29)} = 0.2916$) or surgery (corpus callosum: $p = 0.1875$, $F_{(1-29)} = 1.822$; hippocampus: $p = 0.1551$, $F_{(1-29)} = 2.124$) in the number of nodes in either of the examined regions.

Similarly in the aged animals (Figure 4.9 C and D), no significant effect of genotype (corpus callosum: $p = 0.3568$, $F_{(1-29)} = 0.8768$; hippocampus: $p = 0.4999$, $F_{(1-29)} = 0.4660$) or surgery (corpus callosum: $p = 0.6404$, $F_{(1-29)} = 0.2229$; hippocampus: $p = 0.6659$, $F_{(1-29)} = 0.1900$) in the number of nodes in either region was observed. These findings indicate that hypoperfusion does not result in a change of the number of nodes of Ranvier.

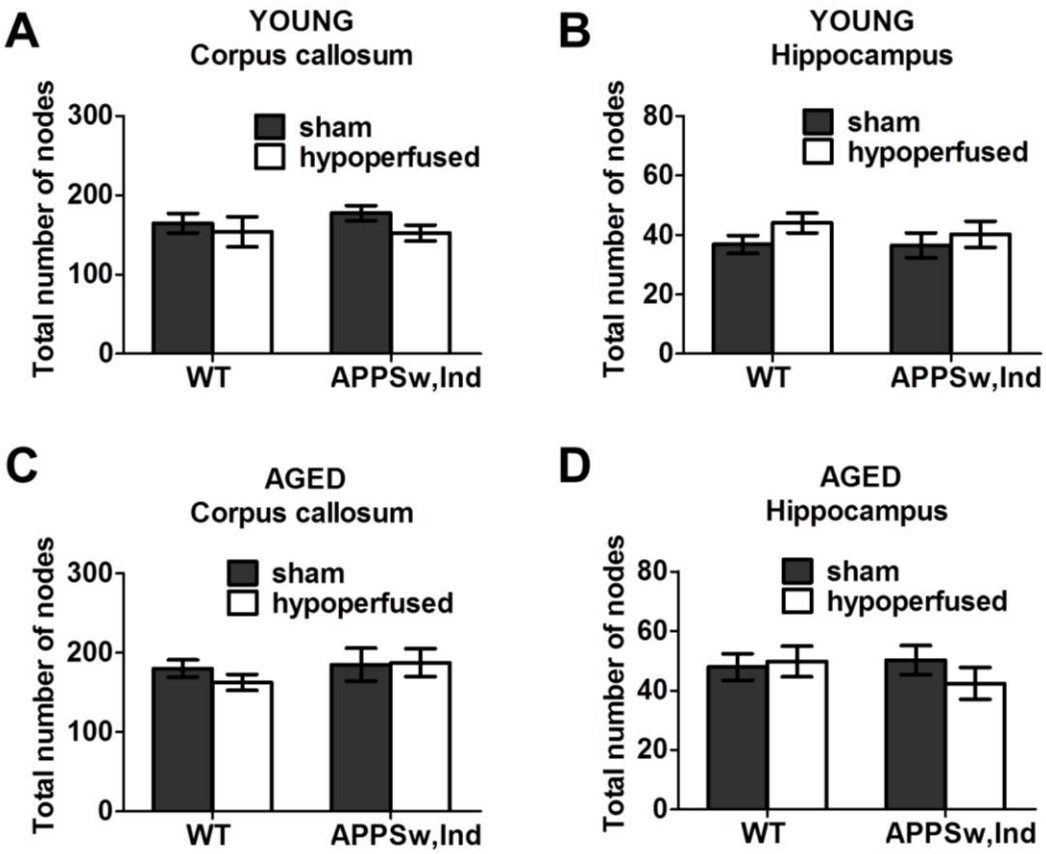

Figure 4.9 ***No change of the number of nodes in response to hypoperfusion either in young or aged animals***. The number of nodes was stereologically counted in 47x47x5 μm^3 confocal stacks of the corpus callosum and in 47x47x10 μm^3 confocal stacks of stratum lacunosum moleculare of the hippocampus. In both regions no significant change ($p > 0.05$) in the nodal number was observed in response to hypoperfusion in either the young [A & B] or the aged animals [C &D].Young: WT sham: *n*=9, WT hypoperfused: *n*=8, TgAPPSw,Ind sham: *n*=8, TgAPPSw,Ind hypoperfused *n*=8; Aged: WT sham: *n*=8, WT hypoperfused: *n*=9, TgAPPSw,Ind sham: *n*=8, TgAPPSw,Ind hypoperfused *n*=8. Graphs show mean ± SEM.

4.3.4 $Na_v1.6$ cluster length to nodal gap length ratio is altered suggesting paranodal disruption in the corpus callosum of young and aged animals

Normally there is a well-defined spatial distribution of Caspr and $Na_v1.6$ in the paranodes and the nodes of Ranvier respectively. Since the length of both the $Na_v1.6$ cluster and nodal gap was reduced in response to hypoperfusion, it was investigated whether this well-defined spatial relationship was maintained or whether this was also disrupted which would suggest paranodal disruption was further investigated. Nodal gap and $Na_v1.6$ cluster lengths were measured on identical nodes in the young and old animals which allowed the ratio between the $Na_v1.6$ cluster and nodal gap length to be calculated. This could serve as a measure of paranodal disruption and expansion of the $Na_v1.6$ channels into the paranodal domain. Lower values would be representative of $Na_v1.6$ clusters restricted in the nodes of Ranvier, while higher values would represent $Na_v1.6$ clusters expanding into the paranodal domain.

In the young animals, the values for the $Na_v1.6$ cluster to nodal gap length ratio were plotted as relative frequency graphs and the distribution of the ratio values was examined. It was shown that in response to hypoperfusion there is a significant shift of the ratio such that there is higher $Na_v1.6$ clusters to nodal gap length ratio in hypoperfused mice as compared to sham. This indicates that that there are more nodes where there is greater expansion of the $Na_v1.6$ channels into the paranodal domains. This observation occurs in both the wild-type ($p < 0.01$, $D = 0.1474$, Figure 4.10 A,) and the TgAPPSw,Ind hypoperfused animals ($p < 0.0001$, $D = 0.3181$, Figure 4.10 B) compared to sham. There was no significant difference between the sham wild-types and TgAPPSw,Ind ($p = 0.372$, $D = 0.0803$, Figure 4.10 C,) mice.

However, it was shown that in response to hypoperfusion the shift towards higher $Na_v1.6$ cluster to nodal gap length ratio was significantly greater in the TgAPPSw,Ind compared to the wild-type mice ($p < 0.001$, $D = 0.1725$, Figure 4.10 D,), suggesting that the there is greater expansion of the $Na_v1.6$ channels into the paranodal domains in the APPSw,Ind hypoperfused animals compared to the wild-type hypoperfused mice.

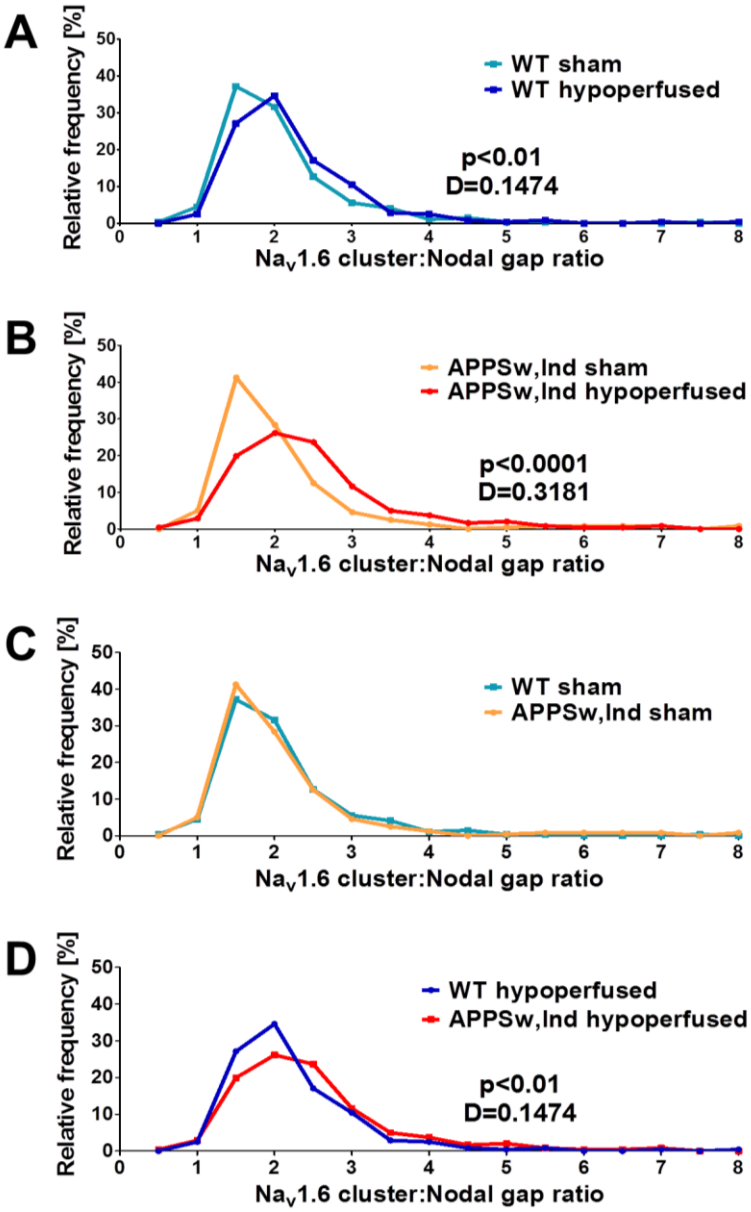

Figure 4.10 ***Expansion of the Na$_v$1.6 cluster into the paranodal domain in response to hypoperfusion exacerbated in TgAPPSw,Ind mice in the corpus callosum of young animals.*** The Na$_v$1.6 cluster to nodal gap length ratio was used as a measure of paranodal disruption and expansion of the Na$_v$1.6 cluster into the paranodal domain. There is a significant increase in the ratio [A-B] of both WT (p < 0.01) and TgAPPSw,Ind (p < 0.0001) hypoperfused animals which is exacerbated in the hypoperfused TgAPPSw,Ind animals (p < 0.01) [D]. No difference (p > 0.05) was observed between genotypes in the sham animals [C]. Na$_v$1.6 cluster and nodal gap length was measured on 30 identical nodes for each animal and the ratio of Na$_v$1.6 cluster to nodal gap length was plotted as distribution of percentage of relative frequencies. WT sham: n=9, WT hypoperfused: n=8, TgAPPSw,Ind sham: n=8, TgAPPSw,Ind hypoperfused n=8.

Similarly, in the aged animals, it was shown that in response to hypoperfusion there is a shift in the $Na_v1.6$ cluster to nodal gap length ratio towards higher values in both the wild-type ($p < 0.0001$, $D = 0.2375$, Figure 4.11 A) and TgAPPSw,Ind mice ($p < 0.01$, $D = 0.1509$, Figure 4.11 B) compared to sham. This again suggests that $Na_v1.6$ channels expand into the paranodal domains with hypoperfusion in aged animals similarly to the young mice. However, there was no significant difference in the $Na_v1.6$ cluster to nodal gap length ratio between the sham wild-type and TgAPPSw,Ind mice ($p = 0.889$, $D = 0.0509$, Figure 4.11 C) or between hypoperfused wild-type and TgAPPSw,Ind ($p = 0.059$, $D = 0.1238$, Figure 4.11 D).

These findings suggest that although the nodes of Ranvier are shortened in response to hypoperfusion the well-defined spatial distribution between the nodal $Na_v1.6$ channels and the paranodal Caspr is disrupted. The $Na_v1.6$ channels are expanded into the Caspr domain indicating a level of paranodal disruption. This is observed in young and aged wild-type animals and TgAPPSw,Ind animals; however, in the young TgAPPSw,Ind mice this phenotype is exacerbated compared to wild-type hypoperfused mice.

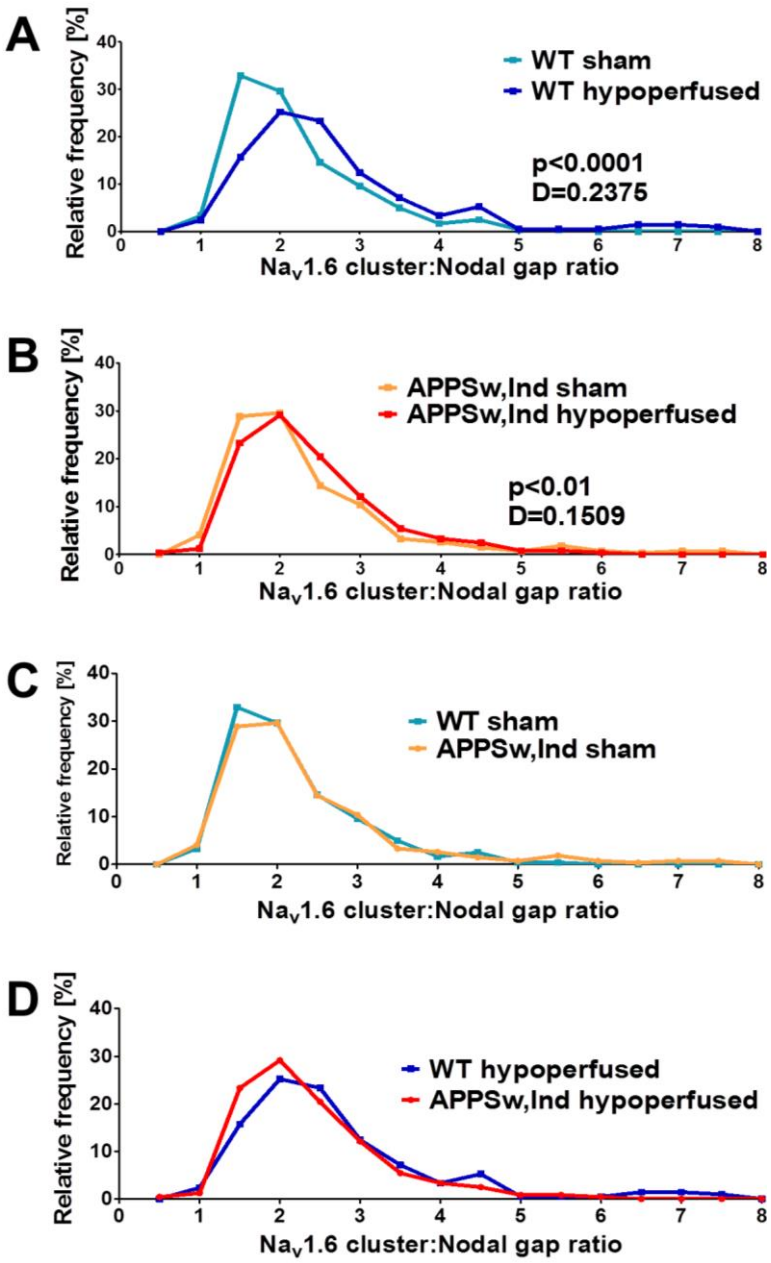

Figure 4.11 ***Expansion of the $Na_v1.6$ channels into the paranodal domains in response to hypoperfusion in the corpus callosum of aged animals***. $Na_v1.6$ cluster to nodal gap length was calculated as a measure of paranodal disruption and expansion of the $Na_v1.6$ channels into the paranodal domain There is a significant increase in the $Na_v1.6$ cluster to nodal gap length ratio [A-B] in both WT (p < 0.0001) and TgAPPSw,Ind (p < 0.01) hypoperfused animals. No difference (p > 0.05) was observed between genotypes in either the sham animals or the hypoperfused [C-D]. $Na_v1.6$ cluster and nodal gap length was measured on 30 identical nodes for each animal and the ratio of $Na_v1.6$ cluster to nodal gap length was plotted as distribution of percentage of relative frequencies. WT sham: n=8, WT hypoperfused: n=9, TgAPPSw,Ind sham: n=8, TgAPPSw,Ind hypoperfused n=8.

4.3.5 No altered distribution of juxtaparanodal $K_v1.2$ channels in response to hypoperfusion

The previous work indicated that cerebral hypoperfusion induced paranodal disruption since $Na_v1.6$ normally contained within the nodes overlapped with Caspr in paranodes. To further investigate paranodal disruption the distribution of the juxtaparanodal $K_v1.2$ channels was investigated by examining the percentage volume of Caspr immunolabeled paranodes that is occupied by $K_v1.2$ channels in a 43.5x43.5x5 μm^3 confocal stack imaged at corpus callosum of young and old, sham and hypoperfused, wild-type and APPSw,Ind mutant mice.

However the data indicated that hypoperfusion does not result in expansion of $K_v1.2$ channels into the paranodal area in either the young of the aged animals. In the young animals [Figure 4.12 A & B], there was no significant effect of genotype (p = 0.5750, $F_{(1-31)}$ = 0.3211) or surgery ($F_{(1-31)}$ = 0.6127, p = 0.4397) in the percentage volume of Caspr immunolabeled paranodes occupied by $K_v1.2$ channels. Moreover, there was no interaction between age and genotype ($F_{(1-31)}$ = 0.4957, p = 0.4866). Similarly in the aged animals [Figure 4.12 C & D] there was no significant effect of genotype ($F_{(1-31)}$ = 0.0704, p = 0.7925) or surgery ($F_{(1-31)}$ = 0.1182, p = 0.7333) in the percentage volume of CASPR immunolabeled paranodes occupied by $K_v1.2$ channels. Moreover, there was no interaction overall between age and genotype ($F_{(1-31)}$ = 0.5037, p = 0.4832).

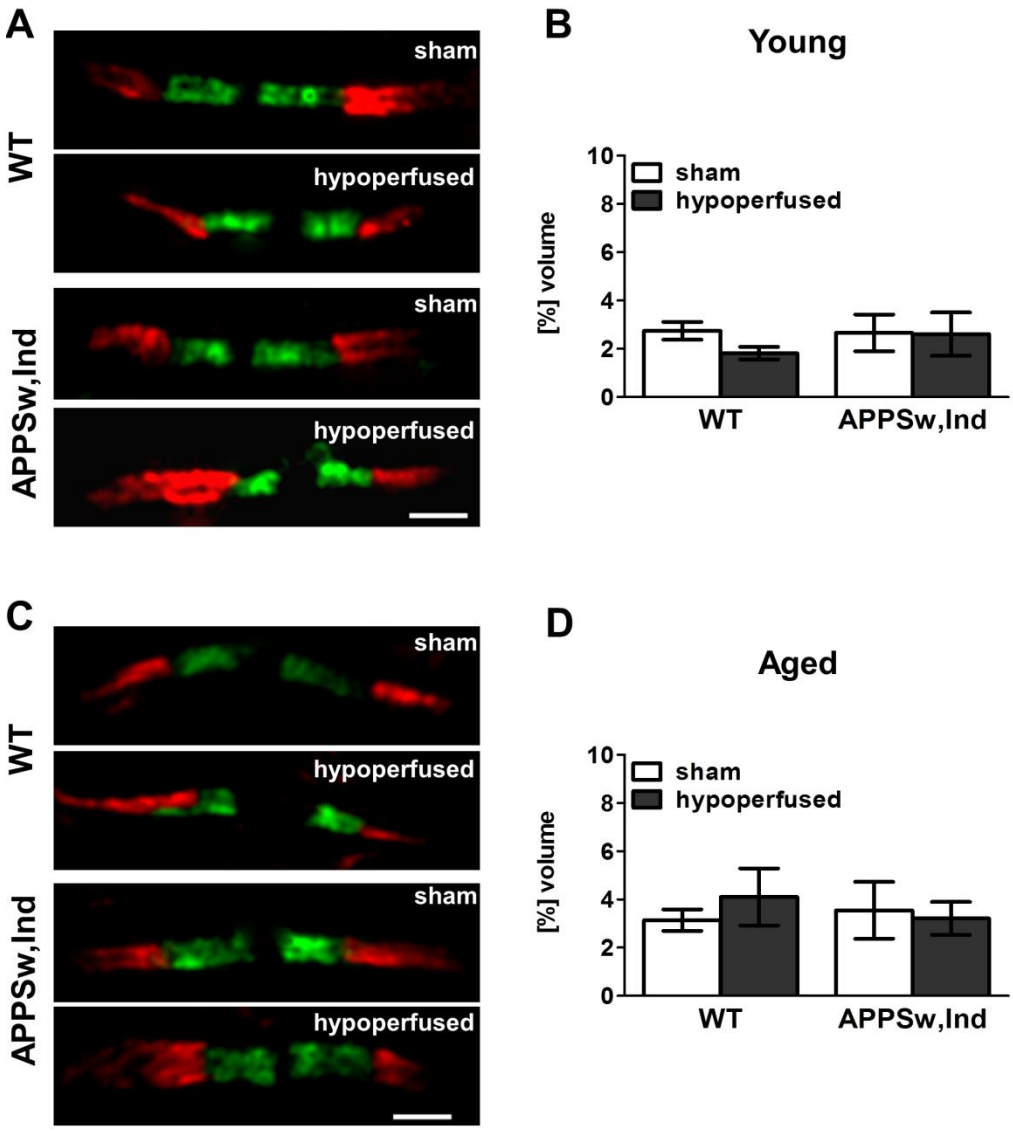

Figure 4.12 ***No evidence of altered K_v1.2 distribution in response to hypoperfusion in young or aged animals.*** Representative images of Caspr (green) and K_v1.2 (red) double immunostaining [A & C]. No change ($p > 0.05$) in [%] volume of Caspr positive domains that are colocalised with K_v1.2 was observed in either the young or the aged animals [B & D]. Colocalisation was analysed in a 43.5x43.5x5 μm^3 confocal stack from the corpus callosum. Young: WT sham: *n*=9, WT hypoperfused: *n*=8, TgAPPSw,Ind sham: *n*=9, TgAPPSw,Ind hypoperfused *n*=9; Aged: WT sham: *n*=9, WT hypoperfused: *n*=9, TgAPPSw,Ind sham: *n*=8, TgAPPSw,Ind hypoperfused *n*=9.Graphs show mean ± SEM. Scale bar 2µm

4.3.6 No evidence of gross myelin or axonal alterations in response to hypoperfusion in young animals

White matter damage is closely related to both cerebral hypoperfusion and AD. In addition, myelin loss has been suggested to be implicated in the disruption of the protein architecture at the nodes of Ranvier, therefore both components of the white matter, the myelin and the axons were investigated in the corpus callosum of young animals. Gross myelin alterations induced by hypoperfusion were examined in corpus callosum using immunolabelling for MBP in young wild-type and TgAPPSw,Ind animals. The percentage area occupied by MBP was assessed (Figure 4.13 A-D). It was shown that neither hypoperfusion (p = 0.6214, $F_{(1-43)}$ = 0.2476) nor genotype (p = 0.6601, $F_{(1-43)}$ = 0.1961) had a significant effect on the percentage area occupied by MBP (Figure 4.13 E). In addition, gross changes in axonal integrity in response to hypoperfusion were examined at the same area using immunolabelling for total neurofilament (SMI312) (Figure 4.14 A-D). There was no significant effect of hypoperfusion (p = 0.0587, $F_{(1-43)}$ = 3.758) or genotype (p = 0.3829, $F_{(1-43)}$ = 0.7761) on the percentage area occupied by total-neurofilament (Figure 4.14 E). This finding suggests that no gross alterations in myelin or axonal integrity are induced by hypoperfusion in the corpus callosum of young wild-type and TgAPPSw,Ind animals.

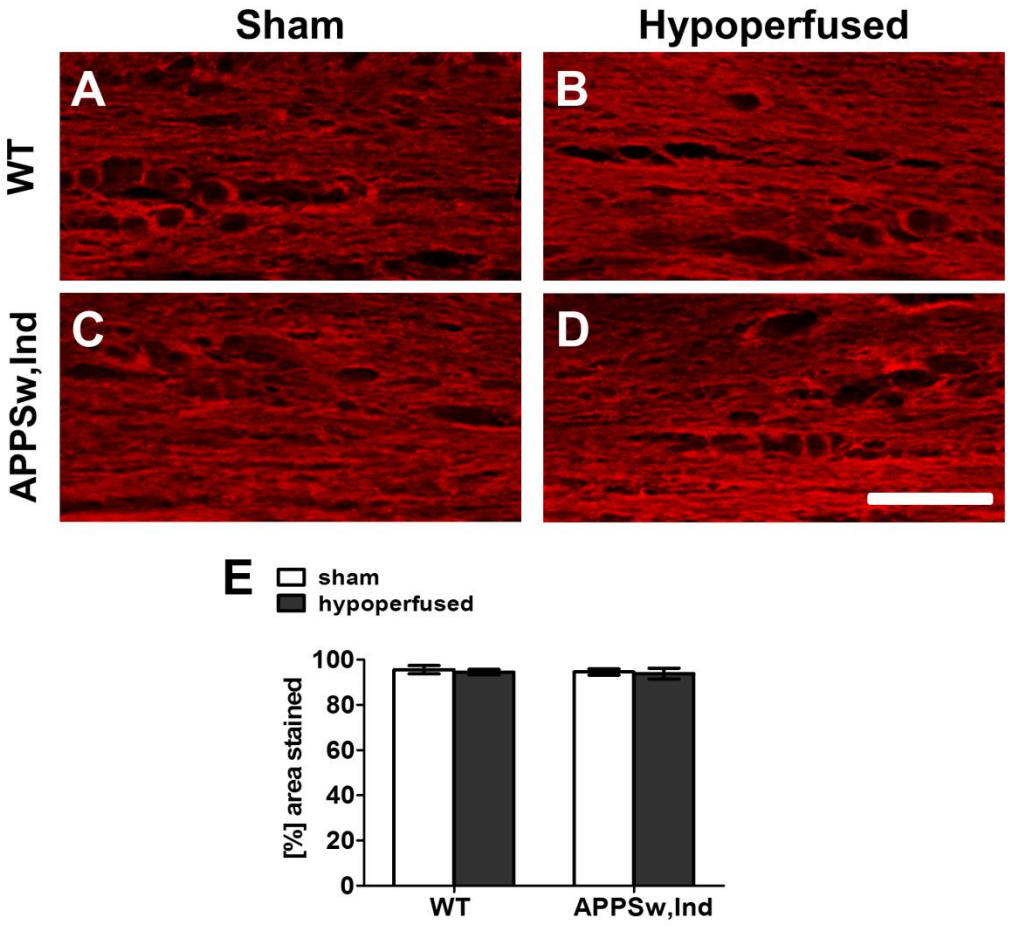

Figure 4.13 ***No myelin alterations in response to hypoperfusion in the corpus callosum of young animals***. Gross myelin integrity was assessed in the corpus callosum using an anti-MBP antibody [A-D]. Analysis of the [%] area of MBP staining did not show any significant ($p > 0.05$) effect of hypoperfusion or genotype [E]. WT sham: n=10, WT hypoperfused: n=12, TgAPPSw,Ind sham: n=13, TgAPPSw,Ind hypoperfused n=10.Scale bar 50 µm. Graphs show mean ± SEM.

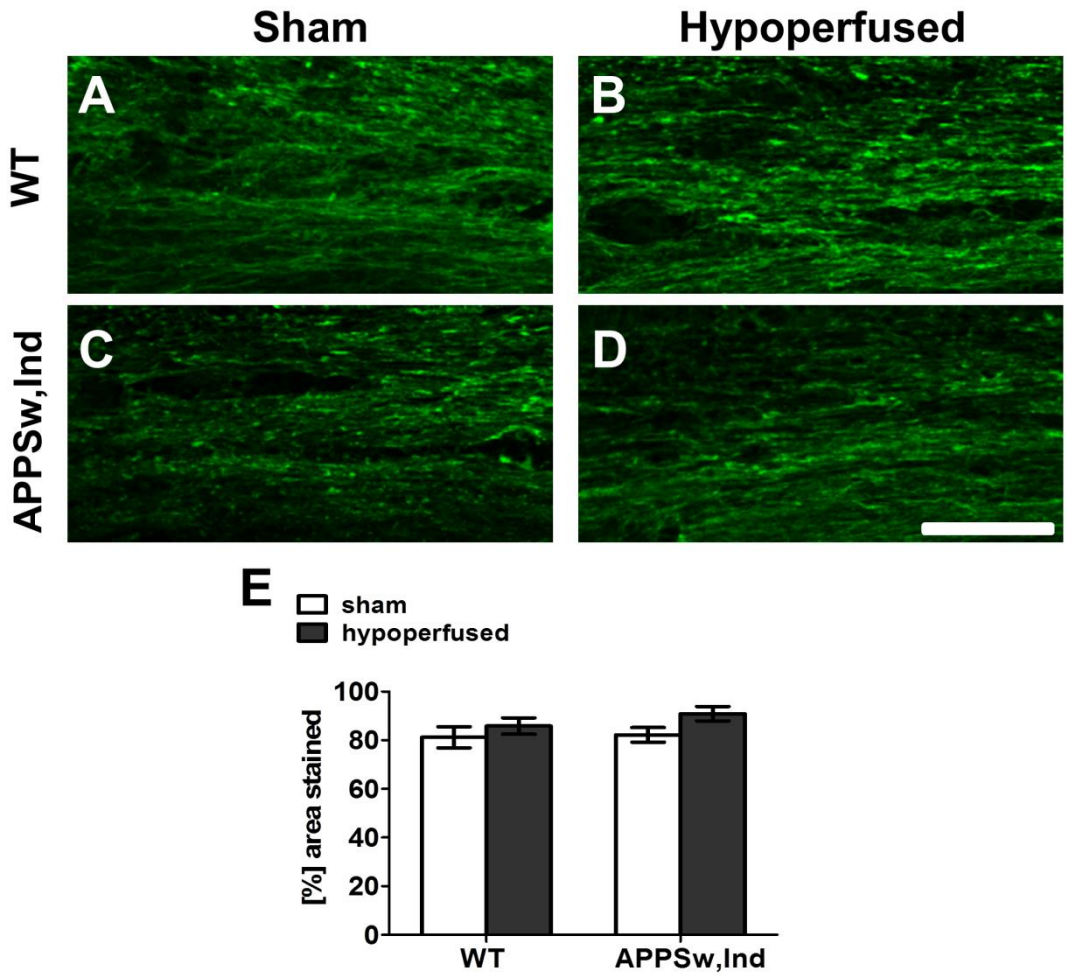

Figure 4.14 ***No axonal alterations in response to hypoperfusion in the corpus callosum of young animals***. Axonal pathology was assessed in the corpus callosum using an anti-total neurofilament antibody (SMI312). Analysis of the [%] area of total neurofilament staining did not show in the young [A-E] or the aged [F-J] animals any significant effect of hypoperfusion in either genotypes ($p > 0.05$). WT sham: n=10, WT hypoperfused: n=12, TgAPPSw,Ind sham: n=13, TgAPPSw,Ind hypoperfused n=10. Scale bar 50 μm. Graphs show mean ± SEM.

4.3.7 No evidence of gross myelin or axonal alterations in response to hypoperfusion in aged animals

Gross myelin and axonal alterations induced by hypoperfusion were also examined in corpus callosum of aged wild-type and TgAPPSw,Ind animals. The percentage area occupied by MBP was assessed. It was demonstrated that neither hypoperfusion (p = 0.4565, $F_{(1-43)}$ = 0.5647) nor genotype (p = 0.0831, $F_{(1-45)}$ = 3.148) have a significant effect on the percentage area occupied by MBP (Figure 4.15 E). In addition, gross changes in axonal integrity in response to hypoperfusion were examined at the same area using immunolabelling for total neurofilament (SMI312) (Figure 4.16 A-D). There was no significant effect of hypoperfusion (p = 0.8101, $F_{(1-43)}$ = 0.05846) or genotype (p = 0.7288, $F_{(1-43)}$ = 0.1218) on the percentage area occupied by total-neurofilament. This finding suggests that no gross alterations in myelin or axonal integrity are induced by hypoperfusion in the corpus callosum of aged wild-type and TgAPPSw,Ind animals.

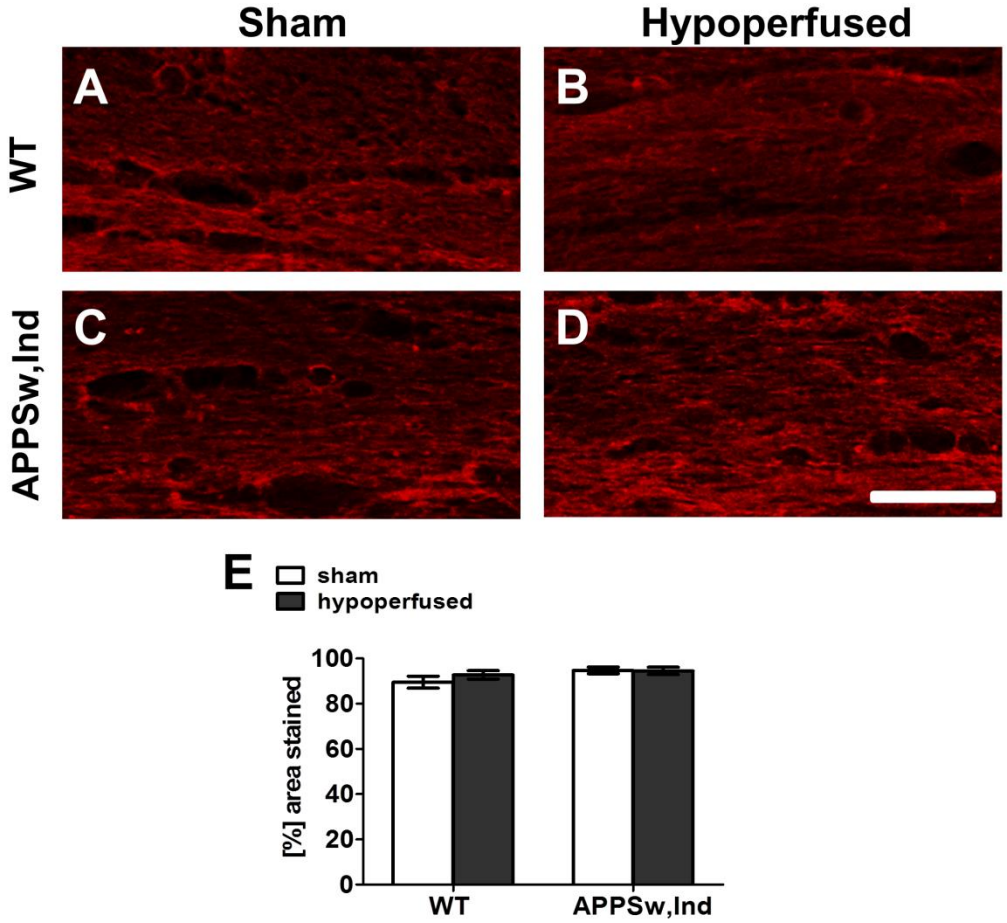

Figure 4.15 ***No myelin alterations in response to hypoperfusion in the corpus callosum of aged animals***. Gross myelin integrity was assessed in the corpus callosum using an anti MBP antibody [A-D]. Analysis of the [%] area of MBP staining did not show any significant ($p > 0.05$) effect of hypoperfusion or genotype [E]. WT sham: n=11, WT hypoperfused: n=13, TgAPPSw,Ind sham: n=11, TgAPPSw,Ind hypoperfused n=12. Scale bar 50 µm. Graphs show mean ± SEM.

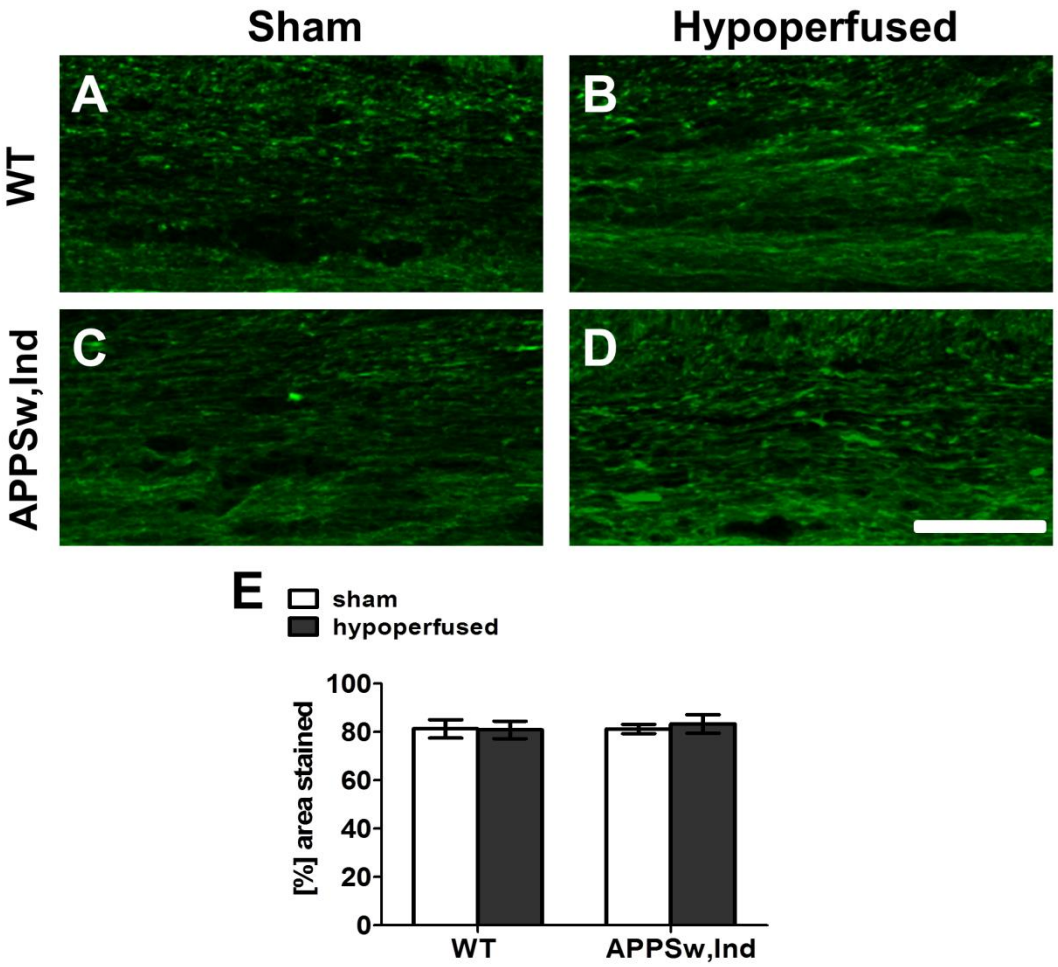

Figure 4.16 ***No axonal alterations in response to hypoperfusion in the corpus callosum of aged animals***. Gross axonal integrity was assessed in the corpus callosum using an anti-total neurofilament antibody (SMI312) [A-D]. Analysis of the [%] area of MBP staining did not show any significant change ($p > 0.05$) in response to hypoperfusion or genotype [E]. WT sham: n=11, WT hypoperfused: n=13, TgAPPSw,Ind sham: n=11, TgAPPSw,Ind hypoperfused n=12. Scale bar 50 µm. Graphs show mean ± SEM.

4.3.8 Myelin basic protein and neurofilament levels are not changed in response to hypoperfusion in young and aged animals

To further confirm that there is no overall change to the protein levels of myelin and axonal markers in response to hypoperfusion, the levels of myelin basic protein (MBP), total neurofilament and heavy neurofilament (NF-H, 200 KDa) were examined in the tissue homogenates of young and old TgAPPSw,Ind and wild-type hypoperfused mice with western blotting. Western blotting for MBP showed four bands at 21.5, 18.5, 17 and 14 KDa All four bands were quantified. Western blotting for total neurofilament and NF-H showed bands at 200 KDa which were quantified.

In the young animals (Figure 4.17 A) no significant change in the protein levels of MBP, total neurofilament or NF-H in response to hypoperfusion (MBP: $p = 0.5223$, $F_{(1-48)} = 0.413$; total neurofilament: $p = 0.7662$, $F_{(1-49)} = 0.0894$; NF-H: $p = 0.6835$, $F_{(1-48)} = 0.1683$) or between the different genotypes (MBP: $p = 0.9019$, $F_{(1-48)} = 0.0153$; total neurofilament: $p = 0.4084$,$F_{(1-49)} = 0.0954$; NF-H: $p = 0.2742$, $F_{(1-48)} = 1.223$) was observed (Figure 4.17 B-D).

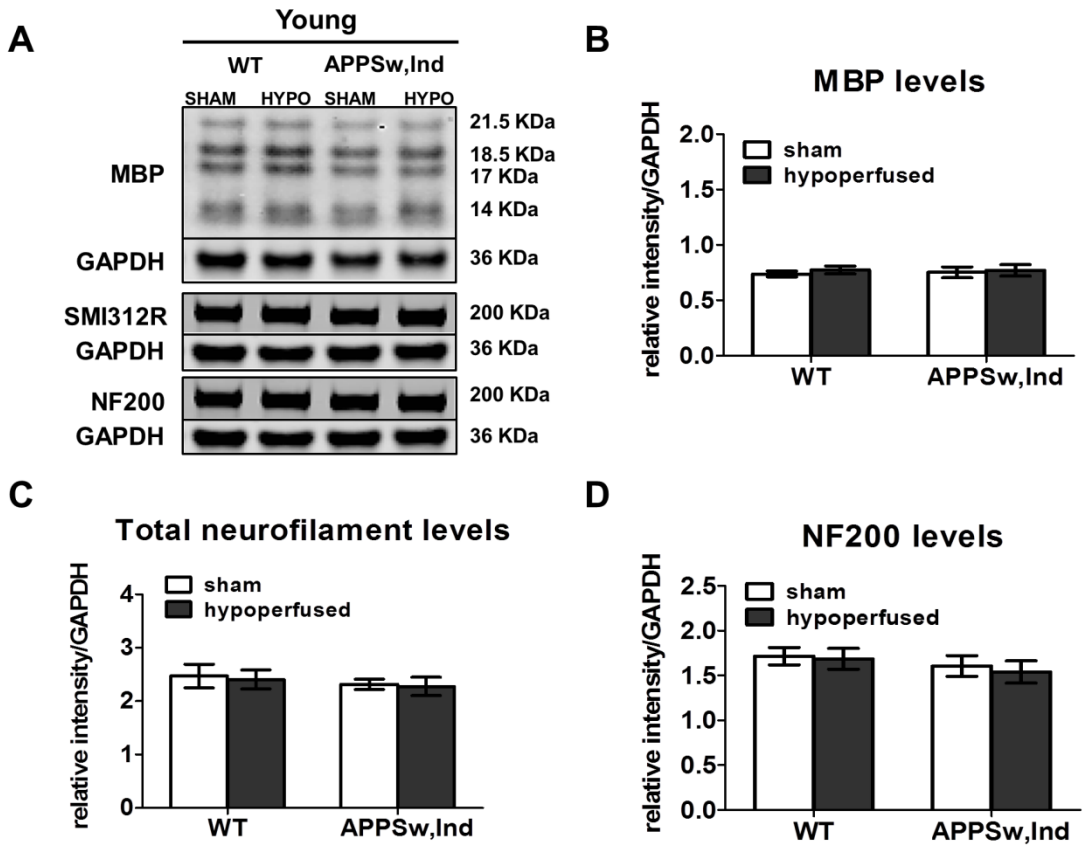

Figure 4.17 ***No change in the protein levels of myelin basic protein, total neurofilament and neurofilament 200 KDa in young animals.*** Total levels of MBP, total neurofilament (SMI312) and NF200 were assessed in tissue homogenates of young animals using western blotting [A]. There is no significant ($p > 0.05$) effect of hypoperfusion or genotype in the levels of MBP [B], total neurofilament [C] or NF200 [D]. Graphs show mean ± SEM.

Similarly in the aged animals the levels of MBP, total neurofilament and NF-H (Figure 4.18 A) were not significantly different in response to hypoperfusion (MBP: p = 0.1609, $F_{(1-47)}$ = 0.2029; total neurofilament: p = 0.8354,$F_{(1-48)}$ = 0.0436; NF-H: p = 0.9256, $F_{(1-48)}$ = 0.0088) between the different genotypes (MBP: p = 0.2656, $F_{(1-47)}$ = 0.1.269; total neurofilament: p = 0.9747; $F_{(1-48)}$ = 0.0010; NF-H: p = 0.7585; $F_{(1-48)}$ = 0.0955) (Figure 4.18 B-D)

These finding combined with those described in the previous chapter suggest that there are no changes in either the protein levels or the pattern of staining of myelin basic protein and neurofilament in response to hypoperfusion.

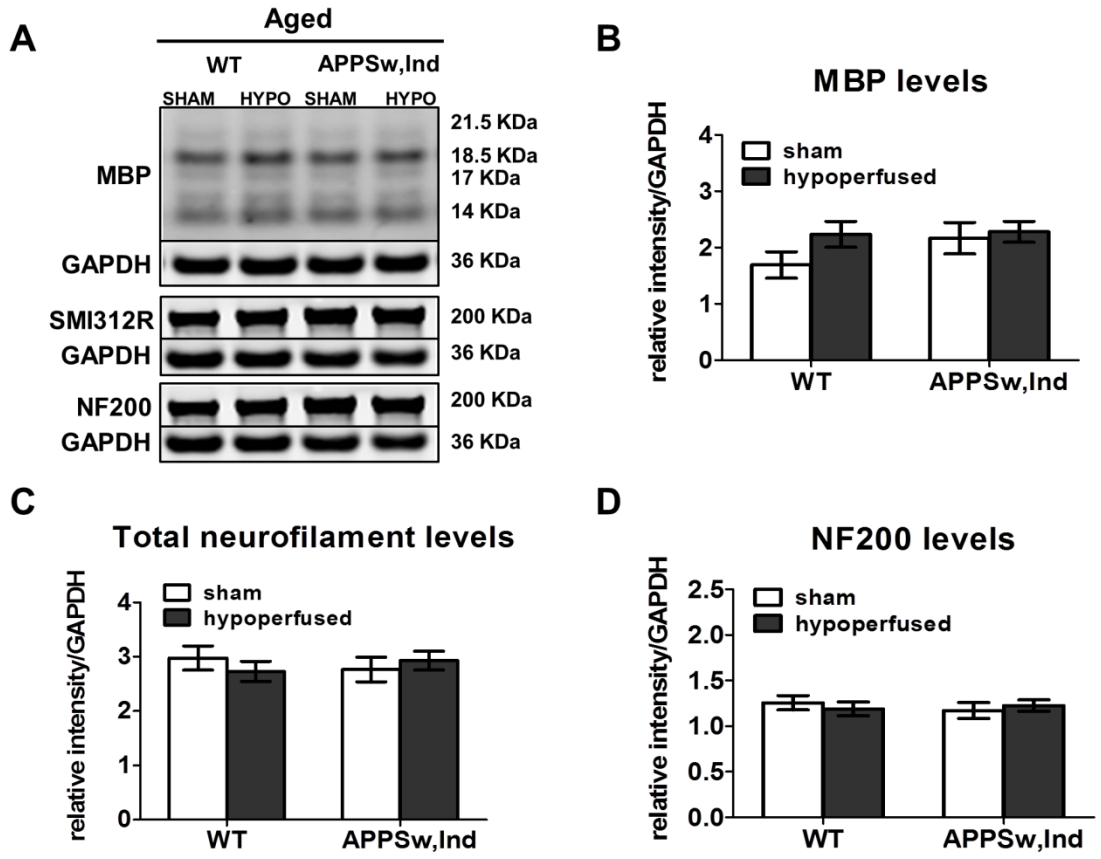

Figure 4.18 ***No change in the protein levels of myelin basic protein, total neurofilament and neurofilament 200 KDa in aged animals.*** Total levels of MBP, total neurofilament (SMI312) and NF200 were assessed in tissue homogenates using western blotting [A]. In the aged animals there was no significant effect of hypoperfusion or genotype ($p > 0.05$) in the levels of MBP [B], total neurofilament [C] or NF200 [D]. Graphs show mean ± SEM.

4.3.9 Human Aβ42 levels change in response to hypoperfusion in young but not aged TgAPPSw,Ind

Some the observed changes in response to hypoperfusion described in this chapter are indicated to be exacerbated in the TgAPPSw,Ind animals which may reflect changes in the Aβ levels. To examine this, the levels of hAβ42 were examined in tissue homogenates of young and aged hypoperfused TgAPPSw,Ind animals.

Interestingly in the young animals, chronic cerebral hypoperfusion significantly reduced hAβ2 levels in the TgAPPSw,Ind animals ($p = 0.0145$, $|t| = 2.665$, Figure 4.19 A) as compared to sham animals.

In the aged animals, however, there was no significant change in the levels of hAβ2 in response to hypoperfusion in the aged TgAPPSw,Ind mice ($p = 0.570$, $|t| = 0.5759$, Figure 4.19 B) as compared to sham.

These finding suggest that cerebral hypoperfusion affects the levels of Aβ42 in the brain of young but not aged TgAPPSw,Ind animals.

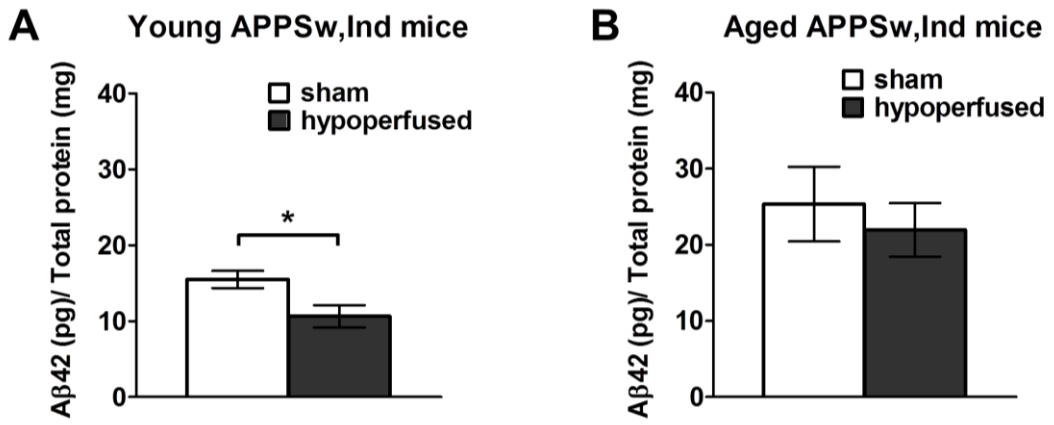

Figure 4.19 ***Human Aβ42 levels are reduced in response to hypoperfusion in young but not aged TgAPPSw,Ind mice***. Human Aβ42 levels detected with ELISA are significantly reduced ($p < 0.01$) in young TgAPPSw,Ind animals [A]. No significant ($p > 0.05$) change is detected in the aged TgAPPSw,Ind hypoperfused animals [B]. Young: TgAPPSw,Ind sham: n=13, TgAPPSw,Ind hypoperfused n=10; Aged: TgAPPSw,Ind sham: n=11, TgAPPSw,Ind hypoperfused n=15. Graphs show mean ± SEM.

4.3.10 Levels of APP and APP processing products unchanged with hypoperfusion

Amyloid precursor protein and the C-terminal products, C83 and C99, of the amyloidogenic and non-amyloidogenic processing of APP were quantified in brain tissue homogenates in order to investigate whether total APP levels of APP-processing are altered in response to hypoperfusion. Western blotting for APP in the TgAPPSw,Ind mice showed a triple band around 100 KDa detecting both mouse and human APP, while in the wild-type animals; it showed only one band around 100 KDa. C83 and C99 are C-terminal fragments deriving from the proteolytic processing of the APP through the non-amyloidogenic and the amyloidogenic pathway respectively. Western blotting for C-terminal fragments showed a C83 band at 9 KDa and C99 at 11 KDa (Figure 4.20 A and 4.21 A).

In the young TgAPPSw,Ind animals, there is a significant increase overall in APP levels ($p < 0.0001$, $F_{(1-49)} = 228.3$) compared to wild-type (Figure 4.20 B). However, it was shown that hypoperfusion did not have any overall effect on APP expression levels ($p = 0.0997$, $F_{(1-49)} = 2.816$). *Post-hoc* analysis showed that both in young hypoperfused and sham TgAPPSw,Ind mice, APP levels are significantly higher compared to young hypoperfused ($p < 0.001$, $|t| = 10.55$) and sham ($p < 0.001$, $|t| = 10.82$) wild-types. Moreover, there is a significant overall increase in the levels of C83 (, $p < 0.0001$, $F_{(1-48)} = 48.04$) and C99 ($p < 0.0001$, $F_{(1-49)} = 27.06$) fragments in the TgAPPSw,Ind mice compared to wild-type (Figure 4.20 C and D). However, hypoperfusion did not have any overall effect on C83 ($p = 0.1515$, $F_{(1-49)} = 2.124$) or C99 ($p = 0.2656$, $F_{(1-49)} = 1.257$) expression levels. *Post-hoc* analysis showed that in young hypoperfused and in young sham TgAPPSw,Ind mice C83 and C99 levels are

significantly higher when compared to young hypoperfused (for C83: $p < 0.001$, $|t| = 5.543$; for C99: $p < 0.001$, $|t| = 4.285$) and young sham (for C83: $p < 0.001$, $|t| = 4.285$; for C99: $p < 0.01$, $|t| = 3.144$) wild-types respectively.

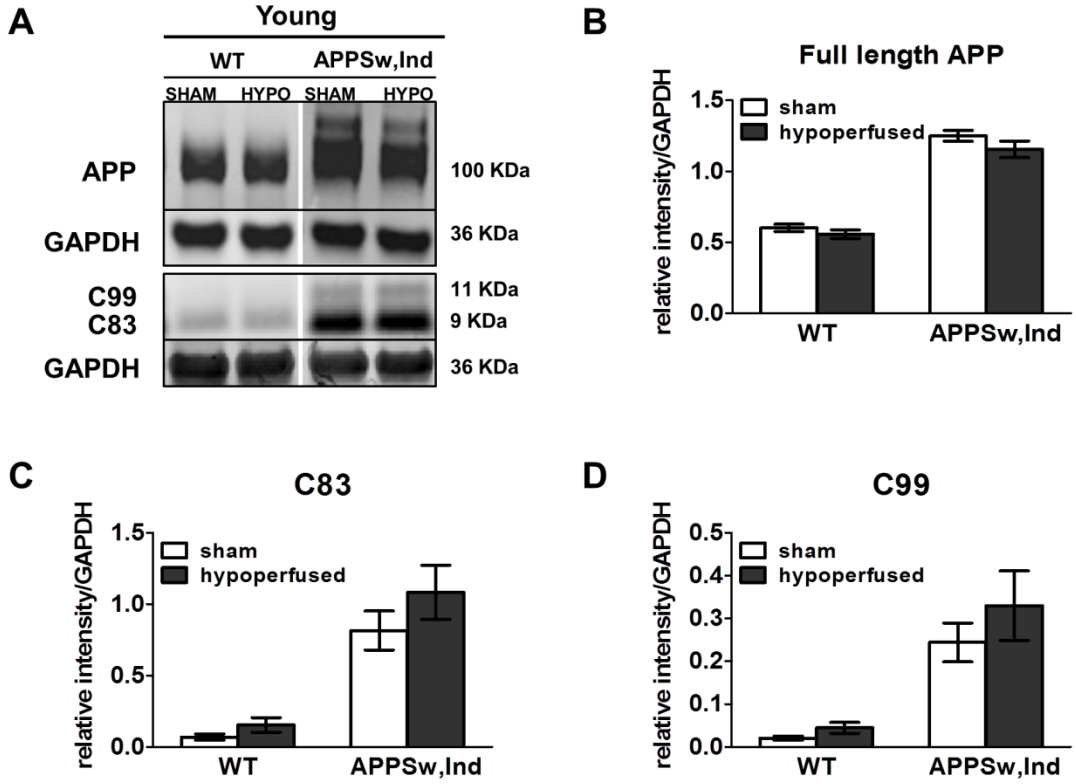

Figure 4.20 ***APP protein levels and APP processing unchanged with hypoperfusion in young animals***. Full length APP and the C-terminal products, C83 and C99, of the amyloidogenic and non-amyloidogenic processing of APP were detected with western blotting [A]. There was a significant increase ($p < 0.0001$) overall in the levels of full length APP, C83 and C99 in the TgAPPSw,Ind animals compared to wild-types, but no change ($p < 0.05$) in response to hypoperfusion in the levels of APP, C83 or C99 was observed. Graphs show mean ± SEM.

Similarly, in the aged TgAPPSw,Ind mice APP levels (Figure 4.21 B) were overall increased compared to wild-type animals ($p < 0.0001$, $F_{(1-48)} = 222.2$). However, it was shown that hypoperfusion did not change overall APP levels ($p = 0.2783$, $F_{(1-48)} = 1.203$). *Post-hoc* analysis for the aged animals showed that in both the hypoperfused and the sham TgAPPSw,Ind mice APP expression levels are significantly increased compared to young hypoperfused ($p < 0.001$, $|t| = 10.64$) and sham ($p < 0.001$, $|t| = 10.48$) wild-types. In addition, a significant increase overall in the levels of C83 ($p < 0.0001$, $F_{(1-49)} = 57.05$) and C99 ($p < 0.0001$, $F_{(1-49)} = 41.69$) fragments compared to wild-type animals was observed (Figure 4.21 C and D). However, hypoperfusion did not have any overall effect on C83 ($p = 0.1515$, $F_{(1-49)} = 0.3842$) or C99 ($p = 0.3113$, $F_{(1-49)} = 1.047$,) expression levels (Figure 4.2 E & G). *Post-hoc* analysis showed that in aged hypoperfused and in aged sham TgAPPSw,Ind mice C83 and C99 levels are significantly higher when compared to young hypoperfused (for C83: $p < 0.001$, $|t| = 6.092$; for C99: $p < 0.001$, $|t| = 4.934$) and aged sham (for C83: $p < 0.001$, $|t| = 4.707$; for C99: $p < 0.001$, $|t| = 4.262$) wild-types respectively.

These findings suggest that hypoperfusion does not alter APP levels or APP processing and not surprisingly the introduction of the APP transgene in the TgAPPSw,Ind increases the levels of full length APP and APP processing products.

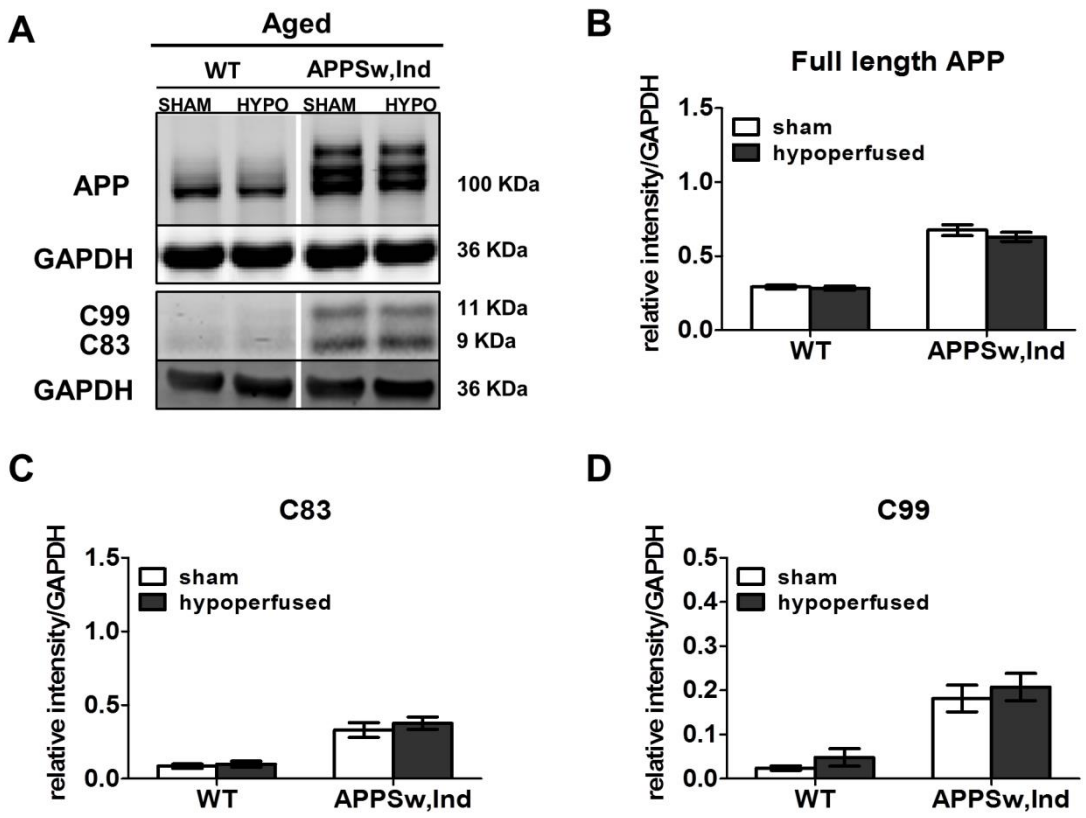

Figure 4.21 ***APP protein levels and APP processing unchanged with hypoperfusion in aged animals***. Full length APP and the C-terminal products, C83 and C99, of the amyloidogenic and non-amyloidogenic processing of APP were detected with western blotting [A]. There was a significant increase ($p < 0.0001$) overall in the levels of full length APP, C83 and C99 in the TgAPPSw,Ind animals compared to wild-types, but no change ($p < 0.05$) in response to hypoperfusion in the levels of APP, C83 or C99 was observed. Graphs show mean ± SEM.

4.3.11 Impairment of spatial working memory in response to hypoperfusion in young animals

Hypoperfusion is suggested to affect spatial working memory, thus this effect may be exacerbated in the TgAPPSw,Ind animals. To investigate that, spatial working memory performance was examined in response to hypoperfusion in young wild-type and TgAPPSw,Ind mice.

Spatial working memory performance was assessed by measuring the number of revisiting errors in the 8-arm radial arm maze. Over the 16-day training period (trial block 1-8) the number of errors made by the animals was reduced ($F_{(5.4, 235)} = 5.569$; $p < 0.001$) which indicated that the mice were able to learn the task (Figure 4.22). There was also a significant main effect of hypoperfusion with hypoperfused mice making more revisiting errors than the shams ($p < 0.001$, $F_{(1, 43)} = 26.172$) demonstrating that hypoperfusion impairs working memory performance (Figure 4.22 A and B). In addition, there was also significant interaction between the different genotype and surgery condition over trial blocks ($p = 0.02$, $F_{(5.4, 235.9)} = 2.645$) which may indicate that the effect of hypoperfusion on spatial working memory is different between wild-type and TgAPPSw,Ind mice.

Moreover, memory acquisition was examined by calculating the gradient of the line generated between the numbers of errors in block 1 to block 8. Each group yielded the following acquisition slopes WT sham: -0.452 ± 0.253, WT hypoperfused: -1.5 ± 0.424, TgAPPSw,Ind sham: -1.093 ± 0.279 and TgAPPSw,Ind hypoperfused: 0.193 ± 0.281 where greater negative values are indicative of good memory acquisition ability and values greater or equal to zero suggest that the animals do not improve

their performance over time. Analysis showed a significant interaction between genotype and hypoperfusion (p = 0.001, $F_{(1, 43)}$ = 13.216) suggesting that the deficit induced by hypoperfusion differently affects wild-type and APPSw,Ind mice. Indeed, there was a significant difference in the acquisition rate between hypoperfused wild-type and TgAPPSw,Ind ($p < 0.01$, $|t| = 3.610$), with the TgAPPSw,Ind hypoperfused mice showing slower memory acquisition (Figure 4.22 D). In addition, no difference in the acquisition rate was observed between the two genotypes under sham conditions ($p > 0.05$, $|t| = 1.462$) (Figure 4.22 C).

These finding suggest that hypoperfusion impairs spatial working memory in both genotypes; however the deficit is more severe in the TgAPPSw,Ind hypoperfused animals.

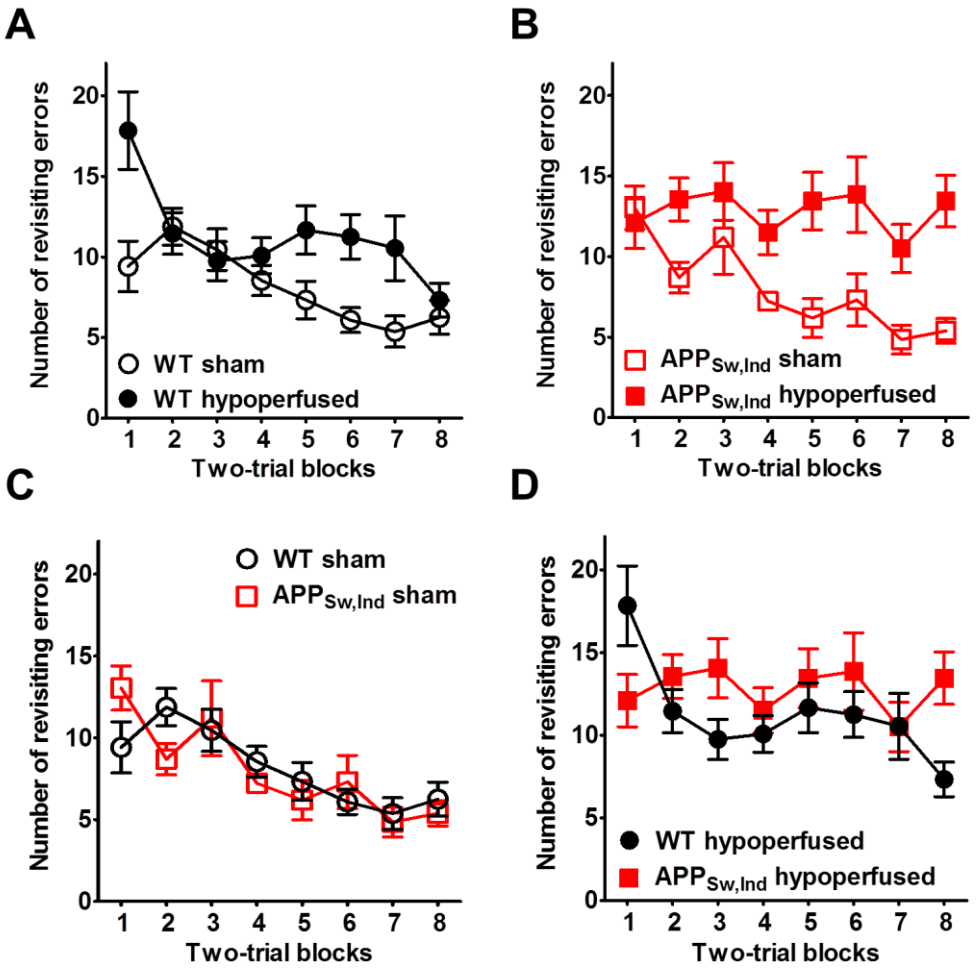

Figure 4.22 ***Spatial working memory impairment induced by hypoperfusion is exacerbated in young TgAPPSw,Ind mice***. Hypoperfused mice make significantly more revisiting errors than the sham mice ($p<0.05$) [A & B]. There is no difference between the genotypes under sham conditions [C] TgAPPSw,Ind hypoperfused mice showing significantly ($p < 0.01$) slower memory acquisition than the WT [D]. WT sham: n=12, WT hypoperfused: n=12, TgAPPSw,Ind sham: n=13, TgAPPSw,Ind hypoperfused n=10. Data presented in two-trial blocks. Graphs show mean ± SEM.

4.3.12 Impairment of spatial working memory in response to hypoperfusion in aged animals

Spatial working memory was next examined in aged wild-type and TgAPPSw,Ind and in response to hypoperfusion.

Over the 16-day training period (trial block 1-8) the number of errors made by the animals was reduced ($F_{(5.29, 259.3)} = 8.058$; $p < 0.001$) which indicated that the mice were able to learn the task (Figure 4.23). There was also a significant main effect of hypoperfusion with hypoperfused mice making more revisiting errors than the shams ($p < 0.001$, $F_{(1, 49)} = 21.549$) demonstrating that hypoperfusion impairs working memory performance (Figure 4.23 A and B). Moreover, memory acquisition was also examined. Each group yielded the following acquisition slopes: WT sham: -0.887 ± 0.292, WT hypoperfused: -1 ± 0.25, APPSw,Ind sham: -0.195 ± 0.332 and TgAPPSw,Ind hypoperfused: -0.305 ± 0.274, however no difference ($p > 0.05$) in the performance of the two genotypes either under sham or hypoperfused conditions (Figure 4.23 C-D) was revealed.

These findings indicate that in both aged wild-type and TgAPPSw,Ind mice hypoperfusion results in an impairment in spatial working memory. This impairment was severe, with both genotypes being poorly able to improve their performance and as a result it was similarly affected in both wild-type and TgAPPSw,Ind mice.

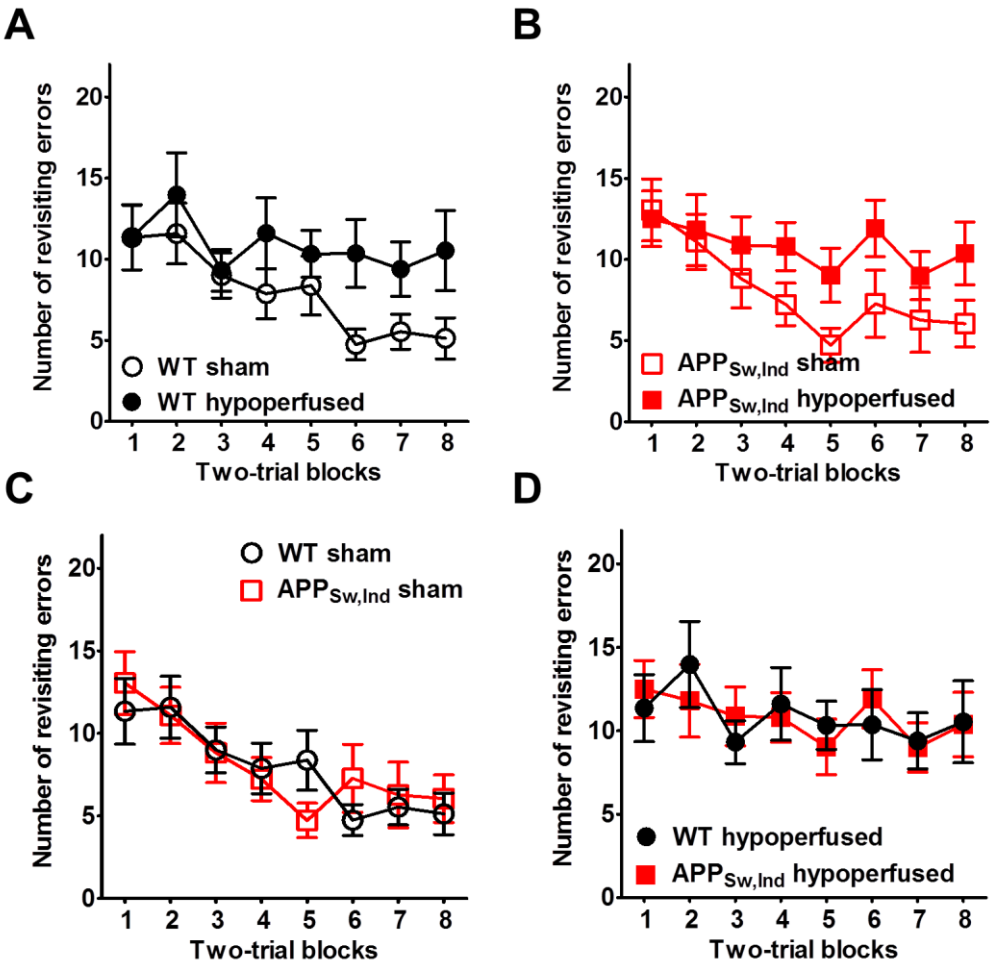

Figure 4.23 ***Spatial working memory impairment induced by hypoperfusion is exacerbated in aged TgAPPSw,Ind mice***. Hypoperfused mice make significantly more revisiting errors than the sham mice ($p<0.05$) [A & B]. There is no difference between the genotypes under sham conditions [C] TgAPPSw,Ind hypoperfused mice made the same number of errors compared to WT [D]. WT sham: *n*=14, WT hypoperfused: *n*=12, TgAPPSw,Ind sham: *n*=11, TgAPPSw,Ind hypoperfused *n*=15. Data presented in two-trial blocks. Graphs show mean ± SEM.

4.3.13 Impairment of spatial working memory associated with nodal alterations in aged animals

It is indicated here that hypoperfusion affects working memory in the eight-arm radial arm maze and causes alterations at the nodal/paranodal regions of the myelinated axons. These regions are important for saltatory conduction hence effective for neural function. Therefore it may be suggested that alterations to paranodal integrity are associated with spatial working memory performance

To investigate that, in the aged animals, where spatial working memory performance was investigated in the same cohort, the association between the number of revisiting errors at trial block 8 with the average $Na_v1.6$ cluster to nodal gap length ratio was determined. A significant correlation between spatial working memory impairment and paranodal disruption was found (Figure 4.24), indicating that the animals which make more errors are more likely to have higher $Na_v1.6$ cluster to nodal gap length ratio ($r = 0.3833$, $p = 0.0303$), hence greater expansion of the $Na_v1.6$ cluster into the paranodal domain. This data provides a link between nodal alterations and cognitive performance. Unfortunately, the same association was not possible in the young animals as different cohorts of animals were used the evaluation of working memory performance and nodal integrity.

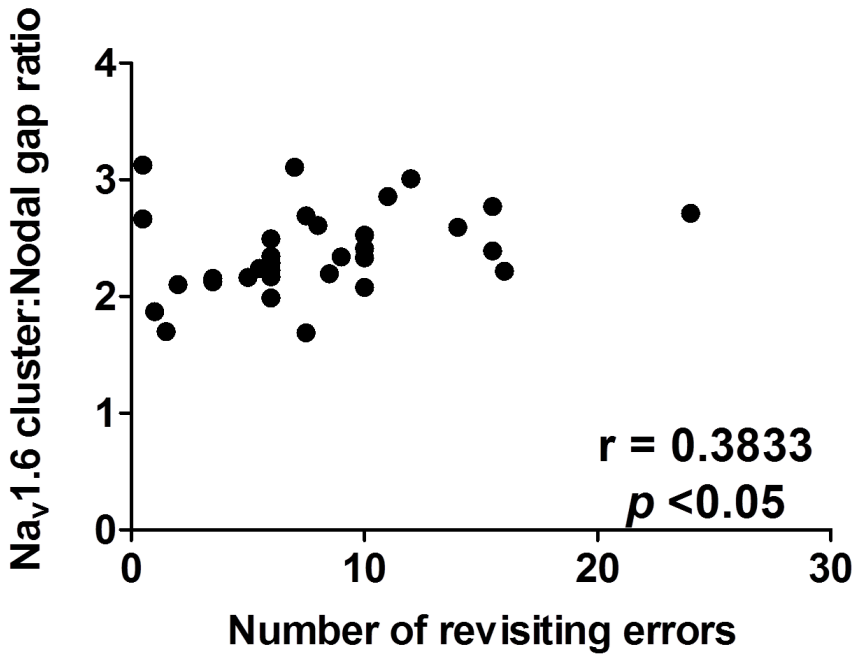

Figure 4.24 ***Working memory performance correlates with Na$_v$1.6 cluster to nodal gap ratio.*** Plotting the number of revisiting errors at trial block 8 with the average Na$_v$1.6 cluster: nodal gap ratio revealed a significant correlation ($p < 0.05$) indicating a link between nodal alterations and cognitive deficits.

4.3.14 Summary of results

The following table (Table 4.3) summarises the findings described in the present chapter

Table 4.3 Summary of results

Feature examined	Age	Findings
$Na_v1.6$ cluster length *(corpus callosum)*	Y	↓ with hypoperfusion (both WT and APPSw,Ind) ↓ in APPSw,Ind hypoperfused compared to WT hypoperfused
	A	↓ with hypoperfusion (both WT and APPSw,Ind)
Nodal gap length *(corpus callosum)*	Y	↓ with hypoperfusion (both WT and APPSw,Ind) ↓ in APPSw,Ind hypoperfused compared to WT hypoperfused
	A	↓ with hypoperfusion (both WT and APPSw,Ind)
$Na_v1.6$ cluster length *(hippocampus)*	Y	↔
	A	↓ with hypoperfusion (both WT and APPSw,Ind)
Nodal gap length *(hippocampus)*	Y	↔
	A	↓ with hypoperfusion (only WT)
Nodal number	Y	↔
	A	↔
MBP (% area)	Y	↓ in aged WT compared to young
	A	
$Na_v1.6$ cluster to nodal gap length ratio	Y	↑ with hypoperfusion (both WT and APPSw,Ind) ↑ in APPSw,Ind hypoperfused compared to WT hypoperfused
	A	↑ with hypoperfusion (both WT and APPSw,Ind)
$K_v1.2$ distrubution	Y	↔
	A	↔

MBP and SMI312 (% area)	Y	↔
	A	↔
Human Aβ42 levels	Y	↓ (in APPSw,Ind)
	A	↔
APP and APP prossessing products (C83 and C99) protein levels	Y	↑ in APPSw,Ind compare to WT ↔ in response to hypoperfusion
	A	↑ in APPSw,Ind compare to WT ↔ in response to hypoperfusion
Spatial working memory (*number of revisiting errors*)	Y	↑ number of revisiting errors in response to hypoperfusion (both WT and APPSw,Ind) WT hypoperfused perform better than the APPSw,Ind hypoperfused perform (fail to improve)
	A	↑ number of revisiting errors in response to hypoperfusion (both WT and APPSw,Ind)

Note: ↑ increase, ↓ decrease, ↔ unchanged, Y: young cohort, A: aged cohort

4.4 Discussion

Disruption of myelinated axons within the brain's white matter in ageing and Alzheimer's disease is associated with cerebral hypoperfusion (Fernando et al., 2006; Scheltens et al., 1995; Ruitenberg et al., 2005). This study sought to investigate the effects of cerebral hypoperfusion in specialized regions of myelinated axons, the nodes of Ranvier and the paranodes. This study demonstrated that these regions are vulnerable to the effects of hypoperfusion. A decrease in nodal length is observed and the well-defined spatial organization of $Na_v1.6$ channels in the Caspr positive paranodes is disrupted in response to hypoperfusion in young and aged animals. This effect was shown to be exacerbated in the young TgAPPSw,Ind animals. Moreover, the disruption of the nodal domain was shown to occur without any gross alterations in myelin integrity or change in nodal density. It was also demonstrated that in response to hypoperfusion, spatial working memory performance is defected in young and aged animals whilst this deficit is exacerbated in young TgAPPSw,Ind animals. Interestingly, working memory performance was associated with nodal integrity.

In support of this study, other work has shown that these regions within the myelinated axons are vulnerable to the effect of ageing. As discussed in Chapter 3, a decrease $Na_v1.6$ cluster and nodal gap length was observed in the stratum lacunosum moleculare of the hippocampus in aged animals. Moreover, reduction in the length of the Na_v cluster at the nodes has also been observed in the optic nerve of 2 year old wild-type mice (Rios et al., 2003). In contrast to the present study, previous work in our lab investigating the length of the $Na_v1.6$ cluster in the same model of cerebral

hypoperfusion demonstrated increased nodal length after three and 30 days of hypoperfusion (Reimer et al., 2011). There are several explanations to account for these differences. Firstly, the duration of hypoperfusion is different between the two studies, here the alterations in nodal size were observed after 8 weeks of hypoperfusion. Secondly, only the distribution of $Na_v1.6$ channels was examined by Reimer et al. (2011) whilst it is not known if the nodal gap also increased. Moreover, both studies are snapshots of the nodal integrity at specific time points which may be representative of a progressive pathology at the nodes induced by hypoperfusion over time. To further investigate that, nodal integrity could be examined at multiple time points after the induction of hypoperfusion which would provide information about the time course of nodal alterations.

In the CNS after injury, the remyelinated axons are associated with a decrease in the length of internodes and a subsequent increase in nodal density (Powers et al., 2012). To determine whether there may be remyelination in the present study, the number of nodes was investigated. Hypoperfusion, however, did not appear to have an effect on the number of nodes in either the young or the aged animals suggesting that remyelination might not be responsible for the observed changes. However, in order to investigate myelin in further detail, ultrastructural analysis of the myelinated axons using electron microscopy may be helpful as new remyelinated axons appear to have thinner myelin sheaths (Patrikios et al., 2006; Peters and Sethares, 2003).

Alternatively, the observed reduction in the size of the nodes could be attributed to a loss of $Na_v1.6$ channels or a failure of $Na_v1.6$ to anchor to the nodal region. In support of this, there is evidence that different Na_v channels are down-regulated with ischemia or injury (Berta et al., 2008; Yao et al., 2005) whilst after stroke there is an

elevation of the βIV spectrin and AnkG calpain-mediated proteolytic products (Schafer et al 2009). For example, Berta et al. (2008) showed in a rat model of spared nerve injury that the levels of $Na_v1.6$ mRNA transcripts are reduced. Reduction in multiple Na_v1 mRNA transcripts has also been observed in rat models of ischaemic brain injury (Yao et al., 2002; Yao et al., 2005). Furthermore, Schafer et al. (2009) showed in a mouse model of stroke an increase in AnkG and βIV spectrin proteolysis at the site of injury. These proteins are responsible for Na_v channel anchoring to the nodal plasma membrane (Yang et al., 2007; Gasser et al., 2012) and their ablation results in abnormally formed nodes of Ranvier (Yang et al., 2004; Dzhashiashvili et al., 2007). Nevertheless, further investigation of the mechanisms underlying the observed changes would include the assessment of levels of $Na_v1.6$ channels or calpain mediated proteolytic products.

Paranodal integrity is crucial for the clustering of $Na_v1.6$ channels at the nodes of Ranvier. Paranodal septate-like junctions act as a diffusion barrier by restricting the $Na_v.16$ channels at the nodal region (Rios et al., 2003). Cerebral hypoperfusion was demonstrated here to have an effect on paranodal integrity. It was shown that the $Na_v1.6$ cluster to nodal gap length ratio, used as a measure of paranodal disruption and expansion of the $Na_v1.6$ channels into the paranodal domain, is increased in the hypoperfused animals. Paranodal disruption in response to hypoperfusion, ageing and disease has been previously described. For example, 30 days after the induction of hypoperfusion in our group using the same model provided evidence of axon-glial disruption resulting in an increase in the $Na_v1.6$ cluster length. This was accomplished by a loss of septate-like junctions in the paranodes and a loss of the paranodal protein NF155 (Reimer et al., 2011). In addition, ageing affects the

number of septate-like junctions in aged rodents. Investigation at ultrastructural level showed that in 22 month old mice the number of paranodes with decreased number of paranodal loops contacting the axolemma, or with lost septate-like junctions was increased (Shepherd et al., 2012). Similarly, in aged rats loss of septate-like junctions (Sugiyama et al., 2002) at the paranodes was observed. In both cases, however, some intact paranodal junctions were preserved. In human patients of demyelinating diseases such as multiple sclerosis as well as in animal models there has also been evidence of paranodal disruption. For example, Howell et al. (2006) demonstrated that in brain demyelinating lesions the pattern of NF155 distribution at the paranodes is altered and there is an increased overlap between the paranodal NF155 and the juxtaparanodal $K_v1.2$ which is indicative of paranodal disruption. Similarly, in a rat model of dysmyelination, the expression profile of juxtaparanodal $K_v1.2$ altered, expanding into the paranodal region (Arroyo et al., 2002). In the present study, despite the observed alterations in $Na_v1.6$ and Caspr overlay indicative of paranodal disruption, there was no alteration in the distribution of the juxtaparanodal $K_v1.2$ channels within the Caspr positive paranodal domain in response to hypoperfusion. A possible explanation for this could be that although the septate-like junctions of the paranodes that act as diffusion barriers Nav1.6 of the nodes of Ranvier may be disrupted, they might not be completely ablated conserving, similarly to what is observed in normal ageing (Shepherd et al., 2012), their role as diffusion barriers for the $K_v1.2$ channels of the juxtaparanodes. However, the approach used here is limited to an evaluation of the space of Caspr positive domain that is occupied by $K_v1.2$ channels and does not take how dense the $K_v1.2$ protein was into account. These findings suggest that the observed changes in response to hypoperfusion are different

from those in demyelinating diseases. The changes in response to cerebral hypoperfusion appear to affect the nodal and paranodal regions rather than the $K_v1.2$ distribution. To further confirm paranodal disruption, ultrastructural investigation of septate-like junction integrity at the paranodes would be useful to provide further evidence of paranodal disruption.

In addition, absence of demyelination and axonal damage was confirmed with the assessment of expression levels and pattern of cellular distribution of myelin basic protein and neurofilament. No axonal damage or myelin loss in response to hypoperfusion was found which is in accordance with previous studies in our lab using the same model which used immunohistochemical and neuroimaging (MRI) approaches for evaluating myelin and axonal integrity (Reimer et al., 2011; Holland et al., 2011). However, the use of MBP and neurofilament is limited to a gross assessment of myelin integrity as other myelin and/or axonal components may be altered and the use of other markers would be more likely to detect alterations if any. For example, other studies using the same model in our lab, have indicated that hypoperfusion may affect axon-glial cross-talk detected by alterations in myelin associated glycoprotein (MAG) immunostaining (Reimer et al., 2011; Holland et al., 2011) and sometimes in the absence of alterations in MBP or neurofilament levels or staining (Reimer et al., 2011). In addition, a recent study by Funfschilling et al. (2012) showed that oligodendrocytes may use glycolytic metabolism as an alternative source for the maintenance of myelin and axonal integrity which if true makes the oligodendrocytes and subsequently myelin and axonal integrity more tolerant to the energy deprivation induced by hypoperfusion. To further investigate myelin integrity, the use of specific markers for myelin damage, such as an anti-

damaged MBP antibody specific for pathological epitopes of MBP (Ihara et al., 2010) or axon-glial integrity such as MAG may be helpful. Axonal integrity may also be further investigated with the use of markers specific for neurofilament phosphorylation which may serve as a marker of axonal injury (Petzold et al., 2011; Singh et al., 2011).

At the onset of this study it was hypothesised that age exacerbates the effects of hypoperfusion. In support of this, it was demonstrated that in the young animals only the corpus callosum is affected whilst in the aged animals the nodes of both the corpus callosum and the hippocampus are affected. Previous studies using this cerebral hypoperfusion model in young animals have shown that it selectively induces diffuse white matter pathology (Shibata et al 2004; Coltman et al 2011). One explanation is that CBF may be compromised in the ageing brain. The white matter constitutes a vascular end zone (Borch et al., 2010) rendering it more sensitive to blood flow fluctuations and vascular insults such as those induced by hypoperfusion. At the same time, there is evidence that cerebral blood flow is attenuated by normal ageing (Park et al., 2007) which with the additional challenge induced by the hypoperfusion could result in greater blood flow alterations. However, blood flow measurements were not assessed in the present study which would securely estimate the nature of flood flow attenuation in young and aged animals.

Another goal of this study was to assess nodal and paranodal integrity in a mouse model (TgAPPSw,Ind) which develops increased deposition of amyloid with age and the alterations at nodes and paranodes may be exacerbated. In confirmation of our hypotheses we showed that in young TgAPPSw,Ind hypoperfused mice the length of

the nodes of Ranvier is significantly decreased whilst the Nav1.6 cluster to nodal gap ratio is significantly increased compared to the wild type hypoperfused animals. These results suggest that there is an exacerbation of the effects of hypoperfusion (i.e. paranodal disruption and shorter nodes) in the TgAPPSw,Ind animals. There is a limited number of studies investigating components of the nodes of Ranvier in AD. In another AD model (3xTg) with overt amyloid pathology $Na_v1.6$ immunoreactivity was decreased in the mutant animals (Desai et al., 2009). Similarly in the J20 line of the TgAPPSw,Ind, which develops Aβ pathology earlier than the J9 line that was used in the present study, $Na_v1.6$ protein levels are reduced (Verret et al., 2012). Moreover, there is some evidence that that BACE1, a proteolytic enzymatic complex implicated in the amyloidogenic processing of APP, regulates voltage gated sodium channels (Kovacs et al., 2010). Kim et al. (2007) demonstrated that increased BACE1 protein levels result in reduced $Na_v1\alpha$ subunit recruitment to the cell surface and marked reduction in sodium current examined with electrophysiology.

The observed exacerbation in the changes induced by hypoperfusion at the nodes in the TgAPPSw,Ind animals could be the result of an additional vascular insult to an already compromised system. In support of this are studies which show that cerebral vasculature and cerebral blood flow are altered in animal models that develop Aβ pathology when compared with wild-type mice. For example, in a mouse model (APP23, 10 months of age), examination of the 3D vascular architecture showed pronounced alterations such as vessel deformation and elimination (Beckmann et al., 2003). Similarly, in a study investigating multiple models overexpressing mutant human APP at a relatively young age, it was demonstrated that vascular autoregulation was disrupted and associated with Aβ levels (Niwa et al., 2002a).

Interestingly, the difference in nodal length observed between young TgAPPSw,Ind and wild-type mice in response to hypoperfusion was not maintained in ageing. One explanation could be that there is a limit by which the length can be reduced with hypoperfusion and with ageing this could have been reached.

A few studies have investigated the impact of hypoperfusion in transgenic mouse models overexpressing human mutant APP to determine whether hypoperfusion increases Aβ levels and deposition. However the findings have been conflicting (Kitaguchi et al., 2009; Yamada et al., 2011; Lee et al., 2011; Koike et al., 2010). Here it was demonstrated that the levels of human Aβ42 are reduced in young hypoperfused TgAPPSw,Ind mice whist they are unchanged in aged animals. Moreover, the levels of APP and C-terminal fragments from the non- and amyloidogenic processing of APP remain unchanged in response to hypoperfusion. In contrast to the present study, Kitaguchi et al. (2009) using the same transgenic model showed a significant increase in perinuclear Aβ42 immunostaining in neurons and an increase in the levels of fibrilar but not monomeric Aβ after one month of cerebral hypoperfusion. In another APP mutant model (3xTg) at a relatively young age, where blood flow was interrupted by occlusion of the common carotid arteries for 4 minutes, there was an increase in the levels of soluble and insoluble Aβ42 and the levels of C-terminal proteolytic products of APP without any change in APP levels in response to oligemia (Koike et al., 2010). Furthermore, Yamada et al. (2011) showed that for TgAPPSw,Ind mice (J20), after 6 months of hypoperfusion, soluble Aβ is increased whilst the deposition of Aβ42 is decreased in the hippocampus but not the cortex. In addition, in Tg2576 mice amyloid plaque pathology was not affected by hypoperfusion (Lee et al 2011). There are several

explanations to account for these differences. Firstly, the protein extraction technique used in the present study did not include extended centrifuging or the use of detergents such as formic acid. These procedures allow the separation of soluble and insoluble fraction and the disassociation and the insoluble Aβ aggregates. The method used here allowed the detection of only soluble Aβ which may be decreased if hypoperfusion induces insoluble Aβ deposition in the young animals. Secondly, there are several differences in the methods used to induce hypoperfusion and measure amyloid: the stage of amyloid pathology development at the onset of hypoperfusion together with underlying differences due to genetic strain which may contribute to the different outcomes of hypoperfusion on amyloid pathology in these studies.

Attenuation of white matter in humans has been linked with poor working memory performance (Appelman et al., 2010; Kennedy and Raz, 2009). At the same time previous studies have shown that hypoperfusion results in poor performance in the 8-arm radial arm maze task (Coltman et al., 2011; Shibata et al., 2004) which is a well-established method to examine working memory in rodents (Cole and Chappell-Stephenson, 2003; Olton and Samuelson, 1976; Hyde et al., 1998). We have confirmed that working memory performance assessed in the 8-arm radial arm maze is impaired with hypoperfusion in young wild-type mice. In addition, working memory impairment is exacerbated in the young TgAPPSw,Ind animals when compared to young wild-type mice in response to hypoperfusion. However, these effects were not observed in the aged animals, as both the hypoperfused wild-type and TgAPPSw,Ind mice were unable to perform well at the task. This suggests that cerebral hypoperfusion combined with the additional challenge of age, results in such

a deficit in working memory performance that does not decipher between the two genotypes. A possible explanation for these finding could lie in the anatomical basis of spatial working memory in rodents which is dependent on multiple brain regions such as the hippocampus, the parahippocampus and the prefrontal cortex (Hodges (Hodges, 1996; Shaw and Aggleton, 1993) and requires their effective communication. In the present study the nodal/paranodal changes observed in response to hypoperfusion were more extensive in the aged animals with both the corpus callosum and the hippocampus being affected whilst in the young animals changes were observed in only the corpus callosum. This difference between young and aged animals may be responsible for the observed behavioural changes.

Changes at the nodes and paranodes may result in functional alterations that could be responsible for the observed spatial working memory deficit in response to hypoperfusion. To further investigate that working memory performance was associated with the nodal changes and a strong association was revealed between the numbers of errors in the 8-arm radial arm maze task and the $Na_v1.6$ cluster to nodal ratio which is a measure of paranodal disruption. This finding suggests that alterations to the nodes of Ranvier and paranodes induced by hypoperfusion may impede action potential propagation and lead to defective communication between brain regions impacting cognition. In support of this, Nie et al. (2006) showed that decrease in nodal length and decrease in the $Na_v1\alpha$ subunit resulted in decreased conduction velocity of action potentials. Additionally, it has been demonstrated that a working memory deficit in the T maze is linked with a reduction in action potential velocity (Tanaka et al., 2009). Furthermore a rat model of demyelination of the PNS was demonstrated to have reduced Na_v channel density at the nodes, which was

associated with slower action potential conduction (Lonigro and Devaux, 2009). Similarly, in a mouse model where Caspr is ablated, which develops paranodes without septate-like junctions, action potential velocity is reduced (Boyle et al., 2001). Moreover, Huff et al. (2011) showed that in spinal cord white matter, high frequency stimulation results in retraction of myelin from the paranodes suggesting that they can undergo activity-dependent alterations in the paranodes. Moreover, a study in an AD transgenic model, (TgAPPSw,Ind, J20 line) that develops spatial learning and memory deficits in the Morris water maze and has decreased protein levels of Na_v channels, showed that induction of the $Na_v1.1$ expression can improve cognitive performance to the level of the wild-types (Verret et al 2012). Although there is evidence that nodal alterations are linked with altered action potential conduction and cognitive performance, investigation of these aspects on the same cohort of hypoperfused animals would provide confirmation of their association. This could be achieved with use of the developed system of in vivo recording in freely behaving animals (Lin et al., 2006; Ye et al., 2008) which would provide information on neural activity as the animals are performing in cognitive tasks with neuropathological analysis to follow.

The question that needs to be answered, however, is how hypoperfusion drives the observed changes at the nodes of Ranvier and subsequently working memory in the wild-type animals and why these are exacerbated in the young but not the aged TgAPPSw,Ind mice. Firstly, there is evidence from studies in our lab that hypoperfusion alters the numbers of mature oligodendrocytes and the pool of oligodendrocyte precursor cells (McQueen et al, submitted) suggesting that the vascular insult affects the survival of oligodendrocytes. This is further supported by

studies using a rat model of chronic cerebral hypoperfusion where seven days after the induction of hypoperfusion the number of oligodendroglia decreased (Tomimoto et al., 2003). Given that nodal assembly and maintenance is under glial control (Mathis et al., 2001; Boiko et al., 2003) alterations in the oligodendroglial cell number may have an impact on nodal integrity. The oligovascular niche has been proposed as a model by which cross-talk occurs between the oligodendrocytes and the vascular elements and thus is necessary for maintaining the integrity and homeostasis of the white matter (Arai and Lo, 2009). From studies in our lab, the vasculature appears to be affected in response to hypoperfusion with the vessels increasing in width, suggesting vascular dysfunction (Dr G. Scullion, unpublished data). Furthermore, there is evidence that the oligodendrocytes are susceptible to oxidative stress and inflammatory signalling (Balabanov et al., 2007; Cammer and Zhang, 1999; Deng et al., 2004; French et al., 2009) which are suggested to be up-regulated by hypoperfusion (Kasparova et al., 2005; Wang et al., 2010). Oxidative stress has been directly linked with paranodal abnormalities in the rat optic nerve (Szymanski et al., 2013) and mitochondrial dysfunction (Lin and Beal, 2006). Mitochondria are distributed along the axons and serve the metabolic demands of the distinct regions (Zhang et al., 2010a; Chiu, 2011) which suggests that the deterioration of mitochondrial metabolic capacity may affect nodal and paranodal integrity as they are regions with high metabolic demands. In addition, microglia have been demonstrated to be activated in response to hypoperfusion (Shibata et al., 2004; Holland et al., 2011) and have been implicated in paranodal disruption in a mouse model of experimental autoimmune encephalomyelitis (EAE) (Howell et al., 2010). Additionally, analysis of gene expression in response to hypoperfusion has

pointed out multiple altered genes implicated in inflammation, vasculature, and cell-adhesion (Reimer et al., 2011) suggesting that there are multiple mechanisms involved in the mechanisms of damage driven by hypoperfusion.

In the young TgAPPSw,Ind mice the effects of hypoperfusion are exacerbated. A possible explanation for this is the baseline difference between TgAPPSw,Ind and wild type mice in the vascular structure i.e. larger size vessels (Dr G Scullion, unpublished data) which may potentially result in baseline CBF differences between the two genotypes and subsequently to the effects of hypoperfusion. Additionally, there is evidence that transgenic models overexpressing hAPP are more susceptible to ischemic injury (Zhang et al., 1997) which is potentially mediated by increased microglial activation (Koistinaho et al., 2002). Moreover, as described earlier processes such as oxidative stress and mitochondrial dysfunction may be implicated in nodal and paranodal integrity and there are several studies that have demonstrated that these processes are upregulated both in humans and in AD models (Markesbery, 1997; Korolainen et al., 2006; Dumont et al., 2010; Zhu et al., 2004; Aliev et al., 2004; Aliev et al., 2003). Another potential mechanism implicated in nodal alterations could be the down-regulation of voltage gated sodium channels mediated by BACE1. BACE1 levels and activity are elevated in AD both in humans and animal models (Heneka et al., 2005; Corbett et al., 2013; Fukumoto et al., 2002). In animal models, cognitive performance and defective neuronal activity is associated with reduced recruitment of $Na_v1.1$ channels at the membranes (Kim et al., 2007; Corbett et al., 2013). This suggests that Na_v channel dysregulation may be a potential mechanism for neuronal network dysfunction observed in AD (Bakker et al., 2012

(Bakker et al., 2012; Verret et al., 2012; Sanchez et al., 2012); Sanchez et al., 2012; Verret et al., 2012).

In conclusion, this study highlights the vulnerability of specific molecular domains (nodes and paranodes) within myelinated axons to the effects of hypoperfusion which may be associated with a deficit cognitive performance. In the future it would be interesting to investigate how the alterations at the nodes and paranodes affect neuronal excitability using electrophysiology and also to identify the molecular mechanisms behind the observed structural alterations.

Chapter 5 Discussion

5.1 Summary

The studies described within the thesis indicate the vulnerability of specialised regions within myelinated axons to ageing, cerebral hypoperfusion and to a lesser extent levels of amyloid. Importantly, breakdown of the nodal/paranodal regions is associated with working memory impairment. These findings may have implications for the development of strategies aimed to ameliorate cognitive impairment observed in ageing and AD.

5.2 Vulnerability of the AIS and nodes of Ranvier

Studying the effects of normal ageing, cerebral hypoperfusion or increasing Aβ levels on brain function in humans is highly complicated as they coexist with each other and/or other comorbidities. Therefore, the utilization of animal models is helpful because it allows the investigation of these pathological processes in isolation, under controlled conditions and the least possible genetic variability, and facilitates the unraveling of mechanisms that may drive changes in brain function.

As discussed in chapter 3 cerebral hypoperfusion was suggested to underlie the changes observed in normal ageing. In the cerebral hypoperfusion model used in the second study, one month after induction of hypoperfusion, CBF is reduced by 10-15% of the baseline (Shibata et al., 2004) which is comparable to the modest blood flow reduction observed in normal ageing where CBF is reduced by ~20% between the age of 20 and 60 years (Leenders et al., 1990). The effects of hypoperfusion on nodal integrity were examined in isolation and in relation with increased Aβ levels in young and aged animals. It was demonstrated that hypoperfusion induces age-related changes to the nodes by reducing their size and producing disruption at the paranodes, which was associated with the severity of the spatial working memory deficit. Similarly to ageing, these changes are occurring without overt myelin loss suggesting that they are an early event in pathology progression and possibly a therapeutic target. Furthermore, both the disruption at the nodes and cognitive decline were exacerbated in the young TgAPPSw,Ind animals. As discussed in chapter 4 this difference may be due to intrinsic changes in the vasculature between the wild-type and the TgAPPSw,Ind mice (Dr G. Scullion, unpublished data) which may induce a greater reduction in CBF. However, when ageing is combined with hypoperfusion nodal integrity in more regions is affected and the effects on nodal integrity and cognition are independent of the genotype. These findings indicate the susceptibility of the ageing brain and the necessity for early interventions against the effects of hypoperfusion.

5.3 Repairing the nodes of Ranvier

Currently, there are not any therapeutic strategies that specifically repair the nodes of Ranvier. The majority of the strategies that examine nodal repair are investigated in the context of demyelination in diseases such as the leukodystrophies, where demyelination has a genetic basis, or diseases such as multiple sclerosis where autoimmunity is responsible (Franklin and Ffrench-Constant, 2008). In these diseases, damage at the oligodendrocytes is usually responsible for demyelination (Franklin and Ffrench-Constant, 2008). Therefore, the research on the development of therapeutic approaches focuses on restoring the integrity of the myelinated axons both structurally and functionally in a process known as remyelination (Smith et al., 1979). The two main strategies followed are cell therapy which includes the transplantation of stem cells that would differentiate into myelinating oligodendrocytes, and promotion of myelination by the endogenous population of OPCs, and both have shown positive results. For example, Sasaki et al. (2006) showed, in demyelinating lesions of rat spinal cord, repair of the molecular architecture of the nodes of Ranvier in remyelinated mediated fibres after transplantation with olfactory ensheathing cells. Moreover, administration of the leukaemia inhibitory factor (LIF) results in the activation of OPCs and subsequent remyelination (Deverman and Patterson, 2012).

The studies presented in this thesis do not suggest that demyelination is occurring in response to ageing or cerebral hypoperfusion. However, it has been proposed that a cross-talk between the oligodendrocytes and vascular elements is necessary for maintaining the integrity and homeostasis of the white matter (Arai and Lo, 2009).

Therefore, strategies that focus on the restoration of oligodendroglial function may be relevant.

There is also evidence that the oligodendrocytes are susceptible to oxidative stress and inflammation (Balabanov et al., 2007; Cammer and Zhang, 1999; Deng et al., 2004; French et al., 2009) which are suggested to be up-regulated by normal ageing, hypoperfusion and AD (Kasparova et al., 2005; Wang et al., 2010). Oxidative stress and microglial activation have been directly linked with paranodal abnormalities (Szymanski et al., 2013; Howell et al., 2010) which suggests that the use of antioxidant or anti-inflammatory agents may attenuate the damage at the nodal region. Indeed, administration of a known antioxidant (Vitamin E) prevents paranodal disruption in a rat of diabetic peripheral neuropathy (Algaidi, 2011) whilst administration of anti-inflammatory agents such as ibuprofen attenuates white matter damage after ischemia (Carty et al., 2011). Furthermore, administration of edaravone, which is an antioxidant that scavenges free radicals, attenuates white matter damage by reducing the loss of oligodendrocytes and demyelination in a rat model of chronic cerebral hypoperfusion (Ueno et al., 2009). In the same model, treatment with gypenosive, a compound with anti-inflammatory and antioxidant effects, is shown to decrease vacuolation and demyelination of the corpus callosum (Zhang et al., 2011).

5.4 Attenuating cerebral hypoperfusion

Chronic cerebral hypoperfusion occurs in normal ageing (Stoquart-ElSankari et al., 2007) and is further exacerbated in the presence of vascular risk factors (Leenders et al., 1990). The effect of chronic hypoperfusion is the deprivation of the brain from the necessary energy and metabolites for brain function (Leenders et al., 1990) resulting in white matter damage and changes in cognition which may further develop to dementia (Pantoni, 2002; Appelman et al., 2010). However, cerebral hypoperfusion is observed prior to the development of any clinical symptoms of cognitive decline (de la Torre, 2009) indicating that that there is a window for intervention after hypoperfusion is first observed and before cognition is impaired. The data presented in this thesis also highlight the importance of hypoperfusion in the development of white matter alteration - particularly within the excitable regions of the myelinated axons - and cognition, and also indicate that increasing age may render the brain more susceptible to its detrimental effects.

The development of strategies to prevent, delay or attenuate hypoperfusion becomes necessary for prolonging cognitively healthy ageing. This may be achieved by the accurate diagnosis of the vascular risk factors underlying hypoperfusion and by applying the appropriate therapeutic strategies to ameliorate them. Jack de la Torre (2010) proposes a series of screens for the identification of individuals at risk. The primary screen includes low-cost, simple, and non-invasive procedures such as ultrasounds, blood tests and physical examination which will highlight any potential risk factor. The secondary screen includes neuroimaging, cognitive tests and biomarkers of cerebrospinal fluid (CSF) which would determine the white matter

damage and the extent of cognitive decline. Accurate detection of the risk factors may promote healthy ageing as a number of them are modifiable by either a change in lifestyle or commonly available drug treatments. For example, lifestyle changes could include a shift towards a healthy diet, low alcohol consumption and increased exercise (Pope et al., 2003), whilst diabetes mellitus, hypercholesterolemia and hypertension could be treated with insulin therapy, statins and angiotensin converting enzyme (ACE) inhibitors respectively (Rockwood et al., 1997).

Furthermore, studies in animal models have indicated pharmacological compounds that attenuate hypoperfusion and its effects, such as white matter damage or cognitive decline. For example, Maki et al. (2011) demonstrated in a mouse model of chronic cerebral hypoperfusion that treatment with andromedullin attenuated the induced hypoperfusion, induces angiogenesis and conserved white matter integrity and cognition. Moreover, treatment with nimodipine, a dihydropyridine which is a calcium entry blocker specific for cerebral vasculature, after ischemic injury may ameliorate cerebral blood flow by reversing cerebral vasoconstriction (Milde et al., 1986). However, further investigation is necessary in order to utilise these compounds as a therapeutic strategy for hypoperfusion.

5.5 Future studies

In the future, further investigation could strengthen and expand the observations presented in this thesis in an effort to identify the molecular mechanism underlying structural alterations and also to specify the implication of Aβ in these mechanisms. For example, computational modeling (Baalman et al., 2013) of the observed alterations at the nodes of Ranvier and/or the AIS would offer some information about specific alterations in the size of the AIS and the nodes similar to those induced by ageing and hypoperfusion are affecting the firing properties of the neurons. In a more detailed approach, electrophysiological examination of firing properties of the axons at the same regions where pathological alterations at the nodes or the AIS are observed in animals that have developed cognitive deficit would provide the necessary link between pathological alterations, altered signal conduction and cognition.

To further identify the nature of the alterations at the myelinated axons as well as the mechanisms responsible, further investigation would be necessary. Detailed ultrastructural analysis of myelinated axons using transmission electron microscopy (Shepherd et al., 2012) could provide evidence for structural alterations in the myelin sheath such as ballooning, decompaction and thinning, and in the paranodal junction (loss of septate-like junction, paranodal loops pilling or disconnection from the axolemma) as well as an estimation of changes in number of myelinated or unmyelinated axons. Other hypoperfusion studies (Coltman et al., 2011; Holland et al., 2011; Reimer et al., 2011) have highlighted MAG to be a sensitive marker of axon-glial disruption in response to hypoperfusion, therefore, examining its protein

levels and cellular distribution would provide additional evidence for myelin disruption. Additionally, down-regulation or proteolytic processing of components of the nodes of Ranvier of the AIS could be confirmed with western blot analysis. In order to gain further insight on the relevance of AD and Aβ pathology in the observed changes, the effect of specific Aβ species on the structure of AIS and the nodes of Ranvier as well as neuronal excitability could be investigated in vitro in combined neuronal and glial cultures. Finally, cerebral blood flow measurements in aged and in TgAPPSw,Ind animals would be helpful for examining whether there are age-related or genotype-dependent baseline alterations in CBF that hypoperfusion exacerbates.

5.6 Conclusion

The data presented in this thesis indicate the necessity for developing strategies to minimize injury at the nodes of Ranvier and drive their repair. In order to be successful it is necessary to ensure that the nodes are formed properly and maintained. Moreover, the importance of therapeutic approaches against the vascular insults that induce hypoperfusion and lead to white matter attenuation and cognitive decline is highlighted.

REFERENCES

Al-Chalabi A and Miller CC. (2003) Neurofilaments and neurological disease. *Bioessays* 25: 346-355.

Algaidi S. (2011) The Effect of Antioxidants on Experimentally Induced Diabetic Peripheral Neuropathy in Adult Male Albino Rats. *Journal of American Science* 7: 671-677.

Aliev G, Obrenovich ME, Smith MA, et al. (2003) Hypoperfusion, Mitochondria Failure, Oxidative Stress, and Alzheimer Disease. *J Biomed Biotechnol* 2003: 162-163.

Aliev G, Smith MA, de la Torre JC, et al. (2004) Mitochondria as a primary target for vascular hypoperfusion and oxidative stress in Alzheimer's disease. *Mitochondrion* 4: 649-663.

Allen JS, Bruss J, Brown CK, et al. (2005) Normal neuroanatomical variation due to age: the major lobes and a parcellation of the temporal region. *Neurobiol Aging* 26: 1245-1260; discussion 1279-1282.

Allen NJ and Barres BA. (2005) Signaling between glia and neurons: focus on synaptic plasticity. *Curr Opin Neurobiol* 15: 542-548.

Alpar A, Ueberham U, Bruckner MK, et al. (2006) Different dendrite and dendritic spine alterations in basal and apical arbors in mutant human amyloid precursor protein transgenic mice. *Brain Res* 1099: 189-198.

Alzheimer A. (1907) Uber eine eigenartige Erkrankung der Hirnrinde. *Allgemeine Zeitschrift fur Psychiatrie und phychish-Gerichtliche Medizin* 64: 146-148.

Ango F, di Cristo G, Higashiyama H, et al. (2004) Ankyrin-based subcellular gradient of neurofascin, an immunoglobulin family protein, directs GABAergic innervation at purkinje axon initial segment. *Cell* 119: 257-272.

Appelman AP, van der Graaf Y, Vincken KL, et al. (2010) Combined effect of cerebral hypoperfusion and white matter lesions on executive functioning - The SMART-MR study. *Dement Geriatr Cogn Disord* 29: 240-247.

Arai K and Lo EH. (2009) An oligovascular niche: cerebral endothelial cells promote the survival and proliferation of oligodendrocyte precursor cells. *J Neurosci* 29: 4351-4355.

Arroyo EJ, Xu T, Grinspan J, et al. (2002) Genetic dysmyelination alters the molecular architecture of the nodal region. *J Neurosci* 22: 1726-1737.

Asllani I, Habeck C, Scarmeas N, et al. (2008) Multivariate and univariate analysis of continuous arterial spin labeling perfusion MRI in Alzheimer's disease. *J Cereb Blood Flow Metab* 28: 725-736.

Auffret A, Gautheron V, Mattson MP, et al. (2010) Progressive age-related impairment of the late long-term potentiation in Alzheimer's disease presenilin-1 mutant knock-in mice. *J Alzheimers Dis* 19: 1021-1033.

Austin BP, Nair VA, Meier TB, et al. (2011) Effects of hypoperfusion in Alzheimer's disease. *J Alzheimers Dis* 26 Suppl 3: 123-133.

Baalman KL, Cotton RJ, Rasband SN, et al. (2013) Blast wave exposure impairs memory and decreases axon initial segment length. *J Neurotrauma* 30: 741-751.

Bach ME, Barad M, Son H, et al. (1999) Age-related defects in spatial memory are correlated with defects in the late phase of hippocampal long-term potentiation in vitro and are attenuated by drugs that enhance the cAMP signaling pathway. *Proc Natl Acad Sci U S A* 96: 5280-5285.

Badea A, Johnson GA and Jankowsky JL. (2010) Remote sites of structural atrophy predict later amyloid formation in a mouse model of Alzheimer's disease. *Neuroimage* 50: 416-427.

Bagh MB, Thakurta IG, Biswas M, et al. (2011) Age-related oxidative decline of mitochondrial functions in rat brain is prevented by long term oral antioxidant supplementation. *Biogerontology* 12: 119-131.

Bailey JA, Ray B, Greig NH, et al. (2011) Rivastigmine lowers Abeta and increases sAPPalpha levels, which parallel elevated synaptic markers and metabolic activity in degenerating primary rat neurons. *PLoS One* 6: e21954.

Bakker A, Krauss GL, Albert MS, et al. (2012) Reduction of hippocampal hyperactivity improves cognition in amnestic mild cognitive impairment. *Neuron* 74: 467-474.

Balabanov R, Strand K, Goswami R, et al. (2007) Interferon-gamma-oligodendrocyte interactions in the regulation of experimental autoimmune encephalomyelitis. *J Neurosci* 27: 2013-2024.

Balthazar ML, Yasuda CL, Pereira FR, et al. (2009) Differences in grey and white matter atrophy in amnestic mild cognitive impairment and mild Alzheimer's disease. *Eur J Neurol* 16: 468-474.

Barnes CA, Nadel L and Honig WK. (1980) Spatial memory deficit in senescent rats. *Can J Psychol* 34: 29-39.

Bartzokis G. (2004) Age-related myelin breakdown: a developmental model of cognitive decline and Alzheimer's disease. *Neurobiol Aging* 25: 5-18; author reply 49-62.

Bartzokis G. (2011) Alzheimer's disease as homeostatic responses to age-related myelin breakdown. *Neurobiol Aging* 32: 1341-1371.

Bartzokis G, Cummings JL, Sultzer D, et al. (2003) White matter structural integrity in healthy aging adults and patients with Alzheimer disease: a magnetic resonance imaging study. *Arch Neurol* 60: 393-398.

Bartzokis G, Sultzer D, Cummings J, et al. (2000) In vivo evaluation of brain iron in Alzheimer disease using magnetic resonance imaging. *Arch Gen Psychiatry* 57: 47-53.

Bartzokis G, Sultzer D, Lu PH, et al. (2004) Heterogeneous age-related breakdown of white matter structural integrity: implications for cortical "disconnection" in aging and Alzheimer's disease. *Neurobiol Aging* 25: 843-851.

Baumann N and Pham-Dinh D. (2001) Biology of oligodendrocyte and myelin in the mammalian central nervous system. *Physiol Rev* 81: 871-927.

Bear MF, Connors BW and Paradiso MA. (2007) *Neuroscience : exploring the brain,* Philadelphia, Penn. ; London: Lippincott Williams & Wilkins.

Beatty WW, Clouse BA and Bierley RA. (1987) Effects of long-term restricted feeding on radial maze performance by aged rats. *Neurobiol Aging* 8: 325-327.

Becker JA, Hedden T, Carmasin J, et al. (2011) Amyloid-beta associated cortical thinning in clinically normal elderly. *Ann Neurol* 69: 1032-1042.

Beckmann N, Schuler A, Mueggler T, et al. (2003) Age-dependent cerebrovascular abnormalities and blood flow disturbances in APP23 mice modeling Alzheimer's disease. *J Neurosci* 23: 8453-8459.

Bell KF, de Kort GJ, Steggerda S, et al. (2003) Structural involvement of the glutamatergic presynaptic boutons in a transgenic mouse model expressing early onset amyloid pathology. *Neurosci Lett* 353: 143-147.

Bell RD, Deane R, Chow N, et al. (2009) SRF and myocardin regulate LRP-mediated amyloid-beta clearance in brain vascular cells. *Nat Cell Biol* 11: 143-153.

Bell RD and Zlokovic BV. (2009) Neurovascular mechanisms and blood-brain barrier disorder in Alzheimer's disease. *Acta Neuropathol* 118: 103-113.

Benes FM, Turtle M, Khan Y, et al. (1994) Myelination of a key relay zone in the hippocampal formation occurs in the human brain during childhood, adolescence, and adulthood. *Arch Gen Psychiatry* 51: 477-484.

Bennett V and Baines AJ. (2001) Spectrin and ankyrin-based pathways: metazoan inventions for integrating cells into tissues. *Physiol Rev* 81: 1353-1392.

Berghs S, Aggujaro D, Dirkx R, Jr., et al. (2000) betaIV spectrin, a new spectrin localized at axon initial segments and nodes of ranvier in the central and peripheral nervous system. *J Cell Biol* 151: 985-1002.

Bernath E, Kupina N, Liu MC, et al. (2006) Elevation of cytoskeletal protein breakdown in aged Wistar rat brain. *Neurobiol Aging* 27: 624-632.

Berta T, Poirot O, Pertin M, et al. (2008) Transcriptional and functional profiles of voltage-gated Na(+) channels in injured and non-injured DRG neurons in the SNI model of neuropathic pain. *Mol Cell Neurosci* 37: 196-208.

Bertoni-Freddari C, Fattoretti P, Casoli T, et al. (1990) Morphological adaptive response of the synaptic junctional zones in the human dentate gyrus during aging and Alzheimer's disease. *Brain Res* 517: 69-75.

Bhat MA, Rios JC, Lu Y, et al. (2001) Axon-glia interactions and the domain organization of myelinated axons requires neurexin IV/Caspr/Paranodin. *Neuron* 30: 369-383.

Billings LM, Oddo S, Green KN, et al. (2005) Intraneuronal Abeta causes the onset of early Alzheimer's disease-related cognitive deficits in transgenic mice. *Neuron* 45: 675-688.

Black JA, Waxman SG and Smith KJ. (2006) Remyelination of dorsal column axons by endogenous Schwann cells restores the normal pattern of Nav1.6 and Kv1.2 at nodes of Ranvier. *Brain* 129: 1319-1329.

Bland JM and Altman DG. (1995) Multiple significance tests: the Bonferroni method. *BMJ* 310: 170.

Boiko T, Rasband MN, Levinson SR, et al. (2001) Compact myelin dictates the differential targeting of two sodium channel isoforms in the same axon. *Neuron* 30: 91-104.

Boiko T, Van Wart A, Caldwell JH, et al. (2003) Functional specialization of the axon initial segment by isoform-specific sodium channel targeting. *J Neurosci* 23: 2306-2313.

Borch K, Lou HC and Greisen G. (2010) Cerebral white matter blood flow and arterial blood pressure in preterm infants. *Acta Paediatr* 99: 1489-1492.

Borchelt DR, Davis J, Fischer M, et al. (1996) A vector for expressing foreign genes in the brains and hearts of transgenic mice. *Genet Anal* 13: 159-163.

Borchelt DR, Ratovitski T, van Lare J, et al. (1997) Accelerated amyloid deposition in the brains of transgenic mice coexpressing mutant presenilin 1 and amyloid precursor proteins. *Neuron* 19: 939-945.

Bosch B, Arenaza-Urquijo EM, Rami L, et al. (2012) Multiple DTI index analysis in normal aging, amnestic MCI and AD. Relationship with neuropsychological performance. *Neurobiol Aging* 33: 61-74.

Boumezbeur F, Mason GF, de Graaf RA, et al. (2010) Altered brain mitochondrial metabolism in healthy aging as assessed by in vivo magnetic resonance spectroscopy. *J Cereb Blood Flow Metab* 30: 211-221.

Bourgeois JP and Rakic P. (1996) Synaptogenesis in the occipital cortex of macaque monkey devoid of retinal input from early embryonic stages. *Eur J Neurosci* 8: 942-950.

Boveris A and Navarro A. (2008) Brain mitochondrial dysfunction in aging. *IUBMB Life* 60: 308-314.

Bowley MP, Cabral H, Rosene DL, et al. (2010) Age changes in myelinated nerve fibers of the cingulate bundle and corpus callosum in the rhesus monkey. *J Comp Neurol* 518: 3046-3064.

Boyle ME, Berglund EO, Murai KK, et al. (2001) Contactin orchestrates assembly of the septate-like junctions at the paranode in myelinated peripheral nerve. *Neuron* 30: 385-397.

Braak H and Braak E. (1997) Diagnostic criteria for neuropathologic assessment of Alzheimer's disease. *Neurobiol Aging* 18: S85-88.

Braak H, Del Tredici K, Schultz C, et al. (2000) Vulnerability of select neuronal types to Alzheimer's disease. *Ann N Y Acad Sci* 924: 53-61.

Bradl M and Lassmann H. (2010) Oligodendrocytes: biology and pathology. *Acta Neuropathol* 119: 37-53.

Breteler MM. (2000) Vascular involvement in cognitive decline and dementia. Epidemiologic evidence from the Rotterdam Study and the Rotterdam Scan Study. *Ann N Y Acad Sci* 903: 457-465.

Breteler MM, van Swieten JC, Bots ML, et al. (1994) Cerebral white matter lesions, vascular risk factors, and cognitive function in a population-based study: the Rotterdam Study. *Neurology* 44: 1246-1252.

Brill MH, Waxman SG, Moore JW, et al. (1977) Conduction velocity and spike configuration in myelinated fibres: computed dependence on internode distance. *J Neurol Neurosurg Psychiatry* 40: 769-774.

Brown WR and Thore CR. (2011) Review: cerebral microvascular pathology in ageing and neurodegeneration. *Neuropathol Appl Neurobiol* 37: 56-74.

Brun A and Englund E. (1981) Regional pattern of degeneration in Alzheimer's disease: neuronal loss and histopathological grading. *Histopathology* 5: 549-564.

Brun A and Englund E. (1986a) Brain changes in dementia of Alzheimer's type relevant to new imaging diagnostic methods. *Prog Neuropsychopharmacol Biol Psychiatry* 10: 297-308.

Brun A and Englund E. (1986b) A white matter disorder in dementia of the Alzheimer type: a pathoanatomical study. *Ann Neurol* 19: 253-262.

Bucur B, Madden DJ, Spaniol J, et al. (2008) Age-related slowing of memory retrieval: contributions of perceptual speed and cerebral white matter integrity. *Neurobiol Aging* 29: 1070-1079.

Buffington SA and Rasband MN. (2011) The axon initial segment in nervous system disease and injury. *Eur J Neurosci* 34: 1609-1619.

Buijs PC, Krabbe-Hartkamp MJ, Bakker CJ, et al. (1998) Effect of age on cerebral blood flow: measurement with ungated two-dimensional phase-contrast MR angiography in 250 adults. *Radiology* 209: 667-674.

Bunce D, Anstey KJ, Christensen H, et al. (2007) White matter hyperintensities and within-person variability in community-dwelling adults aged 60-64 years. *Neuropsychologia* 45: 2009-2015.

Burkarth N, Kriebel M, Kranz EU, et al. (2007) Neurofascin regulates the formation of gephyrin clusters and their subsequent translocation to the axon hillock of hippocampal neurons. *Mol Cell Neurosci* 36: 59-70.

Burke SN and Barnes CA. (2010) Senescent synapses and hippocampal circuit dynamics. *Trends Neurosci* 33: 153-161.

Buttermore ED, Piochon C, Wallace ML, et al. (2012) Pinceau organization in the cerebellum requires distinct functions of neurofascin in Purkinje and basket neurons during postnatal development. *J Neurosci* 32: 4724-4742.

Caldwell JH, Schaller KL, Lasher RS, et al. (2000) Sodium channel Na(v)1.6 is localized at nodes of ranvier, dendrites, and synapses. *Proc Natl Acad Sci U S A* 97: 5616-5620.

Calhoun ME, Kurth D, Phinney AL, et al. (1998) Hippocampal neuron and synaptophysin-positive bouton number in aging C57BL/6 mice. *Neurobiol Aging* 19: 599-606.

Calhoun ME, Mao Y, Roberts JA, et al. (2004) Reduction in hippocampal cholinergic innervation is unrelated to recognition memory impairment in aged rhesus monkeys. *J Comp Neurol* 475: 238-246.

Cammer W and Zhang H. (1999) Maturation of oligodendrocytes is more sensitive to TNF alpha than is survival of precursors and immature oligodendrocytes. *J Neuroimmunol* 97: 37-42.

Campagnoni AT and Macklin WB. (1988) Cellular and molecular aspects of myelin protein gene expression. *Mol Neurobiol* 2: 41-89.

Caprioli A, Ghirardi O, Giuliani A, et al. (1991) Spatial learning and memory in the radial maze: a longitudinal study in rats from 4 to 25 months of age. *Neurobiol Aging* 12: 605-607.

Carty ML, Wixey JA, Reinebrant HE, et al. (2011) Ibuprofen inhibits neuroinflammation and attenuates white matter damage following hypoxia-ischemia in the immature rodent brain. *Brain Res* 1402: 9-19.

Castellani R, Hirai K, Aliev G, et al. (2002) Role of mitochondrial dysfunction in Alzheimer's disease. *J Neurosci Res* 70: 357-360.

Castellani RJ, Rolston RK and Smith MA. (2010) Alzheimer disease. *Dis Mon* 56: 484-546.

Celone KA, Calhoun VD, Dickerson BC, et al. (2006) Alterations in memory networks in mild cognitive impairment and Alzheimer's disease: an independent component analysis. *J Neurosci* 26: 10222-10231.

Chakrabarti S, Munshi S, Banerjee K, et al. (2011) Mitochondrial Dysfunction during Brain Aging: Role of Oxidative Stress and Modulation by Antioxidant Supplementation. *Aging Dis* 2: 242-256.

Chambers JK, Uchida K and Nakayama H. (2012) White matter myelin loss in the brains of aged dogs. *Exp Gerontol* 47: 263-269.

Chapman PF, White GL, Jones MW, et al. (1999) Impaired synaptic plasticity and learning in aged amyloid precursor protein transgenic mice. *Nat Neurosci* 2: 271-276.

Chartier-Harlin MC, Crawford F, Houlden H, et al. (1991) Early-onset Alzheimer's disease caused by mutations at codon 717 of the beta-amyloid precursor protein gene. *Nature* 353: 844-846.

Chen G, Chen KS, Knox J, et al. (2000) A learning deficit related to age and beta-amyloid plaques in a mouse model of Alzheimer's disease. *Nature* 408: 975-979.

Chen H, Epelbaum S and Delatour B. (2011) Fiber Tracts Anomalies in APPxPS1 Transgenic Mice Modeling Alzheimer's Disease. *J Aging Res* 2011: 281274.

Chen TF, Lin CC, Chen YF, et al. (2009) Diffusion tensor changes in patients with amnesic mild cognitive impairment and various dementias. *Psychiatry Res* 173: 15-21.

Chiu SY. (2011) Matching mitochondria to metabolic needs at nodes of Ranvier. *Neuroscientist* 17: 343-350.

Choy M, Ganesan V, Thomas DL, et al. (2006) The chronic vascular and haemodynamic response after permanent bilateral common carotid occlusion in newborn and adult rats. *J Cereb Blood Flow Metab* 26: 1066-1075.

Chui DH, Tanahashi H, Ozawa K, et al. (1999) Transgenic mice with Alzheimer presenilin 1 mutations show accelerated neurodegeneration without amyloid plaque formation. *Nat Med* 5: 560-564.

Chung YA, O JH, Kim JY, et al. (2009) Hypoperfusion and ischemia in cerebral amyloid angiopathy documented by 99mTc-ECD brain perfusion SPECT. *J Nucl Med* 50: 1969-1974.

Cipolla MJ. (2009) *The Cerebral Circulation,* San Rafael (CA): Morgan & Claypool Life Sciences.

Cole MR and Chappell-Stephenson R. (2003) Exploring the limits of spatial memory in rats, using very large mazes. *Learn Behav* 31: 349-368.

Cole SL and Vassar R. (2007) The Alzheimer's disease beta-secretase enzyme, BACE1. *Mol Neurodegener* 2: 22.

Coleman PD and Yao PJ. (2003) Synaptic slaughter in Alzheimer's disease. *Neurobiol Aging* 24: 1023-1027.

Coltman R, Spain A, Tsenkina Y, et al. (2011) Selective white matter pathology induces a specific impairment in spatial working memory. *Neurobiol Aging* 32: 2324 e2327-2312.

Coman I, Aigrot MS, Seilhean D, et al. (2006) Nodal, paranodal and juxtaparanodal axonal proteins during demyelination and remyelination in multiple sclerosis. *Brain* 129: 3186-3195.

Corbett BF, Leiser SC, Ling HP, et al. (2013) Sodium channel cleavage is associated with aberrant neuronal activity and cognitive deficits in a mouse model of Alzheimer's disease. *J Neurosci* 33: 7020-7026.

Cordonnier C. (2011) Brain microbleeds: more evidence, but still a clinical dilemma. *Curr Opin Neurol* 24: 69-74.

Coyle JT and Schwarcz R. (2000) Mind glue: implications of glial cell biology for psychiatry. *Arch Gen Psychiatry* 57: 90-93.

Craik FI, Moscovitch M and McDowd JM. (1994) Contributions of surface and conceptual information to performance on implicit and explicit memory tasks. *J Exp Psychol Learn Mem Cogn* 20: 864-875.

de la Torre JC. (2002) Vascular basis of Alzheimer's pathogenesis. *Ann N Y Acad Sci* 977: 196-215.

de la Torre JC. (2009) Cerebrovascular and cardiovascular pathology in Alzheimer's disease. *Int Rev Neurobiol* 84: 35-48.

de la Torre JC. (2010) Vascular risk factor detection and control may prevent Alzheimer's disease. *Ageing Res Rev* 9: 218-225.

De Strooper B, Simons M, Multhaup G, et al. (1995) Production of intracellular amyloid-containing fragments in hippocampal neurons expressing human amyloid precursor protein and protection against amyloidogenesis by subtle amino acid substitutions in the rodent sequence. *EMBO J* 14: 4932-4938.

de Toledo-Morrell L, Morrell F, Fleming S, et al. (1984) Pentoxifylline reverses age-related deficits in spatial memory. *Behav Neural Biol* 42: 1-8.

Deane R, Sagare A, Hamm K, et al. (2008) apoE isoform-specific disruption of amyloid beta peptide clearance from mouse brain. *J Clin Invest* 118: 4002-4013.

Deane R, Wu Z, Sagare A, et al. (2004) LRP/amyloid beta-peptide interaction mediates differential brain efflux of Abeta isoforms. *Neuron* 43: 333-344.

Deary IJ, Bastin ME, Pattie A, et al. (2006) White matter integrity and cognition in childhood and old age. *Neurology* 66: 505-512.

Debette S and Markus HS. (2010) The clinical importance of white matter hyperintensities on brain magnetic resonance imaging: systematic review and meta-analysis. *BMJ* 341: c3666.

DeCarli C, Murphy DG, Tranh M, et al. (1995) The effect of white matter hyperintensity volume on brain structure, cognitive performance, and cerebral metabolism of glucose in 51 healthy adults. *Neurology* 45: 2077-2084.

Delatour B, Guegan M, Volk A, et al. (2006) In vivo MRI and histological evaluation of brain atrophy in APP/PS1 transgenic mice. *Neurobiol Aging* 27: 835-847.

Deng W, Wang H, Rosenberg PA, et al. (2004) Role of metabotropic glutamate receptors in oligodendrocyte excitotoxicity and oxidative stress. *Proc Natl Acad Sci U S A* 101: 7751-7756.

Denisenko-Nehrbass N, Oguievetskaia K, Goutebroze L, et al. (2003) Protein 4.1B associates with both Caspr/paranodin and Caspr2 at paranodes and juxtaparanodes of myelinated fibres. *Eur J Neurosci* 17: 411-416.

Desai MK, Mastrangelo MA, Ryan DA, et al. (2010) Early oligodendrocyte/myelin pathology in Alzheimer's disease mice constitutes a novel therapeutic target. *Am J Pathol* 177: 1422-1435.

Desai MK, Sudol KL, Janelsins MC, et al. (2009) Triple-transgenic Alzheimer's disease mice exhibit region-specific abnormalities in brain myelination patterns prior to appearance of amyloid and tau pathology. *Glia* 57: 54-65.

deToledo-Morrell L, Stoub TR and Wang C. (2007) Hippocampal atrophy and disconnection in incipient and mild Alzheimer's disease. *Prog Brain Res* 163: 741-753.

Deverman BE and Patterson PH. (2012) Exogenous leukemia inhibitory factor stimulates oligodendrocyte progenitor cell proliferation and enhances hippocampal remyelination. *J Neurosci* 32: 2100-2109.

Dickson DW, Crystal HA, Bevona C, et al. (1995) Correlations of synaptic and pathological markers with cognition of the elderly. *Neurobiol Aging* 16: 285-298; discussion 298-304.

Disterhoft JF and Matthew Oh M. (2003) Modulation of cholinergic transmission enhances excitability of hippocampal pyramidal neurons and ameliorates learning impairments in aging animals. *Neurobiol Learn Mem* 80: 223-233.

Dodart JC, Meziane H, Mathis C, et al. (1999) Behavioral disturbances in transgenic mice overexpressing the V717F beta-amyloid precursor protein. *Behav Neurosci* 113: 982-990.

Dong H, Martin MV, Chambers S, et al. (2007) Spatial relationship between synapse loss and beta-amyloid deposition in Tg2576 mice. *J Comp Neurol* 500: 311-321.

Douaud G, Menke RA, Gass A, et al. (2013) Brain microstructure reveals early abnormalities more than two years prior to clinical progression from mild cognitive impairment to Alzheimer's disease. *J Neurosci* 33: 2147-2155.

Dragicevic N, Mamcarz M, Zhu Y, et al. (2010) Mitochondrial amyloid-beta levels are associated with the extent of mitochondrial dysfunction in different brain regions and the degree of cognitive impairment in Alzheimer's transgenic mice. *J Alzheimers Dis* 20 Suppl 2: S535-550.

Du Y and Dreyfus CF. (2002) Oligodendrocytes as providers of growth factors. *J Neurosci Res* 68: 647-654.

Duff K, Eckman C, Zehr C, et al. (1996) Increased amyloid-beta42(43) in brains of mice expressing mutant presenilin 1. *Nature* 383: 710-713.

Duflocq A, Le Bras B, Bullier E, et al. (2008) Nav1.1 is predominantly expressed in nodes of Ranvier and axon initial segments. *Mol Cell Neurosci* 39: 180-192.

Dumont M, Lin MT and Beal MF. (2010) Mitochondria and antioxidant targeted therapeutic strategies for Alzheimer's disease. *J Alzheimers Dis* 20 Suppl 2: S633-643.

Dzhashiashvili Y, Zhang Y, Galinska J, et al. (2007) Nodes of Ranvier and axon initial segments are ankyrin G-dependent domains that assemble by distinct mechanisms. *J Cell Biol* 177: 857-870.

Dziewczapolski G, Glogowski CM, Masliah E, et al. (2009) Deletion of the alpha 7 nicotinic acetylcholine receptor gene improves cognitive deficits and synaptic pathology in a mouse model of Alzheimer's disease. *J Neurosci* 29: 8805-8815.

Edgar JM, McLaughlin M, Yool D, et al. (2004) Oligodendroglial modulation of fast axonal transport in a mouse model of hereditary spastic paraplegia. *J Cell Biol* 166: 121-131.

Einheber S, Bhat MA and Salzer JL. (2006) Disrupted axo-glial junctions result in accumulation of abnormal mitochondria at nodes of ranvier. *Neuron Glia Biol* 2: 165-174.

Eisele YS, Obermuller U, Heilbronner G, et al. (2010) Peripherally applied Abeta-containing inoculates induce cerebral beta-amyloidosis. *Science* 330: 980-982.

Eisenbach M, Kartvelishvily E, Eshed-Eisenbach Y, et al. (2009) Differential clustering of Caspr by oligodendrocytes and Schwann cells. *J Neurosci Res* 87: 3492-3501.

Englund E, Brun A and Alling C. (1988) White matter changes in dementia of Alzheimer's type. Biochemical and neuropathological correlates. *Brain* 111 (Pt 6): 1425-1439.

Enzinger C, Smith S, Fazekas F, et al. (2006) Lesion probability maps of white matter hyperintensities in elderly individuals: results of the Austrian stroke prevention study. *J Neurol* 253: 1064-1070.

Farkas E, Donka G, de Vos RA, et al. (2004) Experimental cerebral hypoperfusion induces white matter injury and microglial activation in the rat brain. *Acta Neuropathol* 108: 57-64.

Farkas E, Institoris A, Domoki F, et al. (2006) The effect of pre- and posttreatment with diazoxide on the early phase of chronic cerebral hypoperfusion in the rat. *Brain Res* 1087: 168-174.

Farkas E and Luiten PG. (2001) Cerebral microvascular pathology in aging and Alzheimer's disease. *Prog Neurobiol* 64: 575-611.

Farkas E, Luiten PG and Bari F. (2007) Permanent, bilateral common carotid artery occlusion in the rat: a model for chronic cerebral hypoperfusion-related neurodegenerative diseases. *Brain Res Rev* 54: 162-180.

Farrer LA, Cupples LA, Haines JL, et al. (1997) Effects of age, sex, and ethnicity on the association between apolipoprotein E genotype and Alzheimer disease. A meta-analysis. APOE and Alzheimer Disease Meta Analysis Consortium. *JAMA* 278: 1349-1356.

Feldman ML and Peters A. (1998) Ballooning of myelin sheaths in normally aged macaques. *J Neurocytol* 27: 605-614.

Fernando MS, Simpson JE, Matthews F, et al. (2006) White matter lesions in an unselected cohort of the elderly: molecular pathology suggests origin from chronic hypoperfusion injury. *Stroke* 37: 1391-1398.

Fields RD. (2008) White matter in learning, cognition and psychiatric disorders. *Trends Neurosci* 31: 361-370.

Findeis MA. (2007) The role of amyloid beta peptide 42 in Alzheimer's disease. *Pharmacol Ther* 116: 266-286.

Franklin KBJ and Paxinos G. (1997) *The mouse brain in stereotaxic coordinates*, San Diego ; London: Academic Press.

Franklin RJ and Ffrench-Constant C. (2008) Remyelination in the CNS: from biology to therapy. *Nat Rev Neurosci* 9: 839-855.

French HM, Reid M, Mamontov P, et al. (2009) Oxidative stress disrupts oligodendrocyte maturation. *J Neurosci Res* 87: 3076-3087.

Fukumoto H, Cheung BS, Hyman BT, et al. (2002) Beta-secretase protein and activity are increased in the neocortex in Alzheimer disease. *Arch Neurol* 59: 1381-1389.

Funfschilling U, Supplie LM, Mahad D, et al. (2012) Glycolytic oligodendrocytes maintain myelin and long-term axonal integrity. *Nature* 485: 517-521.

Furukawa K, Sopher BL, Rydel RE, et al. (1996) Increased activity-regulating and neuroprotective efficacy of alpha-secretase-derived secreted amyloid precursor protein conferred by a C-terminal heparin-binding domain. *J Neurochem* 67: 1882-1896.

Games D, Adams D, Alessandrini R, et al. (1995) Alzheimer-type neuropathology in transgenic mice overexpressing V717F beta-amyloid precursor protein. *Nature* 373: 523-527.

Garbern JY, Yool DA, Moore GJ, et al. (2002) Patients lacking the major CNS myelin protein, proteolipid protein 1, develop length-dependent axonal degeneration in the absence of demyelination and inflammation. *Brain* 125: 551-561.

Gasser A, Ho TS, Cheng X, et al. (2012) An ankyrinG-binding motif is necessary and sufficient for targeting Nav1.6 sodium channels to axon initial segments and nodes of Ranvier. *J Neurosci* 32: 7232-7243.

Gaudet AD, Popovich PG and Ramer MS. (2011) Wallerian degeneration: gaining perspective on inflammatory events after peripheral nerve injury. *J Neuroinflammation* 8: 110.

Geinisman Y, de Toledo-Morrell L and Morrell F. (1986) Loss of perforated synapses in the dentate gyrus: morphological substrate of memory deficit in aged rats. *Proc Natl Acad Sci U S A* 83: 3027-3031.

Geula C. (1998) Abnormalities of neural circuitry in Alzheimer's disease: hippocampus and cortical cholinergic innervation. *Neurology* 51: S18-29; discussion S65-17.

Giannakopoulos P, Herrmann FR, Bussiere T, et al. (2003) Tangle and neuron numbers, but not amyloid load, predict cognitive status in Alzheimer's disease. *Neurology* 60: 1495-1500.

Gilbert PE and Brushfield AM. (2009) The role of the CA3 hippocampal subregion in spatial memory: a process oriented behavioral assessment. *Prog Neuropsychopharmacol Biol Psychiatry* 33: 774-781.

Gleichmann M and Mattson MP. (2010) Alzheimer's disease and neuronal network activity. *Neuromolecular Med* 12: 44-47.

Glenner GG, Wong CW, Quaranta V, et al. (1984) The amyloid deposits in Alzheimer's disease: their nature and pathogenesis. *Appl Pathol* 2: 357-369.

Golgi C. (1870) Sulla sostanza connettiva del cervello (nevroglia). *Rendiconti del R Instituto Lombardo di Scienze e Lettere.* 275-277.

Gouw AA, Seewann A, Vrenken H, et al. (2008) Heterogeneity of white matter hyperintensities in Alzheimer's disease: post-mortem quantitative MRI and neuropathology. *Brain* 131: 3286-3298.

Grubb MS and Burrone J. (2010a) Activity-dependent relocation of the axon initial segment fine-tunes neuronal excitability. *Nature* 465: 1070-1074.

Grubb MS and Burrone J. (2010b) Building and maintaining the axon initial segment. *Curr Opin Neurobiol* 20: 481-488.

Guerreiro R, Wojtas A, Bras J, et al. (2013) TREM2 variants in Alzheimer's disease. *N Engl J Med* 368: 117-127.

Gunn-Moore D, Moffat K, Christie LA, et al. (2007) Cognitive dysfunction and the neurobiology of ageing in cats. *J Small Anim Pract* 48: 546-553.

Gunning-Dixon FM, Brickman AM, Cheng JC, et al. (2009) Aging of cerebral white matter: a review of MRI findings. *Int J Geriatr Psychiatry* 24: 109-117.

Hardy J. (2009) The amyloid hypothesis for Alzheimer's disease: a critical reappraisal. *J Neurochem* 110: 1129-1134.

Hardy J and Selkoe DJ. (2002) The amyloid hypothesis of Alzheimer's disease: progress and problems on the road to therapeutics. *Science* 297: 353-356.

Hardy JA and Higgins GA. (1992) Alzheimer's disease: the amyloid cascade hypothesis. *Science* 256: 184-185.

Harold D, Abraham R, Hollingworth P, et al. (2009) Genome-wide association study identifies variants at CLU and PICALM associated with Alzheimer's disease. *Nat Genet* 41: 1088-1093.

Harris JA, Devidze N, Verret L, et al. (2010) Transsynaptic progression of amyloid-beta-induced neuronal dysfunction within the entorhinal-hippocampal network. *Neuron* 68: 428-441.

Hattori H, Takeda M, Kudo T, et al. (1992) Cumulative white matter changes in the gerbil brain under chronic cerebral hypoperfusion. *Acta Neuropathol* 84: 437-442.

Head E. (2011) Neurobiology of the aging dog. *Age (Dordr)* 33: 485-496.

Hebert F, Grand'maison M, Ho MK, et al. (2013) Cortical atrophy and hypoperfusion in a transgenic mouse model of Alzheimer's disease. *Neurobiol Aging* 34: 1644-1652.

Hedden T, Mormino EC, Amariglio RE, et al. (2012) Cognitive profile of amyloid burden and white matter hyperintensities in cognitively normal older adults. *J Neurosci* 32: 16233-16242.

Hedstrom KL, Ogawa Y and Rasband MN. (2008) AnkyrinG is required for maintenance of the axon initial segment and neuronal polarity. *J Cell Biol* 183: 635-640.

Heneka MT, Sastre M, Dumitrescu-Ozimek L, et al. (2005) Focal glial activation coincides with increased BACE1 activation and precedes amyloid plaque deposition in APP[V717I] transgenic mice. *J Neuroinflammation* 2: 22.

Heyman A, Wilkinson WE, Stafford JA, et al. (1984) Alzheimer's disease: a study of epidemiological aspects. *Ann Neurol* 15: 335-341.

Hinman JD, Peters A, Cabral H, et al. (2006) Age-related molecular reorganization at the node of Ranvier. *J Comp Neurol* 495: 351-362.

Hinman JD, Rasband MN and Carmichael ST. (2013) Remodeling of the axon initial segment after focal cortical and white matter stroke. *Stroke* 44: 182-189.

Hodges H. (1996) Maze procedures: the radial-arm and water maze compared. *Brain Res Cogn Brain Res* 3: 167-181.

Holland PR, Bastin ME, Jansen MA, et al. (2011) MRI is a sensitive marker of subtle white matter pathology in hypoperfused mice. *Neurobiol Aging* 32: 2325 e2321-2326.

Hollingworth P, Sweet R, Sims R, et al. (2012) Genome-wide association study of Alzheimer's disease with psychotic symptoms. *Mol Psychiatry* 17: 1316-1327.

Holmes C, Boche D, Wilkinson D, et al. (2008) Long-term effects of Abeta42 immunisation in Alzheimer's disease: follow-up of a randomised, placebo-controlled phase I trial. *Lancet* 372: 216-223.

Horresh I, Poliak S, Grant S, et al. (2008) Multiple molecular interactions determine the clustering of Caspr2 and Kv1 channels in myelinated axons. *J Neurosci* 28: 14213-14222.

Howell OW, Palser A, Polito A, et al. (2006) Disruption of neurofascin localization reveals early changes preceding demyelination and remyelination in multiple sclerosis. *Brain* 129: 3173-3185.

Howell OW, Rundle JL, Garg A, et al. (2010) Activated microglia mediate axoglial disruption that contributes to axonal injury in multiple sclerosis. *J Neuropathol Exp Neurol* 69: 1017-1033.

Hsia AY, Masliah E, McConlogue L, et al. (1999) Plaque-independent disruption of neural circuits in Alzheimer's disease mouse models. *Proc Natl Acad Sci U S A* 96: 3228-3233.

Hsiao K, Chapman P, Nilsen S, et al. (1996) Correlative memory deficits, Abeta elevation, and amyloid plaques in transgenic mice. *Science* 274: 99-102.

Hu L, Wong TP, Cote SL, et al. (2003) The impact of Abeta-plaques on cortical cholinergic and non-cholinergic presynaptic boutons in alzheimer's disease-like transgenic mice. *Neuroscience* 121: 421-432.

Hu W, Tian C, Li T, et al. (2009) Distinct contributions of Na(v)1.6 and Na(v)1.2 in action potential initiation and backpropagation. *Nat Neurosci* 12: 996-1002.

Huang ZJ, Di Cristo G and Ango F. (2007) Development of GABA innervation in the cerebral and cerebellar cortices. *Nat Rev Neurosci* 8: 673-686.

Huff TB, Shi Y, Sun W, et al. (2011) Real-time CARS imaging reveals a calpain-dependent pathway for paranodal myelin retraction during high-frequency stimulation. *PLoS One* 6: e17176.

Hutton M, Lendon CL, Rizzu P, et al. (1998) Association of missense and 5'-splice-site mutations in tau with the inherited dementia FTDP-17. *Nature* 393: 702-705.

Hyde LA, Hoplight BJ and Denenberg VH. (1998) Water version of the radial-arm maze: learning in three inbred strains of mice. *Brain Res* 785: 236-244.

Iadecola C, Zhang F, Niwa K, et al. (1999) SOD1 rescues cerebral endothelial dysfunction in mice overexpressing amyloid precursor protein. *Nat Neurosci* 2: 157-161.

Ichinohe N, Hayashi M, Wakabayashi K, et al. (2009) Distribution and progression of amyloid-beta deposits in the amygdala of the aged macaque monkey, and parallels with zinc distribution. *Neuroscience* 159: 1374-1383.

Ihara M, Polvikoski TM, Hall R, et al. (2010) Quantification of myelin loss in frontal lobe white matter in vascular dementia, Alzheimer's disease, and dementia with Lewy bodies. *Acta Neuropathol* 119: 579-589.

Ikegami S. (1994) Behavioral impairment in radial-arm maze learning and acetylcholine content of the hippocampus and cerebral cortex in aged mice. *Behav Brain Res* 65: 103-111.

Irizarry MC, Soriano F, McNamara M, et al. (1997) Abeta deposition is associated with neuropil changes, but not with overt neuronal loss in the human amyloid precursor protein V717F (PDAPP) transgenic mouse. *J Neurosci* 17: 7053-7059.

Jacobs HI, Leritz EC, Williams VJ, et al. (2013) Association between white matter microstructure, executive functions, and processing speed in older adults: the impact of vascular health. *Hum Brain Mapp* 34: 77-95.

Janowsky JS, Kaye JA and Carper RA. (1996) Atrophy of the corpus callosum in Alzheimer's disease versus healthy aging. *J Am Geriatr Soc* 44: 798-803.

Jarrett JT, Berger EP and Lansbury PT, Jr. (1993) The carboxy terminus of the beta amyloid protein is critical for the seeding of amyloid formation: implications for the pathogenesis of Alzheimer's disease. *Biochemistry* 32: 4693-4697.

Jellinger KA. (2002) Alzheimer disease and cerebrovascular pathology: an update. *J Neural Transm* 109: 813-836.

Jellinger KA. (2010) Prevalence and impact of cerebrovascular lesions in Alzheimer and lewy body diseases. *Neurodegener Dis* 7: 112-115.

Jernigan TL, Archibald SL, Fennema-Notestine C, et al. (2001) Effects of age on tissues and regions of the cerebrum and cerebellum. *Neurobiol Aging* 22: 581-594.

Jorm AF, Korten AE and Henderson AS. (1987) The prevalence of dementia: a quantitative integration of the literature. *Acta Psychiatr Scand* 76: 465-479.

Juurlink BH, Thorburne SK and Hertz L. (1998) Peroxide-scavenging deficit underlies oligodendrocyte susceptibility to oxidative stress. *Glia* 22: 371-378.

Kalaria RN. (1996) Cerebral vessels in ageing and Alzheimer's disease. *Pharmacol Ther* 72: 193-214.

Kalaria RN. (2002) Small vessel disease and Alzheimer's dementia: pathological considerations. *Cerebrovasc Dis* 13 Suppl 2: 48-52.

Kamboh MI, Demirci FY, Wang X, et al. (2012) Genome-wide association study of Alzheimer's disease. *Transl Psychiatry* 2: e117.

Kanak DJ, Rose GM, Zaveri HP, et al. (2013) Altered network timing in the CA3-CA1 circuit of hippocampal slices from aged mice. *PLoS One* 8: e61364.

Kaphzan H, Buffington SA, Jung JI, et al. (2011) Alterations in intrinsic membrane properties and the axon initial segment in a mouse model of Angelman syndrome. *J Neurosci* 31: 17637-17648.

Kaplan MR, Cho MH, Ullian EM, et al. (2001) Differential control of clustering of the sodium channels Na(v)1.2 and Na(v)1.6 at developing CNS nodes of Ranvier. *Neuron* 30: 105-119.

Kaplan MR, Meyer-Franke A, Lambert S, et al. (1997) Induction of sodium channel clustering by oligodendrocytes. *Nature* 386: 724-728.

Kasparova S, Brezova V, Valko M, et al. (2005) Study of the oxidative stress in a rat model of chronic brain hypoperfusion. *Neurochem Int* 46: 601-611.

Kemper TL. (1994) Neuroanatomical and neuropathological changes during aging and in dementia. In: Albert ML and Knoefel JE (eds) *Clinical neurology of aging*. Second edition. ed. New York ; Oxford: OUP, 3–67.

Kennedy KM and Raz N. (2009) Aging white matter and cognition: differential effects of regional variations in diffusion properties on memory, executive functions, and speed. *Neuropsychologia* 47: 916-927.

Kerchner GA, Racine CA, Hale S, et al. (2012) Cognitive processing speed in older adults: relationship with white matter integrity. *PLoS One* 7: e50425.

Kettenmann H. (2006) Triggering the brain's pathology sensor. *Nat Neurosci* 9: 1463-1464.

Kim DY, Carey BW, Wang H, et al. (2007) BACE1 regulates voltage-gated sodium channels and neuronal activity. *Nat Cell Biol* 9: 755-764.

Kirkman TW. (1996) *Statistics to Use*. Available at: http://www.physics.csbsju.edu/stats/.

Kitaguchi H, Tomimoto H, Ihara M, et al. (2009) Chronic cerebral hypoperfusion accelerates amyloid beta deposition in APPSwInd transgenic mice. *Brain Res* 1294: 202-210.

Kitazawa M, Medeiros R and Laferla FM. (2012) Transgenic mouse models of Alzheimer disease: developing a better model as a tool for therapeutic interventions. *Curr Pharm Des* 18: 1131-1147.

Koike MA, Green KN, Blurton-Jones M, et al. (2010) Oligemic hypoperfusion differentially affects tau and amyloid-{beta}. *Am J Pathol* 177: 300-310.

Koistinaho M, Kettunen MI, Goldsteins G, et al. (2002) Beta-amyloid precursor protein transgenic mice that harbor diffuse A beta deposits but do not form plaques show increased ischemic vulnerability: role of inflammation. *Proc Natl Acad Sci U S A* 99: 1610-1615.

Kole MH and Stuart GJ. (2012) Signal processing in the axon initial segment. *Neuron* 73: 235-247.

Komatani A, Yamaguchi K, Sugai Y, et al. (1988) Assessment of demented patients by dynamic SPECT of inhaled xenon-133. *J Nucl Med* 29: 1621-1626.

Korolainen MA, Goldsteins G, Nyman TA, et al. (2006) Oxidative modification of proteins in the frontal cortex of Alzheimer's disease brain. *Neurobiol Aging* 27: 42-53.

Kovacs DM, Gersbacher MT and Kim DY. (2010) Alzheimer's secretases regulate voltage-gated sodium channels. *Neurosci Lett* 486: 68-72.

Kuba H. (2010) Plasticity at the axon initial segment. *Commun Integr Biol* 3: 597-598.

Kuba H, Oichi Y and Ohmori H. (2010) Presynaptic activity regulates Na(+) channel distribution at the axon initial segment. *Nature* 465: 1075-1078.

Kudo T, Takeda M, Tanimukai S, et al. (1993) Neuropathologic changes in the gerbil brain after chronic hypoperfusion. *Stroke* 24: 259-264; discussion 265.

Kumar A and Foster TC. (2007) Neurophysiology of Old Neurons and Synapses. In: Riddle DR (ed) *Brain Aging: Models, Methods, and Mechanisms.* Boca Raton (FL).

Kurumatani T, Kudo T, Ikura Y, et al. (1998) White matter changes in the gerbil brain under chronic cerebral hypoperfusion. *Stroke* 29: 1058-1062.

Lacas-Gervais S, Guo J, Strenzke N, et al. (2004) BetaIVSigma1 spectrin stabilizes the nodes of Ranvier and axon initial segments. *J Cell Biol* 166: 983-990.

LaFerla FM, Green KN and Oddo S. (2007) Intracellular amyloid-beta in Alzheimer's disease. *Nat Rev Neurosci* 8: 499-509.

Lambert JC, Heath S, Even G, et al. (2009) Genome-wide association study identifies variants at CLU and CR1 associated with Alzheimer's disease. *Nat Genet* 41: 1094-1099.

Lambert MP, Barlow AK, Chromy BA, et al. (1998) Diffusible, nonfibrillar ligands derived from Abeta1-42 are potent central nervous system neurotoxins. *Proc Natl Acad Sci U S A* 95: 6448-6453.

Laming PR, Kimelberg H, Robinson S, et al. (2000) Neuronal-glial interactions and behaviour. *Neurosci Biobehav Rev* 24: 295-340.

Landfield PW and Lynch G. (1977) Impaired monosynaptic potentiation in in vitro hippocampal slices from aged, memory-deficient rats. *J Gerontol* 32: 523-533.

Lasiene J, Shupe L, Perlmutter S, et al. (2008) No evidence for chronic demyelination in spared axons after spinal cord injury in a mouse. *J Neurosci* 28: 3887-3896.

Lazzarini RA. (2004) Myelin biology and disorders. Sand Diego, Calif.: Elsevier Academic Press,, 1 online resource (2 volumes).

Lebrun C, Durkin TP, Marighetto A, et al. (1990) A comparison of the working memory performances of young and aged mice combined with parallel measures of testing and drug-induced activations of septo-hippocampal and nbm-cortical cholinergic neurones. *Neurobiol Aging* 11: 515-521.

Lee JH, Park SY, Shin YW, et al. (2006) Neuroprotection by cilostazol, a phosphodiesterase type 3 inhibitor, against apoptotic white matter changes in rat after chronic cerebral hypoperfusion. *Brain Res* 1082: 182-191.

Lee JS, Im DS, An YS, et al. (2011) Chronic cerebral hypoperfusion in a mouse model of Alzheimer's disease: an additional contributing factor of cognitive impairment. *Neurosci Lett* 489: 84-88.

Leenders KL, Perani D, Lammertsma AA, et al. (1990) Cerebral blood flow, blood volume and oxygen utilization. Normal values and effect of age. *Brain* 113 (Pt 1): 27-47.

Leon-Espinosa G, DeFelipe J and Munoz A. (2012) Effects of amyloid-beta plaque proximity on the axon initial segment of pyramidal cells. *J Alzheimers Dis* 29: 841-852.

Lesne S, Koh MT, Kotilinek L, et al. (2006) A specific amyloid-beta protein assembly in the brain impairs memory. *Nature* 440: 352-357.

Lewis J, McGowan E, Rockwood J, et al. (2000) Neurofibrillary tangles, amyotrophy and progressive motor disturbance in mice expressing mutant (P301L) tau protein. *Nat Genet* 25: 402-405.

Li S, Pu F, Shi F, et al. (2008) Regional white matter decreases in Alzheimer's disease using optimized voxel-based morphometry. *Acta Radiol* 49: 84-90.

Lierse W and Horstmann E. (1965) Quantitative anatomy of the cerebral vascular bed with especial emphasis on homogeneity and inhomogeneity in small ports of the gray and white matter. *Acta Neurol Scand Suppl* 14: 15-19.

Lin L, Chen G, Xie K, et al. (2006) Large-scale neural ensemble recording in the brains of freely behaving mice. *J Neurosci Methods* 155: 28-38.

Lin MT and Beal MF. (2006) Mitochondrial dysfunction and oxidative stress in neurodegenerative diseases. *Nature* 443: 787-795.

Lin MT, Simon DK, Ahn CH, et al. (2002) High aggregate burden of somatic mtDNA point mutations in aging and Alzheimer's disease brain. *Hum Mol Genet* 11: 133-145.

Lintl P and Braak H. (1983) Loss of intracortical myelinated fibers: a distinctive age-related alteration in the human striate area. *Acta Neuropathol* 61: 178-182.

Liu HX, Zhang JJ, Zheng P, et al. (2005) Altered expression of MAP-2, GAP-43, and synaptophysin in the hippocampus of rats with chronic cerebral hypoperfusion correlates with cognitive impairment. *Brain Res Mol Brain Res* 139: 169-177.

Liu J, Jin DZ, Xiao L, et al. (2006) Paeoniflorin attenuates chronic cerebral hypoperfusion-induced learning dysfunction and brain damage in rats. *Brain Res* 1089: 162-170.

Liu X, Erikson C and Brun A. (1996) Cortical synaptic changes and gliosis in normal aging, Alzheimer's disease and frontal lobe degeneration. *Dementia* 7: 128-134.

Llinas RR. (2003) The contribution of Santiago Ramon y Cajal to functional neuroscience. *Nat Rev Neurosci* 4: 77-80.

Lonie JA, Parra-Rodriguez MA, Tierney KM, et al. (2010) Predicting outcome in mild cognitive impairment: 4-year follow-up study. *Br J Psychiatry* 197: 135-140.

Lonigro A and Devaux JJ. (2009) Disruption of neurofascin and gliomedin at nodes of Ranvier precedes demyelination in experimental allergic neuritis. *Brain* 132: 260-273.

Ludwin SK. (1978) Central nervous system demyelination and remyelination in the mouse: an ultrastructural study of cuprizone toxicity. *Lab Invest* 39: 597-612.

Luebke J, Barbas H and Peters A. (2010) Effects of normal aging on prefrontal area 46 in the rhesus monkey. *Brain Res Rev* 62: 212-232.

Luo XG, Ding JQ and Chen SD. (2010) Microglia in the aging brain: relevance to neurodegeneration. *Mol Neurodegener* 5: 12.

Maki T, Ihara M, Fujita Y, et al. (2011) Angiogenic and vasoprotective effects of adrenomedullin on prevention of cognitive decline after chronic cerebral hypoperfusion in mice. *Stroke* 42: 1122-1128.

Markesbery WR. (1997) Oxidative stress hypothesis in Alzheimer's disease. *Free Radic Biol Med* 23: 134-147.

Marner L, Nyengaard JR, Tang Y, et al. (2003) Marked loss of myelinated nerve fibers in the human brain with age. *J Comp Neurol* 462: 144-152.

Mathis C, Denisenko-Nehrbass N, Girault JA, et al. (2001) Essential role of oligodendrocytes in the formation and maintenance of central nervous system nodal regions. *Development* 128: 4881-4890.

Mayer MC and Meinl E. (2012) Glycoproteins as targets of autoantibodies in CNS inflammation: MOG and more. *Ther Adv Neurol Disord* 5: 147-159.

McDonald-Miszczak L, Hertzog C and Hultsch DF. (1995) Stability and accuracy of metamemory in adulthood and aging: a longitudinal analysis. *Psychol Aging* 10: 553-564.

McIver S, Faideau M and Haydon P. (2013) Astrocyte–Neuron Communications. In: Cui C, Grandison L and Noronha A (eds) *Neural-Immune Interactions in Brain Function and Alcohol Related Disorders.* Springer US, 31-64.

McKhann GM, Knopman DS, Chertkow H, et al. (2011) The diagnosis of dementia due to Alzheimer's disease: recommendations from the National Institute on Aging-Alzheimer's Association workgroups on diagnostic guidelines for Alzheimer's disease. *Alzheimers Dement* 7: 263-269.

McTigue DM and Tripathi RB. (2008) The life, death, and replacement of oligodendrocytes in the adult CNS. *J Neurochem* 107: 1-19.

Meckel JF. (1817) *Tabulae anatomico-pathologicae: modos omnes, quibus partium corporis humani omnium forma externa atque interna a norma recedit exhibentes,* Lipsiae: Gleditsch.

Meier-Ruge W, Ulrich J, Bruhlmann M, et al. (1992) Age-related white matter atrophy in the human brain. *Ann N Y Acad Sci* 673: 260-269.

Mielke MM, Kozauer NA, Chan KC, et al. (2009) Regionally-specific diffusion tensor imaging in mild cognitive impairment and Alzheimer's disease. *Neuroimage* 46: 47-55.

Milde LN, Milde JH and Michenfelder JD. (1986) Delayed treatment with nimodipine improves cerebral blood flow after complete cerebral ischemia in the dog. *J Cereb Blood Flow Metab* 6: 332-337.

Mizumori SJ, Lavoie AM and Kalyani A. (1996) Redistribution of spatial representation in the hippocampus of aged rats performing a spatial memory task. *Behav Neurosci* 110: 1006-1016.

Morgan AR, Turic D, Jehu L, et al. (2007) Association studies of 23 positional/functional candidate genes on chromosome 10 in late-onset Alzheimer's disease. *Am J Med Genet B Neuropsychiatr Genet* 144B: 762-770.

Morris JC, Roe CM, Grant EA, et al. (2009) Pittsburgh compound B imaging and prediction of progression from cognitive normality to symptomatic Alzheimer disease. *Arch Neurol* 66: 1469-1475.

Mucke L, Masliah E, Yu GQ, et al. (2000) High-level neuronal expression of abeta 1-42 in wild-type human amyloid protein precursor transgenic mice: synaptotoxicity without plaque formation. *J Neurosci* 20: 4050-4058.

Mullan M, Crawford F, Axelman K, et al. (1992) A pathogenic mutation for probable Alzheimer's disease in the APP gene at the N-terminus of beta-amyloid. *Nat Genet* 1: 345-347.

Mulligan SJ and MacVicar BA. (2004) Calcium transients in astrocyte endfeet cause cerebrovascular constrictions. *Nature* 431: 195-199.

Nadon NL and West M. (1998) Myelin proteolipid protein: function in myelin structure is distinct from its role in oligodendrocyte development. *Dev Neurosci* 20: 533-539.

Nie DY, Ma QH, Law JW, et al. (2006) Oligodendrocytes regulate formation of nodes of Ranvier via the recognition molecule OMgp. *Neuron Glia Biol* 2: 151-164.

Niwa K, Kazama K, Younkin L, et al. (2002a) Cerebrovascular autoregulation is profoundly impaired in mice overexpressing amyloid precursor protein. *Am J Physiol Heart Circ Physiol* 283: H315-323.

Niwa K, Kazama K, Younkin SG, et al. (2002b) Alterations in cerebral blood flow and glucose utilization in mice overexpressing the amyloid precursor protein. *Neurobiol Dis* 9: 61-68.

Niwa K, Younkin L, Ebeling C, et al. (2000) Abeta 1-40-related reduction in functional hyperemia in mouse neocortex during somatosensory activation. *Proc Natl Acad Sci U S A* 97: 9735-9740.

Nunan J and Small DH. (2000) Regulation of APP cleavage by alpha-, beta- and gamma-secretases. *FEBS Lett* 483: 6-10.

O'Dwyer L, Lamberton F, Bokde AL, et al. (2011) Multiple indices of diffusion identifies white matter damage in mild cognitive impairment and Alzheimer's disease. *PLoS One* 6: e21745.

Oddo S, Caccamo A, Shepherd JD, et al. (2003) Triple-transgenic model of Alzheimer's disease with plaques and tangles: intracellular Abeta and synaptic dysfunction. *Neuron* 39: 409-421.

Ogawa Y, Horresh I, Trimmer JS, et al. (2008) Postsynaptic density-93 clusters Kv1 channels at axon initial segments independently of Caspr2. *J Neurosci* 28: 5731-5739.

Ogawa Y, Oses-Prieto J, Kim MY, et al. (2010) ADAM22, a Kv1 channel-interacting protein, recruits membrane-associated guanylate kinases to juxtaparanodes of myelinated axons. *J Neurosci* 30: 1038-1048.

Ohta H, Nishikawa H, Kimura H, et al. (1997) Chronic cerebral hypoperfusion by permanent internal carotid ligation produces learning impairment without brain damage in rats. *Neuroscience* 79: 1039-1050.

Olichney JM, Ellis RJ, Katzman R, et al. (1997) Types of cerebrovascular lesions associated with severe cerebral amyloid angiopathy in Alzheimer's disease. *Ann N Y Acad Sci* 826: 493-497.

Olton D and Samuelson R. (1976) Remembrance of places passed: Spatial memory in rats. *Journal of Experimental Psychology: Animal Behavior Processes* 2: 97-116.

Omlin FX, Webster HD, Palkovits CG, et al. (1982) Immunocytochemical localization of basic protein in major dense line regions of central and peripheral myelin. *J Cell Biol* 95: 242-248.

Otori T, Katsumata T, Muramatsu H, et al. (2003) Long-term measurement of cerebral blood flow and metabolism in a rat chronic hypoperfusion model. *Clin Exp Pharmacol Physiol* 30: 266-272.

Pan Z, Kao T, Horvath Z, et al. (2006) A common ankyrin-G-based mechanism retains KCNQ and NaV channels at electrically active domains of the axon. *J Neurosci* 26: 2599-2613.

Pantoni L. (2002) Pathophysiology of age-related cerebral white matter changes. *Cerebrovasc Dis* 13 Suppl 2: 7-10.

Pantoni L and Garcia JH. (1997) Cognitive impairment and cellular/vascular changes in the cerebral white matter. *Ann N Y Acad Sci* 826: 92-102.

Papp KV, Kaplan RF, Springate B, et al. (2013) Processing speed in normal aging: Effects of white matter hyperintensities and hippocampal volume loss. *Neuropsychol Dev Cogn B Aging Neuropsychol Cogn*.

Park L, Anrather J, Forster C, et al. (2004) Abeta-induced vascular oxidative stress and attenuation of functional hyperemia in mouse somatosensory cortex. *J Cereb Blood Flow Metab* 24: 334-342.

Park L, Anrather J, Girouard H, et al. (2007) Nox2-derived reactive oxygen species mediate neurovascular dysregulation in the aging mouse brain. *J Cereb Blood Flow Metab* 27: 1908-1918.

Paspalas CD and Papadopoulos GC. (1998) Ultrastructural evidence for combined action of noradrenaline and vasoactive intestinal polypeptide upon neurons, astrocytes, and blood vessels of the rat cerebral cortex. *Brain Res Bull* 45: 247-259.

Patrikios P, Stadelmann C, Kutzelnigg A, et al. (2006) Remyelination is extensive in a subset of multiple sclerosis patients. *Brain* 129: 3165-3172.

Pedraza L, Huang JK and Colman D. (2009) Disposition of axonal caspr with respect to glial cell membranes: Implications for the process of myelination. *J Neurosci Res* 87: 3480-3491.

Peles E and Salzer JL. (2000) Molecular domains of myelinated axons. *Curr Opin Neurobiol* 10: 558-565.

Peters A. (2002) The effects of normal aging on myelin and nerve fibers: a review. *J Neurocytol* 31: 581-593.

Peters A. (2009) The effects of normal aging on myelinated nerve fibers in monkey central nervous system. *Front Neuroanat* 3: 11.

Peters A, Moss MB and Sethares C. (2000) Effects of aging on myelinated nerve fibers in monkey primary visual cortex. *J Comp Neurol* 419: 364-376.

Peters A and Sethares C. (2002) Aging and the myelinated fibers in prefrontal cortex and corpus callosum of the monkey. *J Comp Neurol* 442: 277-291.

Peters A and Sethares C. (2003) Is there remyelination during aging of the primate central nervous system? *J Comp Neurol* 460: 238-254.

Peters A, Sethares C and Killiany RJ. (2001) Effects of age on the thickness of myelin sheaths in monkey primary visual cortex. *J Comp Neurol* 435: 241-248.

Petersen RC. (2004) Mild cognitive impairment as a diagnostic entity. *J Intern Med* 256: 183-194.

Petersen RC, Smith G, Kokmen E, et al. (1992) Memory function in normal aging. *Neurology* 42: 396-401.

Petzold A, Tozer DJ and Schmierer K. (2011) Axonal damage in the making: neurofilament phosphorylation, proton mobility and magnetisation transfer in multiple sclerosis normal appearing white matter. *Exp Neurol* 232: 234-239.

Pillai AM, Thaxton C, Pribisko AL, et al. (2009) Spatiotemporal ablation of myelinating glia-specific neurofascin (Nfasc NF155) in mice reveals gradual loss of paranodal axoglial junctions and concomitant disorganization of axonal domains. *J Neurosci Res* 87: 1773-1793.

Poliak S, Gollan L, Martinez R, et al. (1999) Caspr2, a new member of the neurexin superfamily, is localized at the juxtaparanodes of myelinated axons and associates with K+ channels. *Neuron* 24: 1037-1047.

Pope SK, Shue VM and Beck C. (2003) Will a healthy lifestyle help prevent Alzheimer's disease? *Annu Rev Public Health* 24: 111-132.

Powers BE, Lasiene J, Plemel JR, et al. (2012) Axonal thinning and extensive remyelination without chronic demyelination in spinal injured rats. *J Neurosci* 32: 5120-5125.

Quarles RH. (2002) Myelin sheaths: glycoproteins involved in their formation, maintenance and degeneration. *Cell Mol Life Sci* 59: 1851-1871.

Quarles RH. (2007) Myelin-associated glycoprotein (MAG): past, present and beyond. *J Neurochem* 100: 1431-1448.

Quarles RH, Macklin WB and Morell P. (2006) Myelin Formation, Structure and Biochemistry. In: Siegel GJ, Albers WR, Brady S, et al. (eds) *Basic neurochemistry : molecular, cellular and medical aspects.* 7th edition. ed. Philadelphia: Lippincott-Raven, 51-71.

Raber J, Wong D, Yu GQ, et al. (2000) Apolipoprotein E and cognitive performance. *Nature* 404: 352-354.

Raine C. (1984) Morphology of Myelin and Myelination. In: Morell P (ed) *Myelin.* Springer US, 1-50.

Rapp PR and Gallagher M. (1996) Preserved neuron number in the hippocampus of aged rats with spatial learning deficits. *Proc Natl Acad Sci U S A* 93: 9926-9930.

Rasband MN. (2010) The axon initial segment and the maintenance of neuronal polarity. *Nat Rev Neurosci* 11: 552-562.

Rasband MN. (2011) Composition, assembly, and maintenance of excitable membrane domains in myelinated axons. *Semin Cell Dev Biol* 22: 178-184.

Rasmussen T, Schliemann T, Sorensen JC, et al. (1996) Memory impaired aged rats: no loss of principal hippocampal and subicular neurons. *Neurobiol Aging* 17: 143-147.

Raz N and Rodrigue KM. (2006) Differential aging of the brain: patterns, cognitive correlates and modifiers. *Neurosci Biobehav Rev* 30: 730-748.

Redwine JM, Kosofsky B, Jacobs RE, et al. (2003) Dentate gyrus volume is reduced before onset of plaque formation in PDAPP mice: a magnetic resonance microscopy and stereologic analysis. *Proc Natl Acad Sci U S A* 100: 1381-1386.

Reimer MM, McQueen J, Searcy L, et al. (2011) Rapid disruption of axon-glial integrity in response to mild cerebral hypoperfusion. *J Neurosci* 31: 18185-18194.

Rios JC, Rubin M, St Martin M, et al. (2003) Paranodal interactions regulate expression of sodium channel subtypes and provide a diffusion barrier for the node of Ranvier. *J Neurosci* 23: 7001-7011.

Roach A, Takahashi N, Pravtcheva D, et al. (1985) Chromosomal mapping of mouse myelin basic protein gene and structure and transcription of the partially deleted gene in shiverer mutant mice. *Cell* 42: 149-155.

Rockwood K, Ebly E, Hachinski V, et al. (1997) Presence and treatment of vascular risk factors in patients with vascular cognitive impairment. *Arch Neurol* 54: 33-39.

Roe CM, Fagan AM, Grant EA, et al. (2013) Amyloid imaging and CSF biomarkers in predicting cognitive impairment up to 7.5 years later. *Neurology* 80: 1784-1791.

Rogaeva E, Meng Y, Lee JH, et al. (2007) The neuronal sortilin-related receptor SORL1 is genetically associated with Alzheimer disease. *Nat Genet* 39: 168-177.

Roher AE, Debbins JP, Malek-Ahmadi M, et al. (2012) Cerebral blood flow in Alzheimer's disease. *Vasc Health Risk Manag* 8: 599-611.

Roher AE, Weiss N, Kokjohn TA, et al. (2002) Increased A beta peptides and reduced cholesterol and myelin proteins characterize white matter degeneration in Alzheimer's disease. *Biochemistry* 41: 11080-11090.

Rombouts SA, Goekoop R, Stam CJ, et al. (2005) Delayed rather than decreased BOLD response as a marker for early Alzheimer's disease. *Neuroimage* 26: 1078-1085.

Rosenzweig ES and Barnes CA. (2003) Impact of aging on hippocampal function: plasticity, network dynamics, and cognition. *Prog Neurobiol* 69: 143-179.

Rowbotham GF and Little E. (1965) Circulations of the Cerebral Hemispheres. *Br J Surg* 52: 8-21.

Royeck M, Horstmann MT, Remy S, et al. (2008) Role of axonal NaV1.6 sodium channels in action potential initiation of CA1 pyramidal neurons. *J Neurophysiol* 100: 2361-2380.

Ruitenberg A, den Heijer T, Bakker SL, et al. (2005) Cerebral hypoperfusion and clinical onset of dementia: the Rotterdam Study. *Ann Neurol* 57: 789-794.

Rutten BP, Van der Kolk NM, Schafer S, et al. (2005) Age-related loss of synaptophysin immunoreactive presynaptic boutons within the hippocampus of APP751SL, PS1M146L, and APP751SL/PS1M146L transgenic mice. *Am J Pathol* 167: 161-173.

Salat DH, Greve DN, Pacheco JL, et al. (2009) Regional white matter volume differences in nondemented aging and Alzheimer's disease. *Neuroimage* 44: 1247-1258.

Salat DH, Tuch DS, Greve DN, et al. (2005) Age-related alterations in white matter microstructure measured by diffusion tensor imaging. *Neurobiol Aging* 26: 1215-1227.

Sanchez PE, Zhu L, Verret L, et al. (2012) Levetiracetam suppresses neuronal network dysfunction and reverses synaptic and cognitive deficits in an Alzheimer's disease model. *Proc Natl Acad Sci U S A* 109: E2895-2903.

Sandell JH and Peters A. (2003) Disrupted myelin and axon loss in the anterior commissure of the aged rhesus monkey. *J Comp Neurol* 466: 14-30.

Santuccione AC, Merlini M, Shetty A, et al. (2013) Active vaccination with ankyrin G reduces beta-amyloid pathology in APP transgenic mice. *Mol Psychiatry* 18: 358-368.

Sasaki M, Black JA, Lankford KL, et al. (2006) Molecular reconstruction of nodes of Ranvier after remyelination by transplanted olfactory ensheathing cells in the demyelinated spinal cord. *J Neurosci* 26: 1803-1812.

Savvaki M, Panagiotaropoulos T, Stamatakis A, et al. (2008) Impairment of learning and memory in TAG-1 deficient mice associated with shorter CNS internodes and disrupted juxtaparanodes. *Mol Cell Neurosci* 39: 478-490.

Schafer DP, Jha S, Liu F, et al. (2009) Disruption of the axon initial segment cytoskeleton is a new mechanism for neuronal injury. *J Neurosci* 29: 13242-13254.

Schapira AH. (1996) Oxidative stress and mitochondrial dysfunction in neurodegeneration. *Curr Opin Neurol* 9: 260-264.

Scheff SW, Price DA, Schmitt FA, et al. (2006) Hippocampal synaptic loss in early Alzheimer's disease and mild cognitive impairment. *Neurobiol Aging* 27: 1372-1384.

Scheltens P, Barkhof F, Leys D, et al. (1995) Histopathologic correlates of white matter changes on MRI in Alzheimer's disease and normal aging. *Neurology* 45: 883-888.

Schmidt-Kastner R, Truettner J, Lin B, et al. (2001) Transient changes of brain-derived neurotrophic factor (BDNF) mRNA expression in hippocampus during moderate ischemia induced by chronic bilateral common carotid artery occlusions in the rat. *Brain Res Mol Brain Res* 92: 157-166.

Seiffert D, Bradley JD, Rominger CM, et al. (2000) Presenilin-1 and -2 are molecular targets for gamma-secretase inhibitors. *J Biol Chem* 275: 34086-34091.

Sekhon LH, Morgan MK, Spence I, et al. (1994) Chronic cerebral hypoperfusion and impaired neuronal function in rats. *Stroke* 25: 1022-1027.

Seshadri S, Fitzpatrick AL, Ikram MA, et al. (2010) Genome-wide analysis of genetic loci associated with Alzheimer disease. *JAMA* 303: 1832-1840.

Shankar GM, Li S, Mehta TH, et al. (2008) Amyloid-beta protein dimers isolated directly from Alzheimer's brains impair synaptic plasticity and memory. *Nat Med* 14: 837-842.

Shaw C and Aggleton JP. (1993) The effects of fornix and medial prefrontal lesions on delayed non-matching-to-sample by rats. *Behav Brain Res* 54: 91-102.

Shepherd MN, Pomicter AD, Velazco CS, et al. (2012) Paranodal reorganization results in the depletion of transverse bands in the aged central nervous system. *Neurobiol Aging* 33: 203 e213-224.

Sherman DL, Tait S, Melrose S, et al. (2005) Neurofascins are required to establish axonal domains for saltatory conduction. *Neuron* 48: 737-742.

Shibata M, Ohtani R, Ihara M, et al. (2004) White matter lesions and glial activation in a novel mouse model of chronic cerebral hypoperfusion. *Stroke* 35: 2598-2603.

Shibata M, Yamasaki N, Miyakawa T, et al. (2007) Selective impairment of working memory in a mouse model of chronic cerebral hypoperfusion. *Stroke* 38: 2826-2832.

Silbert LC, Dodge HH, Perkins LG, et al. (2012) Trajectory of white matter hyperintensity burden preceding mild cognitive impairment. *Neurology* 79: 741-747.

Singh P, Yan J, Hull R, et al. (2011) Levels of phosphorylated axonal neurofilament subunit H (pNfH) are increased in acute ischemic stroke. *J Neurol Sci* 304: 117-121.

Sloane JA, Hinman JD, Lubonia M, et al. (2003) Age-dependent myelin degeneration and proteolysis of oligodendrocyte proteins is associated with the activation of calpain-1 in the rhesus monkey. *J Neurochem* 84: 157-168.

Smith KJ. (2007) Sodium channels and multiple sclerosis: roles in symptom production, damage and therapy. *Brain Pathol* 17: 230-242.

Smith KJ, Blakemore WF and McDonald WI. (1979) Central remyelination restores secure conduction. *Nature* 280: 395-396.

Staugaitis SM, Smith PR and Colman DR. (1990) Expression of myelin basic protein isoforms in nonglial cells. *J Cell Biol* 110: 1719-1727.

Stichel CC and Luebbert H. (2007) Inflammatory processes in the aging mouse brain: participation of dendritic cells and T-cells. *Neurobiol Aging* 28: 1507-1521.

Stokin GB, Lillo C, Falzone TL, et al. (2005) Axonopathy and transport deficits early in the pathogenesis of Alzheimer's disease. *Science* 307: 1282-1288.

Stoquart-ElSankari S, Baledent O, Gondry-Jouet C, et al. (2007) Aging effects on cerebral blood and cerebrospinal fluid flows. *J Cereb Blood Flow Metab* 27: 1563-1572.

Sturchler-Pierrat C, Abramowski D, Duke M, et al. (1997) Two amyloid precursor protein transgenic mouse models with Alzheimer disease-like pathology. *Proc Natl Acad Sci U S A* 94: 13287-13292.

Sugiyama I, Tanaka K, Akita M, et al. (2002) Ultrastructural analysis of the paranodal junction of myelinated fibers in 31-month-old-rats. *J Neurosci Res* 70: 309-317.

Sullivan EV, Adalsteinsson E, Hedehus M, et al. (2001) Equivalent disruption of regional white matter microstructure in ageing healthy men and women. *Neuroreport* 12: 99-104.

Summers BA and Appel MJ. (1987) Demyelination in canine distemper encephalomyelitis: an ultrastructural analysis. *J Neurocytol* 16: 871-881.

Susuki K and Rasband MN. (2008a) Molecular mechanisms of node of Ranvier formation. *Curr Opin Cell Biol* 20: 616-623.

Susuki K and Rasband MN. (2008b) Spectrin and ankyrin-based cytoskeletons at polarized domains in myelinated axons. *Exp Biol Med (Maywood)* 233: 394-400.

Szymanski CR, Chiha W, Morellini N, et al. (2013) Paranode Abnormalities and Oxidative Stress in Optic Nerve Vulnerable to Secondary Degeneration: Modulation by 670 nm Light Treatment. *PLoS One* 8: e66448.

Takizawa S, Fukuyama N, Hirabayashi H, et al. (2003) Quercetin, a natural flavonoid, attenuates vacuolar formation in the optic tract in rat chronic cerebral hypoperfusion model. *Brain Res* 980: 156-160.

Tambuyzer BR, Ponsaerts P and Nouwen EJ. (2009) Microglia: gatekeepers of central nervous system immunology. *J Leukoc Biol* 85: 352-370.

Tanaka H, Ma J, Tanaka KF, et al. (2009) Mice with altered myelin proteolipid protein gene expression display cognitive deficits accompanied by abnormal neuron-glia interactions and decreased conduction velocities. *J Neurosci* 29: 8363-8371.

Tang Y, Nyengaard JR, Pakkenberg B, et al. (1997) Age-induced white matter changes in the human brain: a stereological investigation. *Neurobiol Aging* 18: 609-615.

Thomas T, Thomas G, McLendon C, et al. (1996) beta-Amyloid-mediated vasoactivity and vascular endothelial damage. *Nature* 380: 168-171.

Thorburne SK and Juurlink BH. (1996) Low glutathione and high iron govern the susceptibility of oligodendroglial precursors to oxidative stress. *J Neurochem* 67: 1014-1022.

Tomimoto H, Ihara M, Wakita H, et al. (2003) Chronic cerebral hypoperfusion induces white matter lesions and loss of oligodendroglia with DNA fragmentation in the rat. *Acta Neuropathol* 106: 527-534.

Torp R, Head E, Milgram NW, et al. (2000) Ultrastructural evidence of fibrillar beta-amyloid associated with neuronal membranes in behaviorally characterized aged dog brains. *Neuroscience* 96: 495-506.

Traka M, Goutebroze L, Denisenko N, et al. (2003) Association of TAG-1 with Caspr2 is essential for the molecular organization of juxtaparanodal regions of myelinated fibers. *J Cell Biol* 162: 1161-1172.

Tsuchiya M, Sako K, Yura S, et al. (1992) Cerebral blood flow and histopathological changes following permanent bilateral carotid artery ligation in Wistar rats. *Exp Brain Res* 89: 87-92.

Turner PR, O'Connor K, Tate WP, et al. (2003) Roles of amyloid precursor protein and its fragments in regulating neural activity, plasticity and memory. *Prog Neurobiol* 70: 1-32.

Ueno Y, Zhang N, Miyamoto N, et al. (2009) Edaravone attenuates white matter lesions through endothelial protection in a rat chronic hypoperfusion model. *Neuroscience* 162: 317-327.

Uschkureit T, Sporkel O, Stracke J, et al. (2000) Early onset of axonal degeneration in double (plp-/-mag-/-) and hypomyelinosis in triple (plp-/-mbp-/-mag-/-) mutant mice. *J Neurosci* 20: 5225-5233.

Valero J, Espana J, Parra-Damas A, et al. (2011) Short-term environmental enrichment rescues adult neurogenesis and memory deficits in APP(Sw,Ind) transgenic mice. *PLoS One* 6: e16832.

Van Wart A and Matthews G. (2006) Impaired firing and cell-specific compensation in neurons lacking nav1.6 sodium channels. *J Neurosci* 26: 7172-7180.

VanGuilder HD, Farley JA, Yan H, et al. (2011) Hippocampal dysregulation of synaptic plasticity-associated proteins with age-related cognitive decline. *Neurobiol Dis* 43: 201-212.

Verret L, Mann EO, Hang GB, et al. (2012) Inhibitory interneuron deficit links altered network activity and cognitive dysfunction in Alzheimer model. *Cell* 149: 708-721.

Virchow R. (1860) *Cellular pathology : as based upon physiological and pathological histology*, London: Churchill.

von Bernhardi R, Tichauer JE and Eugenin J. (2010) Aging-dependent changes of microglial cells and their relevance for neurodegenerative disorders. *J Neurochem* 112: 1099-1114.

Wakita H, Tomimoto H, Akiguchi I, et al. (2002) Axonal damage and demyelination in the white matter after chronic cerebral hypoperfusion in the rat. *Brain Res* 924: 63-70.

Wang J, Zhang HY and Tang XC. (2010) Huperzine a improves chronic inflammation and cognitive decline in rats with cerebral hypoperfusion. *J Neurosci Res* 88: 807-815.

Weidensteiner C, Metzger F, Bruns A, et al. (2009) Cortical hypoperfusion in the B6.PS2APP mouse model for Alzheimer's disease: comprehensive phenotyping of vascular and tissular parameters by MRI. *Magn Reson Med* 62: 35-45.

Wenk GL. (2003) Neuropathologic changes in Alzheimer's disease. *J Clin Psychiatry* 64 Suppl 9: 7-10.

West MJ. (1993) Regionally specific loss of neurons in the aging human hippocampus. *Neurobiol Aging* 14: 287-293.

Whitley E and Ball J. (2002) Statistics review 4: sample size calculations. *Crit Care* 6: 335-341.

Wirths O, Weis J, Kayed R, et al. (2007) Age-dependent axonal degeneration in an Alzheimer mouse model. *Neurobiol Aging* 28: 1689-1699.

Wisniewski HM, Wegiel J, Wang KC, et al. (1989) Ultrastructural studies of the cells forming amyloid fibers in classical plaques. *Can J Neurol Sci* 16: 535-542.

Wu CC, Chawla F, Games D, et al. (2004a) Selective vulnerability of dentate granule cells prior to amyloid deposition in PDAPP mice: digital morphometric analyses. *Proc Natl Acad Sci U S A* 101: 7141-7146.

Wu EX, Tang H, Asai T, et al. (2004b) Regional cerebral blood volume reduction in transgenic mutant APP (V717F, K670N/M671L) mice. *Neurosci Lett* 365: 223-227.

Xu J, Chen S, Ahmed SH, et al. (2001) Amyloid-beta peptides are cytotoxic to oligodendrocytes. *J Neurosci* 21: RC118.

Yamada M, Ihara M, Okamoto Y, et al. (2011) The influence of chronic cerebral hypoperfusion on cognitive function and amyloid beta metabolism in APP overexpressing mice. *PLoS One* 6: e16567.

Yang X, Yang Y, Luo Y, et al. (2009) Hyperphosphorylation and accumulation of neurofilament proteins in transgenic mice with Alzheimer presenilin 1 mutation. *Cell Mol Neurobiol* 29: 497-501.

Yang Y, Lacas-Gervais S, Morest DK, et al. (2004) BetaIV spectrins are essential for membrane stability and the molecular organization of nodes of Ranvier. *J Neurosci* 24: 7230-7240.

Yang Y, Ogawa Y, Hedstrom KL, et al. (2007) betaIV spectrin is recruited to axon initial segments and nodes of Ranvier by ankyrinG. *J Cell Biol* 176: 509-519.

Yao C, Williams AJ, Cui P, et al. (2002) Differential pattern of expression of voltage-gated sodium channel genes following ischemic brain injury in rats. *Neurotox Res* 4: 67-75.

Yao C, Williams AJ, Hartings JA, et al. (2005) Down-regulation of the sodium channel Na(v)1.1 alpha-subunit following focal ischemic brain injury in rats: in situ hybridization and immunohistochemical analysis. *Life Sci* 77: 1116-1129.

Ye X, Wang P, Liu J, et al. (2008) A portable telemetry system for brain stimulation and neuronal activity recording in freely behaving small animals. *J Neurosci Methods* 174: 186-193.

Yoshita M, Fletcher E, Harvey D, et al. (2006) Extent and distribution of white matter hyperintensities in normal aging, MCI, and AD. *Neurology* 67: 2192-2198.

Young VG, Halliday GM and Kril JJ. (2008) Neuropathologic correlates of white matter hyperintensities. *Neurology* 71: 804-811.

Ypsilanti AR, Girao da Cruz MT, Burgess A, et al. (2008) The length of hippocampal cholinergic fibers is reduced in the aging brain. *Neurobiol Aging* 29: 1666-1679.

Zauner A and Muizelaar P. (1997) Brain metabolism and cerebral blood flow. In: Reilly P and Bullock R (eds) *Head injury : pathophysiology and management of severe closed injury.* London: Chapman & Hall Medical, 89-100.

Zelinski EM and Burnight KP. (1997) Sixteen-year longitudinal and time lag changes in memory and cognition in older adults. *Psychol Aging* 12: 503-513.

Zhang CL, Ho PL, Kintner DB, et al. (2010a) Activity-dependent regulation of mitochondrial motility by calcium and Na/K-ATPase at nodes of Ranvier of myelinated nerves. *J Neurosci* 30: 3555-3566.

Zhang F, Eckman C, Younkin S, et al. (1997) Increased susceptibility to ischemic brain damage in transgenic mice overexpressing the amyloid precursor protein. *J Neurosci* 17: 7655-7661.

Zhang G, Zhao Z, Gao L, et al. (2011) Gypenoside attenuates white matter lesions induced by chronic cerebral hypoperfusion in rats. *Pharmacol Biochem Behav* 99: 42-51.

Zhang HY, Wang SJ, Liu B, et al. (2010b) Resting brain connectivity: changes during the progress of Alzheimer disease. *Radiology* 256: 598-606.

Zhang Y, Schuff N, Camacho M, et al. (2013) MRI markers for mild cognitive impairment: comparisons between white matter integrity and gray matter volume measurements. *PLoS One* 8: e66367.

Zheng H and Koo EH. (2006) The amyloid precursor protein: beyond amyloid. *Mol Neurodegener* 1: 5.

Zhou D, Lambert S, Malen PL, et al. (1998) AnkyrinG is required for clustering of voltage-gated Na channels at axon initial segments and for normal action potential firing. *J Cell Biol* 143: 1295-1304.

Zhu X, Smith MA, Perry G, et al. (2004) Mitochondrial failures in Alzheimer's disease. *Am J Alzheimers Dis Other Demen* 19: 345-352.

Zlokovic BV. (2005) Neurovascular mechanisms of Alzheimer's neurodegeneration. *Trends Neurosci* 28: 202-208.

Zlokovic BV, Deane R, Sagare AP, et al. (2010) Low-density lipoprotein receptor-related protein-1: a serial clearance homeostatic mechanism controlling Alzheimer's amyloid beta-peptide elimination from the brain. *J Neurochem* 115: 1077-1089.

Zonta B, Desmazieres A, Rinaldi A, et al. (2011) A critical role for Neurofascin in regulating action potential initiation through maintenance of the axon initial segment. *Neuron* 69: 945-956.

APPENDIX A

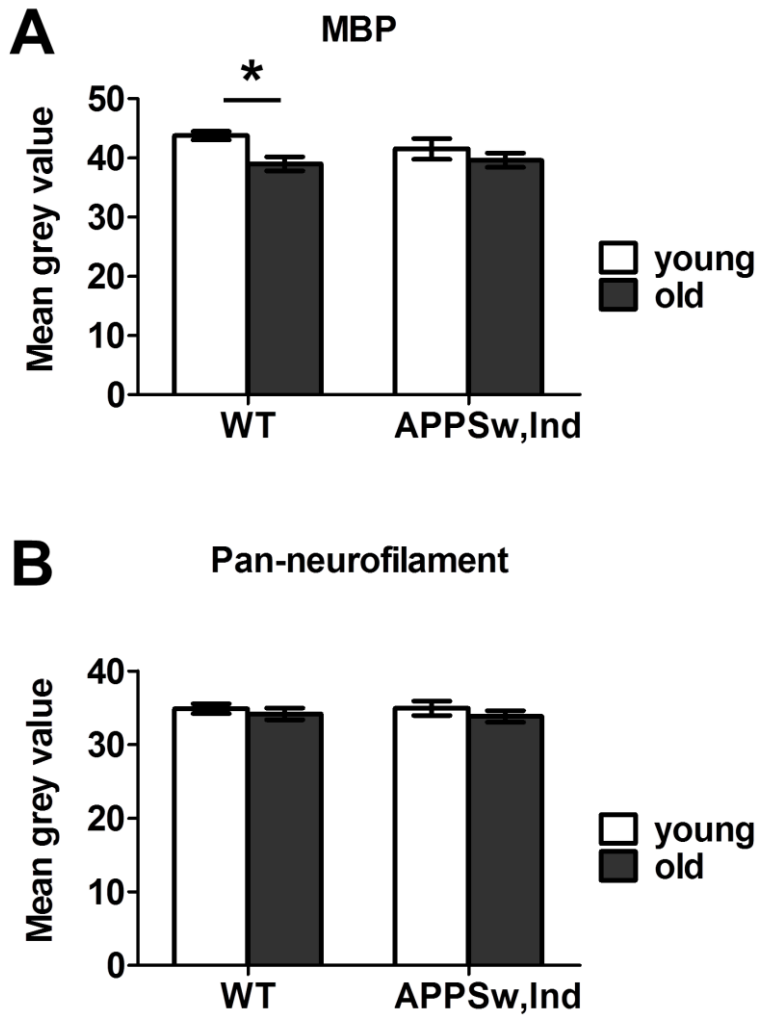

Appendix A1 ***Intensity of MBP and total neurofilament staining in the stratum lacunosum moleculare of the hippocampus*.** [A] There was a significant overall effect of age in intensity of MBP staining (2-way ANOVA: genotype*age; $p < 0.05$). *Post-hoc* testing showed that MBP intensity was significantly reduced ($p < 0.05$) in aged WT when compared to young WT mice. There was no significant difference ($p > 0.05$) in myelin density with increased amyloid in old APPSw,Ind as compared to young APPSw,Ind [B] Analysis of total neurofilament intensity did not show any significant effect of age or genotype. *: $p \leq 0.05$. Graphs show mean ± SEM

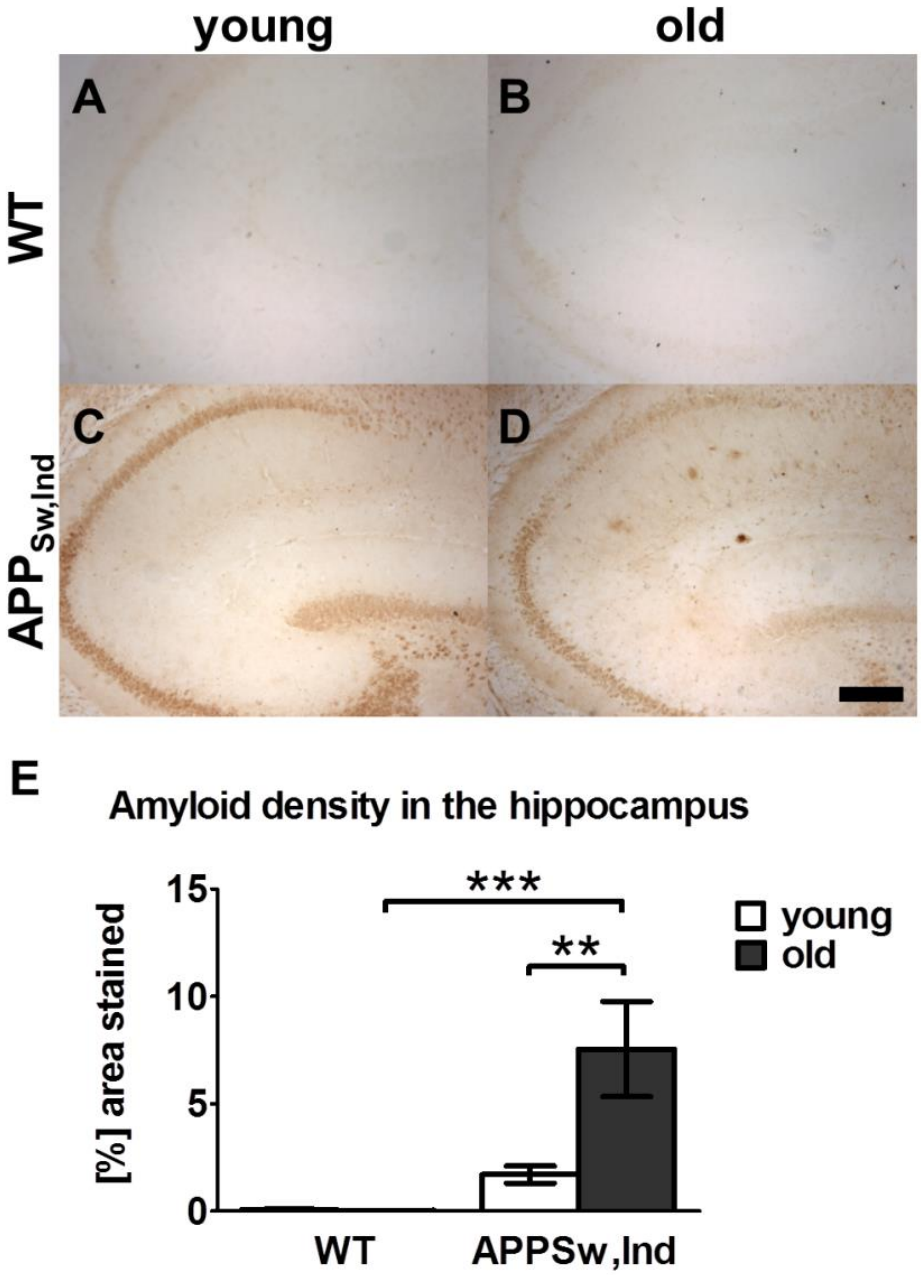

Appendix A2 ***Amyloid deposition in the stratum lacunosum moleculare of the hippocampus of TgAPPSw,Ind mice.*** Amyloid load in the stratum lacunosum moleculare hippocampus was assessed using 6E10 antibody in both WT [A & B] and TgAPPSw,Ind animals [C & D]. Aβ load (percentage area) in the hippocampus was significantly increased by age ($p < 0.05$) and by the TgAPPSw,Ind genotype ($p < 0.05$). *Post-hoc* analysis showed that the aged TgAPPSw,Ind have significantly greater Aβ load in the stratum lacunosum moleculare when compared to young TgAPPSw,Ind ($p < 0.01$) and aged WT ($p < 0.001$). WT young: n=13, WT old: n=12 TgAPPSw,Ind young: n=13, TgAPPSw,Ind old: n=15**: $p < 0.01$, ***: $p < 0.001$. Graphs show mean ± SEM. Scale bar 300μm.

APPENDIX B

MANUSCRIPTS IN PREPARATION

Kanelina Karali, Gillian Scullion, Jill H. Fowler, Karen Horsburgh. Age-related changes of nodes of Ranvier and Axon Initial Segment in the hippocampus of wild-type and mutant APPSw,Ind mice. 2013

Kanelina Karali, Gillian Scullion, Philip Holland, Jill Fowler, Karen Horsburgh. Cerebral hypoperfusion disrupts nodal regions of myelinated axons and impairs spatial working memory, an effect which is exacerbated in APPSw,Ind mice. 2013

ABSTRACTS

Jamie McQueen*, Kanelina Karali*, and Karen Horsburgh. Alterations to nodal and paranodal domains of myelinated axons with ageing and chronic cerebral hypoperfusion. *equal contribution Edinburgh Neuroscience day 2012, Edinburgh UK.

Gillian Scullion, Kanelina Karali, Guiquan Chen, Philip Holland, Jill Fowler, Karen Horsburgh. Changes in cerebrovascular structure and spatial working memory deficits induced by chronic cerebral hypoperfusion are exacerbated by the presence of APP and amyloid, VASCOG 2011, 11-14 September 2011, Lille, France

Kanelina Karali, Stephanie Daumas, Gillian Scullion, Michell Reimer, Jill Fowler, Karen Horsburgh. Age-related cognitive deficits and white matter alterations in a mutant APPSw-Ind mouse model VASCOG 2011, 11-14 September 2011, Lille, France.

Kanelina Karali, Gillian Scullion, Jill Fowler, Karen Horsburgh. Age-related white matter alterations are not influenced by amyloid. Edinburgh Neuroscience day 2011, Edinburgh UK

Kanelina Karali, Gillian Scullion, Karen Horsburgh. Chronic cerebral hypoperfusion results in a working memory deficit which is exacerbated in an animal model of amyloid pathology (J9a). Models of dementia; the good, the bad and the future. 15-17 December 2010, Robinson College, Cambridge, UK.

Jill H. Fowler, Kanelina Karali, Colin Smith, Aisling Spain, Karen Horsburgh. Increased intraneuronal amyloid following a mild brain injury. Alzheimer's & Dementia: The Journal of the Alzheimer's Association July 2010 (Vol. 6, Issue 4, Supplement, Pages S241-S242).

Jill H. Fowler, Kanelina Karali, Karen Horsburgh. Stroke increases oligomeric amyloid and amyloid deposition in mutant APP (J9a) mice. Alzheimer's & Dementia: The Journal of the Alzheimer's Association July 2010 (Vol. 6, Issue 4, Supplement, Page S414).

Gillian A. Scullion, Jill Fowler, Kanelina Karali, Robin Coltman, Ryan Green, Colin Smith, Karen Horsburgh. Increased accumulation of amyloid in white matter in Alzheimer brains and transgenic models. Alzheimer's & Dementia: The Journal of the Alzheimer's Association July 2010 (Vol. 6, Issue 4, Supplement, Pages S244-S245).